The protein network of the Rnf-proline reductase complex required for respiratory energy generation in *Clostridioides difficile*

Von der Fakultät für Lebenswissenschaften

der Technischen Universität Carolo-Wilhelmina zu Braunschweig

zur Erlangung des Grades

einer Doktorin der Naturwissenschaften

(Dr. rer. nat.)

genehmigte

D i s s e r t a t i o n

von: Kim Eileen Rennhack

aus: Braunschweig

1. Referent: Professor Dr. Dieter Jahn

2. Referent: Professor Dr. Lothar Jänsch

Eingereicht am: 16.12.2020

Mündliche Prüfung (Disputation) am: 26.03.2021

Druckjahr 2021

Vorveröffentlichungen der Dissertation

Teilergebnisse aus dieser Arbeit wurden mit Genehmigung der Fakultät für Lebenswissenschaften, vertreten durch den Mentor der Arbeit, in folgenden Beiträgen vorab veröffentlicht:

Tagungsbeiträge:

K. E. Rennhack, J. Wissing, M. Müsken, S. E. Will, I. Pusch, L. Jänsch, M. Rohde, M. Neumann-Schaal, D. Jahn and J. M. Borrero de Acuña: High-ordered electron transfer complex assembly during Stickland fermentation in *Clostridioides difficile*. (Talk). Annual conference of the VAAM, Leipzig (Germany) (2020)

K. E. Rennhack, J. Wissing, M. Müsken, S. E. Will, I. Pusch, L. Jänsch, M. Rohde, M. Neumann-Schaal, D. Jahn and J. M. Borrero de Acuña: High-ordered electron transfer complex assembly during Stickland fermentation in *Clostridioides difficile*. (Progress report). PROCOMPAS Retreat, Königslutter (Germany) (2019)

K. E. Rennhack, J. Wissing, I. Pusch, D. Jahn and J. M. Borrero de Acuña: High-ordered electron transfer complex assembly during Stickland fermentation in *Clostridioides difficile*. (Lightning talk #20). Gordon Research Conference (Molecular Form and Function of Proteins, in Nature and by Design), Holderness (US) (2019)

K. E. Rennhack, J. Wissing, I. Pusch, L. Jänsch, D. Jahn and J. M. Borrero de Acuña: Protein-protein interactions involved in the Stickland fermentation in *Clostridioides difficile*. (Progress report). PROCOMPAS Retreat, Königslutter (Germany) (2018)

Posterbeiträge:

K. E. Rennhack, J. Wissing, I. Pusch, D. Jahn and J. M. Borrero de Acuña: High-ordered electron transfer complex assembly during Stickland fermentation in *Clostridioides difficile*. (Poster). Gordon Research Conference (Molecular Form and Function of Proteins, in Nature and by Design), Holderness (US) (2019)

K. E. Rennhack, J. Wissing, I. Pusch, D. Jahn and J. M. Borrero de Acuña: Interactomic studies of proteins involved in the Stickland fermentation of *Clostridioides difficile*. (Poster). Annual conference of the VAAM, Mainz (Germany) (2019)

K. E. Rennhack, D. Jahn and J. M. Borrero de Acuña: Interactomic studies of proteins involved in the Stickland fermentation of *Clostridioides difficile*. (Poster). 6th ICDS International *C. difficile* Symposium, Bled (Slovenia) (2018)

K. E. Rennhack, D. Jahn and J. M. Borrero de Acuña: Interactomic studies of proteins involved in the Stickland fermentation of *Clostridioides difficile*. (e-Poster). Annual conference of the VAAM, Wolfsburg (Germany) (2018)

Table of contents

Abbreviations

°C	Celsius
A	Abundance
ACN	Acetonitrile
Amp	Ampicillin
ALA	5-aminolevulinic acid
AP	Alkaline phosphatase
Ap^r	Ampicillin resistance
APS	Ammonium peroxodisulphate
ATP	Adenosine triphosphate
BCIP	5-bromo-4-chloro-3-indolyl phosphate
BHI(S)	Brain Heart Infusion Broth with supplements
bp	Base pair(s)
BSA	Bovine serum albumin
catP	Thiamphenicol resistance casette
C. difficile	*Clostridioides difficile*
CDI	*C. difficile* infections
CDT	*C. difficile* transferase
CFU	colony forming units
Cm	Chloramphenicol
DNA	Deoxyribonucleic acid
dNTP	Deoxynucleotide triphosphate
DTT	Dithiothreitol
EDTA	Ethylenediaminetetraacetic acid
EM	Electron microscopy
Etf	Electron-transferring-flavoprotein
EtOH	Ethanol
ermB	Erythromycin resistance casette
erm^r	Erythromycin resistance
FA	Formic acid
FC	Fold change
f.c.	Final concentration
Fd	Ferredoxin
Fe	Iron
g	Gravitation
h	Hour
HRP	Horseradish peroxidase
HZI	Helmholtz Centre for Infection Research

dH_2O	Distilled water
kb	Kilo base(s)
kDa	Kilo-Dalton
LB	Lysogeny broth
LC-MS/MS	Liquid chromatography-mass spectrometry/mass spectrometry
mA	Milliampere
min	Minute
MMTS	Methyl methanethiosulfonate
MQ	Milli-Q® water
NaCl	Sodium chloride
$NAD^+(H)$	Nicotinamide adenine dinucleotide (oxidized and reduced)
NTB	Nitrotetrazolium blue
OD_{xxx}	Optical density at a wavelength of xxx nm
PaLoc	Pathogenicity locus
PBS	Phosphate buffered saline
PCR	Polymerase chain reaction
PPIs	Protein-protein interactions
Prd	D-proline reductase
RNase	Ribonuclease
Rnf	Ferredoxin-NAD^+: oxidoreductase (*origin: rhodobacter nitrogen fixation*)
rpm	Revolutions per minute
s	Second
SDS-PAGE	Sodium dodecyl sulfate polyacrylamid gel electrophoresis
SLP	Substrate-level phosphorylation
SPF	Specific pathogen free conditions
TBS	Tris buffered saline
TEM	Transmission electron microscopy
TEMED	N,N,N',N'-Tetramethyl ethylenediamine
Tm^r	Thiamphenicol resistance
Tm	Thiamphenicol
TFA	Trifluoroacetic acid
Tris	Tris-(hydroxymethyl)-methyl-2-amino-ethansulfonate
TCEP	Tris (2-carboxyethyl) phosphine
U	Unit
UP	Unique peptides

v/v	Volume per volume
w/v	Weight per volume
WLP	Wood-Ljungdahl pathway

1 Introduction

1.1 The gut microbiota of the human gastrointestinal tract

The Germ Theory of diseases proposed by Louis Pasteur ~130 years ago laid the basis for the understanding of the pathogenesis of microbes. It was postulated for the first time that the human health is strongly correlated with the occurrence of non-pathogenic microorganisms that inhabit in our body (Hooper *et al*. 2002; Schottelius 1902). Today, it is established that a large number of microorganisms, mostly various species of bacteria, colonize different parts of the human body and form large, dynamic and complex communities, called the microbiota (Hattori and Taylor 2009; Hooper *et al* 2002). In this line, ~10^{12} of these microorganisms are found on the epidermis and 10^{14} in the intestinal tract of adults (Luckey 1972). The bacterial population of the gut microbiota consists of thousand of different bacteria, whereby the most abundant strains are from the phyla Bacteroidetes, Actinobacteria and Firmicutes (Kho and Lal 2018; Kachrimanidou and Tsintarakis 2020).

In the human intestine, the gut microbiota have the vital function of food processing. The degradation of nutrients leads to the synthesis of different compounds by the gut microbiota. Thus, the human body profits from these metabolic activities by the utilization of formed additional nutrients and also signal molecules. In exchange, the gut microbiota receive a nutrient-rich as well as protected niche. Beyond that, the gut microbiota have further functions like vitamin synthesis or the protection against pathogen colonization (Kachrimanidou and Tsintarakis 2020; Hooper *et al.* 2002; Guarner and Malagelada 2003; Hattori and Taylor 2009). If this microbial balance in the gut is disturbed, e.g. by the intake of antibiotics that destroy the microflora, a dybiosis effect occurs and can lead to severe disease progression like the case of *Clostridioides difficile* infections (CDI) (Kachrimanidou and Tsintarakis 2020; Rao and Safdar 2016).

1.2 The human pathogen Clostridioides difficile *and the CDI*

The human pathogen *Clostridioides* (*Clostridium*) *difficile* belongs to the Firmicutes phylum. It is a Gram-positive, obligate anaerobic, rod-shaped and spore-forming bacterium (figure 1), which was first isolated in 1935 from the stool of a healthy newborn, but was only discovered in 1978 as a pathogen causing antibiotic-associated colitis as well as diarrhea. The broad spectrum of clinical symptoms associated with in infection by this pathogen range from mild diarrhea to toxic megacolon and colonic perforations (Kachrimanidou and Tsintarakis 2020; Mylonakis *et al*. 2001; Bartlett *et al.* 1978; Bartlett *et al.* 1977; Larson *et al.* 1977; Hall and O'Toole 1935; Lawson *et al.* 2016; Eckburg *et al.* 2005).

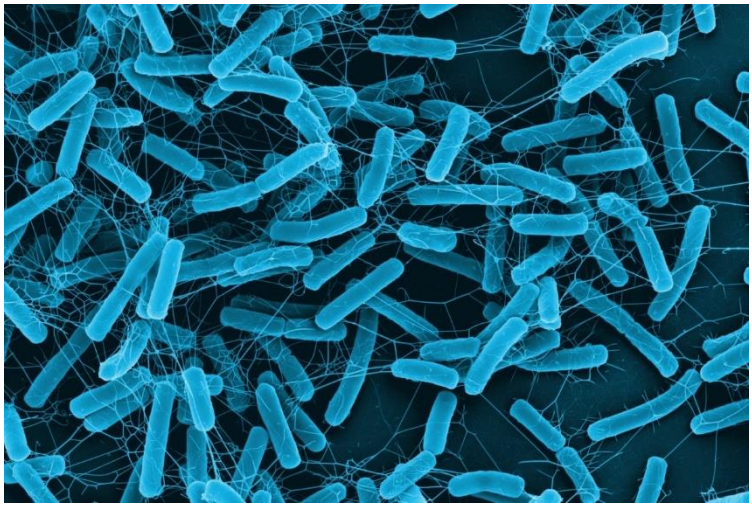

Figure 1: Electron microscopic image (stained) of *Clostridioides difficile* (image was taken by M. Rohde at the Helmholtz Centre for Infection Research, Braunschweig). The pathogenic bacterium *C. difficile* is an obligate anaerobic, Gram-positive and rod-shaped as well as spore-forming bacterium (blue stained) (Mylonakis *et al.* 2001; Bartlett *et al.* 1978; Bartlett *et al.* 1977; Larson *et al.* 1977).

Besides antibiotic treatment, surgery, age and immunosuppression are other major factors sustaining symptomatic infections including CDI which has become a worldwide health problem (Kachrimanidou and Tsintarakis 2020; Rao and Safdar 2016). The severity of nosocomial CDIs in Canada, USA and Europe has increased significantly over the last 20 years, which is reflect by the corresponding mortality rates worldwide. Studies

showed that deaths in the USA have risen to an estimated 14 000 per year (Kachrimanidou and Tsintarakis 2020; Czepiel *et al.* 2019). The CDI infection cycle is illustrated in figure 2.

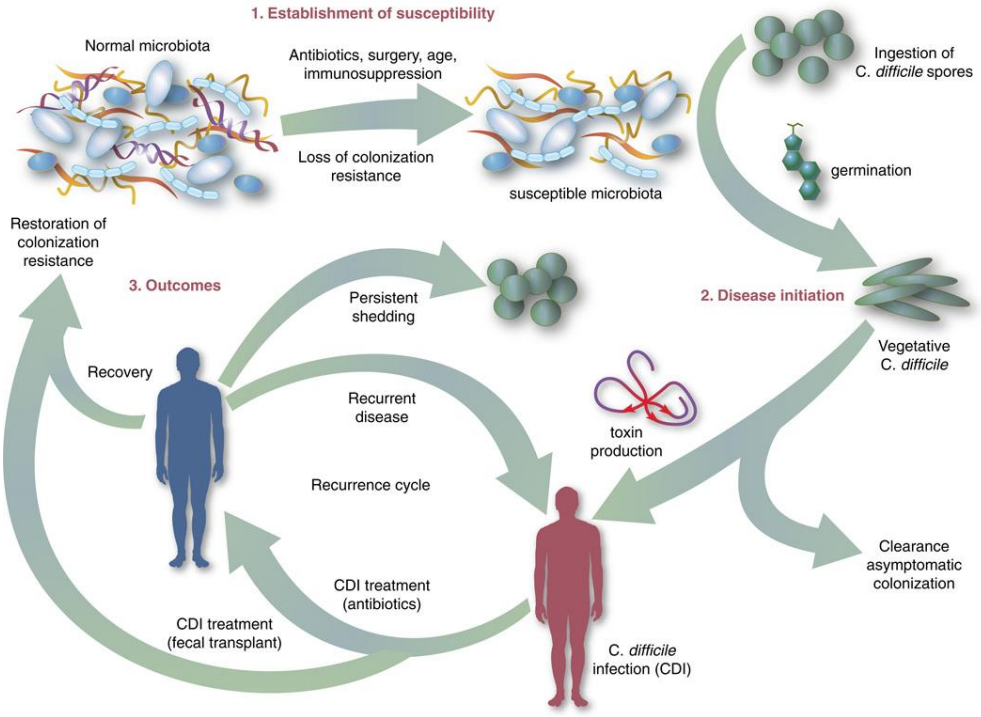

Figure 2: The cycle of *Clostridioides difficile* infections (CDI) (after Rao and Safdar 2016). The figure illustrates the destruction of the normal gut microbiota by various indicated factors and the consequent loss of colonization resistance as well as the generation of a susceptible microbiota. The new circumstances favor the germination of spores of the human pathogen *C. difficile* into the vegetative form of the bacterium, in which it is able to produce epithelial damaging toxins, leading to a CDI. Treatment of the infection with fecal transplantation often contributes to recovery. However, patients treated with antibiotics are sensitive to recurrent infections.

It shows that destruction of the normal microbiota favours the germination of *C. difficile* spores in turn resulting the vegetative bacteria are able to produce toxins that contribute to the damage of the gut epithelium and mucosa. The infection can be treated by various methods (e.g. fecal transplantation, antibiotics) which may lead to either recovery and the rebuilding of colonization resistance or to recurring infections (recurrence cycle) (Rao and Safdar 2016).

1.2.1 The key players of the *C. difficile* pathogenesis

C. difficile is, as already mentioned, able to form spores as a survival strategy. With regard to the disease process of the pathogen, these highly resistant spores can be transmitted from patient to patients via smear infections and unhygienic conditions especially in a hospital environment. Clinical facilities, toilets, telephones and medical equipment can be a temporally limited reservoir for these spores (Czepiel *et al.* 2019). If these spores enter the body of a healthy person, they usually do not germinate. Given the fact that the normal gut microflora is disrupted, spores can germinate by the induction of liver-produced primary bile acids. The natural function of primary bile acids is actually the transport and absorption of fats and water insoluble vitamins in the gut (Kochan *et al.* 2017; Baktash *et al.* 2018; Chiang 2009). Primary bile acids like chenodeoxycholic acid and cholic acid, routinely subjected to 7α-dehydroxylation by the healthy gut microbiota, are converted into secondary bile acids, like deoxycholic acid and lithocholic acid. *In vitro* experiments strongly indicate that some primary bile acids have a promoting effect on the germination of *C. difficile* spores and secondary bile acids rather inhibit the process (Czepiel *et al.* 2019; Chiang 2009; Baktash *et al.* 2018).

After germination of the spores of *C. difficile*, the virulence of the formed vegetative cells is determined by enzymes such as hyaluronidase, collagenase, chondroitin sulfatase and toxins. The pathogen itself is non-invasive. The major toxins of *C. difficile* are enterotoxin A (TcdA) and cytotoxin B (TcdB). These were classified as members of the family of clostridial toxins, which further contain the hemorrhagic and lethal toxin of *C. sordellii*, the α-toxin of *C. novyi* and the TpeL of *C. perfringens*. These toxins are multidomain proteins which are able to transfer glycosyl groups to small Rho-GTPases for their inactivation. TcdA and TcdB of *C. difficile* damage the cytoskeleton of the epithelial cells. This leads to a disturbance of the tight junctions, a neutrophil adhesion, fluid secretion and local inflammation. Finally, the integrity of the intestinal barrier collapses and functionality is lost. This leads to cell rounding and inhibition of cell division, which finally contributes to the death of the cells (Czepiel *et al.* 2019; Smits *et al.* 2016; Shen 2012; Schirmer and Aktories 2004).

Some *C. difficile* strains can produce a third toxin, the so-called *C. difficile* transferase (CDT) or binary toxin. For example, the epidemic ribotype 027 has the ability to produce CDT. It is assumed that it induces the formation of microtubule-based protrusions on epithelium cells (Shen 2012; Popoff *et al.* 1988). Figure 3 shows the regulation of the pathogenic cycle of *C. difficile* spanning from the above-mentioned induction of germination, the toxin formation leading to a strong immune response up to the generation of the pseudomembrane.

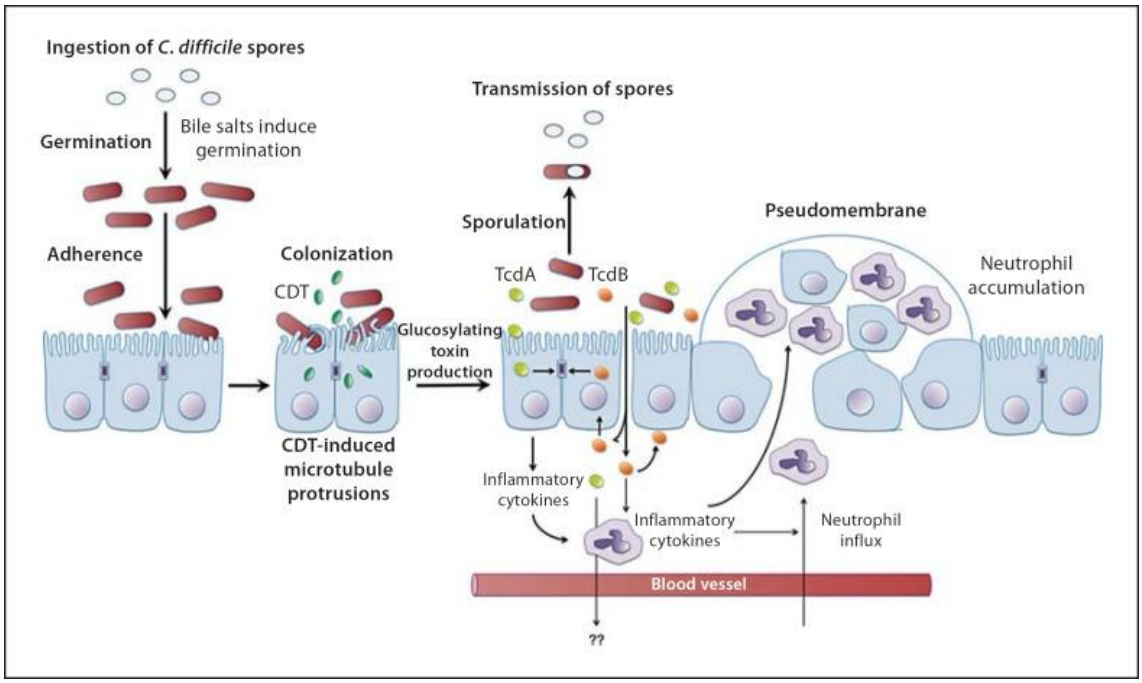

Figure 3: Schematic illustration of the pathogenesis process of *C. difficile* (after Shen 2012). The pathogenesis of the bacterium *C. difficile* in the human small intestine begins with the induction of germination of ingested spores by bile acids. The colonisation of the germ takes place in the colon, which has a disturbed microflora due to e.g. antibiotic treatment. The bacteria can then adhere to the epithelial cells. Strains that form the binary toxin CDT, which induces the formation of microtubule protrusions, can thus increase their adherence to the epithelium via the formed protrusions. Glucosylating toxin-producing (TcdA and TcdB) *C. difficile* strains block cytoskeleton formation and induce cellular disintegration. These processes stimulate inflammation of the mucosa of the colon, resulting in the release of inflammatory cytokines. At this point, the tight junctions are also interrupted, which leads to rounding of the epithelial cells and the formation of cell gaps. This in turn causes lymphocytes and mast cells to release further cytokines. This leads to a strong inflammatory reaction by the aggregation of neutrophils and lymphocytes, which causes the pseudomembrane formation. During this process new spores can be formed and released.

1.2.2 Regulation of toxin gene expression in *C. difficile*

The production of toxins in *C. difficile* depends, among other factors, on nutrient availability, a change in temperature and differences in redox potential (Onderdonk *et al.* 1979; Bouillaut *et al.* 2013; Karlsson *et al.* 2003). Therefore, certain metabolizable carbon sources and amino acids can inhibit the expression of the toxin genes. A significant reduction of the toxin amount occurs, when certain amino acids such as cysteine, leucine, isoleucine, threonine, valine, methionine, tryptophan, proline and glycine are added to the medium during the logarithmic growth phase. Generally, toxins are only produced in the stationary phase when there is a nutrient deficiency (Bouillaut *et al.* 2013; Dupuy and Sonenshein 1998; Karlsson *et al.* 1999).

It has previously been shown that the toxin genes *tcdA* and *tcdB* are genetically organized together in a ~19 kb pathogenicity locus (PaLoc). The genes *tcdR* (for an alternative sigma factor), *tcdE* (for a holin-like protein) and *tcdC* (for an anti-sigma factor) are also located at the same locus (Braun *et al.* 1996; Dineen *et al.* 2010; Fortier and Sekulovic 2013) (figure 4).

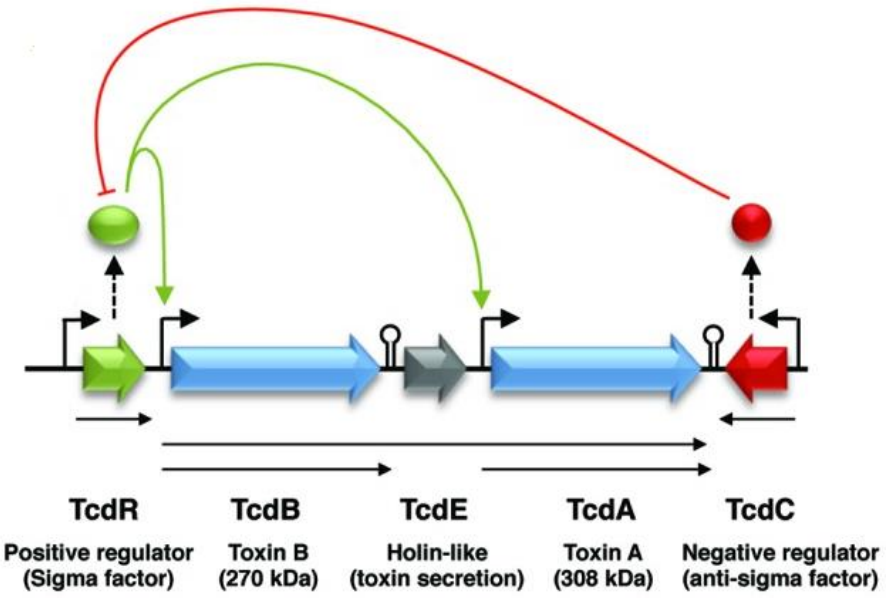

Figure 4: The pathogenicity locus (PaLoc) of *C. difficile* (modified after Fortier and Sekulovic 2013). The PaLoc of *C. difficile* is illustrated in which the toxin genes *tcdB* and *tcdA,* the genes of the alternative sigma factor TcdR, the anti-sigma factor TcdC and the potential holin gene *tcdE* are encoded. The green arrows represent an activation of gene expression of the target gene whereas the red line indicates the inactivation of the sigma factor by binding.

It was also shown that the expression of genes in the PaLoc is repressed by CodY, a global transcriptional regulator. CodY represses the toxin gene transcription by binding to the promoter sequence of the alternative sigma factor TcdR, which induces the transcription of the toxin genes *tcdA* and *tcdB* to promotes of the *tcdR* gene (Dineen *et al.* 2007; Dineen *et al.* 2010; Mani and Dupuy 2001; Martin-Verstraete *et al.* 2016).

1.3 Energy metabolism of the anaerobic bacterium C. difficile

In nature the energy metabolism is classified after the employed energy source (light = phototroph, chemical redox reaction = chemotroph), the used energie donor (inorganic = lithotroph, organic = organotroph) and the utilized electron source (inorganic = autotroph, organic = heterotroph) (Jahn *et al.* 2020; Präve *et al.* 1994). Some Clostridia strains are able to perfom a CO_2- assimilation by using different energy- and carbon substrates as acetate, ethanol and bicarbonate (Jungermann *et al.* 1967). Hence, *C. difficile* was identified as one of the first autotrophic pathogen (Köpke *et al.* 2013).
For many years *C. difficile* was considered as a strict fermentative organism, generating energy via substrate level phosphorylation and generating the essential proton gradient at the membrane using a reverse ATPase. However, only a few years ago ion-gradient formation via the ion-gradient generating Rnf-complex coupled fermentative reaction was discovered. *C. difficile* can use diverse sugars and amino acids for fermentative processes (Neumann-Schaal *et al.* 2019; Neumann-Schaal *et al.* 2015; Jahn *et al.* 2020).

1.3.1 Stickland fermentation reaction

In various *Clostridium* species including *C. sticklandii* and *C. sporogenes*, the primary energy source are amino acids utilized via the Stickland reaction which was first discovered in 1935. This reaction is the linked metabolism of amino acid pairs, with one amino acid serving as an electron donor, which gets oxidatively deaminated and decarboxylated. A second amino acid acts as an electron acceptor and is reductively deaminated. The oxidative and reductive metabolism is coupled with an electron transfer process to the membrane with a formation of an ion-gradient to produce ATP (Nisman 1954; Stickland

1934, 1935a, 1935b; Bouillaut *et. al* 2013; Fonknechten *et al.* 2010; Jahn *et al.* 2020). The next figure gives a schematic representation of the reductive and oxidative pathways in the Stickland fermentation, which is coupled to the Rnf complex in Clostridia.

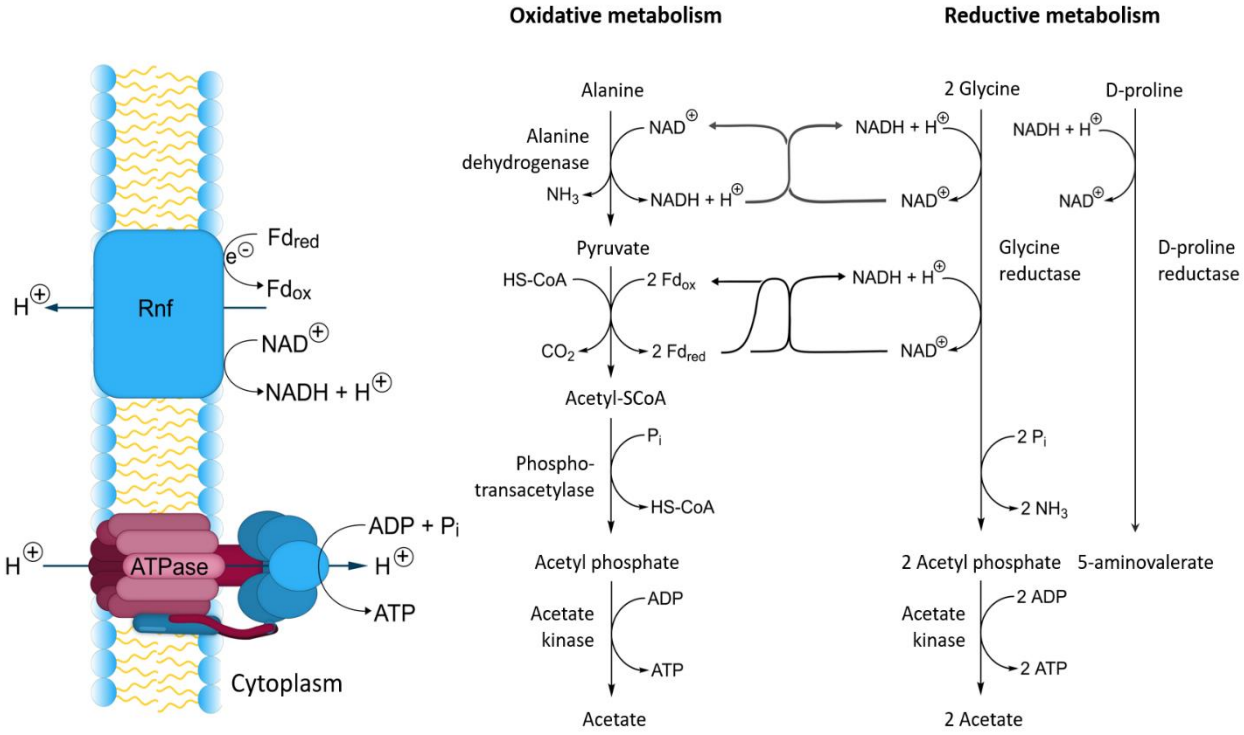

Figure 5: Coupled amino acid fermentation and respiration via the Rnf complex (modified after Jahn *et al*. 2020). The Stickland metabolism is based on the oxidation and reduction of amino acid pairs (oxidative and reductive metabolism). In this process classical fermentation (subrate-level phosphorylation) is combined with an electron transfer process to the membrane to produce an ion-gradient for ATP generation. The process shows the production of acetate by substrate utilization of alanine in the oxidative metabolism and glycine in the reductive metabolsim. In both processes, intermediates such as pyruvate and acetyl-CoA (in the oxidative metabolic pathway) and acetyl phosphate (in the oxidative and reductive metabolic pathway) are formed. Here, generated NADH can be re-oxidized by coupling both pathways. Within the reductive pathway, D-proline is converted to 5-aminovalerate by oxidation of NADH. Electrons can be transferred to the Rnf complex by means of reduced ferredoxin (also from other electron bifurcation pathways), and NAD^+ is generated in the Stickland pathway, whereby ions are transferred across the membrane. At the membrane, the ion-gradient is used by the ATPase to produce ATP.

The amino acids that serve as the mostly efficient electron donors are isoleucine, leucine and alanine (oxidative metabolism), while the most efficient acceptors are glycine, hydroxyproline and proline (reductive metabolism). It is well-known that in the Clostridia species the reduction of the acceptors proline and glycine is catalysed by two selenium-dependent reductases, the D-proline reductase and the glycine reductase. The last enzyme is responsible for the reductive deamination of glycine to acetyl phosphate and ammonium. In contrast, the D-proline reductase converts the substrate D-proline into 5-aminovalerate (Stadtman 1956; Stadtman and Elliott 1957; Cone *et al.* 1977; Seto and Stadtman 1976; Bouillaut *et al.* 2013). In the oxidative metabolism alanine is converted by alanine dehydrogenase to pyruvate and ammonium, which then reacts via acetyl-SCoA to acetyl phosphate. Figure 5 shows that acetyl phosphate is generated to acetate and ATP via the classical fermentation pathway (substrate-level phosphorylation (SLP)). The coupling of both metabolism reactions shows that formed NADH is re-oxidized, whereby formed NAD^+ is also reduced at the membrane-bound Rnf complex. Additionally, reduced ferredoxin is converted at the Rnf complex, which generates the ion-gradient by electron transfer. Finally, the ATPase is able to use the proton gradient to form ATP (Jahn *et al.* 2020; Bouillaut *et al.* 2013).

1.3.2 CO_2-assimilation and energy generation via the Wood-Ljungdahl pathway

An old pathway for CO_2-assimilation discovered in 1980 is the reductive acetyl-CoA pathway and called the Wood-Ljundahl pathway (WLP). The net reaction of $4\ H_2 + 2\ CO_2 \longrightarrow CH_3COO^- + H^+ + 2H_2O$ requires a complex and highly-sensitive enzyme machinery. Overall, one CO_2 gets fixed in the pathway and an additional CO_2 get assimilated, which results no net ATP gain during SLP (Drake *et al.* 2008; Schuchmann and Müller 2014). Moreover, acetate is a major product in energy metabolism. In *C. difficile* and other clostridial species e.g. *C. ljungdahlii* and *C. carboxidivorans* the genes for the WLP are highly conserved. (Köpke *et al.* 2013; Fast and Papoutsakis 2018; Bruant *et al.* 2010).

However, in the context of WLP it was postulated that the clinical isolate *C. difficile* 630 is able to use CO_2 + H_2 autotrophically as sole carbon and energy source when growing in defined medium (Köpke *et al*. 2013). The contrast to real acetogens such as *Clostridium ljungdahlii* or *Acetobacterium woodii,* whose genomes contain genes for acetate formation like acetate kinase (*ack*) and phosphotransacetylase (*pta*), only the acetate kinase gene was found in *C. difficile* (Köpke *et al.* 2013; Köpke *et al.* 2010; Poehlein *et al.* 2012). Using the database Kyoto Encyclopedia of Genes and Genomes (KEGG) a putative phosphotransacetylase was detected (CD630DERM_19200), which could convert the acetyl-CoA into the acetyl-phosphate.

1.3.3 Ion-gradient formation during butyrate fermentation in *C. difficile*

The clostridial butyrate fermentation pathway converts acetyl-CoA, which is the oxidation product after glycolysis, to butyrate. During the butyrate pathway, crotonyl-CoA is formed from acetyl-CoA via the conversation of several intermediates. The bifurcating butyryl-CoA dehydrogenase complex (BcdA/Etf), coupled reduced ferredoxin to an ion-gradient generating process at the membrane, converts crotonyl-CoA into butyryl-CoA. The conversion combines an exergonic reduction (NADH-driven) of crotonyl-CoA into butyryl-CoA and the ferredoxin endergonic reduction (NADH-driven). Finally, butyrate and ATP are formed by SLP (Aboulnaga *et al.* 2013; Neumann-Schaal *et al.* 2019; Bertsch *et al.* 2013; Buckel and Thauer 2013; Li *et al.* 2008). The next figures show the conversion of acetyl-CoA to butyrate in the butyrate fermentation pathway (figure 6) and the principle of electron bifurcation exemplified by the butyryl-CoA dehydrogenase complex reaction (figure 7).

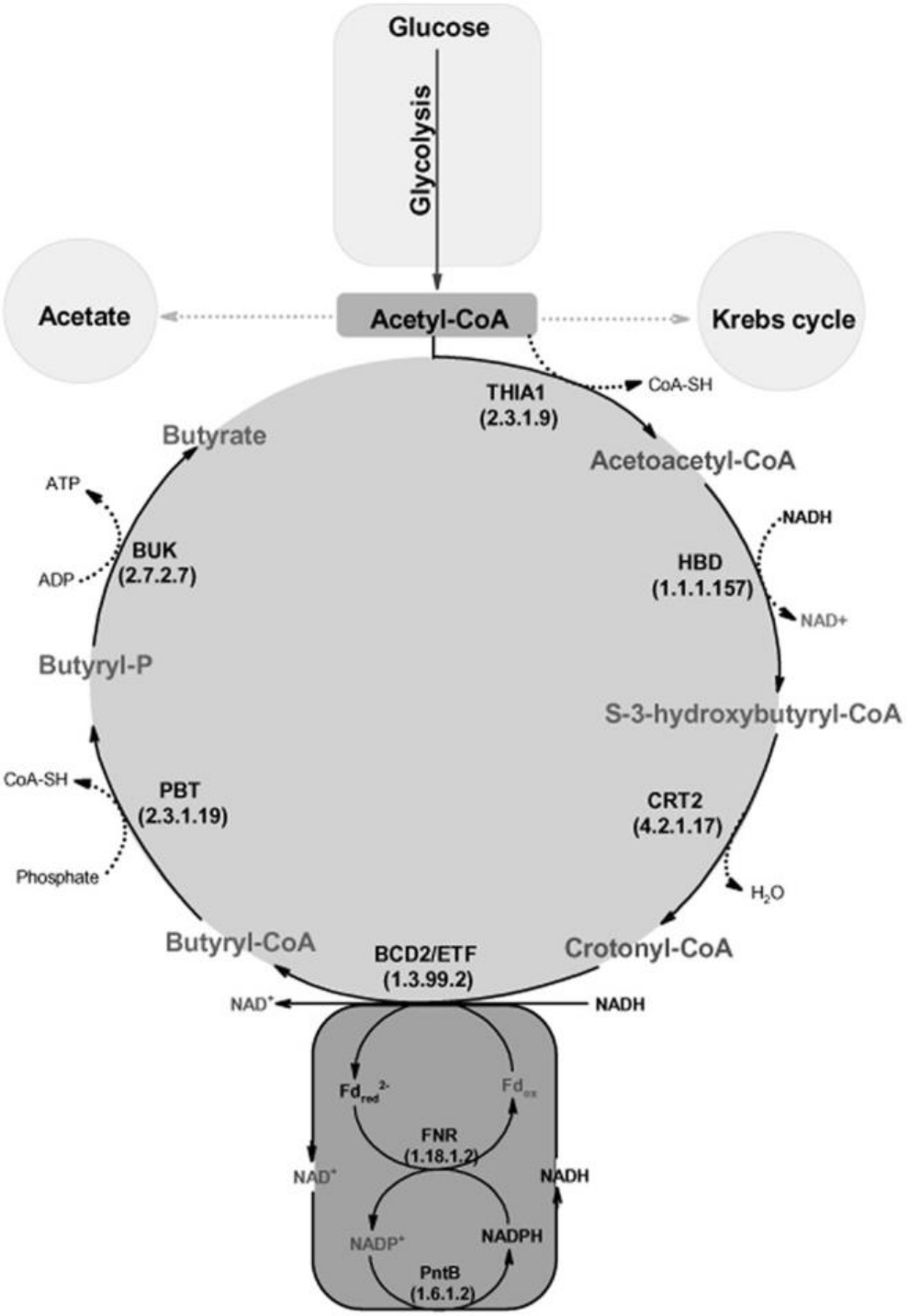

Figure 6: The butyrate fermentation pathway (modified after Aboulnaga *et al.* 2013). The figure shows the butyrate fermentation pathway based on acetyl-CoA, which is converted by the acetoacetyl-CoA thiolase 1 (THIA1) into acetoacetyl-CoA. Subsequently, S-3-hydroxybutyryl-CoA is formed by 3-hydroxybutyryl-CoA dehydrogenase (HBD) which is converted into crotonyl-CoA by 3-hydroxybutyryl-CoA dehydratase (CRT2). Crotonyl-CoA reacts via the bifurcating complex Bcd2/Etf (butyryl-CoA dehydrogenase / electron transfer flavoprotein) and NADH into butyryl-CoA. Here, the bacteria are able to change and conserve further energy by an exergonic reduction and a ferredoxin (Fd) endergonic reduction (with a further NADH molecule) and by the enzymes ferredoxin-$NADP^+$ reductase (FNR) and $NAD(P)^+$ transhydrogenase (PntB). Butyryl-CoA can be converted by phosphate butyryltransferase (PTB) into butyryl-phosphate and then into butyrate by substrate-level phosphorylation via butyrate kinase (BUK), which results ATP (Aboulnaga *et al.* 2013; Buckel and Thauer 2013; Li *et al.* 2008).

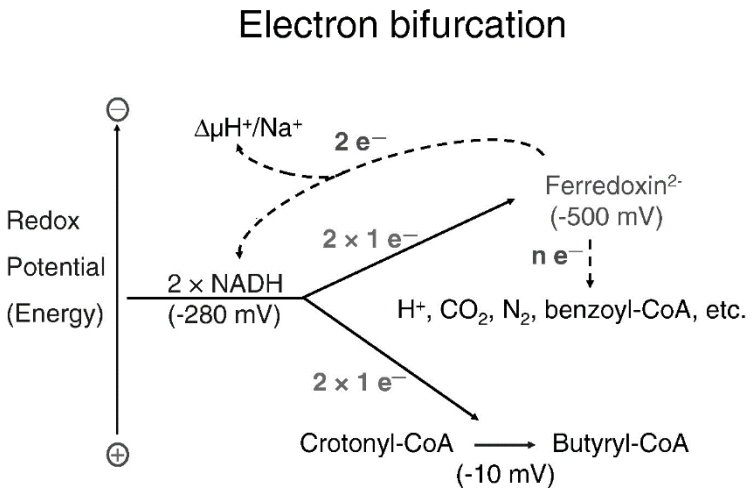

Figure 7: The principle of electron bifurcation at the butyryl-CoA dehydrogenase complex (after Buckel and Thauer 2013). During the NADH coupled electron bifurcation reactions one electron gets transferred to the crotonyl-CoA (high redox potential) and one to ferredoxin (low redox potential), respectively.

1.3.4 Ferredoxin:NAD$^+$-oxidoreductase - Rnf complex

Although different metabolic pathways ultimately provide energy in the form of ATP via SLP like during Stickland fermentation, the WLP or via the last step of butyrate fermentation pathway, significant amounts of ATP are produced by a membrane-localized and ion-gradient driven phosphorylation process (Bouillaut *et al.* 2013; Müller and Wiechmann 2017; Aboulnaga *et al.* 2013). From genome sequences it was deduced that acetogenic bacteria possess the F_1F_0-ATP synthase for ADP phosphorylation by an Na^+/ H^+ ion-gradient. In this context, two complexes are well-known, which are able to couple the energy released by exergonic electron transfer and thus build the gradient chemiosmotically: 1. Ech (energy-conserving hydrogenase) complex and 2. the NAD^+ dependent Rnf complex (Müller and Wiechmann 2017; Müller *et al.* 2001).

Initially, the Rnf (*Rhodobacter* nitrogen fixation) complex was discovered in *Rhodobacter capsulatus*, whose genes *rnfA, rnfB, rnfC, rnfD, rnfE* and *rnfF* encode for six membrane-associated proteins that are involved in nitrogen fixation (Schmehl *et al.* 1993). The *rnf* operon was described for the first time in 2009 for acetogenic bacteria *A. woodii*. With a membrane-spanning ferredoxin:NAD^+-oxidoreductase activity it is simililar to the NADH:quinone-oxidoreductase (Nqr) of other bacteria. The Rnf complex (figure 8) is

able to catalyze the reduction of NAD^+ by ferredoxin (Müller and Wiechmann 2017; Biegel *et al.* 2009; Biegel and Müller 2010; Juárez and Barquera 2012).

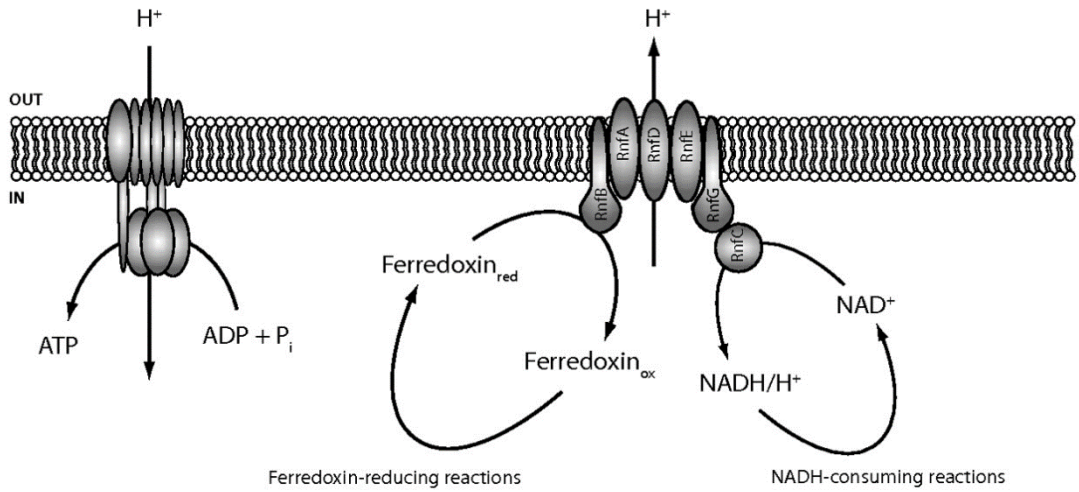

Figure 8: The clostridial Rnf complex in *C. ljungdahlii* (modified after Köpke *et al.* 2010). It is shown the membrane-based Rnf complex with its six subunits RnfB, RnfA, RnfD, RnfE, RnfG and RnfC. These complex drives electron transfer using the resulting free energy to pump ions, most likely H^+, to build up a chemiosmotic ion-gradient at the membrane. The gradient is used by the ATP synthase to phosphorylate ADP. Ferredoxin in its reduced form can be produced in several clostridial species e.g. via bifurcating complexes (e.g. Bcd2/Etf), pathways to conserve energy (Bertsch *et al.* 2013; Aboulnaga *et al.* 2013), and converted by RnfB. The RnfC subunit can reduce NAD^+. During the entire process electrons are transferred from the ferredoxin to the NAD^+.

The employed reduced ferredoxins are generated by various pathways: e.g. via oxidoreductases which are ferredoxin-dependent like in the oxidative Stickland fermentation reaction or via alternative pathways which are depending on bifurcating complexes (Bcd2/Etf) (Bertsch *et al.* 2013; Neumann-Schaal *et al.* 2019; Aboulnaga *et al.* 2013). Moreover, in several Clostridia species, including *C. ljungdahlii* or *C. difficile*, ions can be transported through the Rnf complex, to form an ion-gradient and to finally foster phosphorylation of ADP via the ATP synthase. Therefore, it is conceivable that the reductive pathway of Stickland fermentation, in particular the D-proline reductase might interact with the Rnf complex (Neumann-Schaal *et al.* 2019; Köpke *et al.* 2010).

1.4 Protein-protein interactions (PPIs)

Proteins in living cells never act alone and rather work in complexes. They form dynamic "molecular nanomachines" to perform biological functions to fullfill their function in biochemical pathways or membrane-associated complexes. Therefore, it is crucial to analyze these "interactions" and their time-resolved dynamics more precisely. The discipline that endeavors to elucidate cellular protein-protein interactions (PPIs) (interactomes) is the so-called interactomics (De Las Rivas and Fontanillo 2010; Cusick *et al.* 2005; Feng *et al.* 2014). Experimental verification in orthogonal systems together with projects to identify PPIs can produce data sets with high significance to understand the authenic complex formation and function. Research using model organisms like *Caenorhabditis elegans* or *Saccharomyces cerevisiae* has provided the fundamental know how for "interactome" mapping. Not only basic functional mechanisms of PPIs can be elucidated, furthermore, these data sets might be helpful to investigate the development of malfunction and consequently diseases (Cusick *et al.* 2005; Fromont-Racine *et al.* 1997; Walhout *et al.* 2000).

1.4.1 Interactomics for the determination of cellular protein-protein networks

Deep interactomic analysis aims at the holistic elucidation of protein-protein interaction of a living system. In general, PPIs are described as physical contacts between protein partners. These associations occur *in vivo* in all living organisms. Noteworthily, the special efforts are needed to distinguish between protein interactions which occur specifically and others which are randomly. Moreover, the interactions that a protein encounters during production, folding, quality checking and degradation are normally excluded. These include specific contacts to ribosomes, chaperones and the degradation machinery. Thus, PPIs should be intentional and not random and the interaction should be non-generic (generic functions = e.g. protein production or degradation) (De Las Rivas and Fontanillo 2010). As a dynamic system, the cell is subject to constant change. Some protein compounds, such as ATP synthase or cytochrome oxidase, are stable for longer terms. Other proteins are required short term for specialized functions in the cell. Consequently, their cellular appearance is of transient nature depending for example on the

cell cycle phase, metabolic state and the cell type (De Las Rivas and Fontanillo 2010). The *in vitro* characterization of PPIs relies on well-established biophysical up to genetic methods comprising NMR, X-ray crystallography, surface plasmon resonance (SPR) or yeast two-hybrid system. The holistic interactomic approach combines affinity purification of cellular protein complexes with the mass spectrometrical elucidation of the composition (Meyer and Selbach 2015; Gingras *et al.* 2007). That method offers the possibility of a wide characterization of protein complexes up to the identification of large protein interaction networks. In this context protein complexes are isolated directly from cell lysates and get further purified in one (or more) steps, followed by proteolytic fragmentation. Resulting peptides can subsequently be identified by tandem mass spectrometry (MS/MS). The peptides and the corresponding proteins can be identified by coupling the appropriate databases in suitable proteomic softwares (figure 9) (Gingras *et al.* 2007; Eng *et al.* 2011; Aebersold and Mann 2003).

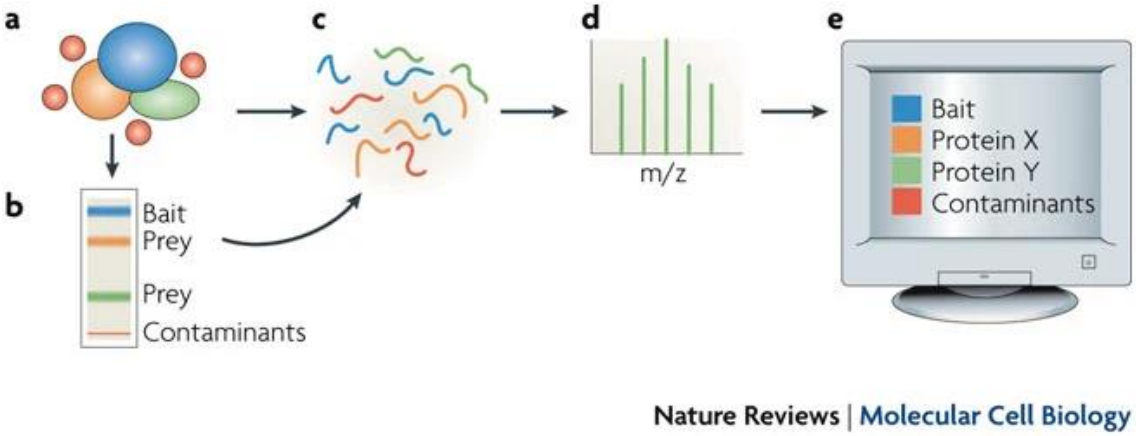

Figure 9: Schematic illustration of the holistic interactomics approach (after Gingras *et al.* 2007). The target protein (bait protein, blue), which is produced in the cell, can be purified from the cell lysate with its interaction partners attached (prey proteins, orange/green) by affinity chromatography using the tag on the bait (a). Isolated protein complexes can be resolved by SDS-PAGE (b) and corresponding proteins can be extracted from the gel and digested with e.g. trypsin (c). It is also possible to analyze isolated complexes directly (gel-free method), which is a generic and quicker method. The individual peptides are separated by liquid chromatography (LC) and identified by tandem mass spectrometry (MS/MS) (d). Obtained masses are assigned to the respective protein using a proteomics software and database matching (e). The interpretation of the data allows to identify the bait protein with its prey bound proteins. Background controls are required to identify contaminants (red).

Usually, strong native PPIs of the intact protein complexes are required to survive the stringent purification conditions. Therefore, a chemical cross-linking step can be used to stabilize transient protein-protein interactions. These cross-linker have two reactive groups, which form a covalent bond with the target protein and proteins in the direct neighbourhood (Gingras *et al.* 2007). Formaldehyde, for instance, which is widely used as an *in vivo* cross-linker, generates covalent cross-links between proteins as well as proteins and nucleotides which are reversible by heating (Larance *et al.* 2016; Tayri-Wilk *et al*. 2020; Metz *et al.* 2004). Hence, the cross-linker has the ability to connect proteins by the production of a stable methylene bridge between two amino acids (Metz *et al.* 2004; Tayri-Wilk *et al*. 2020) (figure 10). A major advantage of using formaldehyde is the small size of the compound that allows to penetrate the membrane into intact cells as well as tissues (Larance *et al.* 2016).

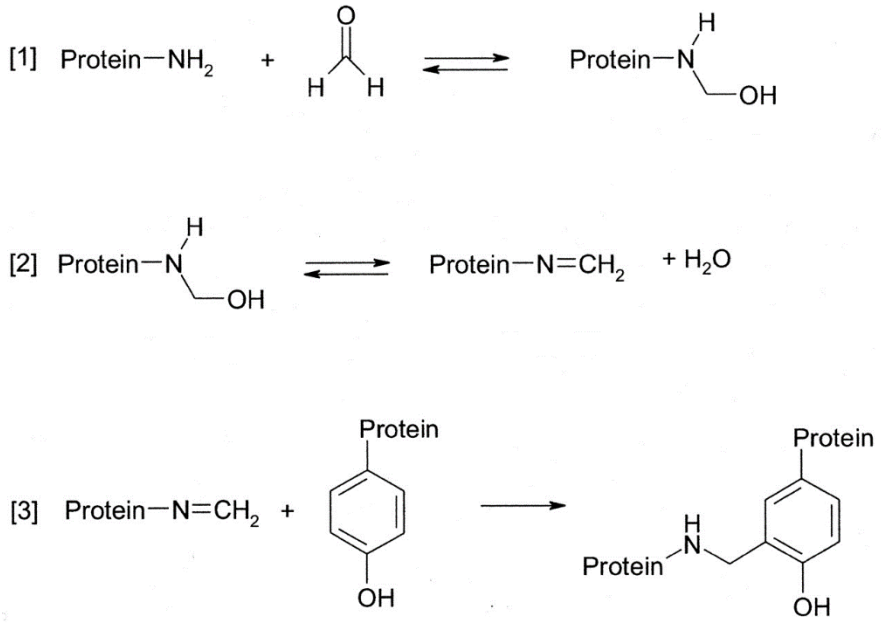

Figure 10: Formaldehyde reaction for the cross-linking of proteins (modified after Metz *et al.* 2004). In the first step [1], the reaction between the amino group of the protein and the formaldehyde begins with the production of a methylol adducts. Subsequently, in [2] a partial dehydration of the methylol adduct at the primary amino group is performed and a labile intermediate product (Schiff-base) is formed. In the final step [3], the Schiff-base can form cross-links with other amino acid residues.

2 Aim of this study

The general aim of this work was to identify the protein-protein interactions of membrane-residing and cytosolic proteins involved in the Stickland fermentation of *C. difficile* 630Δ*erm*. Focusing on the reductive metabolism of the Stickland fermentation, the interaction partners of two key players the D-proline reductase and the Rnf complex had to be investigated.

For this purpose, various bait protein (PrdA, PrdB, RnfB and RnfC) production strains based on *C. difficile* 630Δ*erm* had to be constructed. They provided the basis for the isolation of protein complexes formed in the presence and absence of the cross-linker formaldehyde. The composition of these complexes had to be elucidated by proteomics in cooperation with our partners of the HZI. Obtained results were than used to predict the Rnf-Prd interactions in great detail. Finally, the *in vivo* function of Rnf during the *C. difficile* infection process was of interest and had to be tested with a corresponding *rnfC* mutant strain in a mouse model. Obtained results should provide detailed insights into the dynamic protein-protein interaction underlying a central energy metabolic process of the gut pathogen *C. difficile*.

3 Materials and methods

3.1 Materials

3.1.1 Equipment

The equipment used for this work is listed in Table 1.

Table 1: Used equipment

INSTRUMENT	MODEL	COMPANY
Agarose gel documentation system	CoolSnap™ HQ2 Photometrics	Decon Science Tec GmbH (Hohengandern, Germany)
Agarose gel electrophoresis	Mini-Sub Cell GT Cell Wide Mini-Sub Cell GT Cell	Bio-Rad Laboratories GmbH (Feldkirchen, Germany)
Anaerobic chamber		Coy Laboratory Products inc. (Michigan, USA)
Anaerobic system		Voltcraft
Autoclave	LVSA 50/70	ZIRBUS technology GmbH (Bad Grund, Germany)
Bioanalyzer	Agilent 2100 Bioanalyzer Instrument	Agilent Technologies (Santa Clara, USA)
Blotter	Tetra Blotting Module	Bio-Rad Laboratories GmbH (Feldkirchen, Germany)
Centrifuges	Avanti® J-26XP Centrifuge with the rotor: JLA 8.100	Beckman Coulter GmbH (Krefeld, Germany)
	Megafuge 1.0R	Heraeus Holding GmbH (Hanau, Germany)
	MiniSpin	Eppendorf AG (Hamburg, Germany)
	Optima®L-90K Ultrazentrifuge, Rotor: TI 70.1	Beckman Coulter GmbH (Krefeld, Germany)
Cool sputter coater	SCD 500 (SEM preparation)	BAL-TEC AG (Balzers, Liechtenstein)

Critical Point Dryer and coating rate measuring device	CPD 030 (SEM preparation)	BAL-TEC AG (Balzers, Liechtenstein)
Electrophoresis apparatus (SDS-PAGE)	MiniProteanIII™	Bio-Rad Laboratories GmbH (Feldkirchen, Germany)
FastPrep®	FastPrep®-24	MP Biomedicals™ Germany GmbH (Eschwege, Germany)
Field emission scanning electron microscope	Merlin With Everhart Thornley HESE2 detector and the inlens SE detector in a 25:75 ratio with an acceleration voltage of 5 kV	Carl Zeiss Microscopy GmbH (Jena, Germany)
Fluorescence Spectrometer	FP-8500	JASCO Deutschland GmbH (Pfungstadt, Germany)
GC-MSD system and multi-omics equipment	Agilent GC-MSD system (7890B coupled to a 5977 GC) equipped with a high-efficiency source (HES) and an Agilent VF-5ms column / PAL RTC system (CTC Analytics AG; Zwingen, Switzerland) (Seperationsystem: Agilent VF-WAXms column (0.25 mm 30 m)	Agilent Technologies (Santa Clara, USA)
HPLC system and multi-omic equipment	Agilent 1260 Infinity II HPLC system equipped with a FLD and an Agilent Poroshell HPH-C18 column (4.6 mm x 100 mm, particle size 2.7 mm)	Agilent Technologies (Santa Clara, USA)
LC-MS/MS instruments	Dionex™ UltiMate™ 3000 n-RSLC system connected to an Orbitrap Fusion™ Tribrid™ mass spectrometer ESI Orbitrap Fusion; (Separation: C18 precolumn (3 µm RP18 beads, Acclaim, 0.075 mm × 20 mm) and C18 analytical column (3 mm, Acclaim PepMap RSLC, 0.075 mm × 50 cm, USA)); the effluent was electro-sprayed by a stainless-steel emitter	Thermo Fisher Scientific (Waltham, USA)

LC-QTOF system and multi-omic equipment	Agilent LC-QTOF system (6545 coupled to a 1290 Infinity II UHPLC) equipped with an electrospray interface (Seperation: C18 analytical column (Gemini® 2.0 x 150 mm, particle size 3 mm; Phenomenex®)	Agilent Technologies (Santa Clara, USA)
Microplate reader	Infinite® 200 Serial number: 906000759	Tecan Group Ltd. (Männedorf, Switzerland)
Photometer	Ultrospec 10 Cell Density Meter	Amersham Biosciences
Power supply electrophorese	PowerPac™ Basic Power Supply	Bio-Rad Laboratories GmbH (Feldkirchen, Germany)
Software	Bowtie2 v 2.3.4	(Langmead and Salzberg 2012)
	DNA2.0 - Design and Synthesis	ATUM (California, USA)
	Chromeleon™ software Version 6.8, Thermo Scientific™ Dionex™	Thermo Fisher Scientific (Waltham; MA, USA)
	MS Excel®	Microsoft® Corporation (Washington, USA)
	Prism (version 8.4.3)	GraphPad
	Proteome Discoverer 2.2/2.3	Thermo Fisher Scientific (Schwerte, Germany)
	Peaks® X+	Bioinformatics Solutions Inc. (Waterloo, Canada)
	Rockhopper version 2.03 (available at http://cs.wellesley.edu/~btjaden/Rockhopper)	(McClure *et al.* 2013; Tjaden 2015)
	SnapGene®	GSL Biotech LLC (San Diego, CA, USA)
	Spectra Manager™ II Software	JASCO Deutschland GmbH (Pfungstadt, Germany)
	Tecan i-control™ 1.11.1.0	Tecan Group Ltd. (Männedorf, Switzerland)

	Xcalibur™ software version 3.0.63	Thermo Fisher Scientific (Waltham; MA, USA)
Qubit	Qubit® 3 fluorometer	Thermo Fisher Scientific – Life Technologies GmbH (Schwerte, Germany)
Shakers	3015 (SDS-PAGE)	Gesellschaft für Labortechnik GmbH (Burgwedel, Germany)
	Infors CH-4103	Infors AG (Bottmingen, Germany)
Transmission Electron Microscope (TEM)	Libra® 120 Plus (WinTEM software)	Carl Zeiss Microscopy GmbH (Jena, Germany)
Thermocycler	ProFlex PCR System	Thermo Fisher Scientific (Schwerte, Germany)
Thermomixer	Thermomixer compact	Eppendorf AG (Hamburg, Germany)
Ultrasonic bath	USR57	Merck KGaA (Darmstadt, Germany)
Vortex	Vortex-Genie 2	Scientific Industries (NY, USA)

3.1.2 Resources

Table 2 shows the consumables used for this work.

Table 2: Resources

RESOURCES	MODEL	COMPANY
Anaerobe flask	Transfusion bottle	Gerresheimer Essen GmbH (Essen, Germany)
Falcon	15 mL 50 mL	Sarstedt AG & Co. KG (Nümbrecht, Germany)
Filter	Filtropur BT50 500 mL Bottle Top Filter	Sarstedt AG & Co. KG (Nümbrecht, Germany)
	No. 83.1826 0.45 µm	Sarstedt AG & Co. KG (Nümbrecht, Germany)

	No. 83.1826.001 0.20 µm	Sarstedt AG & Co. KG (Nümbrecht, Germany)
Cuvettes	Polystyrene 10x4x45 mm	Sarstedt AG & Co. KG (Nümbrecht, Germany)
	Precision cuvettes of Quartz glass SUPRASIL® Typ-Nr. 115F-QS SD 10 mm	Hellma GmbH & Co. KG (Osnabrück, Germany)
Discs	Carbon adhesive (SEM preparation)	Plano GmbH (Wetzlar, Germany)
Glass beads	size 70 – 110 µm	
Hungate tubes	16×125 mm	VWR™ International GmbH (Darmstadt, Germany)
Needle	Sterican® 0.90 x 40 mm	Braun Melsungen AG (Melsungen, Germany)
PVDF Membran	PVDF Western Blotting Membrane 0.45 µm pore size	Carl Roth GmbH + Co. KG (Karlsruhe, Germany)
Pipettes	0.1 - 2.5 µL Research 0.5 - 10 µL Research plus 2 - 20 µL Research plus 10 - 100 µL Research plus 20 - 200 µL Research plus 100 - 1000 µL Research plus 1 - 10 mL Research plus	Eppendorf AG (Hamburg, Germany)
Column material	Strep-Tactin® Superflow high capacity affinity purification	IBA GmbH (Göttingen, Germany)
Whattman Paper	Rotilabo®-Blottingpapiere Size: 0.35 mm	Carl Roth GmbH + Co. KG (Karlsruhe, Germany)
Centrifugal concentrators 10K	Amicon® Ultra -0.5 mL Centrifugal Filter Units (Ultracel® - 10K)	Merck KGaA (Darmstadt, Germany)

3.1.3 Chemicals, enzymes and kits

Table 3 lists the chemicals, enzymes and kits employed in this study. All other chemicals not listed herein were purchased from Fluka, Merck, Roth or Sigma-Aldrich

Table 3: Chemicals, enzymes and kits

	PRODUCT	COMPANY
CHEMICALS	5-aminovalerate	Sigma-Aldrich Chemie GmbH (Taufkirchen, Germany)
	5-bromo-4-chloro-3-indolyl phosphate (BCIP)	Merck KGaA (Darmstadt, Germany)
	Ampicillin	Carl Roth GmbH + Co. KG (Karlsruhe, Germany)
	Brain-Heart-Infusion medium	Carl Roth GmbH + Co. KG (Karlsruhe, Germany)
	Chloramphenicol	Carl Roth GmbH + Co. KG (Karlsruhe, Germany)
	Cystein	Carl Roth GmbH + Co. KG (Karlsruhe, Germany)
	d-Desthiobiotin	IBA GmbH (Göttingen, Germany)
	Dithiothreitol (DTT)	Sigma-Aldrich Chemie GmbH (Taufkirchen, Germany)
	Erythomycin	Carl Roth GmbH + Co. KG (Karlsruhe, Germany)
	Formaldehyde	Carl Roth GmbH + Co. KG (Karlsruhe, Germany)
	Nitrotetrazolium blue (NTB)	Merck KGaA (Darmstadt, Germany)
	Proline	Sigma-Aldrich Chemie GmbH (Taufkirchen, Germany)
	ROTIPHORESE®Gel 30 (37,5:1) Acrylamid solution	Carl Roth GmbH + Co. KG (Karlsruhe, Germany)
	Thiamphenicol	Sigma-Aldrich Chemie GmbH (Taufkirchen, Germany)

	Protease inhibitor tablet: cOmplete Protease Inhibitor Cocktail® EDTA-free, *EASY*pack	Roche Deutschland Holding GmbH (Mannheim, Germany)
	Strep-Tactin® AP conjugate	IBA GmbH (Göttingen, Germany)
	InstantBlue® Protein Stain	Expedeon Ltd (Cambridge, UK)
DNA-LADDER	Quick-Load® Purple 1 kb Plus DNA Ladder (or 1 kb Plus DNA Ladder)	New England Biolabs GmbH (Frankfurt am Main, Germany)
ENZYMES	BamHI-HF® (5`-GGATCC-3`)	New England Biolabs GmbH (Frankfurt am Main, Germany)
	BsaI (5`-GGTCTC(N1) /(N5) -3`)	New England Biolabs GmbH (Frankfurt am Main, Germany)
	BsrGI (5`-TGTACA-3`)	New England Biolabs GmbH (Frankfurt am Main, Germany)
	EcoRI-HF® (5`-GAATTC-3`)	New England Biolabs GmbH (Frankfurt am Main, Germany)
	HindIII (5`-AAGCTT-3`)	New England Biolabs GmbH (Frankfurt am Main, Germany)
	T4 DNA Ligase	New England Biolabs GmbH (Frankfurt am Main, Germany)
	Q5® High-Fidelity DNA Polymerase	New England Biolabs GmbH (Frankfurt am Main, Germany)
COMMERCIAL KITS	Agilent RNA 6000 Pico Kit	Agilent Technologies (Santa Clara, USA)
	CloneJET™ PCR Cloning Kit	Thermo Fisher Scientific (Schwerte, Germany)
	ELISA for the separate detection of *Clostridium difficile* Toxin A OR Toxin B in suspensions	tgcBIOMICS GmbH (Bingen, Germany)
	Gibson Assembly® Cloning Kit	New England Biolabs GmbH (Frankfurt am Main, Germany)
	High Sensitivity DNA Analysis Kit (Bioanalyzer)	Agilent Technologies (Santa Clara, USA)
	Monarch® Plasmid Miniprep Kit	New England Biolabs GmbH (Frankfurt am Main, Germany)

	Monarch® Total RNA Miniprep Kit	New England Biolabs GmbH (Frankfurt am Main, Germany)
	NAD^+/NADH Glo Assay kit	Promega GmbH (Madison, Wisconsin, USA)
	NEBNext® Ultra™ II Directional RNA Library Prep with Sample Purification Beads	New England Biolabs GmbH (Frankfurt am Main, Germany)
	NextSeq 500/550 High Output Kit v2.5 (75 cycles)	Illumina Inc (San Diego, USA)
	QIAprep Spin Miniprep Kit	QIAGEN GmbH (Hilden, Germany)
	QIAquick Gel Extraction Kit	QIAGEN GmbH (Hilden, Germany)
	QIAquick PCR Purification Kit	QIAGEN GmbH (Hilden, Germany)
	Ribo-off rRNA Depletion Kit (Bacteria); Protocol after Absource Diagnostics GmbH (Munich, Germany)	Vazyme Biotech Co. (Nanjing, China)
	RNase-free DNase Set / RNeasy Mini Spin Columns	QIAGEN GmbH (Hilden, Germany)
	VAHTS™ RNA Clean Beads	Absource Diagnostics GmbH (Munich, Germany)
	Qubit® 3 fluorometer Kits	Thermo Fisher Scientific (Schwerte, Germany)
PROTEIN LADDER	PageRuler™ Plus Prestained Protein ladder; 10 to 250 kDa	Thermo Fisher Scientific (Schwerte, Germany)
	PageRuler™ Prestained Protein Ladder, 10 to 180 kDa	Thermo Fisher Scientific (Schwerte, Germany)
POLYCLONALE PEPTIDE ANTIBODIES	PAB against 3 synthetic peptides (15 mer each *): - PrdA PAB-2107 - RnfB PAB-2107 - RnfC PAB-2107	Metabion international AG (Planegg, Germany) / Primm

3.1.4 Strains of bacteria, plasmids and primers

Bacterial strains, plasmids and primers that were used in this work are listed in Table 4 and 5. All primers were purchased from Invitrogen (Thermo Fisher Scientific, Schwerte, Germany).

Table 4: Strains of bacteria and plasmids

	DESCRIPTION/GENOTYPE	SOURCES OF REFERENCES
BACTERIA STRAINS		
Escherichia coli DH10B[1]	*F- mcrA Δ(mrr-hsdRMS-mcrBC) Φ80dlacZΔM15 ΔlacX74 recA1 endA1 araD139Δ(ara, leu) 7697 galU galK-rpsL nupG λ-*	Thermo Fisher Scientific (Schwerte, Germany)
E. coli DH10B pMTL82151*prdA*-strep II	Carries pMTL82151*prdA*-strep II vector; Cm^r	Master thesis Ilka Pusch (2018)
E. coli DH10B pJET1.2®*prdB*-strep II	Carries pJET1.2®*prdB*-strep II vector; Amp^r	This study
E. coli DH10B pMTL82151*prdB*-strep II	Carries pMTL82151*prdB*-strep II vector; Cm^r	This study
E. coli DH10B pJET1.2®*rnfB*-strep II	Carries pJET1.2®*rnfB*-strep II vector; Amp^r	This study
E. coli DH10B pMTL82151*rnfB*-strep II	Carries pMTL82151*rnfB*-strep II vector; Cm^r	This study
E. coli DH10B pMTL82151*rnfC*-strep II	Carries pMTL82151*rnfC*-strep II vector; Cm^r	This study
Escherichia coli ST18[2]	S17 λpirΔ*hemA* (*pro thi hsdR*$^+$ Tp^r Sm^r; chromosome::RP4-2 Tc::Mu-Kan::Tn7/λpir) (DSM 22074)	(Thoma and Schobert 2009)
E. coli ST18 pMTL82151*prdA*-strep II	Carries pMTL82151*prdA*-strep II vector; Cm^r	Master thesis Ilka Pusch (2018)

E. coli ST18 pMTL82151*prdB*-strep II	Carries pMTL82151*prdB*-strep II vector; Cm^r	This study
E. coli ST18 pMTL82151*rnfB*-strep II	Carries pMTL82151*rnfB*-strep II vector; Cm^r	This study
E. coli ST18 pMTL82151*rnfC*-strep II	Carries pMTL82151*rnfC*-strep II vector; Cm^r	This study
Clostridioides difficile 630Δ*erm*[3] (CD630Δ*erm*)	Wildtype, Synonym: *Clostridium difficile,* DSM 28645, α-proteobacteria, ((Hall and O'Toole 1935) Prévot 1938)	(Hussain *et al*. 2005; Lawson *et al.* 2016); DSMZ, Braunschweig
CD630Δ*erm*_ pMTL82151	Carries pMTL82151; Tm^r	This study
C. difficile 630Δ*erm*_ pMTL82151*prdA*-strep II	Carries pMTL82151*prdA*-strep II vector; Tm^r	Master thesis Ilka Pusch (2018)
C. difficile 630Δ*erm*_ pMTL82151*prdB*-strep II	Carries pMTL82151*prdB*-strep-II vector; Tm^r	This study
C. difficile 630Δ*erm*_ pMTL82151*rnfB*-strep II	Carries pMTL82151*rnfB*-strep II vector; Tm^r	This study
C. difficile 630Δ*erm*_ pMTL82151*rnfC*-strep II	Carries pMTL82151*rnfC*-strep II vector; Tm^r	This study
C. difficile 630Δ*erm*:: pMTL007C-E2:316671 (CD630Δ*erm_rnfC* 636/637s::*ermB)*	Group II intron based *C. difficile rnfC* mutant strain; intron 636/637s; ClosTron® technology (Heap *et al.* 2007; Heap *et al.* 2010a; Heap *et al.* 2010b;), *ermB*^{r}	This study
CD630Δ*erm_rnfC* 636/637s::*ermB*_ pMTL82151	Carries pMTL82151 vector; Tm^r	This study

CD630Δ*erm_rnfC* 636/637s::*ermB_* pMTL82151*rnfC*-strep II	Carries pMTL82151*rnfC*-strep II vector; Tm^r	This study
PLASMIDS		
pJET1.2®	size: 2974 bp features: pJET1.2/blunt cloning vector, T7 promoter, rep(pMB1), Amp^r	Thermo Fisher Scientific (Schwerte, Germany)
pJET1.2®*prdB*-strep II	size: 4197 bp *prdB* gene with corresponding natural Rnf promoter sequence (461 bp upstream + 723 bp *prdB* gene of *C. difficile* 630Δ*erm*); Strep-tag®II (24 bp); stop codon TGA (3 bp); restriction sites: BamHI-HF®/EcoRI-HF® (12 bp); cloning strategy: Multiple PCR and CloneJET™ further features: see pJET1.2®	This study
pJET1.2®*rnfB*-strep II	size: 4495 bp *rnfB* gene with corresponding natural Rnf promoter sequence (502 bp upstream + 980 bp *rnfB* gene of *C. difficile* 630Δ*erm*); Strep-tag®II (24 bp); stop codon TGA (3 bp); restriction sites: BamHI-HF®/EcoRI-HF® (12 bp); cloning strategy: Golden-gate cloning (BsaI methode) and CloneJET™ further features: see pJET1.2®	This study
pMTL82151	size: 5254 bp ColE1 + *tra*; *catP* (= Tm^r)*;* pBP1	(Heap *et al.* 2009)/ CHAIN Biotechnplogy Ltd (Nottingham, UK)
pMTL007C-E2:316671	Size: 9034 bp Ori_pBr; traJ_*;M_LtrA_*; MRepH_*; *catP* (= Tm^r)*; ermB;* Term_rrnBT1T2; P_fdx; Cdi_*rnfC* intron 636/637s;ClosTron® system	(Heap *et al.* 2007; Heap *et al.* 2010b) / ATUM (Newark, US)
pMTL82151*prdA*-strep II	size: 7566 bp *prdA* gene with corresponding natural Prd promoter sequence (428 bp upstream) + 1878 bp *prdA* gene of *C. difficile* 630Δ*erm*; Strep-tag®II (24 bp); stop codon TGA (3 bp); cloning strategy: Gibson Assembly® (therefore: overlapping	Master thesis Ilka Pusch (2018)

	end (30 bp)); further features: see pMTL82151	
pMTL82151*prdB*-strep II	size: 6450 bp *prdB* gene with corresponding natural Prd promoter sequence (461 bp upstream) + 723 bp *prdB* gene of *C. difficile* 630Δ*erm*; Strep-tag®II (24 bp); stop codon TGA (3 bp); restriction sites: BamHI-HF®/EcoRI-HF® (12 bp); cloning strategy: T4 Ligation; further features: see pMTL82151	This study
pMTL82151*rnfB*-strep II	size: 6731 bp *rnfB* gene with corresponding natural Rnf promoter sequence (496 bp upstream) + 969 bp *rnfB* gene of *C. difficile* 630Δ*erm*; Strep-tag®II (24 bp); stop codon TGA (3 bp); restriction sites: BamHI-HF®/EcoRI-HF® (12 bp); cloning strategy: T4 Ligation; further features: see pMTL82151	This study
pMTL82151*rnfC*-strep II	size: 6795 bp *rnfC* gene with corresponding natural Rnf promoter sequence (200 bp upstream) + 1335 bp *rnfC* gene of *C. difficile* 630Δ*erm*; Strep-tag®II (24 bp); stop codon TGA (3 bp); cloning strategy: Gibson Assembly® (therefore: overlapping end (30 bp)); further features: see pMTL82151	This study

[1]Host for cloning steps and carrying all of the pMTL shuttle vector; [2]Donor strain in mating experiments and carrying all of the pMTL shuttle vector; [3]Expression strain with the respective pMTL82151 vector and/or without vector as reference strain

Table 5: List of primer

PRIMER	SEQUENCE
CDiff16S_fw	5`-GTGAGCCAGTACAGG-3`
CDiff16S_rev	5`-TTAAGGAGATGTCATTGG-3`
Downstream_prdA_rev	5`-ATAGTCACTCCACCGCCTTT-3`
Erm_fw	5`-CGCTGGCAGCTTAAGCAATTGCTGAATCGA-3`
Erm_rev	5`-AAAACTTACCCGCCATACCACAGATGTTCC-3`
M13_fw	5`-CAGGAAACAGCTATGAC-3`
M13_rev	5`-GTAAAACGACGGCCAGT-3`
NEB_pprdA_fw	5`-ATGACCATGATTACGCACATGACTAAATTTTGA-3`
NEB_pprdA_rev	5`-CGACTCTAGAGGATCTCACTTTTCAAATTG-3`
NEB_pRnfC_for	5`-ATGACCATGATTACGGACTTTAGAAAGCTATATG-3`
NEB_pstrep_rev	5`-ACGTCGACTCTAGAGGATCTCACTTTTCAAATTGT-3`
NEB_strep_rev	5`-TCACTTTTCAAATTGTGGGTGGCTCCATTTCTGAGCAGCTTGCT-3`
pJET1.2_fw	5`-CGACTCACTATAGGGAGAGCGGC-3`
pJET1.2_rev	5`-AAGAACATCGATTTTCCATGGCAG-3`
prdA-strep_rev	5`TCACTTTTCAAATTGTGGGTGGCTCCAGTTTTCGTCTTTTTCGT-3`
prdBFw	5`-ATGAGCCTTACAACAGTACAAGGA-3`
prdBRV	5`-AACGTGAGCTTTATATTCGTA-3`
prdBRV2	5`-GGATCCTCATTTTTCGAACTGCGGGTGGCTCCAAACGTGAGCTTTATATTCGTA-3`
prdBPmFw	5`-GAATTCGACCAATACAAAATAGATGTGTCTAAA-3`
prdBPmRv	5`-CCTTGTACTGTTGTAAGGCTCATAGTATAAAATACCTCCTTACA-3`
RnfC_for	5`GACTTTAGAAAGCTATATGAAAAGGAT-3`
RnfC_rev_ohne_ stop	5`-TTTCTGAGCAGCTTGCT-3`
rnfBFw	5`-ATGGTGATACTTACAGCTGTA-3`
rnfBPmFw	5`-GAATTCGTTTTTGGTCGAATGCTGAAA-3`
rnfBPmRv	5`-TACAGCTGTAAGTATCACCATTGTTTTACCCCCTTATCTATA-3`
rnfBRv	5`-GGTCTCATCCACAAAATTTTAATAGCTTTCTT-3`
rnfBRvStreptagII	5`- GGATCCTCATTTTTCGAACTGCGGGTGGCTCCACAAAATTTTAATAGCTTTCTTTGGA-3`
Seq2_fw	5`-GGAGCTGGTGAAGTACATC-3`
Seq2_rev	5`-AAGGCGATTAAGTTGGGTAA-3`
Seq_prdA_fw	5`-AGATAACGTAGAAGGATACAAAGCAGGAGA-3`
Seq_prdA_rev	5`-TCAACTTTTGGAGCTACTTCTGCTGCTGCA-3`
Upstream_prdA_fw	5`-TCAGGTGCATTTACAGGAGC-3`

3.2 Microbiological methods

3.2.1 Sterilisation

The sterilisation of solutions and media was conducted using heating steam at 121 °C and 1 bar overpressure for 20 min. Heat-sensitive media supplements and solutions were sterilized using sterile filters (SARSTEDT, Nümbrecht, Germany) with a pore size of 0.2 µm and 0.45 µm.

3.2.2 Media and media supplements

Lysogeny broth (LB) complex medium

E. coli DH10b and ST18 strains were cultivated in LB medium (Bertani 1951, 2004). Stated media supplements were added (table 6). For cultivation on agar plates 15 g/L agar was added to the medium.

LB-medium:	Trypton	10 g/L
	Yeast extract	5 g/L
	NaCl	10 g/L

Brain Heart Infusion medium with supplements (BHI(S)):

The commercially available Brain Heart Infusion medium (BHI) supplemented with 10 mL per 1 L medium of a 10 % (w/v) cystein stock solution was used for *C. difficile* 630Δ*erm* strains. For the cultivation on agar plates 15 g/L agar-agar were added separately to the medium. Additionally, commercially available CHROMID® *C. difficile* plates (bioMérieux GmbH, Nürtingen, Germany) were used to grow bacteria for subsequent glycerol stock preservation.

BHI(S):	BHI	37 g/L
	Yeast extract	5 g/L
	Cysteine	0.1 % (v/v)

Clostridium difficile minimal medium (CDMM):

This *C. difficile* specific defined minimal medium (after Neumann-Schaal *et al.* 2015; origin: Cartman and Minton 2010) was used for growth of *C. difficile* for multi-omic experiments. In general, the components were autoclaved. Heat-sensitive substances were sterilized by filtration.

10 x Salt mix:	Na_2HPO_4	50	g/L
	NaH_2PO_4 x H_2O	20	g/L
	KH_2PO_4	9	g/L
	NaCl	9	g/L
5 x Casamino Mix:	Casamino acids	50	g/L
	L-Cystein	2.5	g/L
	L-Tryptophan	0.5	g/L
100 x Trace salts:	$(NH_4)_2SO_4$	4	g/L
	$CaCl_2$ x 2 H_2O	2.6	g/L
	$MgCl_2$ x 6 H_2O	2	g/L
	$MnCl_2$x 4 H_2O	1	g/L
	$CoCl_2$ x 6 H_2O	0.1	g/L
	$NaHSeO_3$	0.015	g/L
500 x Iron:	$FeSO_4$ x 7 H_2O	2	g/L
200 x Vitamins:	D-Biotin (B_7)	0.06	g/L
	Ca-D-pantho-tenate (B_5)	0.2	g/L
	Pyridoxine (B_6)	0.2	g/L
20 x Glucose:	D-Glucose	200	g/L

All components described below correspond to 1 L of the final minimal medium CDMM:

10 x Salt mix:	100	mL
5 x Casamino Mix:	200	mL
100 x Trace salts:	10	mL
500 x Iron:	2	mL
200 x Vitamins:	5	mL
20 x Glucose:	50	mL
MQ dH_2O	633	mL

Media supplements:

Media supplements were prepared as concentrated stock solution with dH_2O or EtOH/MeOH and sterile filtered. The stock solutions were stored at -20 °C. The media supplements were added after heat sterilization of the corresponding medium. The final concentrations are shown in table 6.

Table 6: Final concentrations of media supplements

Media supplement	Stock solution	Final concentration	Bacterial strains
ALA	50 mg/mL in dH_2O	50 µg/mL	*E. coli* ST18
Ampicillin	100 mg/mL in dH_2O	100 µg/mL	*E. coli* strains
Chloramphenicol	34 mg/mL in ethanol	34 µg/mL	*E. coli* strains
Erythromycin	5 mg/mL in ethanol	2.5 µg/mL	*C. difficile* 630Δ*erm*
Thiamphenicol	15 mg/mL in methanol	15 µg/mL	*C. difficile* 630Δ*erm*
Cysteine	10 % (w/v) in dH_2O	0.1 % (v/v)	*C. difficile* 630Δ*erm*

3.2.3 Anaerobisation of solutions

The anaerobisation of sterile BHI(S) medium with supplements was accomplished in transfusion bottles with septum in an anaerobisation system. The apparatus ensures the gas exchange against nitrogen by the 2-minute change between vacuum phase and nitrogen gassing (1 bar). The solutions were anaerobized for 2 h to 4 h depending on the volume.

3.2.4 Determining the cell density

Optical density was measured by a spectrophotometer at a wavelength of 578 nm for *E. coli* and 600 nm for *C. difficile* 630Δ*erm*.

3.2.5 Cultivation of *E. coli* DH10B and *E. coli* ST18 strains

The cultivation of *E. coli* strains in liquid culture was performed by inoculating the bacterial cells from an LB agar plate. Cells were transferred to normally 10 mL fresh LB liquid medium with the specific media supplements and cultivated overnight at 200 rpm and 37 °C. For the cultivation of *E. coli* strains on agar plates, biomass was transferred from a glycerol stock or an overgrown agar plate and transferred onto LB agar plate with specific media supplements. The plates were cultivated overnight at 37 °C.

3.2.6 Cultivation of *C. difficile* 630Δ*erm*

C. difficile 630Δ*erm* cells were transferred from a glycerol stock to a commercial CHROMID® plate (bioMérieux GmbH, Nürtingen, Germany), if necessary, with media supplements and incubated anaerobically at 37°C for 2 - 3 days. Cell biomass was inoculated in anaerobic BHI(S) liquid medium with media supplements and allowed to grow anaerobically at 37°C, for 12 h. Main cultures were inoculated from the preculture with an initial $OD_{600\ nm}$ of 0.05. Afterwards, the main culture was cultivated anaerobically at 37 °C until further use. All of the cultivation steps were conducted in the anaerobic chamber.

3.2.7 Characterization of the growth behavior of *C. difficile* 630Δ*erm*

To determine the growth behavior of the constructed *C. difficile* strains a preculture was prepared as described above. The main culture inoculated likewise and grown in 10 mL BHI(S) in Hungate tubes (VWR™ International GmbH, Darmstadt, Germany). The cultures were measured every hour at an $OD_{600\ nm}$ until the stationary growth phase was achieved (16 - 24 h growth).

3.2.8 Bacteria storage

Glycerol stocks were prepared for long-term storage of bacterial strains. For this purpose, 700 µL were taken from an *E. coli* liquid culture and mixed with 300 µL 80 % (w/v) glycerol under steril conditions. *C. difficile* 630Δ*erm* glycerol stocks were prepared by withdrawing 10 mL of liquid culture and centrifuging at 4`000 rpm for 3 min. The bacterial pellet was resuspended with 800 µL fresh bacterial cells from the liquid culture and then mixed with 200 µL 80 % (w/v) sterile glycerol. Glycerol cultures can be stored at -80 °C.

3.3 Molecular biological methods

3.3.1 Preparation of chemocompetent *E. coli* strains using $CaCl_2$

For the preparation of *E. coli* $CaCl_2$-competent cells a 30 mL preculture was grown overnight in LB at 37°C by 200 rpm. The preculture was used to inoculate 100 mL main culture at an $OD_{578\ nm}$ of 0.05. The culture was further cultivated at 37 °C and 200 rpm to $OD_{578\ nm}$ 0.5 to 0.6. After cell density determination the cells were chilled on ice for 10 min. Cells were harvested at 4 °C by 4`000 x g for 10 min. The cell pellet was resuspended with 10 mL ice-cold $CaCl_2$ buffer and centrifuged again at 4 °C, 4`000 x g for 10 min. Afterwards, the pellet was resuspended in 1 mL $CaCl_2$ buffer. Aliquots of the competent cells were prepared and stored at -80 °C.

$CaCl_2$ buffer		
	$CaCl_2$	100 mM
	Glycerol	10 % (v/v)

3.3.2 Transformation of *E. coli* cells

The transformation of chemocompetent *E. coli* cells (50 µL) with the different constructs was performed by adding 0.2 - 1 µg plasmid DNA or 5 µL of a ligation mixture. Afterwards, the mixture was chilled on ice for 30 min followed by a heat shock for 45 sec at 42 °C. Subsequently, 500 µL fresh LB-medium were added to the sample and incubated at 37 °C by 300 rpm for 1 h. Finally, 50 µL, 150 µL and 250 µL of the transformation mixture were plated onto LB agar plates with the corresponding antibiotic concentration. The plates were incubated overnight at 37 °C.

3.3.3 Transfer of plasmid DNA in *C. difficile* 630Δ*erm* (conjugation)

Plasmid DNA was introduced into the *C. difficile* 630Δ*erm* recipient strains by conjugation employing an aminolevulinic acid auxotrophic *E. coli* donor strain. The protocol used for this is based on Bouillaut *et al.* 2011 with minor modifications.

One mL was taken from an overnight *E. coli* ST18 preculture, centrifuged at 16`000 x g for 5 min and the pellet was washed twice in 500 µl 1x PBS. A further centrifugation step was performed as previously described. The pellet containing the donor cells was transferred into the anaerobic chamber and mixed with the recipient strain at a ratio of 1:5 (recipient : donor). For this purpose, the *E coli* ST18 pellet was resuspended with 200 µl of a *C. difficile* preculture and the bacterial suspension was dropped onto BHI(S) agar

plates with the corresponding media supplements. The conjugation plate was then incubated anaerobically at 37 °C for 6 h. After the incubation step, the visible cell biomass was scraped off and transferred onto a selection plate (in this case BHI(S) with supplements and devoid of ALA to suppress *E. coli* ST18 growth). The selection plates were then incubated anaerobically at 37 °C for 2 - 3 days. The resulting colonies were tested by PCR using the genomic or plasmidial DNA as templates.

10x PBS-Puffer, pH 7.4:	NaCl	137 mM
	KCl	27 mM
	Na_2HPO_4	100 mM
	KH_2PO_4	20 mM
1x PBS-Puffer, pH 7.4:	10 x PBS-Puffer	10 % (v/v)

3.3.4 Isolation of DNA from *C. difficile* 630Δ*erm*

The quick protocol of Bouillaut *et al*. 2011 was slightly modified for the isolation of genomic and plasmidial DNA. The clone of interest was taken from a plate and transferred onto a BHI(S) plate with corresponding supplements. The plate was cultivated overnight anaerobically 37 °C. Abundant material was scrapped off from *C. difficile* 630Δ*erm* overnight grown plate to inoculate a preculture. 2 mL of the preculture was withdrawn and centrifuged at 16`000 x g for 5 min. The pellet was washed twice with 1 mL 1x PBS. Afterwards, the pellet was dissolved in 500 µl dH_2O. Cell disruption was performed in a subsequent heating step. The cell suspension was incubated at 95 °C for 15 min. 2 µL from the cell lysate was used for a specific PCR.

3.3.5 Isolation of RNA from *C. difficile* 630Δ*erm*

The RNA isolation procedures were based on the protocol by Monarch Total RNA Miniprep Kit Protocol (New England Biolabs®, Frankfurt am Main, Germany). Cells were pelleted and mechanical disruption was performed as follows: The harvested cells (1.5 g wet weight) were washed with 1 mL 1x PBS and centrifuged at 16`000 x g, 4 °C for 15 min. Subsequently, the pellets were dissolved in 800 µL 1x Protection Reagent (New England Biolabs®, Frankfurt am Main, Germany) and 0.7 g glass beads were added. The cell disruption was performed by FastPrep®-24 (MP Biomedicals™ Germany GmbH, Eschwege, Germany) in two rounds at 6.5 m/s, 4 °C for 30 s. The separation of cell debris and glass beads was performed by a centrifuging at 16`000 x g, 4 °C for 10 min. The supernatant was treated with RNA lysis buffer (New England Biolabs®, Frankfurt am Main, Germany) in a ratio of 1:1 (v/v) and prepared according to the previously specified

protocol. The RNA was eluted with 50 µL nuclease-free water from the column and the concentration was determined with the Qubit® 3 fluorometer (Thermo Fisher Scientific – Life Technologies GmbH, Schwerte, Germany). The samples were then stored at -80 °C until further usage.

3.3.6 Isolation of plasmid DNA from *E. coli* cells

Plasmid DNA was isolated from *E. coli* cells using the commercially available QIAprep® Spin Miniprep Kit (QIAGEN GmbH, Hilden, Germany) or Monarch® Plasmid Miniprep Kit (New England Biolabs®, Frankfurt am Main, Germany). For this purpose, 8 mL of an *E. coli* liquid culture were prepared and incubated at 37 °C by 200 rpm overnight. Four mL were collected from this culture and centrifuged at 16`000 x g for 3 min at room temperature. The pellet was handled as specified by the manufacturer. The elution of plasmid DNA from the silica membrane was performed with 20 - 30 µL Buffer EB.

3.3.7 Determination of the DNA or RNA concentration by using Qubit® 3 fluorometer

The determination of the DNA or RNA concentration was performed on a Qubit® 3 fluorometer (Life Technologies; Thermo Fisher Scientific, Schwerte, Germany). This method is selective for measuring double-stranded DNA (dsDNA)/single-stranded DNA (ssDNA) in a range of 0.01 - 1000 ng/µL. The Qubit® assay dyes bind selectively to DNA/RNA facilitating fluorescence-based quantification. The procedure was performed according to the specifications of the manufacturers.

3.3.8 Agarose gel electrophoresis

A common molecular biological method for the separation of high molecular nucleic acids is the agarose gel electrophoresis. Various agarose concentrations (0.3 to 2 % (w/v)) can be used for the separation of DNA according to the molecular weight. Routinely, DNA fragments were separated in a 1 % (w/v) agarose gel. The DNA samples were mixed with gel loading dye® (purple (6X), New England Biolabs®, Frankfurt am Main, Germany) and transferred onto the gel. The commercially available length standard e.g. 1 kb Plus DNA Ladder (New England Biolabs®, Frankfurt am Main, Germany) was used for sizing. The samples were separated for 50 min at a voltage of 100 V. Subsequently, the gel was stained with ethidium bromide and the separated fragments were visualized by the agarose gel documentation system at a wavelength of λ=312 nm.

TAE-buffer, pH 8.0:	Tris-acetate EDTA	40 mM 1 mM
Agarose gel:	Agarose in TAE-buffer	1 % (w/v)
Ethidium bromide:	Ethidium bromide in dH_2O	0.1 % (w/v)

3.3.9 Polymerase chain reaction (PCR)

The polymerase chain reaction is a molecular method that allows DNA amplification by applying different temperatures in multiple cycles using specific primers and a thermostable DNA polymerase. This method was used for the verification of a pure culture status of *C. difficile* 630Δ*erm* cultivations, for the amplification of *C. difficile* 630Δ*erm* genes as inserts for specific cloning methods (e.g. Gibson Assembly® Cloning Kit, New England Biolabs®, Frankfurt am Main, Germany) and for the verification of various plasmids. The PCR mixture based on the Q5® High-Fidelity DNA-Polymerase protocol (New England Biolabs®, Frankfurt am Main, Germany) was prepared as shown in table 7 and the PCR program was individually customized to amplify the specific DNA sequence in the Pro Flex PCR System (Thermo Fisher Scientific, Schwerte, Germany).

Table 7: PCR mixture

	Volume per mixture [µL]	**Final concentration**
Template DNA	2	<1000 ng
Primer Forward [10 µM]	1.25	0.5 µM
Primer Reverse [10 µM]	1.25	0.5 µM
5x Q5 Reaction Buffer	5	1x
10 mM dNTPs	0.5	200 µM
Q5 High-Fidelity DNA Polymerase	0.25	0.02 U/µl
dH_2O	14.75	-
Final volume	∑ 25	-

Verification of *C. difficile* 630Δ*erm* pure cultures with the 16S rRNA PCR analysis

To verify the absence of contaminations in *C. difficile* 630Δ*erm* strains, sterile colonies were taken from a grown agar plate and the genomic DNA was isolated (see chapter 3.3.4). 16S rRNA primers were used of *C. difficile* 630Δ*erm* showing a clear band of 800 bp on an agarose gel. The mixture was prepared as referred to in table 7 with the Primer CDiff16S_fw and CDiff16S_rev. The specific PCR program is shown in table 8.

***Table 8: PCR program for the verification of a pure culture of* C. difficile *630Δ*erm**

	Temperature [°C]	Time	Cycles
Initial denaturation	95	3 min	1
Denaturation	95	30 s	30
Annealing	48	1 min	
Elongation	72	1 min	
Final Elongation	72	5 min	1
Hold	4	∞	

3.3.10 Construction of Prd and Rnf bait protein production vectors

The bait genes *prdA*, *prdB*, *rnfB* and *rnfC* from *C. difficile* 630Δ*erm* lacking the stop codon were amplified via PCR. Approximately 200 - 500 bp upstream region of the first gene of the operon was amplified together or separately and subsequently fused to the 5´of each gene. These regions putatively contained the native promoter for each genetic unit. Therfore, a 10 mL *C. difficile* 630Δ*erm* overnight culture was grown and the genomic DNA isolated (see chapter 3.3.4) and used as a template for PCR-amplification (table 7). The primers were designed to suit each fragment amplification and/or different cloning strategies. Additionally, the Strep-tag® II sequence was fused to the C-terminal. After amplification, proper size of the fragments was verified by electrophoresis (see chapter 3.3.8) and finally cloned into the shuttle vector pMTL82151.

Construction of the PrdA and RnfC bait protein production vectors

The bait genes *prdA* (master thesis, Ilka Pusch 2018) and *rnfC* were cloned into the vector pMTL82151 using the cloning strategy of the Gibson Assembly® Cloning Kit (New England Biolabs®, Frankfurt am Main, Germany). For this purpose, the above-mentioned gene amplification and subcloning steps were perfomed with a 15 - 30 bp overhang at the 5`and 3` ends complementary to the shuttle vector pMTL82151. And the Strep-tag® II sequence was fused to the C-terminal. The program and primers in table 9 and 10 were used, respectively. The purified final fragment called *prdA*-strep II with a size of ~2300 bp and *rnfC*-strep II with a size of ~1500 bp.

The concentration of the purified fragments was determined via the Qubit® 3 fluorometer (Thermo Fisher Scientific – Life Technologies GmbH, Schwerte, Germany) (see chapter 3.3.7). Finally, the bait insert was stored until further use at -20 °C.

Table 9: PCR program for* prdA-*strep II (master thesis, Ilka Pusch 2018)

	Temperature [°C]	Time	Cycles
Initial denaturation	95	3 min	1
Denaturation	95	30 s	30
Annealing	57[1] | 65[2] | 59[3]	1 min	
Elongation	72	1 min 45 s[1] | 1min 30 s[2,3]	
Final Elongation	72	5 min	1
Hold	4	∞	

[1]Annealing temperature for the first PCR with the primers Upstream_prdA_fw and Downstream_prdA_rev, [2]Annealing temperature for the second PCR with the primers Upstream_prdA_fw and prdA_Strep_rev [3]Annealing temperature for the third PCR with the primers NEB_pprdA_fw and NEB_pprdA_rev

Table 10: PCR program for* rnfC-*strep II

	Temperature [°C]	Time	Cycles
Initial denaturation	95	3 min	1
Denaturation	95	30 s	30
Annealing	57[1] | 70[2,3]	1 min	
Elongation	72	1 min	
Final Elongation	72	5 min	1
Hold	4	∞	

[1]Annealing temperature for the first PCR with the primer RnfC_for and RnfC_rev_ohne_ stop, [2]Annealing temperature for the second PCR with the primer NEB_pRnfC_for and NEB_strep_rev, [3]Annealing temperature for the third PCR with the primer NEB_pRnfC_for and NEB_pstrep_rev

The construction of the final vector pMTL82151*prdA*-strep II (master thesis, Ilka Pusch 2018) and pMTL82151*rnfC*-strep II was achieved using the Gibson Assembly® Cloning Kit, (New England Biolabs®, Frankfurt am Main, Germany) (figure 11). The above-mentioned purified inserts were further employed for subsequent cloning. Therefore, the target vector pMTL82151 was digested with BamHI® and EcoRI® (New England Biolabs®, Germany) (table 11) and purified with the QIAquick PCR Purification Kit (QIAGEN GmbH, Hilden, Germany). The concentration was determined by using Qubit® 3 fluorometer (Thermo Fisher Scientific – Life Technologies GmbH, Schwerte, Germany). The Gibson Assembly® Mix was prepared in a ratio of approximately 1:3 (vector : insert) and with a minimum concentration of 50 ng of the vector as specified by the Gibson Assembly® Protocol (New England Biolabs®, Frankfurt am Main, Germany) (table 12). Finally, the mix were transformed into *E. coli* DH10b cells (see chapter 3.3.2).

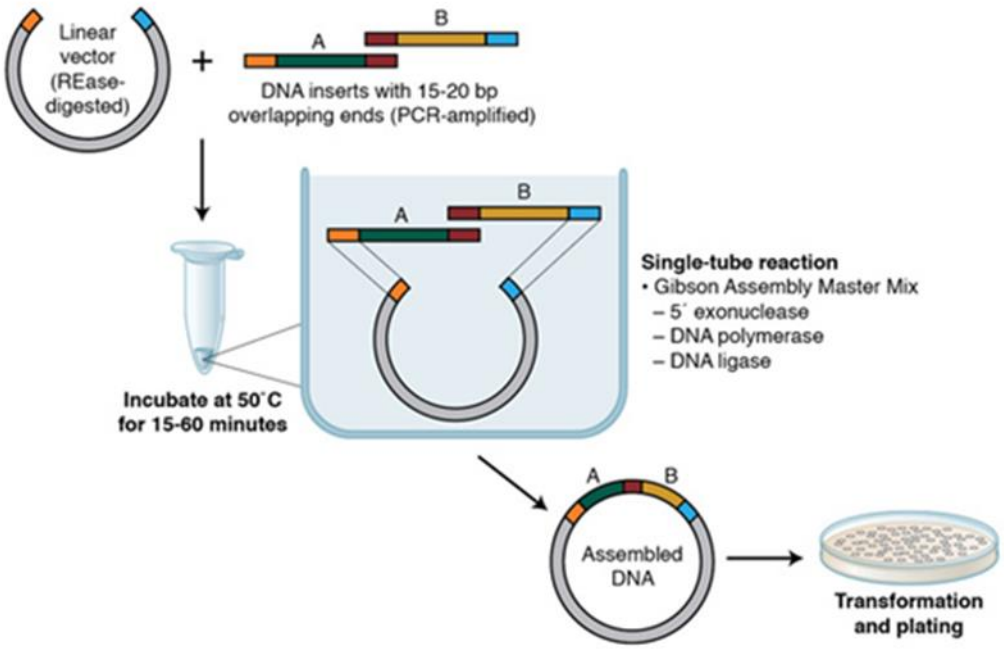

Figure 11: Cloning strategy based on Gibson Assembly® (modified after New England Biolabs®, Frankfurt am Main, Germany). The inserts with the complementary sequence (15 - 20 bp) to the vector ends were used for the Gibson Assembly® approach. Three enzymatic activities in one single reaction step were implemented: a 5' exonuclease activity, DNA polymerase (3`extension activity) and DNA ligase activity (at 50 °C for 15 - 60 min). The exonuclease digests the 5' end sequences to expose a sticky end overhang which is complementary to the vector. The DNA polymerase fills the gaps and a DNA ligase closes the gaps and binds the DNA fragments together.

Table 11: General restriction digestion (modified after New England Biolabs®), 1 h by 37 °C

	Volume per mixture [µL]	Final concentration
Restriction Enzyme	1	10 units
DNA	X	1-2 µg
10X NEBuffer	5	1x
dH_2O	Add to 50	-
Total reaction volume	∑ 50	

Table 12: Gibson Assembly® Mix (modified after New England Biolabs®), 20 min by 50 °C

	Volume per mixture [µL]	Final concentration
Gibson Assembly Master Mix (2X)	10	1x
Vector DNA	X	~ 0.020 pmol
Insert DNA	X	~ 0.060 pmol
dH_2O	Add to 20	-
Total reaction volume	∑ 20	

Clones were transferred from the selective plates into 10 mL LB medium with 34 µg/mL chloramphenicol and were cultivated at 200 rpm, 37 °C overnight. The culture was used to isolate the plasmid which were checked via double digestion using the corresponding enzymes (table 11). Positive clones were also corroborated by DNA sequencing at Eurofins Genomics Germany GmbH (Ebersberg, Germany). For this, the primers Seq2_fw/Seq2_rev and Seq_prdA_fw/Seq_prdA_rev were used. The competent *E. coli* ST18 cells were transformed seperately with the final constructs pMTL82151*prdA*-strep II (master thesis, Ilka Pusch 2018) and pMTL82151*rnfC*-strep II and used for the mating into *C. difficile* 630Δ*erm* (see chapter 3.3.3).

Construction of the PrdB and RnfB bait protein production vectors

The bait genes *prdB* and *rnfB* were amplified and cloned finally into the vector pMTL82151. For this, the amplification of the genes fused to their corresponding promoter sequences and the addition of a C-terminal Strep-tag® II were achieved using separate PCR programs (table 13 and 14).
The Golden Gate method relying on the BsaI restriction was used as a strategy for the cloning of *rnfB*-strep II. The type IIs restriction enzyme BsaI cuts 5 nt upstream its recognition sequence. With the help of this enzyme and the T4 DNA ligase, a simultaneous assembly of several DNA fragments is feasible. The annotated recognition sequence for this enzyme is 5'-GGTCTC(N1)/(N5)-3', which was included within the rnfBRv primer sequence. Afterwards the amplified *rnfB* and the corresponding upstream sequence containing the promoter region were assembled using BsaI. The Strep-tag® II sequence was spliced to the C-terminal of each insert by PCR (table 14). The purified final fragments called *prdB*-strep II (~ 1220 bp) and *rnfB*-strep II (~ 1500 bp) and the concentration was determined on the Qubit® 3 fluorometer (Thermo Fisher Scientific – Life Technologies GmbH, Schwerte, Germany) (see chapter 3.3.7). Afterwards, the bait inserts were stored at -20 °C until further use.

Table 13: PCR program for prdB-strep II

	Temperature [°C]	Time	Cycles
Initial denaturation	95	3 min	1
Denaturation	95	30 s	30
Annealing	53[1,2,3,4]	1 min	
Elongation	72	1 min	
Final Elongation	72	5 min	1
Hold	4	∞	

[1]Annealing temperature for the promoter amplification with the primers prdBPmFw and prdBPmRv, [2]Annealing temperature for the amplification of *prdB* with the primer pair prdBFw and prdBRV, [3]Annealing temperature for the fusion PCR with the primer prdBPmFw and prdBRV; [4]Annealing temperature to add the C-terminal Strep-tag® II with the primer prdBPmFw and prdBRV2

Table 14: PCR program for rnfB-strep II

	Temperature [°C]	Time	Cycles
Initial denaturation	95	3 min	1
Denaturation	95	30 s	30
Annealing	51[1] | 50[2] | 60[3]	1 min	
Elongation	72	1 min	
Final Elongation	72	5 min	1
Hold	4	∞	

[1]Annealing temperature for the promoter amplification using the primer rnfBPmFw and rnfBPmRv, [2]Annealing temperature for amplification of the *rnfB* sequence employing the primers rnfBFw and rnfBRv, [3]Annealing temperature to add the C-terminal Strep-tag® II with the primer rnfBPmFw and rnfBRvStreptagII

The respectively bait insert *prdB*-strep II and *rnfB*-strep II were further transferred into the pJET1.2® as a subcloning step (Thermo Fisher Scientific, Schwerte, Germany). The CloneJET™ PCR Cloning Kit protocol was carried out as specified in the manufacturer´s guidelines. *E. coli* DH10b cells were employed to propagate the plasmids.
The resulting constructs pJET1.2®*prdB*-strep II and pJET1.2®*rnfB*-strep II were digested using BamHI® and EcoRI® (New England Biolabs®, Frankfurt am Main, Germany). The final digested fragments *prdB*-strep II and *rnfB*-strep II were subsequently cloned into the target vector pMTL82151 using the T4 ligase (New England Biolabs®, Frankfurt am Main, Germany). For this purpose, the target vector was also digested with the enzymes BamHI® and EcoRI® (New England Biolabs®, Frankfurt am Main, Germany) (table 11). Afterwards the samples were purified using the QIAquick PCR Purification Kit (QIAGEN GmbH, Hilden, Germany) and the concentration was determined using a Qubit® 3 fluorometer (Thermo Fisher Scientific – Life Technologies GmbH, Schwerte, Germany). The purified fragments were then ligated using the Ligation Protocol with T4 DNA ligase (New England Biolabs®, Germany) (table 15) and finally the ligation mixture was transformed into *E. coli* DH10b cells (see chapter 3.3.2).

Table 15: General Ligation Protocol with T4 DNA Ligase (after New England Biolabs®) at 16 °C

	Volume per mixture [µL]	Final concentration
T4 DNA Ligase Buffer (10X)	2	1x
Vector DNA	X	0.020 pmol
Insert DNA	X	0.060 pmol
T4 DNA Ligase	1	20.000 units
dH_2O	Add to 20	-
Total reaction volume	∑ 20	overnight

Clones were transferred from the selective plates into 10 mL LB medium with 34 µg/mL chloramphenicol or 100 µg/mL ampicillin (depending of the plasmid) and were cultivated by 200 rpm at 37 °C overnight. Afterwards, the culture was used to isolate the

plasmid which were checked via double digestion using the corresponding enzymes (table 11). Positive pJET1.2® clones were used for DNA sequencing at Eurofins Genomics Germany GmbH (Ebersberg, Germany). For this, the primers pJET1.2_fw/pJET1.2_rev were used. The competent *E. coli* ST18 cells were transformed with the final bait protein production vector pMTL82151*prdB*-strep II and pMTL82151*rnfB*-strep II, respectively and used for the mating into *C. difficile* 630Δ*erm* (see chapter 3.3.3).

Confirmation of the constructed *C. difficile* pMTL82151 strains by PCR

The successful mating of *C. difficile* 630Δ*erm* which finally harbors the different bait protein production constructs based of the vector pMTL82151 was PCR confirmed by using the primers M13_fw and M13_rev. The empty vector pMTL82151 was used as a control. After the mating, different clones were picked from the BHI(S) selection plates containing 15 µg/mL thiamphenicol and inoculated in 10 mL fresh supplemented BHI(S) medium. The cultures were grown anaerobically at 37 °C overnight. Two mL of these were taken and the plasmid DNA of *C. difficile* 630Δ*erm* was isolated (see chapter 3.3.4). The PCR master mix was prepared as described in table 7. Additionally, table 16 shows the implemented PCR program. After PCR-amplification the mixture was resolved by agarose gel electrophoresis and the products were visualized (see chapter 3.3.8). A DNA band with the length of 153 bp corresponded to the empty vector pMTL82151 while larger DNA bands matching the expected size of each insert in this vector. The PCR observation confirmed the proper construction of the *C. difficile* 630Δ*erm* recombinant strains.

Table 16: PCR program for the confirmation of recombinant* C. difficile *630Δ*erm *strains

	Temperature [°C]	Time	Cycles
Initial denaturation	95	3 min	1
Denaturation	95	30 s	30
Annealing	50	1 min	
Elongation	72	1 min – 1 min 30 s[1]	
Final Elongation	72	5 min	1
Hold	4	∞	

[1]Elongation time depends on the amplicon product size

3.3.11 Mutagenesis in *C. difficile* 630Δ*erm* using ClosTron® technology

Mutagenesis is a classical tool of genetic research. For directed mutagenesis strategies molecular biology-based approaches are needed. Various molecular biology tools have been developed to mutagenize distinct bacteria in this context. A customized molecular approach for genetic engineering has been developed for *C. difficile* to modify genes in a targeted manner.

The most widely employed genome engineering technique in the Clostridia scientific community is termed ClosTron® (Heap *et al.* 2007, Heap *et al.* 2010a; Kuehne and Minton 2012). In recent years, novel strategies have been explored such as the CRISP-CAS9 system (Wang *et al.* 2018).

In this work the ClosTron® approach was used to mutate the *rnfC* gene, which encodes for a subunit of the Rnf complex. The ClosTron® system is based on an intron puntual mutagenesis strategy, during which the intron integrates specifically into a preselected insertion sequence. Thus, an insertional, but not a knock out mutant are generated. This intron belongs to the mobile group II intron family (Mohr *et al.* 2000). The intron possesses a retrotransposition activated marker (RAM) based on the *ermB* gene. Acquired resistance to erythromycin is used for the selection of clones harboring an intron-based gene disruption (Heap *et al.* 2007; Kuehne and Minton 2012). A commercially synthesized shuttle vector pMTL007C-E2 (Heap *et al.* 2010b), which contains the pre-designed intron targeting sequence and the group II intron is introduced into *C. difficile* 630Δ*erm* by conjugal gene transfer (Heap *et al.* 2007; Heap *et al.* 2010a; Kuehne und Minton 2012). Figure 12 shows the strategy of intron insertion.

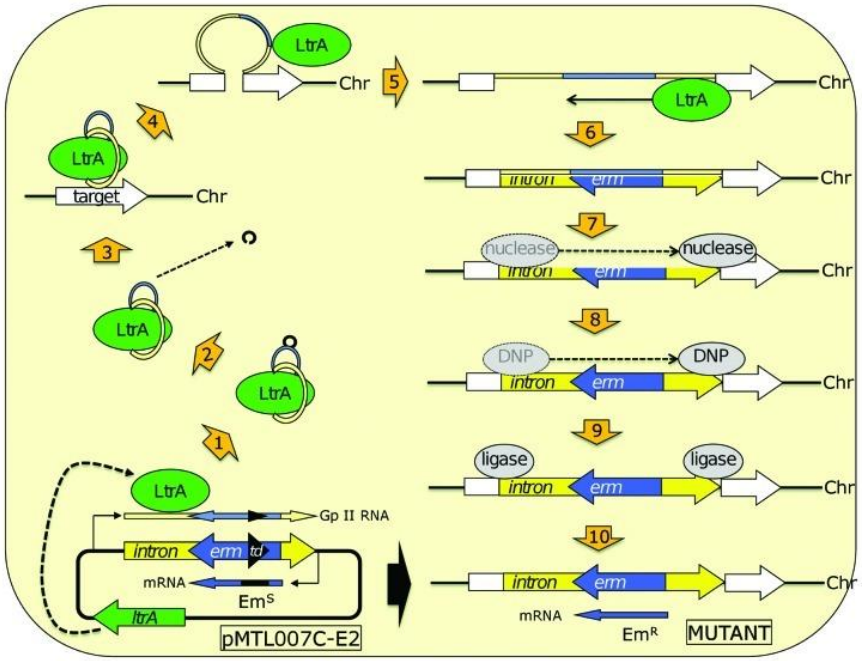

Figure 12: Representation of the ClosTron® technique for the generation of mutants in *C. difficile* (after Kuehne and Minton 2012). The ClosTron® plasmid pMTL007C-E2 (Heap *et al.* 2010b) carrying a group II intron [yellow] with the *td* sequence (own splicing activity) [black] that inactivated *ermB* gene [blue] and the *ltrA* gene [green] is shown. The mRNA transcript of *ermB* contains the *td* intron without an own splicing effect. That mechanism leads to an erythromycin sensivity at first. Next, the transcription of the lagging DNA strand, which includes the group II intron region, is generated and a ribonuclear protein complex [RNP] is formed by the binding of the LtrA protein and the transcript [1], whereby the *td* is now in the correct orientation and the splicing effect is elicited [2]. The complex RNP binds specifically to the target gene within the chromosome [3], and the LtrA cleaves the target region of the chromosome and the RNA can be inserted [4]. LtrA has reverse transcriptase activity and synthesizes the DNA strand [5,6], whereby the nucleases of the host degrade the inserted RNA [7]. A DNA polymerase reconstitutes the complementary strand [8]. Finally, ligases fill the gaps [9,10].

The *rnfC* mutant strain (hereafter termed CD630Δ*erm*_*rnfC*636/637s::*ermB*) was generated by using this system of ClosTron®. The group II intron was designed to be integrated in the middle of the *rnfC* sequence of the wildtype strain *C. difficile* 630Δ*erm*. Using the intron targeting design tool by ClosTron®, the program identified possible intron target sites (Perutka method (Perutka *et al.* 2004)). Based on the algorithm of the exon target site of the *rnfC* sequence (CD630DERM_11370 (KEGG)), the position with the highest score of 8.401 was selected:
636|637s (5`-ATTGAAACGAATAAACCAGATGCTATAGAAGCAATTCAAAATGTA-3`) (digital appendix). Afterwards, the plasmid for mutagenesis on the basis of the vector pMTL007C-E2 was designed and synthesized with the tool DNA2.0 from ATUM (US) (Heap *et al.* 2007; Heap *et al.* 2010a; Heap *et al.* 2010b; Kuehne and Minton 2012). *E. coli* DH10b cells were transformed with the purchased plasmid pMTL007C-E2:316671 (CDi_*rnfC*) and selected on LB with 34 µg/ml chloramphenicol overnight at 37 °C. The plasmid was isolated from the resulting clones and the DNA concentration was determined on a Qubit™ 3 fluorometer (Thermo Fisher Scientific – Life Technologies GmbH, Schwerte Germany). Once the intron targeting sequence (CDi_*rnfC*) was present, the plasmid pMTL007C-E2:316671 (CDi_*rnfC*) was digested with the enzymes BsrGI and HindIII at 37 °C for 1 h. The digested DNA fragment was loaded onto an 1 % agarose gel and checked for presence at ~340 bp DNA fragment lenght. Afterwards, the plasmid was transferred into *E. coli* ST18 cells and finally into the wildtype strain *C. difficile* 630Δ*erm*. Bacteria cells which are carrying the target vector were selected twice onto BHI(S) plates with 15 µg/mL thiamphenicol. Clones were then selected on BHI(S) with 2.5 µg/mL erythromycin to ensure the insertion of the intron. Clones grown on this selection plate were used for DNA isolation. The presence of the insertion of the group II intron was determined by PCR. With that aim, *rnfC* gene specific primers (RnfC_for and RnfC_rev_ohne_stop) were used. The expected lenght of the DNA fragment product was 1535 bp for the intron-free chromosome and 3335 bp when the group II intron (~1800 bp) was integrated within the *rnfC* gene. A second PCR was conducted with erythromycin gene specific primers (Erm_fw and Erm_rev). The PCR product with a lenght of ~1700 bp and ~1500 bp confirmed the intron insertion. The final verification of the proper construction of the *rnfC* mutant strain was carried out by DNA sequencing (Eurofins Genomics Germany GmbH, Ebersberg, Germany) using the amplified DNA fragments containing the intron sequence.

Table 17: PCR program for the control of the group II intron insertion in CD630Δerm

	Temperature [°C]	Time	Cycles
Initial denaturation	95	3 min	1
Denaturation	95	30 s	30
Annealing	55[1] |60[2]| 62[3]	1 min	
Elongation	72	2 min[1] |1 min 30 s[2,3]	
Final elongation	72	5	1
Hold	4	∞	

[1]Conditions for the *rnfC* specific PCR employing the primers RnfC_for and RnfC_rev_ohne_stop; [2]Conditions for the PCR with erythromycin gene and *rnfC* gene primers Erm_fw and RnfC_rev_ohne_stop; expected length of PCR product ~1500 bp; [3]Annealing temperature for the PCR by using erythromycin and *rnfC* specific primers: RnfC_for and Erm_rev; expected length of PCR product ~1700 bp

3.4 Affinity purification coupled with mass spectrometry – Protein production and bait-prey purification

An interactomic approach based of affinity purification coupled with mass spectrometry was used for the identification of *in vivo* protein-protein interactions in *C. difficile* 630Δ*erm* (see chapter 1.4). This method was employed to analyse in depth the interaction partners (preys) of the target proteins (baits). This approach encompassed the genomic part and the interactomic methodology. Figure 13 shows the generic workflow illustrating the process of the method. The host native organism *C. difficile* 630Δ*erm* was chosen as a production strain. Thereby, the naturally occuring interactions were observed without artifacts derived from exogenous proteins. Firstly, the strains were purified in absence of an *in vivo* cross-linker for qualitative analysis of the baits and the determination of a bait-prey interaction. Additionally, formaldehyde-driven *in vivo* cross-linking was carried out to capture transient interactions. The wildtype strain *C. difficile* 630Δ*erm* harboring the empty vector pMTL82151 was included as a background control and subjected to the complete affinity chromatography process to rule out proteins unspecifically binding to the column material.

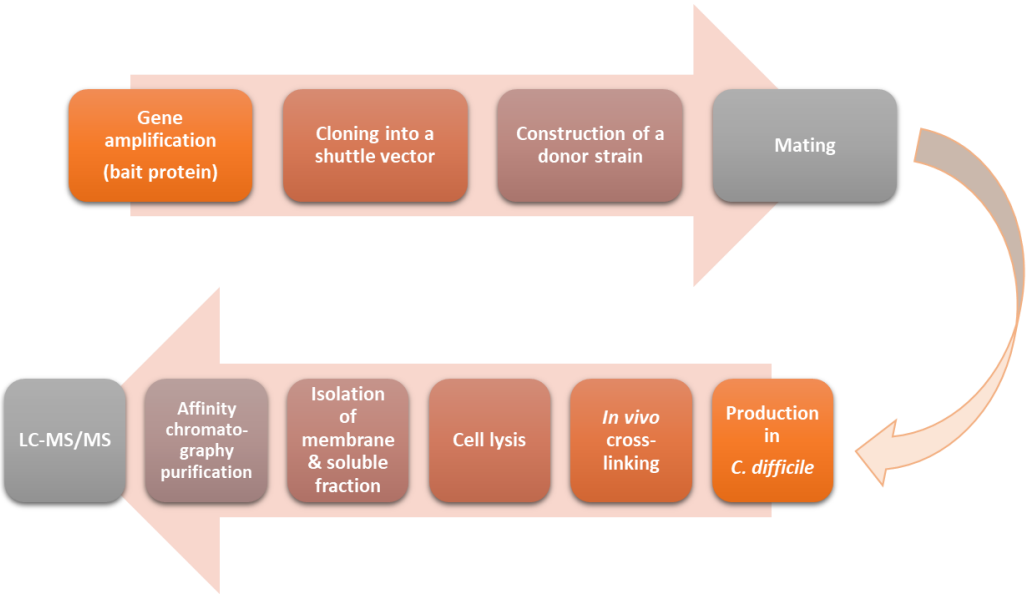

Figure 13: Schematic representation of the interactomic workflow based of affinity chromatography coupled with LC-MS/MS in *C. difficile* 630Δ*erm*. The figure shows stepwise the workflow of the interactomic technique encompassing affinity chromatography coupled with LC-MS/MS. The methods are divided into the sections: the genetic part [upper right arrow] and the the interactomic procedures [below left arrow].

3.4.1 Recombinant bait protein production and cross-linking in *C. difficile* 630Δ*erm*

Strains *C. difficile* 630Δ*erm*_pMTL82151*prdA*-strep II (master thesis, Ilka Pusch 2018), *C. difficile* 630Δ*erm*_pMTL82151*prdB*-strep II, *C. difficile* 630Δ*erm*_pMTL82151*rnfB*-strep II and *C. difficile* 630Δ*erm*_pMTL82151*rnfC*-strep II, and the background control (wildtype harboring the empty plasmid pMTL82151) were grown anaerobically in 40 mL BHI(S) supplemented with 15 µg/mL thiamphenicol at 37 °C for 12 h and used as preculture. The main culture was inoculated to an $OD_{600\ nm}$ of 0.05 in 2 L BHI(S) containing 15 µg/mL thiamphenicol and further grown anaerobically at 37 °C over 12 h. One protein-protein interaction experimental set up included the formaldehyde treatment to accomplish *in vivo* cross-linking ($OD_{600\ nm}$ = 1, addition of 0.156 % cross-linker). After addition of formaldehyde, the cultures were incubated anaerobically at 37 °C for 20 min to allow the cross-linker to penetrate the cell membrane and react with proteins. The reaction was quenched by adding 270 mM glycine and incubating the culture for additional 5 min.

Afterwards, cultures with and without cross-linker treatment were handled similary. Cells were harvested anaerobically at 4 °C, 3`000 x g for 20 min. After that, the cells were washed with 20 mL 1 x PBS and centrifuged again at 4 °C, 3`000 x g for 15 min. Finally, cells were resuspended in 10 mL resuspension buffer.

Resuspension buffer:		
	Tris-HCl, pH 7.5	100 mM
	EDTA	1 mM
	NaCl	150 mM
	DTT	5 mM
	1 tablet protease inhibitor per 10 mL buffer	

3.4.2 Cell disruption and separation of the insoluble and soluble fraction

Cell disruption was accomplished by the FastPrep®-24 (MP Biomedicals™ Germany GmbH, Eschwege, Germany) with in total 12 g glass beads per resuspended cell suspension. The disruption was carried out at 4 °C and 6.5 m/s for 30 s in two cycles. Following by an ultrasonic bath (Merck KGaA, Darmstadt, Germany) treatment for 5 min. The separation of cell debris and spores from the residual cell free extract was achieved by centrifugation at 4 °C, 2`000 x g for 20 min. Subsequent separation of the soluble and insoluble phase of the cell free extracts was performed by ultracentrifugation at 4 °C, 40`000 rpm for 65 min (Optima®L-90K ultracentrifuge, Rotor: TI 70.1, Beckman Coulter GmbH, Krefeld, Germany).

3.4.3 Affinity chromatography of the bait-prey complexes

The soluble fractions of the cell free extract from cultures without the cross-linker formaldehyde containing the tagged baits PrdA, PrdB and RnfC were treated with 300 µL Avidin (2 mg/mL), incubated for 10 min and subjected to the affinity chromatography, respectively. In contrast, the insoluble fraction isolated by ultracentrifugation was used after solubilization for the isolation of the membrane-bound RnfB. For this purpose, 0.3 g insoluble fraction was resolved in 5 ml solubilization buffer containing detergent. The proteins were isolated from the membrane at 4 °C for 1.5 h with gentle rotation. Afterwards, the dissolved membrane associated proteins were separated by further centrifugation at 16`000 x g for 10 min. The following affinity chromatography steps were similar for insoluble and the soluble fractions. The protein complexes were immobilzed on an affinity Strep-Tactin® column (Strep-Tactin® Superflow® high capacity, IBA Lifesciences, Göttingen, Germany) with a column volume of 0.5 mL (for insoluble fractions) and 1 mL (for soluble fractions). The flowthrough was collected and the matrix was washed with 5 x 1 column volume washing buffer and the proteins were eluted from the column with 3 x 1 column volume elution buffer after an incubation of 15 min. The protein concentration was determined on a Qubit™ 3 fluorometer (Thermo Fisher Scientific – Life Technologies GmbH, Schwerte Germany). The eluates were concentrated employing a centrifugal concentrator Amicon® Ultra -0.5 mL centrifugal filter units (Ultracel® -10K) (Merck KGaA, Darmstadt, Germany) according to the recommendations of the supplies. Elution of the protein from the membrane of the centrifugal

concentrator was performed by centrifugation at 2`000 rpm for 2 min. After each fractionation, 40 µL samples were collected and mixed with 15 µL SDS sample buffer and stored at -20 °C (for a gel- based LC-MS/MS measurement).

The bait-prey interactions at the membrane level were stabilized by the presence of the cross-linker formaldehyde. This facilitates the identification of cytosolic transient interacting proteins. For this purpose, all bait proteins (PrdA, PrdB, RnfB and RnfC) strains were treated identically. After the cell fractionation of the cell free extract, 0.3 g of the insoluble fraction was solubilized in 5 mL solubilization buffer for at least 1.5 h with gentle rotation at 4 °C and the proteins were solubilized from the membrane using detergent as previously specified. Two hundred µL samples from the solubilized membranes were analyzed by LC-MS/MS and used as an abundance control for the proteomics approach. The remaining insoluble fraction was strep-tagged affinity chromatoghaphed. For this purpose, 0.5 mL of the Strep-Tactin® matrix (Strep-Tactin® Superflow® high capacity, IBA Lifesciences, Göttingen, Germany) was used. The flowthrough was collected and the column was washed with 5 x 1 column volume washing buffer. The elution of each bait protein was performed by adding 3 x 1 column volume elution buffer to the column and incubated for 15 min. Two hundred µL samples were taken from each eluate for LC-MS/MS analysis. The protein concentration was determined using a Qubit™ 3 fluorometer (Thermo Fisher Scientific – Life Technologies GmbH, Schwerte, Germany). The samples were stored at -80°C until further use.
The remaining eluate was concentrated using a centrifugal concentrator Amicon® Ultra -0.5 mL centrifugal filter units (Ultracel® -10K; Merck KGaA, Darmstadt, Germany) according to the recommendations of the company. A 40 µL sample were taken from the elution fraction and 15 µL SDS sample buffer were added. The SDS samples were stored at -20 °C until further use (e.g. for gel-based LC-MS/MS measurement).

Solubilization buffer (pH 8.0):	K_2HPO_4	18.8 mM
	KH_2PO_4	1.2 mM
	Triton X-100	1.8 % (v/v)
Washing buffer:	Tris-HCl, pH 7.5	100 mM
	EDTA	1 mM
	NaCl	150 mM
	DTT	5 mM
Elution buffer:	Tris-HCl, pH 7.5	100 mM
	EDTA	1 mM
	NaCl	150 mM
	DTT	5 mM
	d-desthiobiotin	2.5 mM

4x SDS sample buffer:	Tris-HCl, pH 6.8	100 mM
	Glycerol	40 % (v/v)
	SDS	110 mM
	ß-Mercaptoethanol	2 mM
	Bromphenol blue	3 mM

3.4.4 Storage and regeneration of the Strep-Tactin® column

After protein purification the column material was washed 5 x 1 column volume with washing buffer and stored in 1 x Haba solution (IBA Lifesciences, Göttingen, Germany) at 4 °C until usage. The column was regenerated with 5 x 1 column volume Strep-wash buffer I and 10 x 1 column volume Strep-wash buffer II. Thereby, the column material was optimally regenerated for next protein purification.

Strep-wash buffer I:	Tris-HCl (pH 10.5)	100 mM
	NaCl	150 mM
	EDTA	1 mM
Strep-wash buffer II:	Tris-HCl (pH 8)	100 mM
	NaCl	150 mM
	EDTA	1 mM

3.4.5 Determination of protein concentration with Qubit® 3 fluorometer

The determination of the protein concentration was performed on a Qubit® 3 fluorometer (Life Technologies; Thermo Fisher Scientific, Schwerte, Germany). The Qubit® assay dyes contained in the kit bind selectively to proteins. Afterwards, a fluorescence-based quantification was performed. The procedure was conducted following the recommendations of the supplies.

3.5 Biochemical methodes for the characterization of protein-protein interactions

3.5.1 Discontinuous SDS-PAGE

The characterization of proteins in terms of their relative molecular masses the sodium dodecyl sulfate polyacrylamide gel electrophoresis (SDS-PAGE) was used. In brief, the proteins were denatured by the SDS detergent and heating, and separated electrophoretically. SDS allows to mask the intrinsic charge of proteins with the negative charge of the detergent and subsequently the separation of the proteins is only dependent on their relative molecular mass. An electrical currency was applied to the gel chamber and the negatively charged „SDS-protein complexes“ moved towards the anode and were separated according to their mass in a polyacrylamide gel. Thereby, larger proteins migrate slower than smaller proteins. The gel consisted of a stacking gel and a separation gel. In the stacking gel the pores of the gel were larger and the ionic intensity lower than in the separation gel, which means that the proteins moved faster. In the interface between both gel types, the ratio of pore size and ionic intensity were inverted and the proteins were concentrated. Subsequently, the proteins were separated according to their molecular masses in the separation gel. Afterwards, migration of proteins was compared to those of a reference marker and the relative molecular masses were inferred.

For SDS-PAGE analysis 40 µL protein samples were mixed with 15 µL 4 x SDS sample buffer and heated up at 95 °C for a maximum of 30 min. The samples were centrifuged at 16`000 x g for 5 min. The proteins were normally separated in a 15 % SDS gel. The electrophoresis was performed for 45 min at a constant amperage of 45 mA per gel. The resulting protein bands were stained using commercially available InstantBlue® Protein Stain (Expedeon Ltd, Cambridge, UK). The gel was treated with the staining solution for 30 min and was destained with water until the individual protein bands became visible. The PageRuler™ (Plus) Prestained Protein Ladder (Thermo Fisher Scientific, Schwerte, Germany) was used as reference marker.

Solutions and buffer for the SDS-PAGE (per gel):

Stacking gel (6 %):	Acrylamide (30 % w/v)	0.5 mL
	0.5 M Tris-HCl, pH 6.8	0.625 mL
	dH_2O	1.375 mL
	Ammonium peroxodisulphate (APS) solution (10 %)	25 µL
	N,N,N',N'-Tetramethyl ethylenediamine (TEMED)	2.5 µL

Separation gel (15 %):	Acrylamide (30 % w/v)	2.5 mL
	1.5 M Tris-HCl, pH 8.8	1.75 mL
	dH_2O	1.75 mL
	Ammonium peroxodisulphate (APS) solution (10 %)	50 µL
	N,N,N',N'-Tetramethyl ethylenediamine (TEMED)	5 µL
Separation gel buffer:	SDS	0.4 % (w/v)
	Tris-HCl, pH 8.8	1.5 M
Stacking gel buffer:	SDS	0.4 % (w/v)
	Tris-HCl, pH 6.8	0.5 M
10 x SDS running buffer:	Glycine	192 mM
	SDS	1 % (w/v)
	Tris-HCl, pH 8.8	50 mM

3.5.2 Detection of bait proteins by Western blot analysis

After the purification of the bait-prey protein complex via affinity chromatography, the presence of each tagged bait protein was analyzed by Western blot analysis. For this purpose, Strep-Tactin® AP conjugate was used to bind to the Strep-tag® II of the bait proteins (Strep-tag® detection in Western blots, IBA GmbH, Göttingen, Germany). As described in the previous chapter, the samples were loaded onto a 15 % SDS-PAGE and the proteins were separated. Afterwards, the SDS-PAGE was incubated for 10 min in blotting-transfer buffer. In parallel a methanol activated PVDF membrane and Whatman paper were incubated for 5 min in the same buffer. The Western blot was built up in a sandwich model in the Tetra Blotting Module (Bio-Rad Laboratories GmbH, Feldkirchen, Germany) and protein transfer towards the PVDF membrane was conducted at 4 °C, 30 V overnight. After blotting, the membrane was treated according to the protocol for the chromogenic detection via an alkaline phosphatase reaction by using Strep-Tactin® AP conjugate (Strep-tag® detection in Western blots, IBA GmbH, Göttingen, Germany).

The Western blot membrane was subsequently blocked with 20 mL TBS-blocking buffer for 60 min and washed for 3 times with 20 mL TBS-Tween buffer. Afterwards, 10 mL TBS-Tween containing 2.5 µL Strep-Tactin® AP conjugate (1:4000) was added to the membrane and incubated over 60 min at room temperature by gently shaking. Next, the Western blot membrane was washed with TBS-Tween buffer followed with TBS buffer and each step was repeated twice. For the development of the chromogenic reaction

the membrane was transfered in 20 mL reaction buffer until the expected protein bands became visible.

Finally, the relative molecular masses of Strep-tag® II recombinant proteins compared to the protein lenght ladder PageRuler™ (Plus) Prestained Protein Ladder (Thermo Fisher Scientific, Schwerte, Germany) were observed on the Western blot membrane.

Blotting-transfer buffer:	Tris-HCl, pH 8.5	25 mM
	Glycine	150 mM
	Methanol	10 % (v/v)
TBS buffer:	Tris-HCl, pH 7.4	50 mM
	NaCl	140 mM
TBS-blocking buffer:	TBS buffer	20 mL
	BSA	3 % (w/v)
	Tween20	0.1 % (v/v)
TBS-Tween buffer:	TBS buffer	20 mL
	Tween20	0.1 % (v/v)
Reaction buffer:	Tris-HCl, pH 8.8	100 mM
	NaCl	100 mM
	MgCl2	5 mM
	7.5 % (w/v) nitrotetrazolium blue in 70 % (v/v) dimethylformamid (NTB solution)	10 µL
	5 % (w/v) 5-bromo-4-chloro-3-indolyl phosphate in dH_2O (BCIP solution)	60 µL

3.5.3 Preparation of gel-based LC-MS/MS samples

The concentrated protein eluates of the tagged baits PrdA, PrdB, RnfB and RnfC were transferred onto a 15 % SDS gel, seperated and stained with InstantBlue® Protein Stain (Expedeon Ltd, Cambridge, UK). After 30 min incubation the reaction was quenched with water. Afterwards, the prominent protein bands were cut out of the gel and prepared for LC-MS/MS analysis.
For this purpose, the gel bands were fixed in a solution with 30 % ethanol and 10 % acetic acid. The InstantBlue® stain was treated with 50 mM ammonium hydrogen carbonate with 30 % acetonitrile until the dye was no longer visible. Finally, 100 % acetonitrile (ACN) was added. Remaining solvent was entirely withdrawn. The samples were further processed for LC-MS/MS by Dr. Josef Wissing and Hedwig Schrader at the Helmholtz Centre for Infection Research (HZI) in Braunschweig (group of Prof. Dr. Lothar Jänsch; Cellular Proteome Research). For that, the gel pieces were dried in a SpeedVac and treated with 5 mM Tris (2-carboxyethyl) phosphine (TCEP) at 56 °C for 30 min, dehydrated in 100 % acetonitrile and rehydrated and with 10 mM methyl methanethiosulfonate (MMTS) containing trypsin (Promega GmbH, Walldorf, Germany) in a 10:1 protein/protease ratio. Afterwards, gel pieces were incubated at 37 °C overnight. Peptides were eluted with a 10 gel volume of H_2O, 0.1 % trifluoroacetic acid (TFA) in 3 % ACN and finally with 0.1 % TFA in 30 % ACN for 2 h at 1`000 rpm and room temperature. The observed supernatants were dried separately in a SpeedVac. The dried peptides were resolubilized with 0.1 %/ 3 % (TFA/ACN) and desalted on a RP18 column and treated with 60 % ACN in 0.1 % TFA for elution. Finally, peptides were dried in a SpeedVac and resolubilized with 0.2 % (TFA)/ 3 % (ACN) and transferred to sample vials for LC-MS/MS measurement.

3.5.4 Preparation of gel-free LC-MS/MS samples

The gel-free LC-MS/MS analysis of the complete 200 µL cross-linked bait-prey complex eluates and a corresponding control of 200 µL of the total insoluble fraction-derived proteins prior the affinity chromatography (see chapter 3.4.3) was performed as follows. The samples were prepared for LC-MS/MS analysis as previously described by Dr. Josef Wissing and Hedwig Schrader at the HZI in Braunschweig (group of Prof. Dr. Lothar Jänsch; Cellular Proteome Research). The protein eluates were incubated for 30 min with 5 mM TCEP at 56 °C. For the reduction and protection of cysteine residues, the solution was treated with 10 mM MMTS for 15 min respectively. Afterwards, protein purification, protein digestion as well as peptide purification for LC-MS/MS measurements were performed according to a slightly adapted „Single-Pot Solid-Phase-enhanced Sample Preparation“ (SP3) protocol (Hughes *et al.* 2014; Sielaff *et al.* 2017).
Sequencing grade trypsin (Promega GmbH, Walldorf, Germany) was added in a ratio of 1:50 (w/w) in 50 mM HEPES, pH 8 and incubated at 37 °C overnight. The beads which harbored the digested peptides were acidified, shaken and incubated overnight at room temperature after raising the ACN concentration to 95 %. The adsorbed peptides were

washed with 100 % ACN and air dried. Finally, peptides were eluted with 20 µl 2 % DMSO for 30 min and afterwards with water for 30 min. The peptides were vacuum dried and dissolved in 0.2 % TFA/3 % ACN for subsequent ultracentrifugation at 50`000 × g, 30 min and room temperature.

3.5.5 LC-MS/MS measurements of gel-based and gel-free samples

The LC-MS/MS measurements of purified and desalted peptides were performed by Dr. Josef Wissing at the HZI in Braunschweig (group of Prof. Dr. Lothar Jänsch; Cellular Proteome Research) on a Dionex™ UltiMate™ 3000 n-RSLC system connected to an Orbitrap Fusion™ Tribrid™ mass spectrometer (Thermo Fisher Scientific™, Waltham, USA). Peptides were loaded onto a C_{18} precolumn and washed for 3 min with a flow rate of 6 µl/min. Afterwards, the samples were separated on a C_{18} analytical column with a flow rate of 200 µl/min over a linear 120 min gradient from 97 % MS buffer A to 25 % MS buffer B and following by a gradient from 25 % MS buffer B to 62 % MS buffer B for 30 min.

The effluent was electro-sprayed by a stainless-steel emitter (Thermo Scientific™, Waltham, USA). The LC system was run with the software Chromeleon™ (Version 6.8, Thermo Scientific™ Dionex™, Waltham, USA) embedded in the Xcalibur™ software suite (version 3.0.63, Thermo Scientific™, Waltham, USA). During the use of Xcalibur™ software, the MS was controlled and operated in a “top speed” mode. Here, that mode allows the automatic selection of many doubly/triply charged peptides (in 3 sec) and a subsequent fragmentation of peptides. The peptide fragmentation was carried out by using the higher energy collisional dissociation mode and peptides were measured in the ion trap (HCD/IT).

MS buffer A:	Formic acid (FA)	0.1 %
MS buffer B:	Formic acid (FA)	0.1 %
	Acetonitrile (ACN)	80 %

3.5.6 Analysis of the LC-MS/MS data

For the *.raw data evaluation of the LC-MS/MS results, the Proteome discoverer™ 2.2/2.3 software (Thermo Fisher Scientific™, Schwerte, Germany) (MMTS fixed; oxidation of methionine: variable modification) was used. The parameters were set to: one missing cleavage and a false positive rate of 1 %. The mass errors were allowed to 7 ppm for MS and 0.4 Da for MS/MS data. The m/z spectra were matched to the FASTA files of the actual UniProt database version of *C. difficile*. The data were processed by Dr. Josef

Wissing at the HZI in Braunschweig (group of Prof. Dr. Lothar Jänsch; Cellular Proteome Research). The list of identified proteins from each sample were further processed with the same program. Only the gel-based bait sample RnfB was analysed with Peaks® X+ (Bioinformatics Solutions Inc., Waterloo, Canada).
Processing of gel-based samples (qualitative analysis of prominent covalent interaction partners) was performed using the proteins present in single gel protein bands. The proteins were sorted and evaluated according to their abundance (three most prominent peaks). Cut-off criterias for exclusion of poorly determined proteins were set to: unique peptides > 2, coverage > 5 % and an abundance > 1E+05. A comparison with the wildtype harboring the empty vector pMTL82151 which served as background control allowed to exclude unspecifically bound proteins from further analysis. This gel-based interactomic approach was carried out for all bait proteins in presence and absence of the cross-linker formaldehyde. The procedure allows to enquire the quality of the bait production and elucidate possible bait-prey interactions.

For the gel-free method the above-mentioned process was performed analogously. The data sets included baits and potential preys. After setting the cut-off criteria (unique peptides ≥ 2 and the coverage ≥ 5 %) the data were exported into MS Excel® (Microsoft® Corporation, Washington, USA). Subsequently, the data were normalized to the same protein concentration of 0.24 mg/mL and enrichment factors were calculated by using the following formula: abundance of protein in eluate/abundance in the control (insoluble fraction overall proteomics). The value indicated the enrichment of proteins after affinity chromatography in comparison to their natural abundance in the cell. The mean value of the enrichment factor was determined from three biological replicates. Proteins absent in one of the three replicates or those having an enrichment factor below 1 were eliminated. Proteins that were not the focus of the study i.e. unrelated to the Stickland fermentation, electron transport or specific energy generation process and possible contaminants from background control were also eliminated until further notice. Proteins which were highly enriched (enrichment factor > 1) in the bait-prey eluates after affinity chromatography were considered as potential interaction partners and were further discussed in the upcoming sections.

3.5.7 Double immunogold labeling detecting by transmission electron microscopy

This method was used to determine co-localization of two proteins and simultaneously analyze their subcellular location (figure 14). For this purpose, commercially generated and purified polyclonal antibodies in combination with protein A coupled to gold particles of different sizes were used. Three-peptide mixtures covering different epitopes of each protein of interest were used to raise specific antibodies. Thus, rabbit polyclonal antibodies specific for the baits PrdA, RnfB and RnfC were produced employing synthetic peptides (15mers*) (digital appendix) by the company Metabion international AG and Primm (Planegg, Germany). The obtained immune sera from rabbits were then purified

by Ina Schleicher at the HZI in Braunschweig (group of Prof. Dr. Manfred Rohde; Central Facility for Microscopy).
A prepared preculture of *C. difficile* 630Δ*erm* was used to inoculate a main culture with an $OD_{600\ nm}$ of 0.05. The main culture was cultivated anaerobically at 37 °C for 12 h. Subsequently, 5 mL of the grown culture were removed and centrifuged at 16`000 x g for 5 min. The cells were fixed with 3 % formaldehyde in 100 mM EM-HEPES buffer and stored at 4° C overnight. Following immunogold labeling experiment steps, TEM images and the semi-quantitative image analyses were performed by Dr. Mathias Müsken and Ina Schleicher at the HZI in Braunschweig (group of Prof. Dr. Manfred Rohde; Central Facility for Microscopy). After the fixation, the samples were exposed to glycine with EM-HEPES buffer for 30 min at room temperature and washed with buffer. Afterwards the samples were dehydrated on ice in EtOH (10 %, 30 % and 50 % steps and >50 % EtOH steps, - 28° C). Subsequently, the samples were infiltrated at - 28 °C onto a K4M resin (K4M:EtOH (1:1, 2:1, 2x 100 %)) and with an incubation times of 8 h respectively overnight. Finally, the samples were polymerized at - 40 °C and suspended to UV light (λ 366 nm) for 30 h, followed by additional 48 h UV light step at room temperature.

EM-HEPES buffer, pH 6.9:	HEPES	100 mM
	Sucrose	90 mM
	$CaCl_2$	10 mM
	$MgCl_2$	10 mM

Prior to labeling, ultrathin sections (70 - 80 nm) were collected on droplets of dH_2O. For this purpose, the sections were overlaid with droplets of 1:20 PBS-diluted antibodies against RnfB, RnfC and PrdA for the single labeling and incubated at 4° C overnight. Following by a series of PBS washing steps (15 s with spray bottle, 3 times droplets of PBS, 5 min each) and a blocking step with 0.1 % skim milk (5 min). Next, protein A-gold (15 nm; 1:75 diluted in PBS supplemented with 0.5 mg/mL PEG20000) was incubated for 30 min at room temperature and the samples were washed with a spray bottle containing PBS with Tween 20 (15 s) as well as 2 times of PBS droplets, 1 x TE droplet and 1 x dH_2O droplet (5 min each). To conduct the second labeling, two labeling steps were performed in series as mentioned above separated by a 30 min incubation time with protein A solution to avoid cross reactions. Both primary antibodies were diluted in a ratio of 1:10 and the incubation time of the second antibody reduced to 3 h. The protein A-gold (10 nm) solution directed against the first antibody was diluted 1:200 and the protein A-gold (15 nm) solution against the second antibody 1:75. All samples were counterstained with 4 % aqueous uranyl acetate for 3 min. Finally, all images were acquired with Libra® 120 Plus (Carl Zeiss Microscopy GmbH, Jena, Germany) at an acceleration voltage of 120 kV and at calibrated magnifications. The contrast, brightness adjustments and size measurements were determined with the WinTEM software.

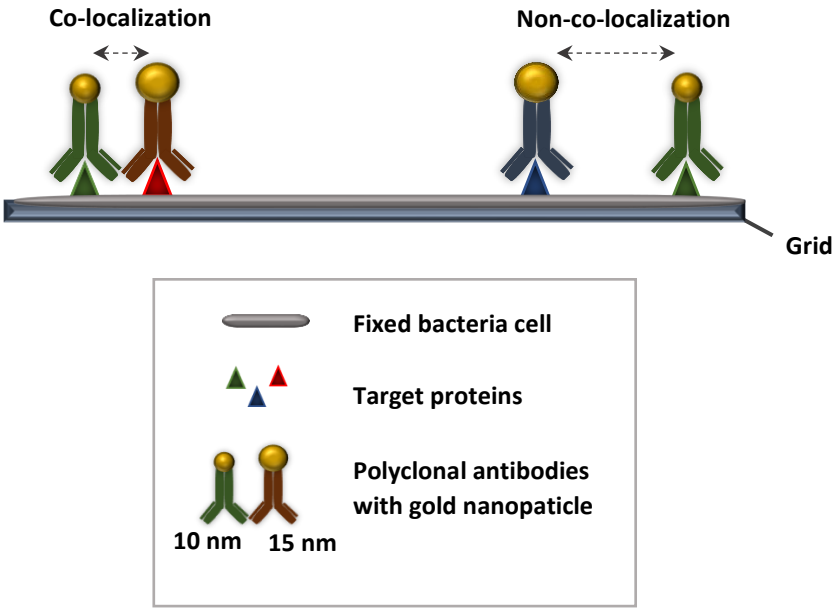

Figure 14: General principle of the immunogold labeling method for the co-localization of two proteins. The so-called double immunogold labeling method to determine the co-localization [left] or non-co-localization [right] of two target proteins [triangle] is shown (here without the protein-A treatment). For this method, purified polyclonal antibodies conjugated with gold nanopaticle of two different sizes [10 nm and 15 nm] against specific epitopes of the bait proteins were used. These antibodies were incubated on ultrathin sections of previously fixed bacterial cells [grey band] and were analyzed using transmission electron microscopy (TEM). A low distance [arrow] of two different size of gold particles indicates a co-localization event of two different target proteins. In comparison, larger distances suggest that both target proteins are not co-localized to each other.

For a semi-quantitative image analysis of single and double labeling events the area of cells in respect to the background (in μm^2) was determined. For this purpose, the cell area was devided into two fractions: cytoplasm 75 % and membrane 25 %. The gold particles were counted in each image and assigned to the three compartments: cytoplasm, membrane and background (for example between cells). For single labeling of PrdA, RnfB and RnfC (gold particle 15 nm), respectively, more than 80 images/label out of 10 image series were averaged out (analyses of mean values of the series were plotted). Double labeling analyses of protein pairs (PrdA and RnfB, RnfB and RnfC, RnfC and PrdA) were performed in three data sets (each combination covered by 21 - 25 images). Co-localization events were counted when a 10 nm and a 15 nm gold particle were in close proximity. The software GraphPad prism (version 8.4.3) was used to plot the data.

3.6 Characterization of the rnfC *mutant strain and multi-omic experiments*

The previously generated *rnfC* mutant strain (CD630Δ*erm_rnfC*636/637s::*ermB)* was employed for further inspection. A holistic multi-omics study encompassing transcriptomics, proteomics and metabolomics was implemented to better characterize the cellular effects resulting from the absence of the Rnf complex. Furthermore, phenotypical characterization of the *rnfC* mutant strain were conducted by electron microscopy, growth behavior experiments, *in vitro* enzymatic assays and toxin quantification.

3.6.1 Growth behavior and phenotypic characterization by scanning electron microscopy

Firstly, the *rnfC* mutant strain CD630Δ*erm_rnfC*636/637s::*ermB* was compared to the wildtype strain in terms of growth behavior and cell morphology. The *rnfC* mutant strain and the wildtype CD630Δ*erm* were grown in BHI(S) and the $OD_{600\ nm}$ was measured hourly to follow the growth of each strain in five biological replicates as descriped in chapter 3.2.7. The bacterial morphology was determined using the scanning electron microscopy (SEM) technique performed by Dr. Mathias Müsken and Ina Schleicher (group of Prof. Dr. Manfred Rohde; Central Facility for Microscopy) at the HZI in Braunschweig.

For this purpose, precultures of the corresponding strain were used (see chapter 3.2.6). As described previously, the main cultures were inoculated to an initial OD_{600nm} of 0.05 and cultivated under anaerobic conditions at 37 °C for 12 h. Bacterial cultures were fixed by addition of fixation solution with a final volume of 2 mL and stored at 4 °C overnight. The cells were washed twice in TE buffer and a 50 µl aliquot added to a round, poly-L-Lysine pretreated coverslip and incubated for 10 min at room temperature. The coverslip was transferred to TE buffer including 1 % (v/v) glutaraldehyde and incubated for an additional 10 min at room temperature and washed twice in TE buffer. The samples were dehydrated on ice with a graded series of acetone (10%, 30%, 50%, 70%, and 90%) for 10 min each, followed, by two steps in 100 % (v/v) acetone at room temperature and subjected to manual critical-point drying with liquid CO_2 (CPD 030, Bal-Tec AG, Balzers, Liechtenstein). The coverslips were mounted onto aluminum stubs with carbon adhesive discs (Plano GmbH, Wetzlar, Germany) and covered with a gold palladium film by sputter coating for 55 sec at 45 mA (SCD 500 Bal-Tec AG, Balzers Liechtenstein). Examination was performed with a field emission scanning electron microscope Zeiss Merlin (Carl Zeiss Microscopy GmbH, Jena, Germany) using the Everhart Thornley HESE2 detector and the inlens SE detector in a 25:75 ratio with an acceleration voltage of 5 kV.

Fixation solution (in HEPES buffer):	Paraformaldehyde	5 % (v/v) f.c.
	Glutaraldehyde	2 % (v/v) f.c.
HEPES buffer, pH 6.9:	HEPES	0.1 % (v/v)
	Sucrose	90 mM
	$CaCl_2$	10 mM
	$MgCl_2$	10 mM
TE buffer, pH 6.9:	TRIS	20 mM
	EDTA	1 mM

3.6.2 Bacteria cell preparation for the D-proline reductase activity assays, NAD^+/NADH ratio determination, toxin ELISA and Omic experiments

Comparative Omic experiments encompassing transcriptomic, proteomic and metabolomic contrasting the wildtype CD630Δ*erm* to the *rnfC* mutant strain CD630Δ*erm*_*rnfC*636/637s::*ermB* were conducted to obtain information about gene regulatory networks and metabolic pathways in the cell, dysfunctional or rewired by missing *rnfC*. With this aim, the *rnfC* mutant strain and wildtype were cultivated in a defined CDMM medium (see chapter 3.2.2). Hundred mL of each preculture were inoculated in CDMM and cultivated anaerobically at 37 °C overnight. The main culture was inoculated to an $OD_{600\,nm}$ of 0.05 in a total volume of 220 mL. Bacteria cells were further cultivated anaerobically at 37 °C until 1/3 of the maximum optical cell density (after ~5 h, exponential growth phase, T1) and the maximum cell density (~14 h, stationary growth phase, T2) of the culture were reached. At these time points the bacterial cells were harvested at 4 °C, 4`000 x g for 10 min. Afterwards, 2 mL were removed from the corresponding supernatant for the measurement of the exometabolome and further 2 mL for the toxin ELISA assay. The bacterial cell pellet from 45 mL of the corresponding culture from T1 and T2 was quenched and washed with 10 ml 50 % MeOH/0,9 % NaCl. After centrifugation at 10`000 x g for 5 min the bacterial cell pellets were frozen in liquid nitrogen for the metabolome experiments. Forty-five mL bacterial culture was pelleted and used for the measurement of CoA-esters. Likewise, 45 mL bacterial culture pellets were employed for transcriptome analyses. Finally, the bacterial cell pellet derived from 15 mL culture was employed for the determination of D-proline reductase activity and the measurement of the NAD^+/NADH ratios. All bacterial cell pellets were frozen in liquid nitrogen and stored at - 80 °C until further measurements. The bacterial cell preperation were performed with Dr. Sabine Will and Dr. Meina Neumann-Schaal (group of Dr. Meina Neumann-Schaal; Bacterial Metabolomics; DSMZ in Braunschweig) at the BRICS in Braunschweig.

3.6.3 Fluorometric assay of the D-proline reductase activity

To elucidate the functionality of the cytosolic enzyme D-proline reductase in the absence of the RnfC subunit of the Rnf complex, an assay based on the fluorometric product detection was performed. Based of the work of Seto 1979 and the dissertation of Kabisch 2001 the fluorometric assay for measuring the production of 5-aminovalerate was slightly modified as follows. One g wet weight of the harvested bacterial cell pellets of the *rnfC* mutant strain and the wildtype from both growth time points (T1 and T2) and of three biological replicates were analyzed. The bacterial cell pelltes were washed with 1 mL 1 x PBS and centrifuged at 4 °C and 3`000 x g for 15 min. The resulting bacterial cell pellets were resuspended with 1.5 mL resuspension buffer (see chapter 3.4.1), 0.5 g glass beads were added to the bacterial cell suspensions and cells were disrupted by using the FastPrep®-24 (MP Biomedicals™ Germany GmbH, Eschwege, Germany). Afterwards, the beads were separated by centrifugation at 4 °C and 16`000 x g for 20 min. The cell free extracts were separated into cytosolic and membrane fractions by ultracentrifugation at 4 °C, 40`000 rpm for 65 min. The total protein concentration of the cytosolic extracts was determined on the Qubit™ 3 fluorometer (Thermo Fisher Scientific – Life Technologies GmbH, Schwerte, Germany) and used to perform the assay.

The enzymatic reaction was started with 5 µg of each cytosolic extract in a given reaction mixture and incubated at 30 °C for 60 min. For the measurements a negative control consisting dH_2O instead of D-proline in the reaction mixture was used. The control samples were prepared identically. The reaction was stopped with 300 µL 5 % (v/v) perchloric acid and the samples were centrifuged at 4 °C, 16`000 x g for 10 min. In parallel, for calibration a standard solution of 20 nM to 80 nM 5-aminovalerate was prepared and dissolved in the reaction buffer. Fifty µL from the supernatant of each sample and in parallel from the 5-aminovalerate standard solution were mixed with 4 mL o-phthaldialdehyde solution and filled into a glass cuvette. Subsequently, the fluorescence was determined using a FP-8500 Fluorescence Spectrometer (JASCO Deutschland GmbH, Pfungstadt, Germany) and the Spectra Manager™ II Software (JASCO Deutschland GmbH, Pfungstadt, Germany). The excitation wavelenght was set at 330 nm (Ex wavelenght) and the fluorescence emission was measured with a scan speed of 200 nm/min from 400 nm until 500 nm. A blank correction with o-phthaldialdehyde solution was prepared.

The data obtained by these measurements were exported as a txt file format. The highest emission peak value was determined around 450 nm. After subtraction of the negative background control from the sample datasets the emissions of the samples showed the normalized relative fluorescence intensity at 450 nm. The concentration of 5-aminovalerate in the sample was determined using the 5-aminovalerate standard. The emzymatic production of 5-aminovalerate observed for the cytosolic extract from CD630Δ*erm_rnfC*636/637s::*ermB* were plotted versus those of CD630Δ*erm* over an assay reaction time of 60 min.

Reaction buffer:	500 mM K_3PO_4	100 µL
	100 mM $MgCl_2$	50 µL
	200 mM DTT	50 µL
	dH_2O	**250 µL**
Reaction mixture:	500 mM K_3PO_4	100 µL
	100 mM $MgCl_2$	50 µL
	200 mM DTT	50 µL
	100 mM D-proline	50 µL
	dH_2O	**Add to 500 µL**
o-phthaldialdehyde solution:	400 mM K_3BO_3-buffer, pH 9.7	100 mL
	ß-mercaptoethanol	0.2 mL
	o-phthaldialdehyde (80 mg/mL EtOH)	1 mL

3.6.4 NAD^+/NADH ratio determination

The *rnfC* mutant CD630Δ*erm_rnfC*636/637s::*ermB* and wildtype CD630Δ*erm* bacteria cells were harvested at the two time points specified in the previous chapter. Five biological replicates were used for the determination of the NAD^+/NADH ratio in the bacterial cells. The ratio was quantified with the NAD^+/NADH Glo Assay kit (Promega GmbH, Madison, USA). For this purpose, the pellets of the bacteria cells were resuspended in 0.6 ml 1 x PBS and transferred into a 2 mL screw cap microtubes harboring 0.4 g glass beads with 0.3 mL chloroform. The samples were thoroughly mixed before being homogenized and disrupted with the FastPrep®-24 (MP Biomedicals™ Germany GmbH, Eschwege, Germany) for three times 30 s using a CoolPrep™ sample holder (MP Biomedicals™ Germany GmbH, Eschwege, Germany). Afterwards, the bacterial cell lysates were centrifuged at 4 °C and 16`000 x g for 10 min. The supernatants were collected and centrifuged again under identically conditions. The assay was conducted using the aqueous phase following company instructions. The luminescence was measured in a white 384 well plate (Greiner AG, Kremsmünster, Austria) after 45 min of incubation at room temperature on a microtiter plate photometer Infinite® M200 (Tecan Group Ltd., Männedorf, Switzerland). The aqueous phase was diluted to match the area of the calibration range (0.01 - 4 µM). All the measurements were performed by Dr. Petra Henke and Dr. Sabine Will (group of Dr. Meina Neumann-Schaal; Bacterial Metabolomics) at the DSMZ in Braunschweig.

3.6.5 Determination of the concentration of the toxins TcdA and TcdB via sandwich ELISA

To determine the concentration of the toxins TcdA and TcdB in the supernatant of the mutant strain CD630Δ*erm*_*rnfC*636/637s::*ermB* and the wildtype CD630Δ*erm* at the outlined two time points in five biological replicates bacteria cells were harvested as described previously. The sandwich ELISA was performed for each bacterial cell sample using a commercially available kit (ELISA for the separate detection of *Clostridium difficile* Toxin A OR Toxin B in suspensions kit; tgcBIOMICS GmbH, Bingen, Germany). In this experiment the samples were used undiluted. Before performing the sandwich ELISA, a standard calibration curve for TcdA and TcdB in the range of 0.31 ng/mL to 40 ng/mL (stock solution of 80 ng/mL TcdA and TcdB included in the kit) was generated by using the including dilution buffer. The sandwich ELISA was performed according to the "Two step protocol" described in the kit´s guidelines.
The sandwich ELISA allows to detect toxins by a colometric reaction step mediated by horseradish peroxidase (HRP). Microtiter plates coated with captured antibodies specific to TcdA and TcdB were provided in the kit. After the immobilization of TcdA or TcdB the second antibody coupled to HRP was added. Addition of the TMB-substrate (3,3',5,5'-tetramethylbenzidine substrate; included in the kit) permitted the enzyme HRP to generate the colorimetrically detectable product.

After quenching the reaction with 50 µL stop solution (included in the kit) ODs at 450 nm and 620 nm (measured twice and averaging out) were measured with the program Tecan i-control™ (Tecan Group Ltd., Männedorf, Switzerland) in a microtiter plate photometer Infinite® 200 (Tecan Group Ltd., Männedorf, Switzerland) to quantify the amount of toxins per sample. Afterwards, the $OD_{450\text{-}620\ nm}$ values were determined (see kit instructions: ELISA for the separate detection of *Clostridium difficile* Toxin A OR Toxin B in suspensions kit; tgcBIOMICS GmbH, Bingen, Germany). Furthermore, the TcdA and TcdB standards were measured and used for a calibration curve (concentration [ng/mL] versus the corresponding $OD_{450\text{-}650\ nm}$). The resulting standard linear equation of both standard controls (concentration area of 0 - 20 ng/mL TcdA or TcdB) were used for the determination of the concentration of the toxins TcdA and TcdB in each sample (see appendix).

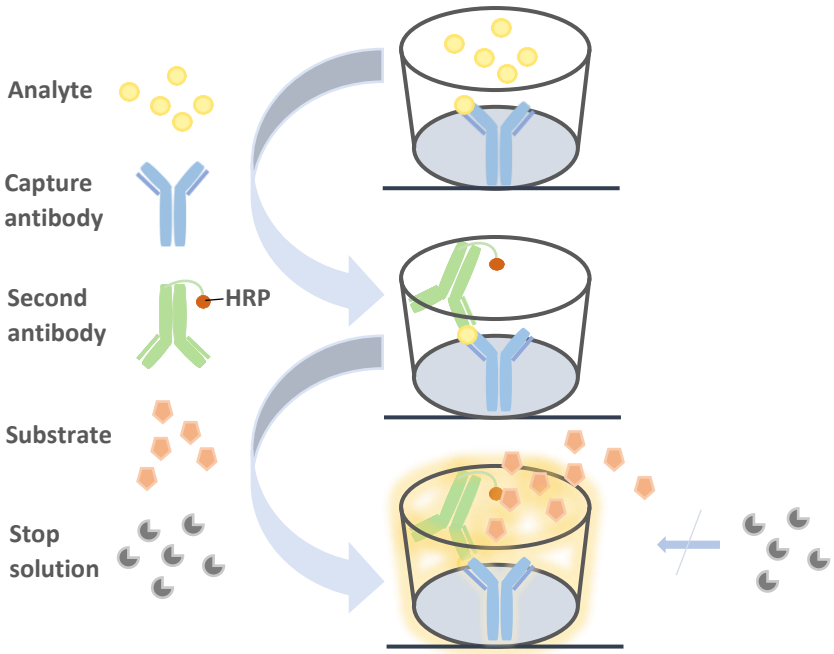

Figure 15: Principle of the colorimetric sandwich ELISA for toxin (TcdA and TcdB) concentration determination. First, a microtiter plate is coated with immobilized antibodies [blue] specifically with affinity to a toxin epitope [yellow]. Next, a sample with analyte molecules was added to the plate and the antibody binds to the toxins. Unbound material was subsequently washed away. Afterwards, the secondary antibody [green], which was coupled with horseradish peroxidase (HRP) [red], was added and binds to the toxin. Unbound secondary antibodies were washed away. Subsequently, the substrate [orange] to drive the chemical reaction of the HRP was added. Color development was occurring in the microtiter plate. The reaction was stopped with the stop solution [grey]. Finally, the extinction at 450 nm (and 620 nm) was photometrically measured.

3.6.6 Multi-omic experiments

GC-MS analysis of polar metabolites

The cell pellets of the *rnfC* mutant strain and the wildtype of five biological replicates were resuspended in 100 µL methanol (with 2 mg/L ribitol) / mg cell dry weight and the extraction was performed as described before (Hofmann *et al.* 2018). Next, for extracellular metabolite measurements, 8 µL of the supernatant were taken and dried with 20 µL methanol (including 8 mg/L ribitol). The metabolome sample preparation, analyses, on an Agilent GC-MSD system (Agilent Technologies, Santa Clara, USA), and data processing were performed by Dr. Sabine Will and Dr. Meina Neumann-Schaal (group of Dr. Meina Neumann-Schaal; Bacterial Metabolomics) at the DSMZ in Braunschweig as described before (Will *et al.* 2019).

GC-MS analysis of volatile compounds

The volatiles were extracted as described in Neumann-Schaal *et al.* 2015. Obtained compounds were identified on an Agilent GC-MSD (Agilent Technologies, Santa Clara, USA) and a PAL RTC system (CTC Analytics AG, Zwingen, Switzerland). The separation was conducted with an Agilent VF-WAXms column (0.25 mm 30 m) as described (Neumann-Schaal *et al.* 2015). The sample preparation, measurement and data processing of five biological replicates were performed by Dr. Sabine Will and Dr. Meina Neumann-Schaal (group of Dr. Meina Neumann-Schaal; Bacterial Metabolomics) at the DSMZ in Braunschweig.

LC-MS analysis of coenzyme A esters

For the analyses of CoA esters frozen cell pellets of the *rnfC* mutant strain and the wildtype were resuspended with 300 µL methanol / 1 mg cell dry weight and 1 mL of the suspension were transfered into 2 mL screw-cap tubes harboring 600 mg glass beads. 250 ng of ^{13}C3-malonyl-CoA was added (internal standard) and the cells were lysed using a FastPrep®-24 classic instrument (here with a CoolPrep™ adapter) (MP Biomedicals™ Germany GmbH, Eschwege, Germany). The extraction of a solid phase was performed as previously described (Wolf *et al.* 2016; Hofmann *et al.* 2018). Next, CoA-derivatives were measured on an Agilent LC-QTOF system (Agilent Technologies, Santa Clara, USA). Afterwards, the separation was carried out on a C_{18} analytical column (Gemini® 2.0 x 150 mm, particle size 3 mm; Phenomenex®) as described (Wolf *et al.* 2016). Here, the sample preparation, measurement and data processing of five biological replicates were performed by Dr. Meina Neumann-Schaal and Dr. Sabine Will (group of Dr. Meina Neumann-Schaal; Bacterial Metabolomics) at the DSMZ in Braunschweig.

HPLC analysis of amino acids

The amino acids were determined using an Agilent 1260 Infinity II HPLC system (Agilent Technologies, Santa Clara, USA). The sample preparations and the HPLC analyses were based on the protocol described in Trautwein *et al.* 2016; Dannheim *et al.* 2017; Hofmann *et al.* 2018 and with a sodium acetate concentration of 25 mM. The sample preparation/measurement of five biological replicates was performed by Dr. Meina Neumann-Schaal as well as Dr. Sabine Will (group of Dr. Meina Neumann-Schaal; Bacterial Metabolomics) at the DSMZ in Braunschweig.

Transcriptomics and proteomics analyses

The harvested *rnfC* mutant cultures CD630Δ*erm_rnfC*636/637s::*ermB* and wildtype cultures CD630Δ*erm* at the two time points T1 and T2 were placed at 4 °C overnight. The RNA isolation was performed after the protocol of the Monarch Total RNA Miniprep Kit Protocol (New England Biolabs®, Frankfurt am Main, Germany) (see chapter 3.3.5).

The RNA/DNA ratios were determined with the Qubit® 3 fluorometer (Life Technologies; Thermo Fisher Scientific, Schwerte, Germany). The rRNA depletion was performed with the Ribo-off rRNA depletion kit (Bacteria) (Vazyme Biotech Co., Nanjing, China) followed by the Absource protocol (Absource Diagnostics GmbH, Munich, Germany) using 1 - 5 µg RNA. The residual DNA was removed with an RNase-free DNase Set and the RNeasy Mini Spin Columns (QIAGEN GmbH, Hilden, Germany) (modification: elution step in 2 times of centrifugation of 15 µl). The quantity and quality post-depletion of the RNA was determined on an Agilent 2100 Bioanalyzer with the kit Agilent RNA 6000 Pico (Agilent Technologies, Santa Clara, USA). Afterwards, the cDNA libraries were produced with the NEBNext® Ultra™ II Directional RNA Library Prep Kit with Sample Purification Beads (New England Biolabs GmbH, Frankfurt am Main, Germany) following the instructions of the manufacturers for a purified mRNA / rRNA depleted input RNA. Here, the PCR enrichment of adaptor ligated DNA (7 cycles) and an RNA fragmentation time of 7 min were used. The following PCR reaction purification step was performed with the kit containing beads and qualities as assessed on the Bioanalyzer with the High Sensitivity DNA Analysis Kit (Agilent Technologies, Santa Clara, USA). Finally, the transcriptome RNA sequencing was performed on the Illumina NextSeq system using the NextSeq 500/550 High Output Kit v2.5 (75 cycles) (Illumina Inc, San Diego, USA).
After RNA isolation the further RNA preparation and processing and RNA sequencing of five biological replicates for transciptomics were performed by Dr. Petra Henke and Dr. Sabine Will (group of Dr. Meina Neumann-Schaal; Bacterial Metabolomics) at the DSMZ in Braunschweig.

To map the rRNA sequences the software Bowtie2 v 2.3.4 (Langmead and Salzberg 2012) was applied and rRNA sequences were removed from the data of total RNA transcriptome. Afterwards, the Rockhopper software version 2.03 (McClure *et al.* 2013; Tjaden 2015) was used for mapping the reads to the archived *Peptoclostridium difficile* 630 reference genome. Here the following parameter settings were used: reverse complement reads, strand specific and verbose output mapped. The transcriptome data was analysed with expression values of each transcript (reported by Rockhopper). After that, the mean value of the gene expression values and the corresponding false discovery rate as the q-value of five replicates were calculated (see digital appendix). Based on that calculation the log2 fold change values of the *rnfC* mutant strain against the wildtype at the time points T1 and T2 were determined. These analyses were performed by Dr. Petra Henke (group of Dr. Meina Neumann-Schaal; Bacterial Metabolomics, DSMZ).

The samples for proteomic analyses of the *rnfC* mutant strain in comparison to the wildtype in T1 (exponentielle growth phase) and T2 (stationary growth phase) were prepared according to the gel-free LC-MS/MS measurement protocol (see chapter 3.5.4, 3.5.5) by Dr. Josef Wissing and Hedwig Schrader at the HZI in Braunschweig (group of Prof. Dr. Lothar Jänsch; Cellular Proteome Research). For this purpose, the cell-free extacts (soluble fraction) of three biological replicates were used for that approach after ultracentrifugation of the samples prepared using the similar protocol of protein purification outlined before (see chapter 3.4.2).

3.7 In vivo *characterization of the rnfC mutant strain*

Comparative mouse infection experiments with the *rnfC* mutant and wildtype strain were performed to gain further insights into the consequences of the *rnfC* gene deletion on adaptation to a host intestinal environment *in vivo*.

3.7.1 Mice infection experiments with *C. difficile* 630Δ*erm*

To analyse the behavior of the *rnfC* mutant strain CD630Δ*erm*_*rnfC*636/637s::*ermB* in a mouse model spore suspensions were prepared from the respective strains CD630Δ*erm*_*rnfC*636/637s::*ermB*_pMTL82151(*rnfC*-mutant), CD630Δ*erm*_*rnfC*636/637s::*ermB*_pMTL82151*rnfC*-strep II (complemented strain) and CD630Δ*erm*_pMTL82151 (wildtype). Therefore, commercially available CHROMID® *C. difficile* plate of bioMérieux GmbH (Nürtingen, Germany) were used for an anaerobically cultivation of the strains at 37 °C for 2 - 3 days. The fresh cultures were used to prepare spore suspensions of the *C. difficile* 630Δ*erm* strains which were used for mouse infection. The mouse wildtype (WTBL/6-SPF1) line from the HZI in Braunschweig was used under the specific pathogen free conditions (SPF).
All animal experiments, e.g. mice infection and organ sampling (colon, cecum and feces), and the preparation of the spore suspension were performed by Dr. Nathiana Smit at the HZI in Braunschweig (group of Prof. Dr. Till Strowig; Microbial Immune Regulation). At that time point all experiments were performed under the strict animal permission of the local government following the protocol of the „Niedersächsisches Landesamt für Verbraucherschutz und Lebensmittelsicherheit “.

The infection is based on single infections of the mice with the one of the mentioned *C. difficile* strains. In additional experiment, mice were co-infected with the *rnfC*-complemented mutant strain and the *rnfC* mutant strain. All the strains were carrying the plasmid pMTL82151 for comparability. The PCR protocol „Confirmation of plasmid DNA“ (see chapter 3.3.10) using the primer M13_fw/M13_rev was determined to reveal the presence of the pMTL82151 plasmid and was therefore used to analyze for the presence of the different strains (haboring pMTL82151 or pMTL82151*rnfC*-strep II (see appendix)) during co-infection in the samples of colon, cecum and feces.

For the *in vivo* experiment, mice were treated with 10 mg/kg clindamycin antibiotic 24 h before infection and infected (oral) with 1000 spores/mice. The behavior of the mice and the body weight were monitored daily. Feces, colon and cecum samples were collected on day 1 (D1) or/and day 3 (D3) after infection. Samples of colon and cecum content were washed with 5 mL 1 x PBS. One mL of the sample was used for elimination the vegetative cells (incubated at 65 °C, 25 min). Spores will survive this heat-treatment and thus only spores will be able to grow out. All samples were homogenized before plating.

Afterwards, heated and non-heated samples were spread on commercially available CLO plates (bioMérieux GmbH, Nürtingen, Germany) added with 0.1 % taurocholate for germination of spores in the heated samples and without taurocholate for vegetative bacteria cells in the non-heated samples. The plates were incubated under anaerobic conditions at 37 °C for 72 h and after that time colony forming units (CFU) of the bacteria were counted and the log CFU of the different single infection samples was determined. After co-infection 100 clones were tested in the above-mentioned PCR to determine the *rnfC*-complemented mutant strain or the *rnfC* mutant strain in the specific organ sample onto the corresponding plates. The infection, sample preparation and determination of the log CFU values were performed by Dr. Nathiana Smit at the HZI in Braunschweig (group of Prof. Dr. Till Strowig; Microbial Immune Regulation).

4 Results

4.1 Identification of protein-protein interactions during Stickland fermentation in C. difficile *630Δ*erm – rationale of the approach

For the identification of protein-protein interactions involved in the Stickland fermentation of the anaerobic bacterium *C. difficile* 630Δ*erm*, protein baits that play an essential role in the reductive part of the fermentation process were selected. These were the subunits PrdA (CD630DERM_32440) and PrdB (CD630DERM_32410) of the cytoplasmic D-proline reductase, and the subunits RnfB (CD630DERM_11420) and RnfC (CD630DERM_11370) of the membrane ferredoxin-NAD^+: oxidoreductase Rnf complex. For a qualitative analysis of the bait protein interaction partners (preys) a combined affinity purification, gel-based separation and LC-MS/MS analyses approach was used (see chapter 3.5.3). The LC-MS/MS measurements and data generation were performed by Dr. Josef Wissing at the HZI in Braunschweig (group of Prof. Dr. Lothar Jänsch; Cellular Proteome Research). The analysis of the generated data was conducted as described in chapter 3.5.5 and 3.5.6.

Firstly, the wildtype genes of the baits PrdA, PrdB, RnfB and RnfC from *C. difficile* 630Δ*erm* and the corresponding promoter sequences were amplified and fused in frame to the target gene to a C-terminal Strep-tag® II encoding DNA sequence for subsequent affinity chromatography purification (see chapter 3.3.9). The resulting DNA-fragments *prdA*-strep II, *prdB*-strep II, *rnfB*-strep II and *rnfC*-strep II were ligated into the shuttle vector pMTL82151 using various cloning strategies (e.g. Gibson assembly or T4 ligation) respectively (see chapter 3.3.10). The resulting constructs harboring the bait genes were finally verified using the DNA sequencing by Eurofins Genomics Germany GmbH (Ebersberg, Germany). The constructs were individually transferred into the wildtype strain *C. difficile* 630Δ*erm* by conjugation employing the *E. coli* ST18 cells harboring the above-mentioned constructs (see chapter 3.3.3). After proper establishment of an interactomic workflow with and without cross-linking treatment (see chapter 3.4) for *C. difficile* 630Δ*erm* the different bait strains and the wildtype harboring the pMTL82151 empty vector as a control were all subjected to worked out procedure to identify appropriate protein interaction partners.

4.1.1 Background control for the used interactomics approach

The cell free extracts of the wildtype strain harboring the cloning vector pMTL82151 (empty vector, control) were chromatographed and served as a quality control to sort out proteins unspecifically bound to the column material. The elution fractions were concentrated with a centrifugal concentrator (Amicon® Ultra -0.5 mL centrifugal filter units (Merck KGaA, Darmstadt, Germany)) and separated on SDS-PAGEs following by a Western blot analyses. After staining the SDS-PAGE all visible proteins were cut out (figure 16) and subjected to LC-MS/MS analysis (see chapter 3.5).

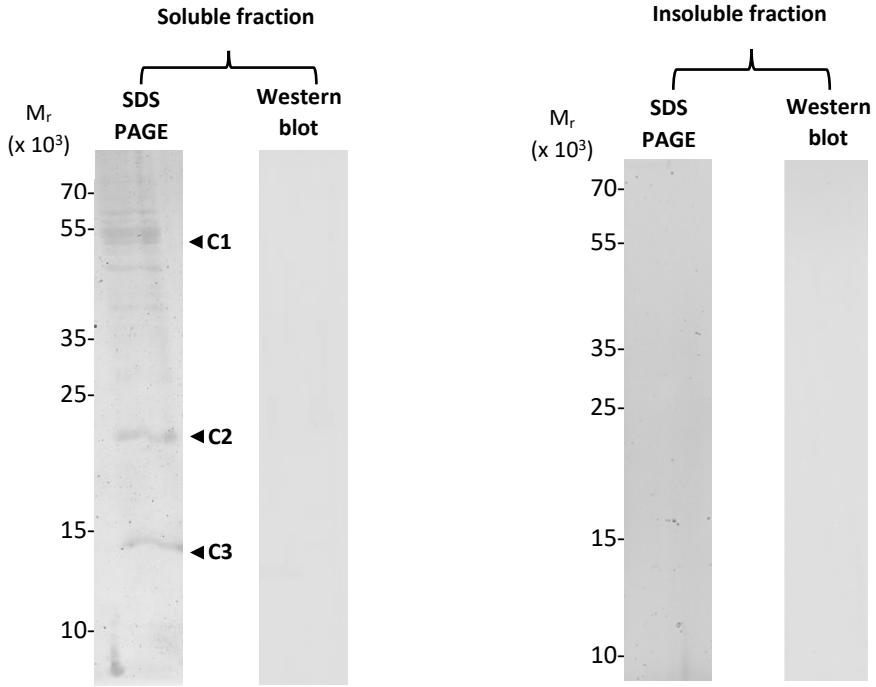

Figure 16: Background control of the interactomics approach. Shown is a stained SDS-PAGE [left lane] and Western blot membrane [right lane] of the affinity chromatography elution fraction of the soluble [left panel] and insoluble fraction [right panel] of the wildtype strain *C. difficile* 630Δ*erm* carrying the empty vector pMTL82151, respectively. The 60-fold (soluble fraction) and 30-fold (insoluble fraction) concentrated elution samples (10 µL) were loaded onto a 15 % SDS-PAGE and separated for 45 min at 45 mA. The SDS-PAGE was stained with InstantBlue® Protein Stain (Expedeon Ltd, Cambridge, UK) solution and the relative molecular masses of absorved proteins were determined using the PageRuler™ Plus Prestained *Protein Ladder* (Thermo Fisher Scientific, Schwerte, Germany). The Western blot analysis was performed with a Strep-Tactin® AP conjugate (IBA GmbH, Göttingen, Germany). The blot development was in general 30 min. Images were grayscaled and the image of the Western blot membranes was taken at 30 % brightness.

The stained SDS-PAGE of the concentrated elution fraction after affinity chromatographic treatment of soluble fraction of all free cell extracts (figure 16, left lane) from the wildtype *C. difficile* 630Δ*erm* pMTL82151 (empty vector, control) revealed proteins of different relative molecular masses. Three major bands with proteins were observed at the relative molecular mass (M_r) of 15.000, 22.000 and 55.000. Importantly, Strep-Tactin® AP conjugate (Strep-tag® detection in Western blots, IBA GmbH, Göttingen, Germany) failed to detect any protein (figure 16, right lane). Nevertheless, the three prominent protein bands found in the SDS-PAGE were cut-out (figure 16, C1-C3) and analyzed by LC-MS/MS. In the average 145 different proteins were found with the highly sensitive LC-MS/MS technique. Unique peptides > 2, an abundance > 1E+05 and a protein coverage > 5 % were the settings used for the analyses with the software Proteome discoverer™ 2.2/2.3 (Thermo Fisher Scientific, Schwerte, Germany) to filter out not securely identified proteins or measurement-derived artifacts. After applying the above-mentioned settings most of the identified contaminants were 30S/50S ribosomal protein, chaperones, aminotransferases, peptidase or elongation factors (see digital appendix). Beside the mentioned contaminats the most present proteins of 56 proteins in the bands C1-C3 are shown in table 26 in the appendix. Consequently, these proteins were excluded from the following interactome analyses.

4.1.2 Interaction partners of the D-proline reductase subunits PrdA and PrdB in the absence of the cross-linker formaldehyde

After the determination of the unspecific binding capacity of the employed Strep-Tactin® affinity chromatography material, first bait-prey experiments for determination of the interaction partners of the D-proline reductase subunits PrdA and PrdB were performed. For this purpose, the soluble fraction from a cell free extract obtained from *C. difficile* cells without cross-linker treatment were affinity chromatographed using the C-terminal Strep-tag® II of the bait protein. The concentrated elution fraction was analyzed by SDS-PAGE and Western blotting using Strep-Tactin® AP conjugate for bait visualization (figure 17). The cut-out visible proteins were subjected to LC-MS/MS analyses.

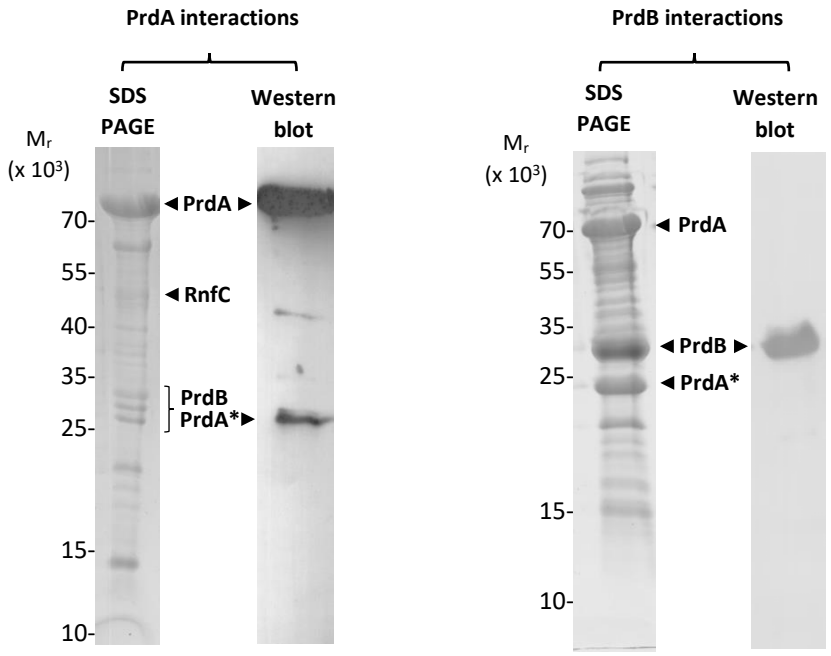

Figure 17: Interaction partners of the D-proline reductase subunits PrdA and PrdB without the cross-linker formaldehyde treatment. The stained SDS-PAGE [left lane] and Western blot analysis [right lane] of the PrdA [left panel] and PrdB [right panel] interaction partner after affinity chromatographic purification. The bait proteins PrdA and PrdB were recombinantly produced in *C. difficile* 630Δ*erm* without treatment of the cross-linking agent formaldehyde, respectively. The soluble fraction of cell free extracts containing the Strep-tagged proteins were chromatographed through the Strep-Tactin® affinity column. Formed bait-prey complexes were eluted and 10 µL of the 60-fold concentrated elution fraction were loaded onto a 15 % SDS-PAGE and separated according to their relative molecular mass with 45 mA for 45 min. The gel was stained with InstantBlue® Protein Stain (Expedeon Ltd, Cambridge, UK) solution. The relative molecular masses were deduced from the PageRuler™ (Plus) Prestained *Protein Ladder* (Thermo Fisher Scientific, Schwerte, Germany). For the Western blot analysis, the bait protein was detected via Strep-Tactin® AP conjugate (IBA GmbH, Göttingen, Germany). The blot development was in general 15 - 30 min. Image quality was improved by colorizing all images in grayscale and setting the image of the Western blot of PrdB to a brightness of 30 % to avoid background noise. The PrdA encoding plasmid was constructed by Ilka Pusch during her master thesis.

Several protein bands were observed for the elution fractions. During the analysis of the PrdA interaction partners an intensive protein band became visible at the relative molecular mass of ~70.000 on the SDS-PAGE (figure 17, left panel). The corresponding Western blot loaded with the identical sample as the SDS-PAGE revealed for the chromogenic detection of the Strep-tag® II using Strep-Tactin® AP conjugate (IBA GmbH, Göttingen, Germany) three protein bands with a relative molecular mass of ~70.000, ~40.000 and ~25.000 (figure 17, left panel, right lane). After cutting out the visible proteins out of the SDS-PAGE (∑ 15 bands) and preparing them according to the gel-based LC-MS/MS analysis protocol, in total 188 proteins were found. The mass spectrometry settings for the identification of the analyzed proteins were unique peptides > 2, an abundance > 1E+05 and a protein coverage > 5 % enabled with the software Proteome

discoverer™ 2.2/2.3 (Thermo Fisher Scientific, Schwerte, Germany). Next, proteins that are highly abundant in the cell, such as chaperones, ribosomal proteins or cell wall binding proteins and some column contaminants (see chapter 4.1.1 and 4.1.6) were excluded. Overall, 32 PrdA bound proteins were determined (original protein list see digital appendix). Firstly, with its relative molecular mass of ~70.000 this way the bait protein **PrdA** (M_r 68.000), a subunit of the D-proline reductase from *C. difficile* 630*Δerm,* was identified. In agreement, the Western blot also identified this protein band as the Strep-tagged bait PrdA. A significant amount of PrdA (**PrdA***) was also detected in the M_r of ~25.000 protein band. This PrdA fragment is the product of a proteolytic cleaving of the major PrdA subunit into two different sized subunit fragments (M_r 23.000 and 45.000) (Kabisch *et al.* 1999; Jackson *et al.* 2006). The second enzyme subunit **PrdB** (M_r 26.000) was also detected in the identical region of the SDS-PAGE as PrdA* indicating heterodimer formation. Furthermore, the membrane-associated Rnf complex subunit **RnfC** (M_r 48.000) was found in the protein band at an M_r of ~53.000 by gel-based LC-MS/MS.

The stained SDS-PAGE loaded with the concentrated elution fraction of the bait PrdB derived from the soluble fraction of the *C. difficile* 630*Δerm*_pMTL82151*prdB*-strep II strain (figure 17, right panel) showed several protein bands of different relative molecular masses with different band intensities. Three bands at a M_r of ~25.000 to ~30.000 and at ~70.000 were more prominent than the other protein bands. All visible SDS-PAGE protein bands (∑19 bands) were cut-out and analyzed by LC-MS/MS and finally identified with the software Proteome discoverer™ 2.2/2.3 (Thermo Fisher Scientific, Schwerte, Germany). The total number of detected proteins were 855. Afterwards, the same cut-off criteria as mentioned before were used and 128 proteins were observed and closely inspected (original protein list see digital appendix). The protein band between a M_r of ~25.000 and ~30.000 contained the purified bait protein **PrdB** (M_r 26.000) of the D-proline reductase. In agreement, the Western blot analysis showed one single visible band in the range between ~25.000 and ~30.000 (figure 17, right panel, right lane). The protein band at ~70.000 contained **PrdA** (M_r 68.000) and at ~25.000 the **PrdA***. The most prominent mass spectrometry identified interaction partners for the baits were classified according to function and different metabolic classes (table 27). An

overview of these proteins in relation to all four baits and in addition with consideration of a cross-linker treatment is given in the chapter 4.1.6.

4.1.3 Interaction partners of the Rnf complex subunits RnfB and RnfC in absence of the cross-linker formaldehyde

After the determination of the D-proline reductase interactions further bait-prey experiments of the membrane complex subunits RnfB and RnfC were perfomed. First, the soluble fraction containing the membrane-associated but soluble RnfC and the insoluble fraction with the membrane-residing RnfB were obtained from a cell free extract from *C. difficile* cells grown without further cross-linking. Both baits were affinity chromatographed using their C-terminal Strep-tag® II. The concentrated elution fractions were analyzed by SDS-PAGE, Western blot analyses via Strep-Tactin® AP conjugate (figure 18) and finally the cut-out protein bands were subjected to LC-MS/MS analyses.

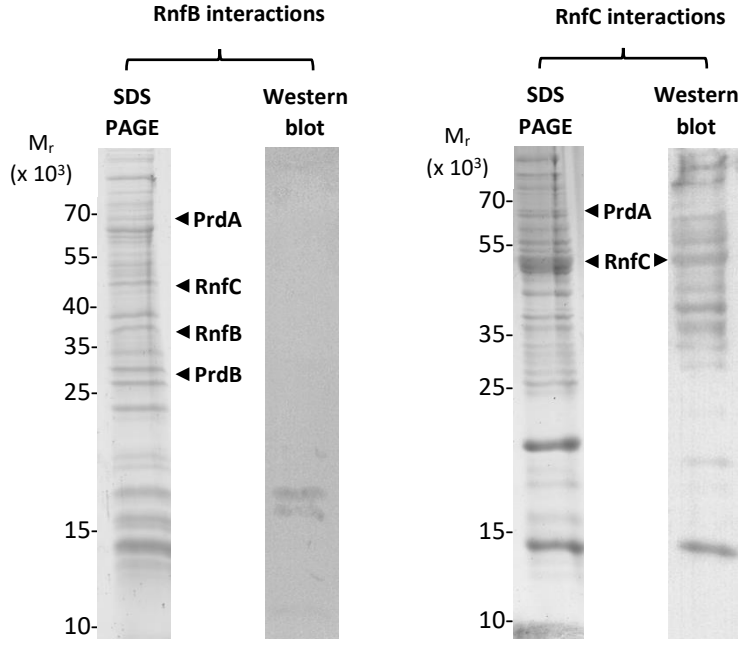

Figure 18: Interaction partners of the Rnf complex subunits RnfB and RnfC without the cross-linker formaldehyde. Shown are stained SDS PAGEs [left lane] and Western blot analyses [right lane] of the RnfB [left panel] and RnfC [right panel] interaction partners after affinity chromatography. Both baits were recombinantly produced in *C. difficile* 630Δ*erm* without the cross-linker. The soluble (RnfC) and insoluble fraction (RnfB) of cell free extracts were chromatographed through a Strep-Tactin® affinity column. Bait-prey complexes were eluted and a volume of 10 µL of the 60-fold (soluble fraction) and 30-fold (insoluble fraction) concentrated elution fraction were loaded onto 15 % SDS-PAGE and separated at 45 mA for 45 min. The PAGEs were stained with InstantBlue® Protein Stain (Expedeon Ltd, Cambridge, UK) solution. The relative molecular masses were deduced from the PageRuler™ (Plus) Prestained *Protein Ladder* (Thermo Fisher Scientific, Schwerte, Germany). The Western blot analyses were subjected to Strep-Tactin® AP conjugate (IBA GmbH, Göttingen, Germany) reaction. Blot development: 60 min until overnight. Image quality was impoved by grayscaled and the images of the Western blot were set to a color saturation of 355 %. The Western blot (RnfC) was set to 30 % brightness.

The stained SDS-PAGE showed several protein bands with different relative molecular masses for the elution fractions. For the analysis of RnfB (figure 18, left panel) interaction partners LC-MS/MS analyses for 18 cut-out protein bands were performed. Overall, 979 individiual proteins were found with the proteomic program Peaks® X+ (Bioinformatics Solutions Inc., Waterloo, Canada). The mass spectrometry settings for the prey protein identification were set to unique peptides > 2, a coverage > 5 % and an abundance > 1E+05. Hence, 56 proteins were left for further inspection (original protein list see digital appendix). Firstly, in the protein band at a relative molecular mass of 37.000 the bait protein **RnfB** (M_r 35.000) was detected via LC-MS/MS analysis, but unfortunately not in the Western blot analysis after a treatment with Strep-Tactin® AP conjugate (Strep-tag® detection in Western blots, IBA GmbH, Göttingen, Germany). The Strep-Tactin® AP conjugate detected two distinct bands in the range between M_r ~15.000 and ~25.000 of unknown identity (figure 18, left panel, right lane). Nevertheless, the LC-MS/MS analyses identified several proteins as RnfB interaction partners including the other subunit of the Rnf complex **RnfC** (M_r 48.000) in the protein band at a M_r of 40.000 - 55.000 and **PrdA** (M_r 68.000) and **PrdB** (M_r 26.000) in the protein bands with a M_r of ~70.000 and ~25.000, respectively.

For the identification of interaction partners of the bait protein RnfC (figure 18, right panel) the SDS-PAGE observed different protein bands with three intensive protein bands at a M_r of ~15.000, ~15.000 - 25.000 and ~55.000. Afterwards, 16 cut out protein bands were subjected to LC-MS/MS analyses. Overall, 577 proteins were found using the program Proteome discoverer™ 2.2/2.3 (Thermo Fisher Scientific, Schwerte, Germany). By setting the same cut-out criteria as described before 40 proteins were identified for further inspection (original protein list see digital appendix). In the protein band at a M_r ~55.000 the bait protein **RnfC** (M_r 48.000) was identified by LC-MS/MS. The Western blot using the Strep-Tactin® AP conjugate (Strep-tag® detection in Western blots, IBA GmbH, Göttingen, Germany) detected different proteins which might include the RnfC at a M_r ~55.000 (figure 18, right panel, right lane). Furthermore, RnfC interaction partners like **PrdA** (M_r 68.000) one subunit of the cytoplasmic D-proline reductase were identified (figure 18, right panel).

Moreover, additional abundant interaction partners of RnfB and RnfC without a formaldehyde cross-link treatment were identified by mass spectrometry (see appendix). In regards to the same LC-MS/MS analysis cut-off criteria which were mentioned before detected prey proteins were classified according to function and metabolic classes: electron transfer proteins, metal ion transport/binding proteins and proteins which are involved in glycolysis/glyconeogenesis, pyruvate metabolism, fatty acid degradation, pentose phosphate pathway, TCA cycle, butanoate metabolism and amino acid metabolism (table 28). The overview of these proteins in relation to all four baits (PrdA, PrdB, RnfB and RnfC) and in comparison of a cross-linker treatment is given in the chapter 4.1.6.

4.1.4 Interaction partners of the D-proline reductase subunits PrdA and PrdB in presence of the cross-linker formaldehyde

In the next experiments the interaction partner of PrdA and PrdB in the presence of the cross-linker formaldehyde were analyzed. Cultures were grown likewise but were treated with 0.156 % formaldehyde ($OD_{600\ nm}$ = 1) as a cross-linker (Fraenkel-Conrat and Olcott 1948; Metz *et al.* 2004) to stabilize transient protein-protein interactions. The Strep-tagged based affinity chromatography and data anlayses were conducted as specified before. In this case, the cross-linked insoluble fraction of the cell free extracts was used, which encompassed proteins from all cellular compartments. For this purpose, the concentrated bait elution fraction after affinity chromatography was prepared for a 15 % SDS-PAGE and for a bait detection via Western blot analysis by using Strep-Tactin® AP conjugate (Strep-tag® detection in Western blots, IBA GmbH, Göttingen, Germany) (figure 19). Visible protein bands in the SDS-PAGE were subjected to a LC-MS/MS analyses. The same cut-off criteria like in the non-cross-linking experiments were selected. For all baits, the protein-protein interactions occuring at the membrane were investigated in detail.

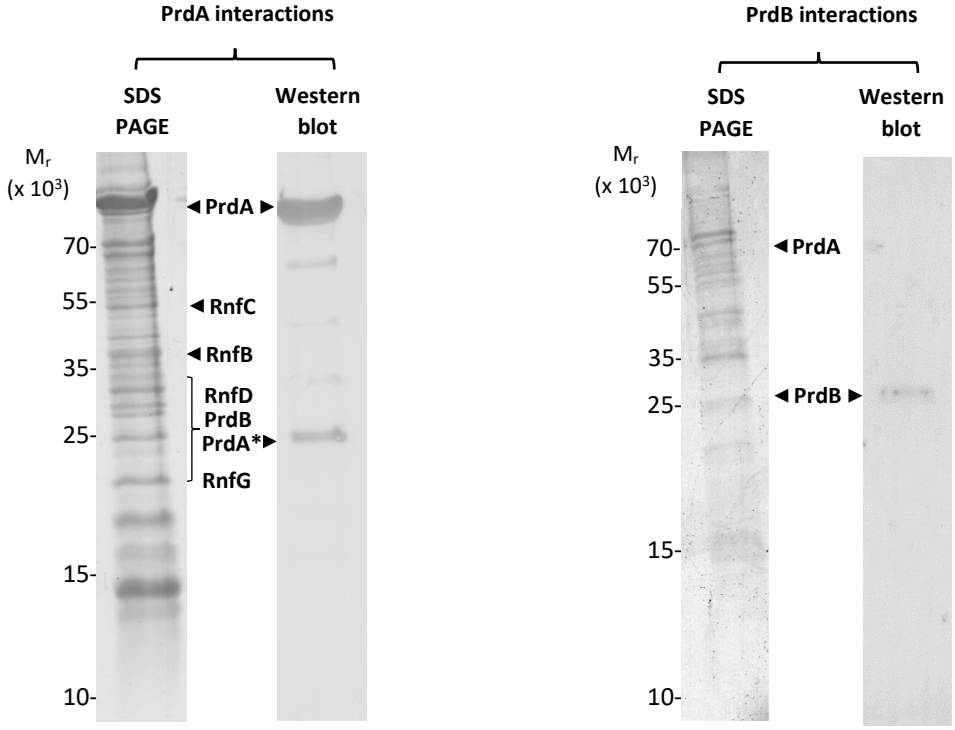

Figure 19: Interaction partners of the D-proline reductase subunits PrdA and PrdB in pesence of the cross-linker formaldehyde. Shown are the stained SDS PAGEs [left lane] and Western blot analyses [right lane] of the PrdA [left panel] and PrdB [right panel] interaction partners after purification via affinity chromatography. PrdA and PrdB as bait proteins were recombinantly produced in *C. difficile* 630Δ*erm.* The respective strain was treated with 0.156 % formaldehyde ($OD_{600\ nm}$ = 1) as a cross-linker before purification. The insoluble fraction of the cell free extacts containing the Strep-tagged baits was chromatographed through the Strep-Tactin® affinity column. Formed bait-prey complexes were eluted and 10 µL of the 30-fold concentrated elution fraction were seperated via 15 % SDS-PAGE with 45 mA for 45 min. The SDS-PAGE was stained with InstantBlue® Protein Stain (Expedeon Ltd, Cambridge, UK) solution. The relative molecular masses were deduced from the PageRuler™ Plus Prestained *Protein Ladder* (Thermo Fisher Scientific, Schwerte, Germany). The bait detection was performed by Western blot analysis using the Strep-Tactin® AP conjugate (IBA GmbH, Göttingen, Germany). The blot development was in general 15 - 30 min. Image quality was improved in grayscale. The image of the SDS-PAGE of PrdB was set to a brightness of 30 % and a color saturation of 355 %. The Western blot image of PrdA was set to a brightness of 30 % and 20 % for PrdB combined with 355 % color saturation to avoid background noise.

The stained SDS-PAGE of the concentrated elution fraction of the cross-linked PrdA (figure 19, left panel, left lane) showed several protein bands with different relative molecular masses. Firstly, the protein band at a M_r of 70.000 showed a higher intensity than the others. For subsequent LC-MS/MS analyses, 18 protein bands were cut-out and subjected to mass spectrometry. On average, 946 individiual proteins were found with the program Proteome discoverer™ 2.2/2.3 (Thermo Fisher Scientific, Schwerte, Germany). The cut-off criteria were unique peptides > 2, a protein coverage > 5 % and an abundance

> 1E+05 and the consideration of background control proteins determined before (see chapter 4.1.1). These settings excluded many proteins from the further analyses. Nevertheless, 140 proteins were considered (original protein list see digital appendix). The visible protein band at a M_r ~70.000 contained the bait protein **PrdA** (M_r 68.000) as confirmed by mass spectrometry. In agreement, the Western blot analysis via Strep-Tactin® AP conjugate (Strep-tag® detection in Western blots, IBA GmbH, Göttingen, Germany) also identified this protein band as the Strep-tagged bait PrdA. Furthermore, the above-mentioned proteolytically generated smaller subunit PrdA* was identified at a M_r of ~25.000 (figure 19, left panel, right lane). Other PrdA cross-linked interaction partner like **PrdB** (M_r 26.000), **RnfB** (M_r 35.000), **RnfC** (M_r 48.000), **RnfD** (M_r 35.000) and **RnfG** (M_r 20.000) were detected (figure 19, left panel).

The cross-linked PrdB interaction partner analysis revealed on a stained SDS-PAGE (figure 19, right panel, left lane) different protein bands. Afterwards, 7 protein bands were cut-out and subjected to LC-MS/MS. In total 49 proteins were identified by the software Proteome discoverer™ 2.2/2.3 (Thermo Fisher Scientific, Schwerte, Germany). The same cut-off criteria as above-mentioned excluded multiple proteins as observed before. Only 6 proteins were considered for further analyses (original protein list see digital appendix). Unfortunately, the bait protein **PrdB** (M_r 26.000) was not identified via mass spectrometry but was observed during the Western blot analysis at a M_r of 25.000 (figure 19, right panel, right lane). Furthermore, cross-linked PrdB interaction partners were identified e.g **PrdA** (M_r 68.000) with a relative molecular mass of ~70.000. Moreover, further important interaction partners of PrdA and PrdB in presence of the formaldehyde cross-linker were identified by LC-MS/MS (see appendix). For this purpose, the cut-off criteria which were mentioned before were selected and the prey proteins in relation to all baits were classified according to function and metabolic classes (table 29). The overview of these preys in comparison of the absence of formaldehyde is given in the chapter 4.1.6.

4.1.5 Interaction partners of the Rnf complex subunits RnfB and RnfC in presence of the cross-linker formaldehyde

Further bait-prey experiments of the membrane complex subunits RnfB and RnfC including 0.156 % formaldehyde cross-linker treatment were perfomed. Cultures were grown as described before and resulting cell free extracts were used for a Strep-tagged based affinity chromatography. For this purpose, the solubilized insoluble fraction of the cell free extracts was used. The concentrated elution fraction after affinity chromatography was separated on a 15 % SDS-PAGE. A subsequent Western blot was used for a bait detection (figure 20). Gel slices of protein bands which were visible in the stained SDS-PAGEs were cut out and contained proteins were subjected to LC-MS/MS analyses. For this purpose, the same cut-off criteria as mentioned before were selected. Thus, for the baits RnfB and RnfC, the protein-protein interactions occuring at the membrane were investigated.

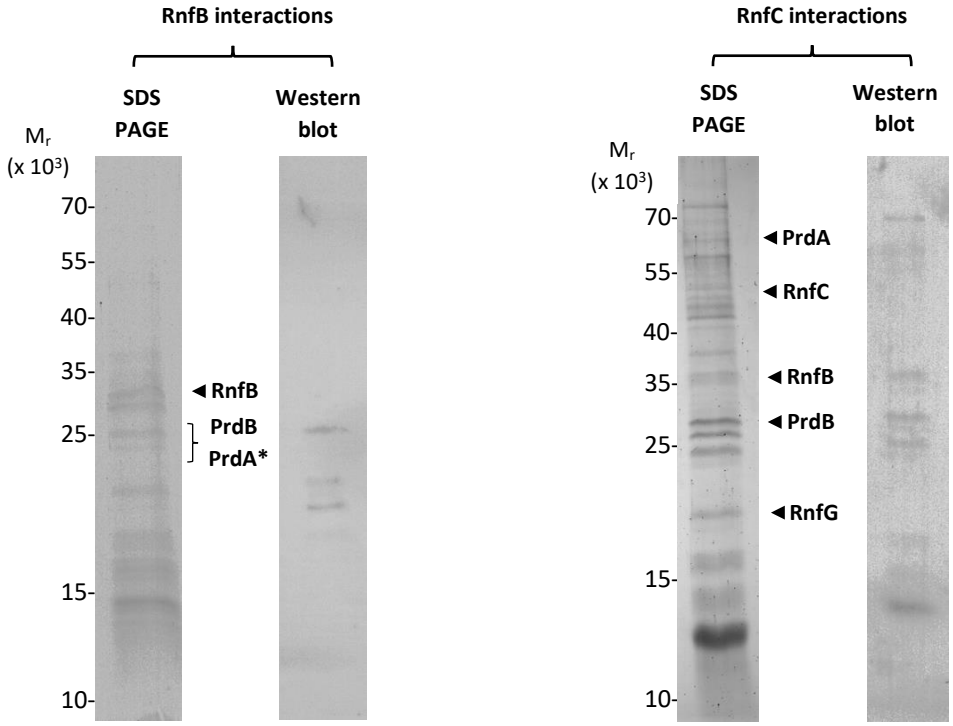

Figure 20: Interaction partners of the Rnf complex subunits RnfB and RnfC in presence of the cross-linker formaldehyde. The stained (InstantBlue® Protein Stain (Expedeon Ltd, Cambridge, UK)) SDS-PAGEs [left lane] and the corresponding Western blot analyses [right lane] of RnfB [left panel] and RnfC [right panel] interaction partners after the affinity chromatography purification are shown. Both baits were recombinantly produced in *C. difficile* 630Δ*erm* and treated with 0.156 % formaldehyde ($OD_{600\,nm}$ = 1) to stabilize protein-protein interactions before purification of the solubilized proteins of the insoluble fraction of the cell free extracts through the Strep-Tactin® affinity column. The bait-prey complexes were eluted and 10 µL of the 30-fold concentrated fraction were separated via 15 % SDS-PAGE at 45 mA for 45 min. The relative molecular masses were deduced using the PageRuler™ Prestained *Protein Ladder* (Thermo Fisher Scientific, Schwerte, Germany). The bait detection was performed via Western blot analyses using the Strep-Tactin® AP conjugate (IBA GmbH, Göttingen, Germany). The blot development was for 15 - 30 min. Images quality was improved in grayscale. The SDS-PAGE of RnfB was set to a brightness of - 20 %, a color saturation of 400 % and a color temperature of 7.220. The PAGE of RnfC was set to a brightness of 10 % and the corresponding Blot image to a brightness of 50 % and a color saturation of 200 % to avoid background noise.

The stained SDS-PAGE showed multiple bright protein bands with different molecular masses after separation of proteins in the concentrated elution fraction of the cross-linked RnfB (figure 20, left panel, left lane). All visible protein bands (∑ 13 bands) were processed according to the gel-based LC-MS/MS approach. In total, 378 individiual proteins were analyzed with the program Peaks® X+ (Bioinformatics Solutions Inc., Waterloo, Canada). The conditions of the settings were unique peptides > 2, a coverage > 5 % and an abundance > 1E+05 and some column contaminants were excluded from further

analyses. After application of these cut-off criteria 36 proteins were considered for further analyses (original protein list see digital appendix). The LC-MS/MS analyses detected the bait protein **RnfB** (M_r 35.000) in the protein band at a relative molecular mass of ~35.000. Unfortunately, the Western blot analysis with the Strep-Tactin® AP conjugate (Strep-tag® detection in Western blots, IBA GmbH, Göttingen, Germany) showed three different protein bands around ~ 25.000 of unknown identity (figure 20, left panel, right lane). Furthermore, several expected RnfB interaction partners were found via mass spectrometry like the subunits of the D-proline reductase **PrdA*** and **PrdB** (M_r 26.000) at a M_r of ~25.000.

For further identification of protein-protein interaction partners of the Rnf complex Strep-tagged-based affinity chromatography of the subunit RnfC was performed. The corresponding prey proteins were detected in the stained SDS-PAGE (figure 20, right panel, left lane). Firstly, multiple protein bands with different brightness and various relative molecular masses became visible which were subsequently cut-out (∑ 18 protein bands) and subjected to gel-based LC-MS/MS analyses. Approximatly 300 proteins (in 18 single cut out protein band files) were identified with the Proteome discoverer™ 2.2/2.3 (Thermo Fisher Scientific, Schwerte, Germany). After set up of the above-mentioned cut-off criteria approximatly 60 proteins (in 18 single cut outs of protein band) were further analyzed. For this purpose, the LC-MS/MS analyses identified the bait protein **RnfC** (M_r 48.000) in the protein band with a M_r of ~45.000. The Western blot analysis via Strep-Tactin® AP conjugate (Strep-tag® detection in Western blots, IBA GmbH, Göttingen, Germany) failed to detect this bait protein. Only other protein bands of unknown identity and with different relative molecular masses became visible (figure 20, right panel, right lane). Nevertheless, additional membrane Rnf complex subunits like **RnfB** (M_r 35.000) and **RnfG** (M_r 20.000) and subunits of the D-proline reductase **PrdA** (M_r 68.000) and **PrdB** (M_r 26.000) were found during LC-MS/MS analyses. Further important interaction partners were identified by LC-MS/MS (table 30). An overview of these preys and in comparison of the absence of formaldehyde is given in the next chapter 4.1.6.

4.1.6 Summary of the strong-binary and cross-linked protein-protein interactions of the baits PrdA, PrdB, RnfB and RnfC

In order to obtain cell systematics overview over the contacts between the Rnf complex, the D-proline reductase Prd and other proteins obtained results were combined in the following table. For this purpose, these identified proteins were separated into different classes: 1. proteins to serve electron transfer and 2. energy production proteins (classified according the database annotation of KEGG or UniProt). An overview over these proteins of high abundance (detail list in the appendix) in relation to all four non-cross-linked and cross-linked baits is given in table 18 - 21. The abundance of these prey proteins was defined with following values:

+++ = > 1E+09

++ = >1E+07 – 1E+09

+ = 1E+05 – 1E+07

- = no hit

Certain previously determined column contaminants of the background control which were highly concentrated and might to be enriched in these protein-protein interaction experiments were included in the analyses and marked in green.

Table 18: Interaction partners from the Stickland fermentation pathway and related functions of non-cross-linked (-CL) and cross-linked (+CL) PrdA, PrdB, RnfB and RnfC: *D-proline reductase (**PrdCDF**), glycine reductase (**GrdBCD**), indolepyruvate ferredoxin oxidoreductase (**IorAB**) and dihydroorotate dehydrogenase electron transfer (**PyrK**)*

D-proline reductase					Oxidoreductase/Lyases					
Baits/Preys		**PrdC**	**PrdD**	**PrdF**	**GrdB**	**GrdC**	**GrdD**	**IorA**	**IorB**	**PyrK**
PrdA	**- CL**	-	-	-	-	-	-	-	-	-
	+ CL	-	++	++	++	-	-	++	-	++
PrdB	**- Cl**	++	-	++	+	-	+	+	-	-
	+ CL	-	-	-	-	-	-	-	-	-
RnfB	**- Cl**	++	-	-	-	++	-	-	++	-
	+ CL	-	-	-	-	-	-	-	-	-
RnfC	**- Cl**	-	-	-	-	+	-	+	-	-
	+ CL	++	-	++	+	-	++	+	-	-

Table 19: Subunits of the F-type and V-type ATPase interacting with PrdA, PrdB, RnfB and RnfC in the presence (+CL) and absence (-CL) of the cross-linker formaldehyde

ATPase								
		V-type ATPase				F-type		
Baits/Preys		**AtpA**	**AtpB**	**AtpD**	**AtpF**	**AtpA1**	**AtpF1**	**AtpG**
PrdA	**- CL**	-	-	-	-	-	-	-
	+ CL	-	+	++	-	++	-	++
PrdB	**- Cl**	-	-	++	-	++	-	+
	+ CL	-	-	-	-	++	-	-
RnfB	**- Cl**	++	++	++	++	++	-	++
	+ CL	-	-	++	++	++	-	++
RnfC	**- Cl**	-	-	+	-	++	-	+
	+ CL	+	-	++	++	++	++	+

Table 20: Interaction partners from electron bifurcating and iron (-transport) proteins of non-cross-linked (-CL) and cross-linked (+CL) PrdA, PrdB, RnfB and RnfC: *Electron transfer flavoprotein (**EtfAB**), ferrous iron transport protein (**FeoB**), Flavodoxin (**FldX**) and Ferritin (**FtnA**)*

Electron bifurcating and iron (-transport)									
Baits/Preys		**EtfA1**	**EtfA3**	**EtfB1**	**EtfB3**	**FeoB1**	**FeoB2**	**FldX**	**FtnA**
PrdA	**- CL**	-	-	+	-	-	-	+	+
	+ CL	++	-	++	-	++	-	-	-
PrdB	**- Cl**	++	-	++	-	+	-	+	+
	+ CL	-	-	-	-	-	-	-	-
RnfB	**- Cl**	-	++	++	++	++	++	-	-
	+ CL	++	++	++	+	++	-	-	-
RnfC	**- Cl**	++	-	++	-	+	-	-	-
	+ CL	+++	-	++	-	++	-	++	++

Table 21: Interaction partners from different energy metabolism pathways of non-cross-linked (-CL) and cross-linked (+CL) PrdA, PrdB, RnfB and RnfC: *3-hydroxybutyryl-CoA dehydratase (Crt2), 3-hydroxybutyryl-CoA dehydrogenase (**Hbd**), 4-hydroxybutyrate CoA-transferase (**Cat2**), 4-hydroxybutyryl-CoA dehydratase (**AbfD**), acyl-CoA dehydrogenase (**AcdB**), acryloyl-CoA reductase electron transfer (**AcrA**), aldehyde-alcohol dehydrogenase (**AdhE/AdhE1**), 6-phosphofructokinase (**PfkA**), butyrate kinase (**Buk**), butyryl-CoA dehydrogenase (**Bcd2**), D-lactate dehydrogenase (**LdhA**), formate acetyltransferase (**PlfB**), fructose-1,6-bisphosphate aldolase (**Fba**), glucose-6-phosphate isomerase (**Pgi**), glyceraldehyde-3-phosphate dehydrogenase (**GapAB**), phosphate butyryltransferase (**Ptb**), pyruvate carboxylase (**PycA**), pyruvate flavodoxin oxidoreductase (**Pfo**), pyruvate kinase (**Pyk**) and succinate-semialdehyde dehyd-rogenase (**SucD**)*

Butanoate-, fatty acid metabolism, glycolysis/glyconeogenesis, pentose phosphate pathway, pyruvate metabolism, TCA cycle												
Baits/Preys		**Crt2**	**Hbd**	**Cat 2**	**AbfD**	**AcdB**	**AcrA**	**AdhE**	**Pfk A**	**Buk**	**Bcd 2**	**Ldh A**
PrdA	**- CL**	-	++	-	+	-	-	+	+	-	-	+
	+ CL	++	+++	++	++	+++	++	++	++	++	+++	++
PrdB	**- Cl**	++	++	++	++	-	-	++	++	++	-	++
	+ CL	-	-	-	-	-	-	-	-	-	-	-
RnfB	**- Cl**	++	++	++	-	-	-	++	++	++	-	++
	+ CL	++	-	++	++	-	-	++	++	-	-	++
RnfC	**- Cl**	-	-	+	++	-	-	-	++	++	-	+
	+ CL	+	++	++	++	-	-	+++	++	++	-	++
Baits/Preys		**PlfB**	**Fba**	**Pgi**	**GapA**	**GapB**	**Ptb**	**PycA**	**Pfo**	**Pyk**	**Suc D**	
PrdA	**- CL**	-	++	-	-	++	+	+	-	-	-	
	+ CL	++	++	+	++	-	+	++	++	++	+++	
PrdB	**- Cl**	-	++	++	++	-	++	++	++	++	++	
	+ CL	-	-	-	-	-	-	-	-	-	-	
RnfB	**- Cl**	-	++	++	++	-	-	-	++	++	-	
	+ CL	++	++	-	++	-	++	++	++	++	++	
RnfC	**- Cl**	-	++	+	++	-	+	++	++	++	++	
	+ CL	+	++	++	++	-	-	++	++	++	++	

In conclusion, a manifold of prey proteins were found via gel-based LC-MS/MS analyses in the different bait-prey experiments in absence and presence of the cross-linker formaldehyde. It is noteworthily that some of identified prey proteins were only present in the cross-linking experiments and others only in absence of the cross-linker. Since the bait proteins were found by LC-MS/MS, the method shows a suitable procedure for the

interactomic approach of Rnf-Prd in *C. difficile*. Interestingly, further important proteins were found, which are involved in Stickland fermentation, ATP generation, electron transfer, iron transport and/or generally in different energy/electron generating metabolic pathways. It is assumed that interaction partners of this type serve for a localized, rapid reaction and electron transfer at the Rnf-Prd complex in the Stickland fermentation pathway. For a more precise information about the protein-protein interactions of the individual baits, a quantification of the preys in a gel-free LC-MS/MS analyses of the baits PrdA, PrdB, RnfB and RnfC was performed in the following chapter.

4.2 Identification and quantification of the bait-prey interactions between the Rnf complex and D-proline reductase with a gel-free LC-MS/MS approach

The gel-based LC-MS/MS approach helped to identify the protein interaction-partner of the bait proteins PrdA, PrdB, RnfB and RnfC with and without formaldehyde cross-linking. Afterwards, the determined protein-protein interactions were further analyzed in more detail via a quantification approach performed by gel-free LC-MS/MS set up. The affinity chromatography-based enrichment of prey proteins via protein interaction to the affinity-tagged baits in comparison to their normal abundance in the cell free extract (solubilized proteins of the insoluble fraction) was determined. For this purpose, the abundance values of identified proteins after attached to affinity chromatographed baits PrdA, PrdB, RnfB and RnfC in comparison to the abundance of the cell free extract control, were used for the calculation of an enrichment factor (see chapter 3.5.6).

According to this, a factor > 1 showed an enrichment of LC-MS/MS identified proteins in the bait elution fraction. It has to be noted that increasing values of this factor indicate either a stronger bait-prey protein interaction or a special polymerization of the prey proteins which were linked to the respective bait.

4.2.1 Quantification of protein-protein interactions of the formaldehyde cross-linked baits PrdA, PrdB, RnfB and RnfC

For the quantification of protein-protein interactions of PrdA, PrdB, RnfB and RnfC similar growth conditions of *C. difficile* 630Δ*erm* as used for the gel-based analyses were selected followed by a formaldehyde treatment of 0.156 % ($OD_{600\,nm}$ = 1), cell fractionation, and Strep-tag® II affinity chromatography steps (see chapter 3.4.3). Three biological replicates were investigated with the gel-free LC-MS/MS method. As mentioned before 200 µL of the solubilized insoluble fraction as abundance control and of the respective chromatographed eluted bait protein in the same amount were taken for the further calculation of an enrichment factor after LC-MS/MS measurement. Procedures were described in detail in chapter 3.5.5 and 3.5.6. All of the samples were analysed with the software Proteome discoverer™ 2.2/2.3 (Thermo Fisher Scientific, Schwerte, Germany).

The list of protein interaction partners of the chromatographed bait proteins compared to the corresponding abundance control was included in one data set. The total amount of LC-MS/MS identified proteins was 1931. The data were exported to MS Excel® (Microsoft® Corporation, Washington, USA) after narrowing down the candidates according to the cut-off criteria: the unique peptides ≥ 2 and the coverage ≥ 5 %. Afterwards the data were normalized to a usually meassured chromatographed bait protein concentration of 0.24 mg/mL as reference and the mean value of the enrichment factor (abundance of proteins in eluate/abundance of proteins in the abundance control) for the quantification of prey proteins in the bait sample was calculated (see digital appendix). Proteins which were not found in all of the three replicates and proteins with an enrichment factor < 1 were excluded from further analyses. After these settings 1196 proteins were found to be enriched in the bait elution fraction (original list in the digital appendix). Furthermore, general proteins which were not specific for energy generation pathways and not directly contribute to the Stickland fermentation process in *C. difficile* were withdrawn from this study. Moreover, several proteins were not considered for further analyses as they are generic and abundantly found in bacterial cells such as: chaperones, ribosomale proteins, not classified enzymes, ligases, polymerases, gyrases, transferases, aldolases, elongation factors, transcriptional regulators, chromosomal replication initia-

tor proteins, DNA repair proteins/binding proteins, cold shock proteins, unspecific sporulation or cell surface proteins and cell division proteins. Overall, **810 enriched potential prey proteins** were encountered (original list in the digital appendix). Among these, several proteins were found in in all four, three, two or one of the baits eluates. The next figure shows the amount of identified prey proteins according to their occurrence in the different bait eluates.

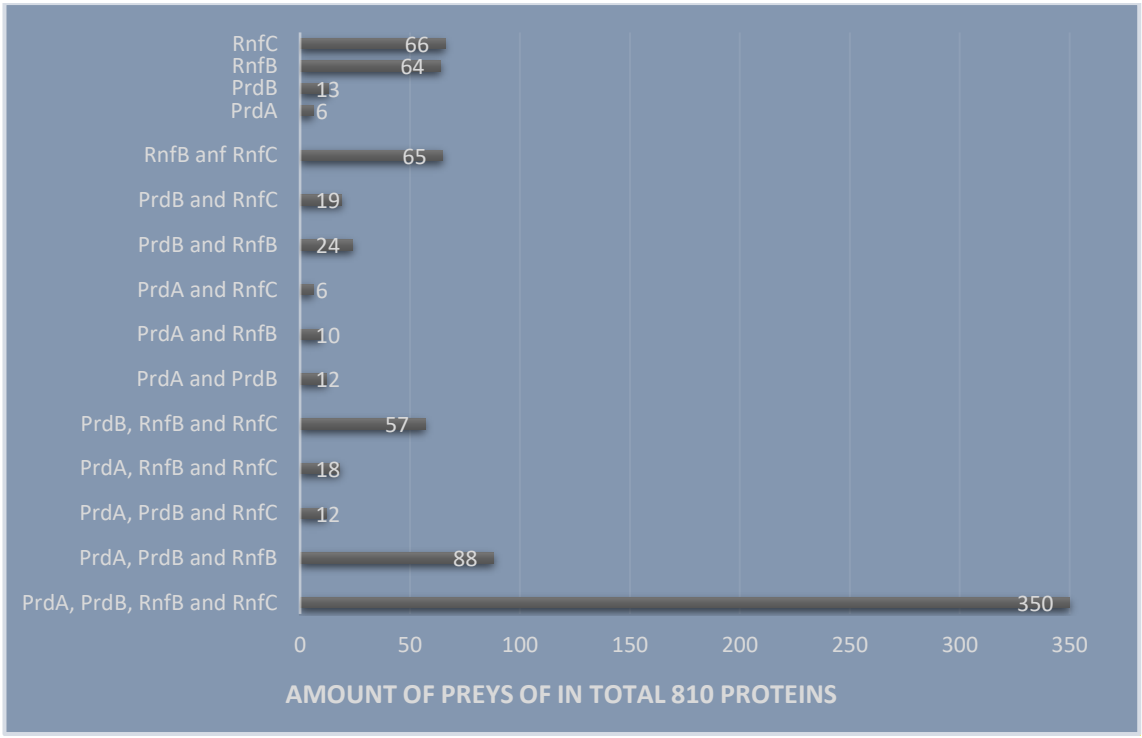

Figure 21: Grouped bar diagram of prey proteins of the baits PrdA, PrdB, RnfB and/or RnfC from *C. difficile* 630Δ*erm* in the total amount of 810 identified proteins. The identified preys of the baits PrdA, PrdB, RnfB and RnfC were determined with the program Proteome discoverer™ 2.2/2.3 (Thermo Fisher Scientific, Schwerte, Germany). After the settings of unique peptides ≥ 2, protein coverage ≥ 5 %, normalization to 0.24 mg/mL protein concentration, excluding non energy generation or Stickland fermentation pathway relevant proteins (e.g. generic proteins) in total 810 proteins were identified via mass spectrometry. Firstly, these proteins were grouped into the occurrence in all four, three, two or in single bait proteins. Interestingly, 350 prey proteins were present in all four baits.

Afterwards, the prey proteins were sorted according to their enrichment factor value in relation to the value of the bait protein. In general, prey proteins with a higher enrichment factor than the bait protein may indicate a strong interaction or that more subunits of the preys interact with the bait protein. The following table shows an overview of the most important prey proteins from the total amount of 810 identified proteins found in

the differerent bait protein eluates (original list in the digital apendix). Furthermore, it has been subdivided into the categories: Stickland fermentation pathway, ATP synthase, electron transfer or iron translocating proteins by the use of the database KEGG or Uni-Prot.

Table 22: Quantification of formaldehyde cross-linked bait-prey proteins identified via gel-free LC-MS/MS approach and dedicated to the Stickland fermentation pathway, ATP synthase and electron transfer or ion translocating proteins

Prey proteins			Enrichment factor of preys in the baits			
Definition		**Gene-ID**	**Bait PrdA**	**Bait PrdB**	**Bait RnfB**	**Bait RnfC**
Stickland fermentation – D-proline reductase						
D-proline reductase PrdA subunit	**PrdA**	CD630DERM_32440	**934.38**	65.42	74.29	7.81
D-proline reductase PrdB subunit	**PrdB**	CD630DERM_32410	127.43	**32.87**	91.25	5.65
D-proline reductase PrdD subunit	**PrdD**	CD630DERM_32400	-	6.94	-	10.57
Proline racemase	**PrdF**	CD630DERM_32370	18.40	7.59	243.96	21.26
Putative electron transfer protein	**PrdC**	CD630DERM_32470	28.24	14.29	28.82	4.50
Transcriptional regulator	**PrdR**	CD630DERM_32450	41.69	-	-	-
Stickland fermentation – Rnf Komplex						
Ion-translocating oxidoreductase complex subunit B	**RnfB**	CD630DERM_11420	31.35	20.80	**41.79**	3.46
Ion-translocating oxidoreductase complex subunit C	**RnfC**	CD630DERM_11370	9.62	10.61	9.40	**3.38**
Ion-translocating oxidoreductase complex subunit D	**RnfD**	CD630DERM_11380	35.65	90.23	229.18	18.17
Ion-translocating oxidoreductase complex subunit G	**RnfG**	CD630DERM_11390	-	15.46	37.50	28.05
Stickland fermentation – Glycine reductase						
Glycine reductase subunit B	**GrdB**	CD630DERM_23510	18.47	13.24	41.52	1.54

Glycine reductase component C subunit beta	**GrdC**	CD630DERM_23490	49.93	4.34	5.93	6.48
Glycine reductase subunit D	**GrdD**	CD630DERM_23480	65.65	28.84	16.56	8.77
Glycine reductase component B subunits alpha and beta	**GrdE**	CD630DERM_23540	39.29	14.93	83.84	83.46
ATP-Synthase						
F-type H^+/Na^+-transporting ATPase subunit alpha	**AtpA1**	CD630DERM_34700	10.99	6.13	199.96	5.43
F-type H^+-transporting ATPase subunit b	**AtpB1**	CD630DERM_34720	8.92	4.97	19.03	1.86
F-type H^+-transporting ATPase subunit c	**AtpC2**	CD630DERM_ 34730	-	-	361.07	8.49
F-type H^+-transporting ATPase subunit delta	**AtpF1**	CD630DERM_34710	64.62	8.03	11.88	-
F-type H^+-transporting ATPase subunit gamma	**AtpG**	CD630DERM_34690	11.08	7.19	43.67	1.38
F-type H^+-transporting ATPase subunit beta	**AtpD**	CD630DERM_34680	9.33	4.22	68.06	24.60
Putative ATPase	**-**	CD630DERM_22490	-	17.68	46.84	2.26
V-type ATP synthase alpha chain	**AtpA**	CD630DERM_29560	-	-	209.60	-
Electron transfer						
Electron transfer flavoprotein subunit alpha	**EtfA1**	CD630DERM_04010	10.10	9.03	159.74	6.91
Electron transfer flavoprotein subunit alpha	**EtfA3**	CD630DERM_10560	11.48	8.10	92.34	4.22
Electron transfer flavoprotein subunit beta	**EtfB1**	CD630DERM_04000	13.92	11.04	108.80	3.27
Electron transfer flavoproteins subunit beta	**EtfB3**	CD630DERM_10550	10.21	9.31	98.21	7.68
Flavodoxin	**FldX**	CD630DERM_19990	20.91	14.09	140.98	15.89

NADH-quinone oxidoreductase subunit E (electron-transferring)	-	CD630DERM_34050	-	-	-	15.18
Iron-dependend/containing/transporter proteins and ferredoxin						
2-oxoglutarate ferredoxin oxidoreductase subunit gamma	-	CD630DERM_01180	20.01	11.59	52.89	35.02
Ferredoxin--NADP(+) reductase subunit alpha	-	CD630DERM_15360	9.73	11.58	81.19	5.00
Ferrous iron transport protein A	**FeoA1**	CD630DERM_14780	100.15	29.05	7.39	-
Ferrous iron transport protein B	**FeoB1**	CD630DERM_14790	6.44	15.63	78.11	2.28
Ferrous iron transport protein B	**FeoB2**	CD630DERM_32740	7.51	11.22	78.43	18.94
Fe-s iron-sulfur cluster assembly protein, nifu family	-	CD630DERM_12800	21.78	18.69	360.42	26.09
Indolepyruvate ferredoxin oxidoreductase	**IorB**	CD630DERM_23800	53.87	15.35	34.30	6.87
Putative dinitrogenase iron-molybdenum cofactor	-	CD630DERM_16930	10.18	18.35	368.73	10.14
Putative iron-dependent hydrogenase	-	CD630DERM_08930	6.57	31.15	390.57	16.04
Putative iron-sulfur assembly protein	-	CD630DERM_36070	7.72	15.44	94.66	13.80

Blue-grey color code of the calculated enrichment factor (F) values of the different proteins in the bait samples: The enrichment of bait proteins by affinity chromatography versus their abundance in the corresponding cell free extract delivered the bait enrichment factor (F) for **PrdA= 934.38**; **PrdB= 32.87**; **RnfB= 41.79** and **RnfC= 3.38.** If these values showed 100 % enrichment of the respective bait protein, the calculated prey enrichment factors for the respective bait were above (**> 100 %, dark blue**) or below (**10 - 100 %, bright blue**; **< 10 %, grey**) to the corresponding bait factor. The illustration of this high or low ratio of prey-bait interaction were highlighted in the above-metioned color code (this shows the enriched prey proteins after affinity chromatography versus their abundance in the respective cell free extract (F) and compared to the employed bait protein enrichment factor).

Other prey proteins (after applying the cut-off) that are also highly abundant, usually with an enrichment factor above their respective bait (dark blue marked, > 100 %) or which are at least as abundant as the bait protein (blue marked =

100 %), were classified according to their pathway or function. Proteins that are very prominent but did not obviously directly contribute to the general energy metabolism of the bacterial cell were placed into the category cellular processes. The following table shows an overview of the proteins that were examined in detail for the analyses (the original list is shown in the digital appendix).

Table 23: Quantification of the formaldehyde cross-linked bait-prey proteins identified via gel-free LC-MS/MS approach and dedicated to general bacterial cell energy generation pathways

Prey proteins			Enrichment factor of preys in the baits			
Definition		**Gene-ID**	**Bait PrdA**	**Bait PrdB**	**Bait RnfB**	**Bait RnfC**
Butanoate metabolism, fatty acid metabolism, glycolysis, pentose phosphate pathway pyruvate metabolism, TCA cycle						
3-hydroxybutyryl-CoA dehydratase (Crotonase)	**Crt2**	CD630DERM_10570	27.92	11.11	132.70	
4-hydroxybutyrate CoA transferase	**Cat2**	CD630DERM_23390	24.74	16.23	52.43	5.40
Acetyl-coenzyme A carboxylase car-boxyl transferase	**AccA**	CD630DERM_19360	34.01	38.45	101.80	5.75
Alcohol dehydrogenase	**Adh**	CD630DERM_30060	12.34	10.18	86.95	3.90
Biotin carboxyl car-rier protein of ace-tyl-CoA carboxylase	**AccB**	CD630DERM_19390	364.51	341.79	677.34	16.54
D-lactate dehydrogenase	**LdhA**	CD630DERM_03940	14.94	11.20	108.43	6.60
Fructose-1,6-bis-phosphate aldolase	**Fba**	CD630DERM_04030	12.48	6.19	170.51	3.78
Glyceraldehyde-3-phosphate dehydro-genase	**GapN**	CD630DERM_05800	9.25	6.00	2.73	6.69
Probable butyrate kinase	**Buk2**	CD630DERM_23790	10.55	8.63	70.60	6.06
Pyruvate car-boxylase	**PycA**	CD630DERM_00210	72.37	55.11	488.24	20.77
Pyruvate formate-ly-ase	**PflE**	CD630DERM_32830	204.06	40.91	8.84	11.84
Pyruvate kinase	**Pyk**	CD630DERM_33940	14.22	8.15	101.07	6.77

Putative 6-phospho-beta-glucosidase	-	CD630DERM_13380	-	-	133.75	234.30
Sedoheptulose-7-phosphate:D-glyceraldehyde-3-phosphate glycolaldehydetransferase	**Tkt`**	CD630DERM_23210	50.08	10.57	284.75	7.44
Succinate-semialdehyde dehydrogenase	**SucD**	CD630DERM_23420	32.09	14.57	40.24	14.53
Biosynthesis of amino acids/amino acid metabolism						
Aspartokinase	**DapG**	CD630DERM_13220	37.75	15.82	248.19	9.94
Glycine decarboxylase	**GcyPB**	CD630DERM_16580	126.81	149.39	45.49	-
Homoserine kinase	**ThrB**	CD630DERM_21190	-	27.54	875.24	108.46
Imidazoleglycerol-phosphate dehydratase	**HisB**	CD630DERM_15500	10.04	94.31	-	24.17
Phospho-2-dehydro-3-deoxyheptonate aldolase	**AroF**	CD630DERM_14530	1454.82	229.40	42.21	4.68
Prephenate dehydrogenase	**TyrC**	CD630DERM_18390	42.43	27.85	827.33	50.80
PTS system						
PTS system, mannitol-specific, IICB component	**MtlA**	CD630DERM_23340	11.91	9.91	634.18	3.77
PTS system, glucose-like IIBC component	-	CD630DERM_30890	3.00	20.52	43.04	72.64
Cellular Processes						
Bifunctional carbon monoxide dehydrogenase/acetyl-CoA synthase,nickel-inserting subunit	-	CD630DERM_07240	12.20	49.98	305.87	-
Cyclic-di-AMP phosphodiesterase	-	CD630DERM_36590	-	-	-	723.44
Flagellar assembly factor	**FliW**	CD630DERM_02330	56.14	72.64	999.73	30.01
Flagellar basal body protein	**FlgG**	CD630DERM_02690	269.45	183.29	23.71	13.20

Flagellar motor switch phosphatase FliN1	**FliN1**	CD630DERM_02710	-	37.23	1049.96	9.92
Putative ferric-uptake regulator	**-**	CD630DERM_08260	102.07	-	42.77	9.47
Putative flagellar biosynthesis protein	**FlgN**	CD630DERM_02300	215.03	17.38	435.09	6.51
Putative pyridine nucleotide-disulphide oxidoreductase	**-**	CD630DERM_30090	-	-	1235.63	-
Toxin A	**TcdA**	CD630DERM_06630	18.41	12.88	45.29	4.00
Two-component response regulator, CheY family	**-**	CD630DERM_36000	2896.21	118.51	21.96	12.13
Xanthine dehydrogenase iron-sulfur binding subunit	**XdhC3**	CD630DERM_21000	-	34.16	1401.87	-

Blue-grey color code of the calculated enrichment factor (F) values of the different proteins in the bait samples: The enrichment of bait proteins by affinity chromatography versus their abundance in the corresponding cell free extract delivered the bait enrichment factor (F) for **PrdA= 934.38**; **PrdB= 32.87**; **RnfB= 41.79** and **RnfC= 3.38.** If these values showed 100 % enrichment of the respective bait protein, the calculated prey enrichment factors for the respective bait were above (**> 100 %, dark blue**) or below (**10 - 100 %, bright blue**; **< 10 %, grey**) to the corresponding bait factor. The illustration of this high or low ratio of prey-bait interaction were highlighted in the above-metioned color code (this shows the enriched prey proteins after affinity chromatography versus their abundance in the respective cell free extract (F) and compared to the employed bait protein enrichment factor).

Both tables showed an overview of the abundant preys for the respective bait protein. Due to Stickland fermentation, proteins of D-proline reductase, glycine reductase and the Rnf complex were found in almost all bait eluates. Various subunits of ATPase (F-type and V-type), the Etf complex and iron-dependent proteins were identified in most bait eluates and highly enriched in the Rnf subunit bait eluates. In addition, highly abundant preys specifically related to energy metabolism were found in almost all eluates.

4.3 Verification of bait-prey interactions using transmission electron microscopy (TEM)

In order to verify some of the results obtained by the interactomics approach, a second independent method based on electron microscopy was used. For this purpose, a double immunogold labeling experiment of the bait and prey proteins and their potential co-localization using TEM was performed. This method allows for the cellular co-localization of the two proteins by means of polyclonal antibodies which carry different-sized gold particles. For the generation of the corresponding antibodies three peptide epitopes of the target protein were selected based on their soluble nature and their exposure to the protein surface according to bioinformatic predictions from the company Metabion international AG and Primm (Planegg, Germany) (see chapter 3.5.7 and appendix). Preparation of the labelled antibodies, images collection and analyses were performed using TEM by Dr. Mathias Müsken and Ina Schleicher at the HZI in Braunschweig (group of Prof. Dr. Manfred Rohde; Central Facility for Microscopy).

For the interaction studies of PrdA, RnfB and RnfC corresponding rabbit polyclonal antibodies were raised as mentioned before. Ultrathin sections of *C. difficile* 630Δ*erm* were incubated with pairs of antibodies. Images were taken of the labeled cells via TEM and co-localization events of protein pairs (PrdA with RnfB, PrdA with RnfC and RnfC with RnfB) were monitored in detail. The binding specificity of each antibody was tested by incubating it individually with *C. difficile* 630Δ*erm* cells. The figure below illustrates the single and double immunogold labeling events encountered for each pair of proteins analyzed:

PrdA AB (15 nm)

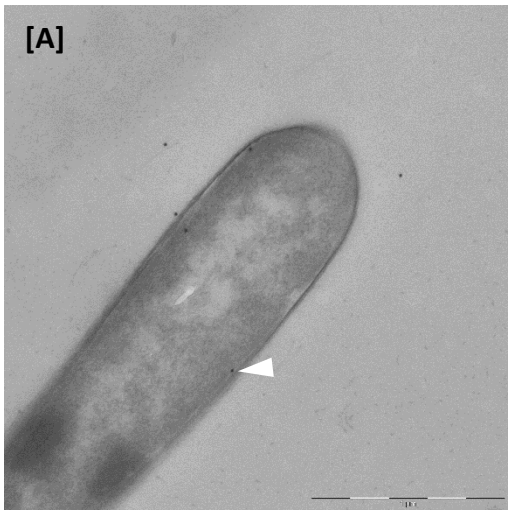

RnfB AB (15 nm)

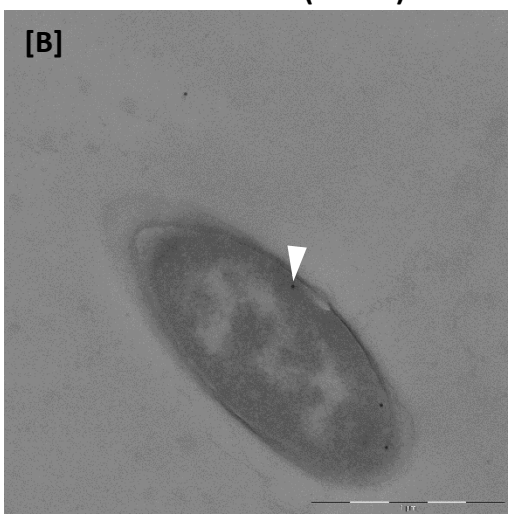

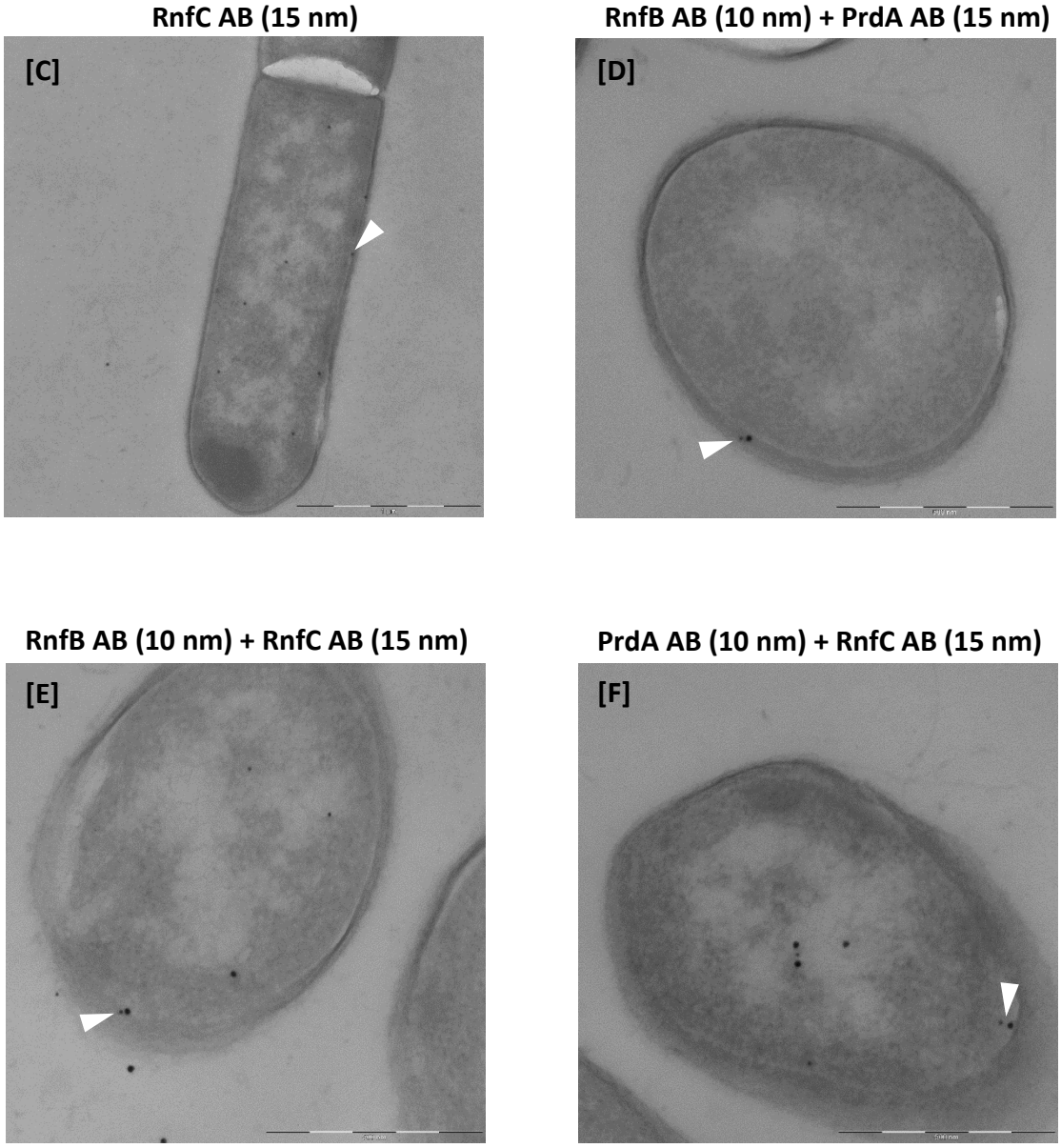

Figure 22: Interaction studies using antibodies directed against PrdA, RnfB and RnfC coupled with gold particles of different size (immunogold co-localization) visualized by TEM. Panels [A] to [C] show the control reactions of individually applied antibodies coupled with 15 nm insize gold particles directed against the cytoplasmic subunit of D-proline reductase PrdA and the membrane-bound subunits RnfB and RnfC as indicated above every image. Panels [D] to [F] show the images of the co-localization studies for the indicated protein pairs: RnfB and PrdA; RnfB and RnfC; PrdA and RnfC (labeled with gold particles size of 10 nm or 15 nm). The specific events occurring localized to the membrane are marked with white arrows. The images show a scale of 1 µm for single events and 500 nm for double events. The images were provided by Dr. Mathias Müsken at the HZI in Braunschweig (group of Prof. Dr. Manfred Rohde; Central Facility for Microscopy).

In the TEM images shown in panels [A] to [C] of figure 22 the localization of the gold particles (15 nm) labeled antibodies directed against PrdA, RnfB and RnfC were tested alone. The proteins were observed mainly localized to the bacterial membrane (white arrow) and to a minor extent inside the cytoplasm. The co-localization studies shown in panels [D] to [F] of figure 22 were mainly observed at the membrane (white arrow). To a certain degree, single antibodies were found in the cytoplasm or in the background. In addition, the single antibody localization and the co-localization events of PrdA, RnfB and RnfC were subjected to semi-quantitative analyses. For this purpose, GraphPad prism (version 8.4.3) was applied to plot the data. In detail, the area of cells respectively background was measured in µm^2 and split in different fractions: cytoplasm (75 %) and membrane (25 %). Afterwards, the gold particles in single or double labeling were counted (see chapter 3.5.7) and classified into cell cytoplasm, cell membrane and background. The following figures illustrate the single and double antibody detection in the cell according to the cell compartment.

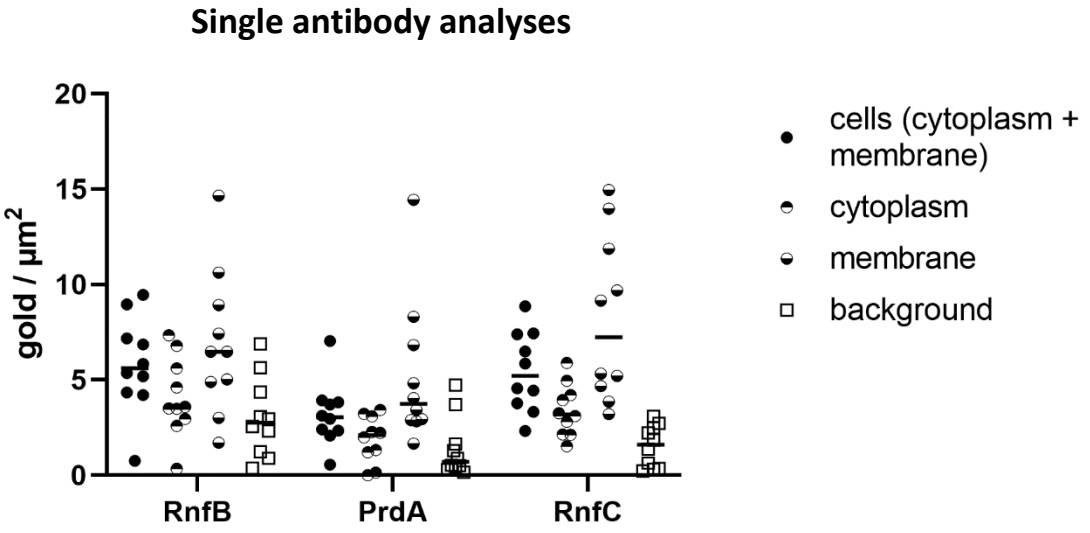

Figure 23: Semi-quantitative image analyses of single antibody detections of PrdA, RnfB and RnfC in *C. difficile* 630Δ*erm*. The figure shows the counted events out of a 10 images series of antibodies directed to PrdA, RnfB and RnfC coupled with protein A-gold (15 nm). The mean value of the series was plotted and the area of the cell respectively backround (in µm^2) was measured in advance (gold/µm^2). The occurring events in each image were counted and assigned to the different (cell)-regions (cytoplasm, membrane and background). The figure was provided by Dr. Mathias Müsken at the HZI in Braunschweig (group of Prof. Dr. Manfred Rohde; Central Facility for Microscopy).

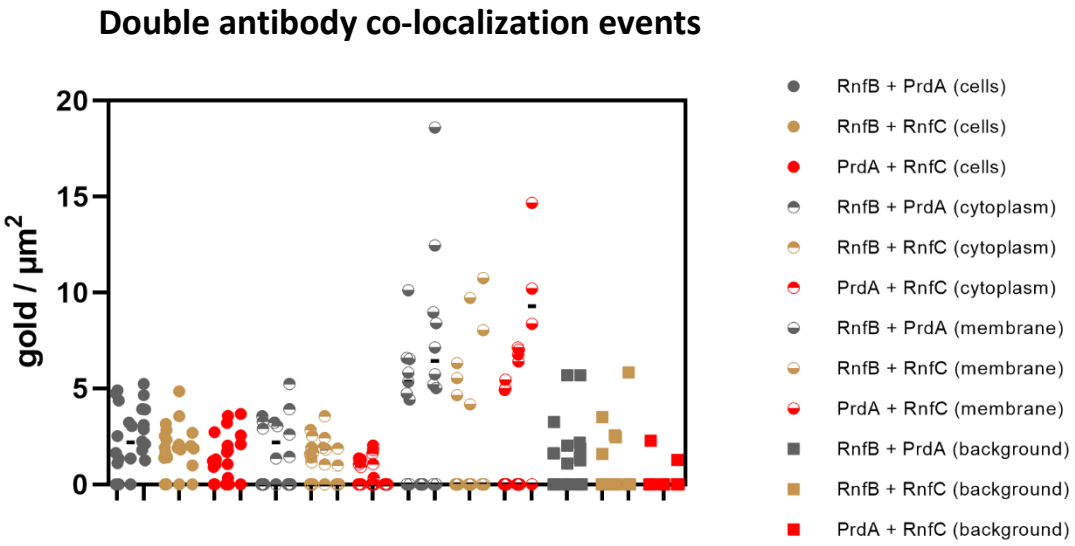

Figure 24: Semi-quantitative image analyses of co-localization events for the protein combinations PrdA and RnfB, RnfB and RnfC as well as RnfC and PrdA in *C. difficile* 630Δ*erm*. The figure shows the counted events out of three data sets (each combination covered by 21 - 25 images) for the co-localization of antibodies directed to PrdA, RnfB and RnfC coupled with protein A-gold (10 nm and 15 nm). The mean value of the series was included and the area of the cell respectively backround (in µm²) was measured in advance (gold/µm²). The gold particle events in each image were counted and assigned to the different (cell)-regions (cytoplasm, membrane and background). The figure was provided by Dr. Mathias Müsken at the HZI in Braunschweig (group of Prof. Dr. Manfred Rohde; Central Facility for Microscopy).

Figure 23 shows the semi-quantitative cell localization of the antibodies directed against RnfB, PrdA and RnfC alone in *C. difficile* 630Δ*erm*. Based on the measured cell area in relation to the background, the gold particles were counted and the localization events in gold particles/µm² were determined. The full circles show the occurence of the respective gold particles in the cell (cytoplasm and/or membrane), while the semicircles (closed at the top) indicate the presence of the gold particles in the cytoplasm, and the semicircles (closed at the bottom) the presence of the gold particles at the membrane. The white squares indicate the presence of the gold particles in the background. One circle or square represents 1 image series in which the gold particles have been counted. The mean values are indicated by the black bar of the respective sample.

The localization analyses showed that the RnfB alone has a mean value of > 5 gold particles/µm² in the cell. Most hits were at the membrane (> 5 gold particles/µm²) and less in the cytoplasm (< 5 gold particles/µm²). In the background a mean value below 5 gold particles/µm² was found, indicating a low unspecific binding of antibody against RnfB. Antibodies specific for PrdA showed that the mean value of gold particles in the cell was

below 5 gold particles/µm^2, with more events found at the membrane than in the cytoplasm. The mean value of the detected gold particles in the background was slightly above 0 gold particles/µm^2. The same relation was observed for the RnfC specific antibodies. Most of the hits were found at about 5 gold particles/µm^2 in the cell and most of them were observed at the membrane (> 5 gold particles/µm^2) and less in the cytoplasm (< 5 gold particles/µm^2). The background had the lowest number of events (< 5 gold particles/µm^2).

Figure 24 shows the semi-quantitative analyses of the co-localization events of PrdA and RnfB, RnfB and RnfC as well as RnfC and PrdA in *C. difficile* 630Δ*erm*. As described above, identical conditions for measuring the cell area and nomenclature (circle, semicircle, square, bar) were applied. In contrast to the single localization, events were counted from three data sets (with 21 - 25 images). On average for all tested double label combinations with a co-localization event value of under 5 gold particles/µm^2 was found in the cell. A more detailed inspection revealed that in all three combinations the co-localization events were mostly found at the membrane (on average > 5 gold particles/µm^2) and to a lower extent inside the cytoplasm (< 5 gold particles/µm^2). Although the co-localization events were not frequent, the semi-quantitative analyses showed a clear-cut tendency towards the binary-association of Prd and Rnf. It is also evident that gold particles were identified increasingly in the background.

4.4 In vitro *biochemically characterization of the* rnfC *mutant strain*

In order to gain better functional insights in terms of physiology and biochemistry into the pivoting role of the Rnf complex in *Clostridioides difficile* 630Δ*erm* in the frame work of the reductive energy-generating processes of the Stickland fermentation, the RnfC-encoding locus was truncated using the ClosTron® technique (see chapter 3.3.11). Thus, the group II intron harbored into the specific shuttle vector pMTL007C-E2 (tool: DNA2.0 from ATUM (US)), was designed to be integrated in the middle of the *rnfC* sequence CD630DERM_11370 at position 636|637s (Heap *et al.* 2007; Heap *et al.* 2010a; Heap *et al.* 2010b; Kuehne and Minton 2012). After transformation of the *E. coli* ST18 cells with the plasmid pMTL007C-E2:316671 (CDi_*rnfC*), this strain was used for genetic material transfer via mating into the *C. difficile* 630Δ*erm* wildtype (see chapter 3.3.3).
Afterwards, erythromycin-resistant clones were PCR-screened and a sanger sequenced to monitor proper integration of the group II intron. The resulting *rnfC*-deficient strain was termed CD630Δ*erm*_*rnfC*636/637s::*ermB* and employed for further characterization. The growth behavior of the newly generated strain was registered spectrophotometrically. The morphological phenotype of this strain was inspected by SEM imaging. Furthermore, the strain was biochemically explored *in vitro* (D-proline activity assay, toxin ELISA and NAD^+/NADH ratio) and it was studied at diverse omics levels.

4.4.1 Growth behavior and morphological characterization of a *rnfC* mutant

Firstly, the growth behavior of the constructed *rnfC* mutant strain CD630Δ*erm*_*rnfC*636/637s::*ermB* in comparison to the wildtype CD630Δ*erm* as descriped in chapter 3.2.7 was performed. Furhter, the cell morphology was monitored by SEM performed by Dr. Mathias Müsken (group of Prof. Dr. Manfred Rohde; Central Facility for Microscopy) at the HZI in Braunschweig according to the protocol described in chapter 3.6.1. For the growth behavior experiment both strains were inoculated at the same time point with an optical density of 0.05 and monitored over a 16 h period (figure 25). Five biological replicates were performed and the average measurements (cell density) were plotted (see appendix).

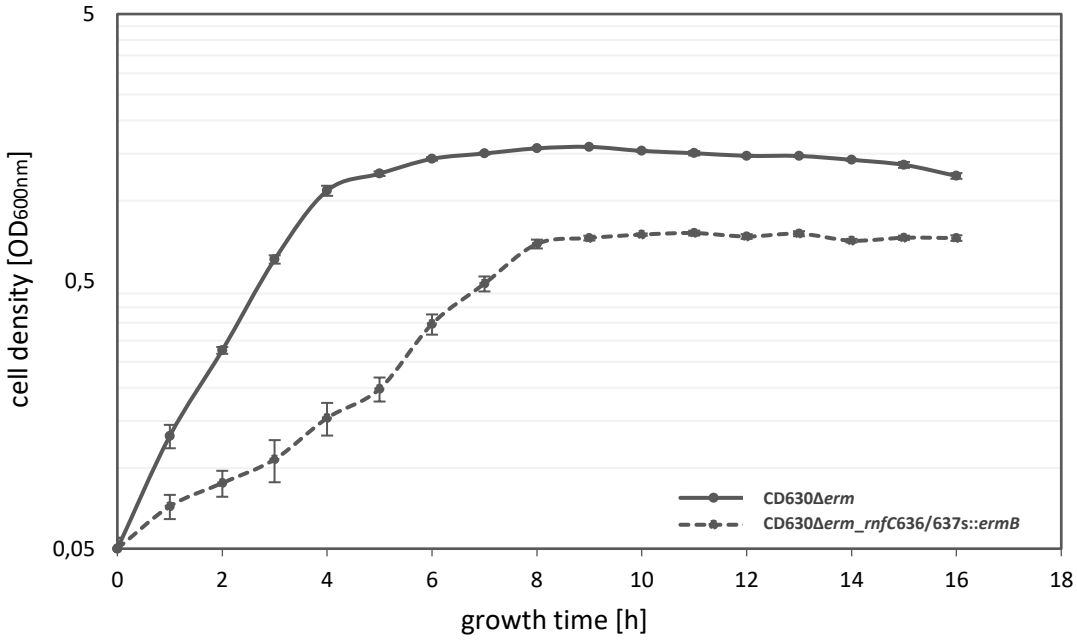

Figure 25: Growth curves of the wildtype (CD630Δ*erm*) (solid line) and the *rnfC* mutant (CD630Δ*erm_rnfC*636/637s::*ermB*) (dashed line) in BHI(S) medium over 16 h growth time. Both strains were inoculated at a cell density $OD_{600\ nm}$ of 0.05 and were grown for 16 hours under anaerobic conditions and at 37 °C until the stationary phase was reached. The cell densities of five replicates were measured every hour (see appendix) and the mean values with the corresponding standard deviation were determined. The data were presented in logarithmic scale (base 10).

The logarithmic curve in figure 25 represents the observed growth behavior of the wildtype (solid line) and the *rnfC* mutant strain (dashed line). The measured cell densities (at $OD_{600\ nm}$) were plotted on the Y-axis against the corresponding time points [X-axis]. The wildtype strain displayed the distinctive *C. difficile* growth phases. It showed a reduced lag phase and an exponential phase with a maximum cell density in terms of $OD_{600\ nm}$ value of 1.6 after 9 h. Subsequently, the bacterium entered the stationary phase.

In contrast, the *rnfC* mutant strain revealed an arrested growth behavior characterized by an extended exponential phase of over 11 h, reaching a maximum optical density of 0.76 [$OD_{600\ nm}$]. Clearly, a mutation of a gene for a subunit of the ion-pumping Rnf complex significantly impaired the growth of *C. difficile*. Besides the growth behavior, SEM imaging provided with further insights into morphological divergences between the two cell types (figure 26, panels [A] - [D]).

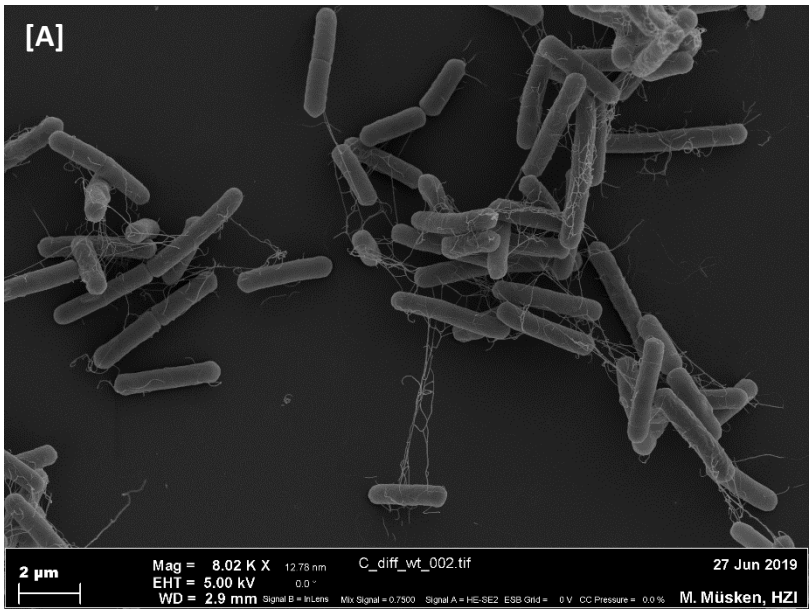
[A]
2 µm
Mag = 8.02 K X 12.78 nm
EHT = 5.00 kV 0.0 °
WD = 2.9 mm Signal B = InLens Mix Signal = 0.7500 Signal A = HE-SE2 ESB Grid = 0 V CC Pressure = 0.0 %
C_diff_wt_002.tif
27 Jun 2019
M. Müsken, HZI


[B]
2 µm
Mag = 8.02 K X 12.78 nm
EHT = 5.00 kV 0.0 °
WD = 2.9 mm Signal B = InLens Mix Signal = 0.7500 Signal A = HE-SE2 ESB Grid = 0 V CC Pressure = 0.0 %
C_diff_DrnfC_002.tif
27 Jun 2019
M. Müsken, HZI

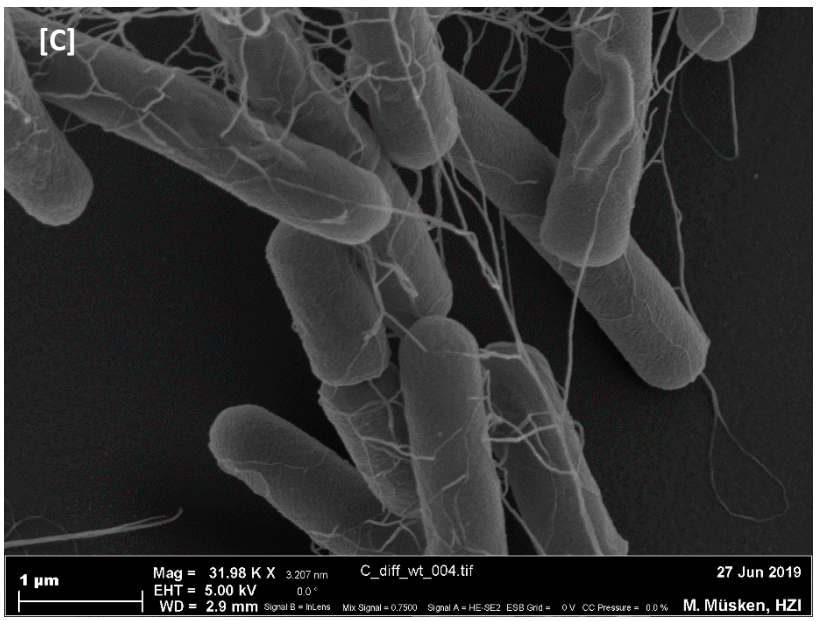
[C]
1 µm
Mag = 31.98 K X 3.207 nm
EHT = 5.00 kV 0.0 °
WD = 2.9 mm Signal B = InLens Mix Signal = 0.7500 Signal A = HE-SE2 ESB Grid = 0 V CC Pressure = 0.0 %
C_diff_wt_004.tif
27 Jun 2019
M. Müsken, HZI

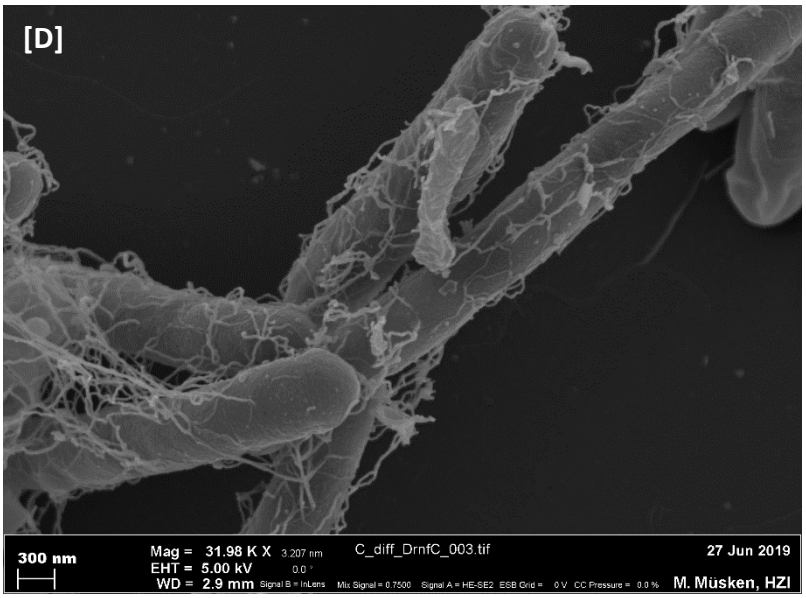

Figure 26: Scanning electron microscopy images of the wildtype and the *rnfC* mutant strain. Shown are the wildtype CD630Δ*erm* in panels [A] and [C] and the corresponding *rnfC* mutant CD630Δ*erm_rnfC*636/637s::*ermB* in panels [B] and [D]. Images in panels [A] and [B] show both strains at a magnification (Mag) of 8.02 K X and [C] and [D] of 31.98 K X. The scale bars were inserted. The images were taken at 5.00 kV (EHT) and 2.9 mm (WD) on Merlin (Carl Zeiss Microscopy GmbH, Jena, Germany) with the Everhart Thornley HESE2 detector and the inlens SE detector in a 25:75 ratio by Dr. Mathias Müsken at the HZI in Braunschweig (group of Prof. Dr. Manfred Rohde; Central Facility for Microscopy).

The SEM images show the wildtype strain CD630Δ*erm* in panels [A] and [C] and the *rnfC* mutant CD630Δ*erm_rnfC*636/637s::*ermB* in panels [B] and [D]. The figures showed both strains in different magnifications. Obviously, the wildtype formed rod-shaped cells, which were flagellated peritrichely. Clearly, the *rnfC* mutant had to an impaired flagellum formation and an attachement of the cells via the flagella and accumulated extracellular material sticking to the flagella.

4.4.2 D-proline reductase activity in dependence of a functional Rnf complex

To check if the absence of the RnfC subunit of the membrane ferredoxin-NAD^+: oxidoreductase Rnf complex of *C. difficile* 630Δ*erm* has an impact on the D-proline reductase a fluorometric activity assay was performed based on the work by Seto 1979 and Kabisch 2001. This assay monitors the activity of the enzyme D-proline reductase by the conversion of its substrate D-proline into the product 5-aminovalerate in a time-dependent manner. The bacterial cells of the wildtype CD630Δ*erm* and the *rnfC* mutant strain

CD630Δ*erm_rnfC*636/637s::*ermB* were grown anaerobically in the defined minimal medium CDMM. Samples were taken in the exponential (T1) and the stationary growth phase (T2). Afterwards, the cells were harvested and three biological replicates were analyzed as described in chapter 3.6.2 and 3.6.3. For this purpose, 5 µg protein of cytosolic extract containing the D-proline reductase were mixed with the substrate D-proline and incubated for 60 min at 30 °C. Seperately, a negative control carrying solely dH_2O instead of D-proline was included and the samples were treated identically. Thereby, the 5-aminovalerate which had already been formed intracellulary during cell growth in CDMM was determined and excluded from the data. A 5-aminovalerate calibration curve was also performed (see digital appendix). After quenching the reaction with 5 % perchloric acid, the samples were mixed with the reagent o-phthaldialdehyde. The non-fluorescence reagent reacted with 5-aminovalerate producing a fluorescent PH-5-aminovalerate with a fluorescence excitation peak around 330 nm and an emission peak at 450 nm (Seto 1979; Kabisch 2001). Consequently, the relative fluorescence intensities were measured at the emission peak point (450 nm) using the FP-8500 Fluorescence Spectrometer (JASCO Deutschland GmbH, Pfungstadt, Germany) (see appendix and digital appendix).

For both strains (wildtype and *rnfC* mutant) at T1 and T2 the normalized fluorescence intensities were deduced by substraction of the relative fluorescence intensities of PH-5-aminovalerate in the negative control sample (already formed 5-aminovalerate in the cell) from the values obtained for corresponding samples containing reacted D-proline. Afterwards, the actual concentrations [nmol] of the enzymatically formed 5-aminovalerate were calculated utilizing the calibration curve (linear regression, see appendix). The comparison of the product formation (mean values) by the D-proline reductase from the wildtype and the *rnfC* mutant strain cell free extracts at the exponential (T1) and stantionary growth phase (T2) were graphically represented in the figure 27.

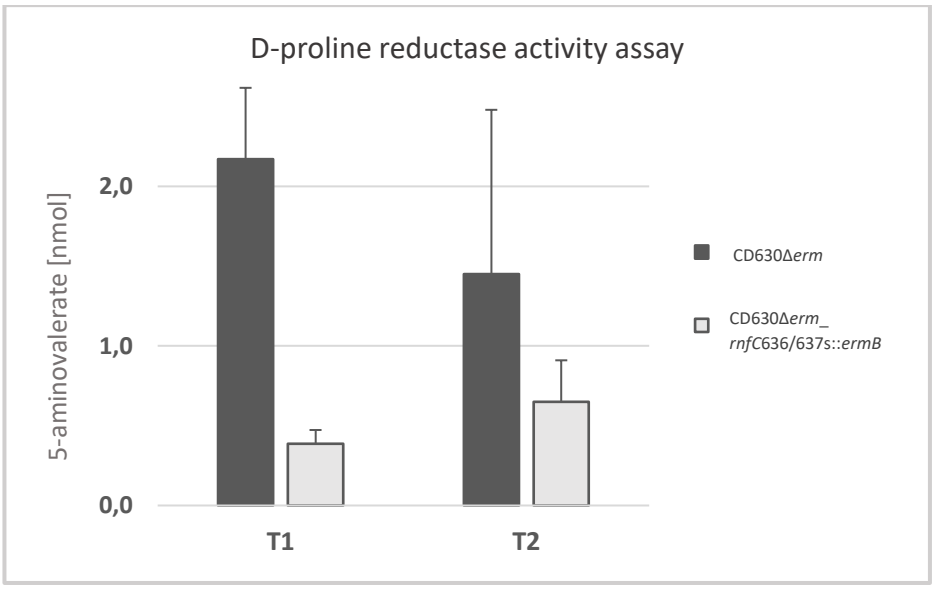

Figure 27: The 5-aminovalerate production by D-proline reductase in cell free extracts of the wildtype and the *rnfC* mutant strain. In the activity assay for D-proline reductase 5 µg protein of cytosolic cell free extracts of each strain (dark bars: wildtype CD630Δ*erm* and bright bars: *rnfC* mutant CD630Δ*erm*_*rnfC*636/637s::*erm*B) were incubated with the substrate (100 mM D-proline) at 30 °C for 60 min. Before, samples were taken in the exponential (T1) and stationary (T2) growth phases. The emission at 450 nm was determined after addition of o-phthaldialdehyde using a FP-8500 Fluorescence Spectrometer (JASCO Deutschland GmbH, Pfungstadt, Germany). Using a 5-aminovalerate standard, the concentrations of the product in the respective sample were determined.

Figure 27 shows the amounts of 5-aminovalerate [nmol] formed by the cytosolic cell free extract containing D-proline reductase from the wildtype (dark grey bar) and the *rnfC* mutant strain (bright grey bar) determined at two different time points during the growth phase. The diagram illustrates that the D-proline reductase activity of the wildtype cell free extract yielded a total amount of 2.17 nmol 5-aminovalerate at T1 and 1.45 nmol at T2. In contrast, the values of the 5-aminovalerate formed by the D-proline reductase contained in *rnfC* mutant cell free extract at T1 and T2 were 0.39 nmol and 0.65 nmol, respectively (see appendix). Obviously, an intact Rnf complex is a functional prerequisite for efficient D-proline reductase activity in *C. difficile*.

4.4.3 Cellular NAD$^+$/NADH ratio of the wildtype and the *rnfC* mutant strain

The NAD$^+$/NADH ratio in the wildtype CD630Δ*erm* and in the *rnfC* mutant strain CD630Δ*erm_rnfC*636/637s::*ermB* were determined to test for the physiological consequences of a lack of the RnfC subunit. As mentioned above, both strains were grown anaerobically until the time points T1 (exponential growth phase) and T2 (stationary growth phase) were reached in defined minimal medium CDMM and the bacteria cells were subsequently harvested. The cell pellets of five biological replicates were prepared according to the protocol described in chapter 3.6.4 by Dr. Petra Henke and Dr. Sabine Will (group of Dr. Meina Neumann-Schaal; Bacterial Metabolomics) at the DSMZ in Braunschweig. The mean values of NAD$^+$ and NADH were determined using the NAD$^+$/NADH Glo Assay kit (Promega GmbH, Madison, USA). The following table 24 shows the NAD$^+$ and NADH content of both strains at time point T1 and T2. The values were provided by Dr. Petra Henke.

Table 24: Determination of the NAD$^+$/NADH ratio in the wildtype CD630Δerm and in the rnfC mutant strain CD630Δerm_rnfC636/637s::ermB in the exponential (T1) and stationary growth phases (T2)

Strain	Time point	Mean value NAD$^+$ [nmol/mg]	Mean value NADH [nmol/mg]	NAD$^+$/ NADH ratio
CD630Δ*erm*	T1	924.05	12.11	**76**
	T2	2407.58	195.60	**12**
CD630Δ*erm_rnfC*636/637s::*ermB*	T1	977.28	26.48	**37**
	T2	1686.73	10.31	**164**

The table 24 shows the cellular content of NAD$^+$ [nmol/mg], NADH [nmol/mg] and the ratio of both cofactors (NAD$^+$/ NADH) of the wildtype CD630Δ*erm* and the *rnfC* mutant strain CD630Δ*erm_rnfC*636/637s::*ermB*. The wildtype generated at T1 a total amount of 924.05 nmol/mg NAD$^+$ and 12.11 nmol/mg NADH. At the time point T2 the values increased up to 2407.58 nmol/mg NAD$^+$ and 195.60 nmol/mg NADH. This led to a 76-fold NAD$^+$ excess compared to NADH at the exponential growth phase (T1). This ratio was reduced by a factor of 12 in the stationary growth phase (T2).

In contrast, the mutant strain showed 977.28 nmol/mg NAD^+ and 26.48 nmol/mg NADH at T1, whereas in the stationary growth phase (T2) the NAD^+ level increased to 1686.73 nmol/mg and the NADH level decreased to 10.31 nmol/mg. These values resulted in a NAD^+/NADH ratio of 37 at T1 and a clearly detectable accumulation of the NAD^+ in the mutant strain cells at the stationary growth phase T2 by a factor of 164. Clearly, the *rnfC* mutant had to deficient NADH formation with an overall decreased NAD^+ amount. A disturbed central energy metabolism can be concluded.

4.4.4 Influence of the *rnfC* mutant on the formation of the toxins TcdA and TcdB

The human pathogenic bacterium *C. difficile* has the ability to produce the toxins TcdA and TcdB. The production is strictly linked to the reductive part of the Stickland fermentation (Bouillaut *et al.* 2013). The impact of RnfC subunit absence on toxin production was tested using the kit: „ELISA for the separate detection of *Clostridium difficile* Toxin A OR Toxin B in suspensions kit" (tgcBIOMICS GmbH; Bingen, Germany). The production of both toxins was determined seperately. For the test, both strains were grown in defined CDMM until they reached the exponential (T1) and the stationary growth phase (T2) according to chapter 3.6.2. Afterwards, cells were separated from the growth medium via centrifugation. The cell-free growth medium expected to contain secreted toxins of both strains obtained at indicated time points was tested immunologically for the presence of toxins using a sandwich ELISA kit as described in chapter 3.6.5. In this test the toxins were detected by a colometric chemical reaction step driven by horse radish peroxidase coupled to antibodies specific for TcdA or TcdB. Afterwards the colometric reaction was stopped and the ODs at 450 nm and 620 nm were measured spectrophotometrically in a microtiter plate photometer Infinite® 200 (Tecan Group Ltd., Männedorf, Switzerland). A standard and a negative control were also tested likewise. Afterwards, $OD_{450\text{-}620\ nm}$ values were determined. The TcdA and TcdB concentration in each sample of five biological replicates was calculated using the standard in linear equation (see appendix and digital appendix).

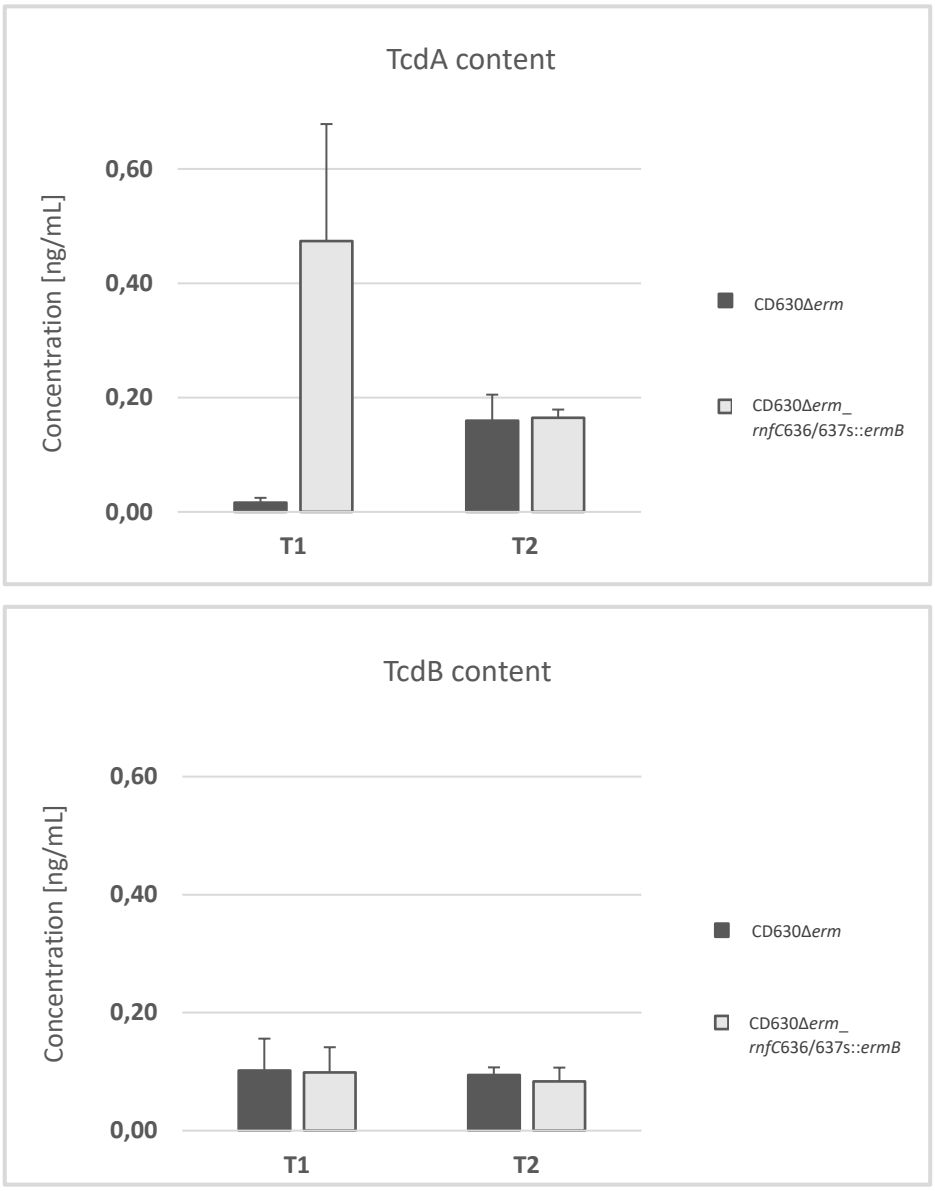

Figure 28: Toxin formation in the wildtype and the *rnfC* mutant strain. The toxin content (TcdA and TcdB) in the growth medium of the wildtype (CD630Δ*erm*) (dark bar) and the *rnfC* mutant strain (CD630Δ*erm*_*rnfC*636/637s::*ermB*) (bright bar) were determined in the exponential (T1) and stationary growth phase (T2). Using a colometric horse radish peroxidase-driven reaction in a sandwich ELISA by the measurement of $OD_{450\text{-}620\,nm}$ the TcdA or TcdB concentrations were determined in the samples. The TcdA concentration in the growth medium of the wildtype at T1 was 0.016 ng/mL and 0.160 ng/mL at T2. In the *rnfC* mutant strain growth medium the TcdA concentration at T1 was 0.474 ng/mL and 0.164 ng/mL at T2. The TcdB concentration in the wildtype growth medium was 0.102 ng/mL at T1 and 0.094 ng/mL at T2. In comparison the TcdB concentration of the *rnfC* mutant strain at T1 was 0.099 ng/mL and 0.083 ng/mL at T2.

Figure 28 shows the amount of toxin TcdA and TcdB, which is released into the growth medium during cell growth of the different strains in CDMM. The concentrations of TcdA and TcdB in the medium of the wildtype (dark grey bar) and the *rnfC* mutant strain (bright grey bar) at the time points T1 and T2 are shown. The TcdA concentrations in the wildtype CD630Δ*erm* growth medium were 0.016 ng/mL at T1 and 0.160 ng/mL at T2. In contrast, the TcdA concentrations in the growth medium of the *rnfC* mutant at T1 was 0.474 ng/mL and 0.164 ng/mL in T2. Strikingly, the values measured at T1 show that the TcdA concentration in the growth medium of the mutant strain was 30-fold higher as of the wildtype. The figure also shows that the concentrations of TcdB formation did not vary significantly between the two strains. TcdB concentrations of 0.102 ng/mL at T1 and 0.094 ng/mL at T2 were determined for the wildtype strain. The TcdB concentrations in the growth medium of the *rnfC* mutant were 0.099 ng/mL at T1 and 0.083 ng/mL at T2. Obviously, the *rnfC* mutant strain leads to the re-programming of the central energy metabolism causing a drastic increase in TcdA formation.

4.4.5 Changes in the metabolism of the *rnfC* mutant holistically measured by metabolomics, transcriptomics and proteomics

Measured D-proline reductase activity levels, the NAD^+/NADH ratio and the TcdA values indicated a major re-organization of the energy metabolism of *C. difficile* by the *rnfC* mutation. To obtained detailed insights into underlying data products and intermediate metabolites including cytoplasmatically metabolites, CoA derivates, exometabolites and volatile derivatives from different metabolic pathways were measured for both strains. For this purpose, both strains were grown under anaeobic conditions at 37 °C in defined medium CDMM as described above and the bacteria cells were harvested in the exponential (T1) and in the stationary growth phase (T2). The resulting cell pellets were used for the subsequent experiments (see chapter 3.6.6).

The measurements of polar metabolites, volatile compounds and coenzyme A derivatives were performed by GC-MS (Agilent GC-MSD system (Agilent Technologies, Santa Clara, USA)/ PAL RTC system (CTC Analytics AG; Zwingen, Switzerland)) or Agilent LC-QTOF system (Agilent Technologies, Santa Clara, USA). Here, the measurements and the corresponding analyses of the resulting raw data were performed by Dr. Meina Neumann-Schaal and Dr. Sabine Will (group of Dr. Meina Neumann-Schaal; Bacterial Metabolomics) at the DSMZ in Braunschweig. The data were provided in a MS Excel® file (Microsoft® Corporation, Washington, USA) (see digital appendix). Free amino acids in the growth medium were measured on a HPLC system (Agilent Technologies, Santa Clara, USA) following the protocol described by Trautwein *et al.* 2016; Dannheim *et al.* 2017; Hofmann *et al.* 2018 (see chapter 3.6.6). The measurements and corresponding values were also performed and provided by Dr. Meina Neumann-Schaal and Dr. Sabine Will in MS Excel® (Microsoft® Corporation, Washington, USA).

The analyzed metabolites in the wildtype and the *rnfC* mutant strain

A total amount of 84 metabolites were found in the cell free extracts of both strains (wildtype CD630Δ*erm* and *rnfC* mutant strain CD630Δ*erm*_*rnfC*636/637s::*ermB*) at the time points T1 and T2 during the different growth phases. The data represent the mean values of five biological replicates and the fold changes were extracted (mean values of the peak areas of the *rnfC* mutant devided to mean values of the peak areas of the wildtype) at the time points T1 and T2. Subsequently, the compounds that were within a fold change threshold range of 0.67 to 1.5 at both time points were ruled out. Fold change values of compounds above 1.5 indicated a significant accumulation and values below the limit of 0.67 indicated a reduced presence in the *rnfC* mutant strain compared to the wildtype strain at T1 or T2 (see appendix and digital appendix). After applying this cut-off criteria 56 metabolites (figure 29) were analyzed in more detail.

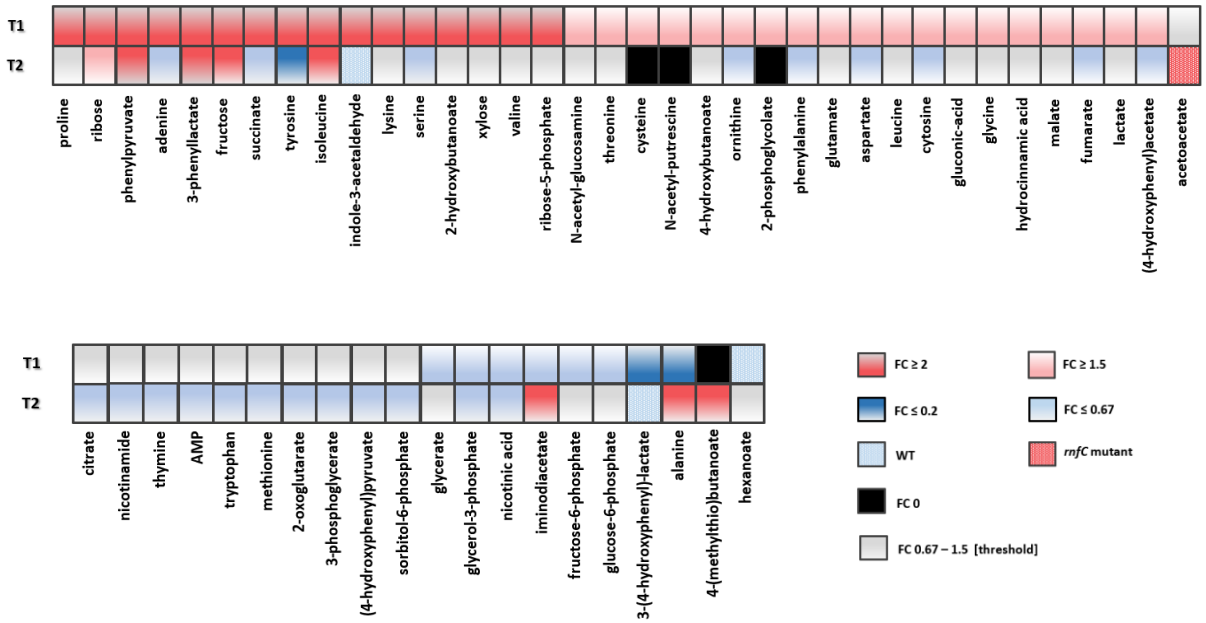

Figure 29: Heatmap of the determined fold changes (FC) of the values for metabolites extracted from the *rnfC* mutant strain CD630Δ*erm*_*rnfC*636/637s::*ermB* in comparison to the wildtype CD630Δ*erm* at time points T1 and T2. Shown are the fold change (FC) values (*rnfC* mutant versus wildtype) of the 56 GC-MS measured metabolites of the *rnfC* mutant strain compared to the wildtype in the exponential growth phase T1 (upper row) and in the stationary growth phase T2 (lower row). By using the threshold values of FC 0.67 to 1.5 (grey) (indicating no significant change between mutant strain and wildtype) the metabolites were sorted according to their relative amount. The coloration shows the accumulation (FC > 1.5 and 2, red color) and the reduced amounts (FC < 0.67 and 0.2, blue color) of metabolites in the cell free extracts of the *rnfC* mutant strain compared to the wildtype strain. Here, the order of the metabolites in the graph shows the development of the highly accumulated (FC > 2) to the reduced amounts of derivatives (FC < 0.2) at T1. The graph shows by far the highest accumulation of proline with FC of 60 at T1. Followed by ribose (FC of 7.8) and phenylpyruvate (FC of 7.4). Compounds such as alanine (FC of 0.05) or 3-(4-hydroxyphenyl)-lactate (FC of 0.1) at T1 were found highly reduced in the mutant strain. The highest accumulation of phenylpyruvate (FC of 7.9) and a reduced amount of tyrosine (FC of 0.2) in the mutant cell free extract compared to the wildtype was observed at T2. Acetoacetate was only present in the mutant strain at T2. 3-(4-hydroxyphenyl)-lactate, indole-3-acetaldehyde at T2 and hexanoate at T1 were only present in the wildtype strain. The metabolites that were not found in both strains at T1 or T2 are marked in black.

The figure 29 shows the heatmap of the 56 metabolites that were accumulated or decreased at T1 or T2 in the *rnfC* mutant strain compared to the wildtype. The values at T1 begin with the most abundant metabolite, proline with an FC value of 60 and end with the most reduced metabolite of alanine (FC of 0.05). It is observed that metabolites like ribose (FC of 7.8), phenylpyruvate (FC of 7.4), adenine (FC of 6.1) and 3-phenyllactate (FC of 5.3) were significantly accumulated in the mutant strain in the exponential growth phase T1.

Metabolites like phenylpyruvate (FC_{T1} of 7.4; FC_{T2} of 7.85), 3-phenyllactate (FC_{T1} of 5.3; FC_{T2} of 6.1) and fructose (FC_{T1} of 4.1; FC_{T2} of 2.6) were found highly accumulated in the *rnfC* mutant cell at T1 and T2, while tyrosine (FC of 0.2) and succinate (FC of 0.2) were found reduced at T2. Acetoacetate was also only detected in the *rnfC* mutant at T2.

Nicotinic acid (FC_{T1} of 0.6; FC_{T2} of 0.4) and glycerol-3-phosphate (FC_{T1} of 0.6; FC_{T2} of 0.5) were found rarely present in the *rnfC* mutant at T1 and T2. In contrast hexanoate, 3-(4-hydroxyphenyl)-lactate and indole-3-acetaldehyde were only present in the wildtype at T1 or T2. Derivates that were not found in both strains at the same time (T1 or T2) were marked in black in figure 29.

The CoA-esters found in the wildtype and the *rnfC* mutant strain

A total amount of 52 CoA-esters were found in the cell free extracts of the wildtype and the *rnfC* mutant strain at the time points T1 and T2. Subsequently, the identically treshhold range as mentioned before were used and the corresponding fold change values were determined. After applying this cut-off criteria 41 CoA-esters (figure 30) were found.

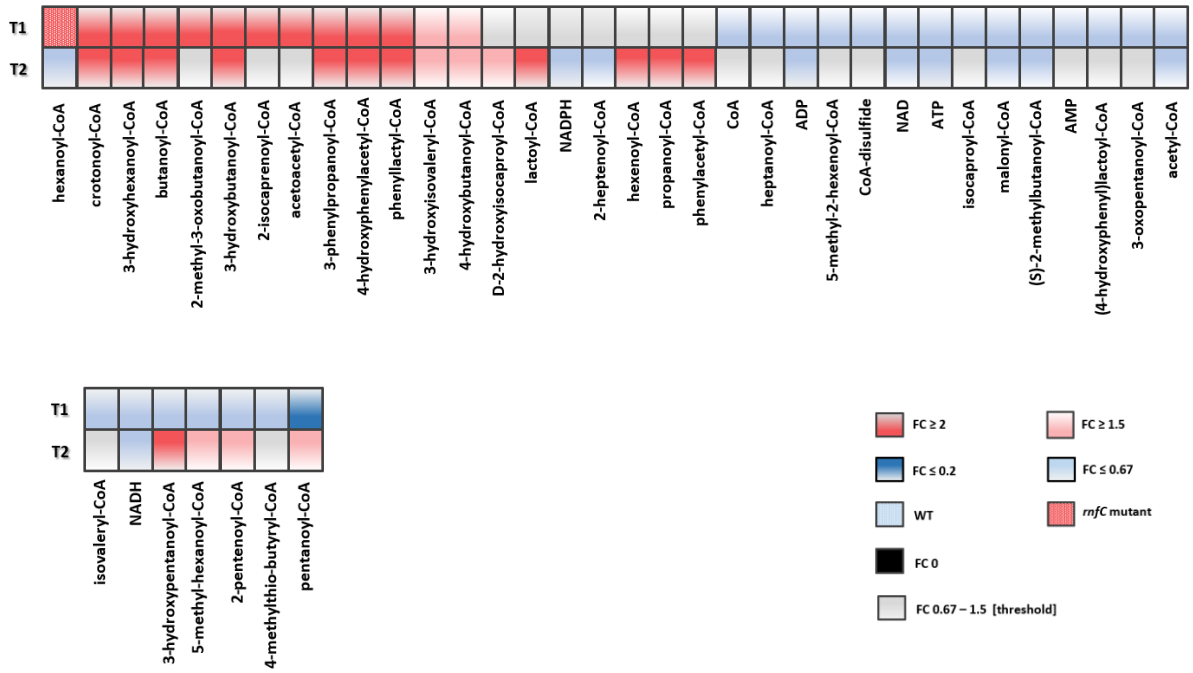

Figure 30: Heatmap of the determined fold changes (FC) for CoA-esters extracted from the *rnfC* mutant strain CD630Δ*erm*_*rnfC*636/637s::*ermB* in comparison to the wildtype CD630Δ*erm* at the time points T1 and T2. Shown are the fold change (FC) values (*rnfC* mutant versus wildtype) of the 41 LC-MS measured CoA-esters of the *rnfC* mutant in comparison to the wildtype in the exponential growth phase T1 (upper row) and in the stationary growth phase T2 (lower row). FC 0.67 to 1.5 (grey) (indicating no significant change between the *rnfC* mutant strain and wildtype). CoA-ester accumulation was determined by a FC > 1.5 and 2 shown in red color, while values of FC < 0.67 and 0.2 shown a reduced ester amount (blue color). Here, the accumulation of e.g. crotonyl-CoA (FC of 9.4), 3-hydroxyhexanoyl-CoA (FC of 7.5) and butanoyl-CoA (FC of 7.2) at T1 were visible. Derivatives such as pentanoyl-CoA (FC of 0.2) or 4-methylthio-butyryl-CoA (FC of 0.3) at T1 were highly reduced in the *rnfC* mutant strain. Interestingly, hexanoyl-CoA was only present in the *rnfC* mutant strain at T1. CoA-esters that were not found in both strains at the same time are marked in black.

The heatmap in figure 30 shows the fold changes of CoAs at T1 or T2 in the *rnfC* mutant strain compared to the wildtype. Here, 2-methyl-3-oxobutanoyl-CoA (FC of 6.0), 2-isocaprenoyl-CoA (FC of 5.4) and acetoacetyl-CoA (FC of 3.3) were found highly accumulated in the mutant strain at T1. In contrast, pentanoyl-CoA (FC of 0.2), 4-methylthio-butyryl-CoA (FC of 0.3) and 2-pentenoyl-CoA (FC of 0.3) were only present in highly reduced quantities. At T2 lactoyl-CoA (FC of 4.1), 3-hydroxypentanoyl-CoA (FC of 4.0), hexenoyl-CoA (FC of 2.7), phenylacetyl-CoA (FC of 2.3) and propanoyl-CoA (FC of 2.1) were accumulated and NADH (FC of 0.3), hexanoyl-CoA (FC of 0.4) and ATP (FC of 0.4) were quantitatively reduced in the *rnfC* mutant strain.

NADH (FC_{T1} of 0.3; FC_{T2} of 0.3), ATP (FC_{T1} of 0.6; FC_{T2} of 0.4), NAD^+ (FC_{T1} of 0.6; FC_{T2} of 0.5), ADP (FC_{T1} of 0.6; FC_{T2} of 0.5), malonyl-CoA (FC_{T1} of 0.5; FC_{T2} of 0.6), (S)-2-methyl-butanoyl-CoA (FC_{T1} of 0.5; FC_{T2} of 0.6) and acetyl-CoA (FC_{T1} of 0.4; FC_{T2} of 0.6) revealed reduced amounts in the *rnfC* mutant strain at T1 and T2 in comparison to the wildtype. In contrast, 3-hydroxybutanoyl-CoA (FC_{T1} of 5.6; FC_{T2} of 4.9), crotonoyl-CoA (FC_{T1} of 9.4; FC_{T2} of 4.1), phenyllactyl-CoA (FC_{T1} of 2; FC_{T2} of 3.2), 3-hydroxyhexanoyl-CoA (FC_{T1} of 7.5; FC_{T2} of 2.9), 3-phenylpropanoyl-CoA (FC_{T1} of 2.3; FC_{T2} of 2.7), butanoyl-CoA (FC_{T1} of 7.2; FC_{T2} of 2.5) and 4-hydroxyphenylacetyl-CoA (FC_{T1} of 2.3; FC_{T2} of 2.3) were found highly enriched in the mutant strain. Only hexanoyl-CoA was present in the *rnfC* mutant strain at T1.

The volatiles of the *rnfC* mutant strain in comparison to the wildtype

Furthermore, 20 volatile acids were found in the cell free extracts of the wildtype and the *rnfC* mutant strain and at the time points T1 and T2 during the different growth phases. Fold change values in consideration of the mentioned-above threshold were determined. Finally, 15 volatile acids were analyzed in more detail (figure 31).

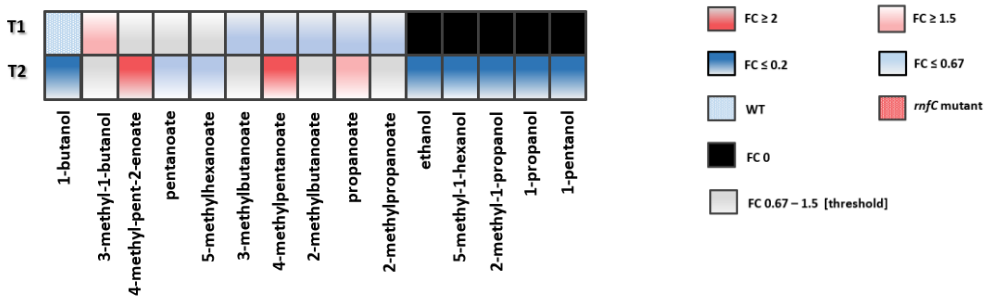

Figure 31: The heatmap of the determined fold changes (FC) of volatile acids extracted from the *rnfC* mutant strain CD630Δ*erm*_*rnfC*636/637s::*ermB* in comparison to the wildtype CD630Δ*erm* at T1 and T2. Shown are the FC values of the 15 GC-MS measured volatile acids of the *rnfC* mutant strain in comparison to the wildtype at T1 (upper row) and at T2 (lower row). By using the threshold values FC 0.67 to 1.5 (grey) volatiles out of that range were focused in more detail. Here, 3-methyl-1-butanol (FC of 1.6) at T1 and 4-methyl-pent-2-enoate (FC of 2.7) at T2 were highly accumulated in the *rnfC* mutant strain. Whereby, 2-methylpropanoate (FC of 0.4) at T1 and 2-methyl-1-propanol (FC of 0.1), 1-propanol (FC of 0.1), 1-pentanol (FC of 0.1), ethanol (FC of 0.2) and 5-methyl-1-hexanol (FC of 0.2) at T2 were detected in a highly reduced amount in the *rnfC* mutant strain. Only 1-butanol was found in the wildtype at T1 and with a highly reduced value at T2 in the mutant strain.

The figure 31 describes the determined fold change values for the detected volatile acids in the *rnfC* mutant strain compared to the wildtype at T1 and T2. It is evident that 3-methyl-1-butanol (FC of 1.6) was highly accumulated at T1, while 2-methylpropanoate (FC of 0.4), propanoate (FC of 0.5), 2-methylbutanoate (FC of 0.5), 4-methylpentanoate (FC of 0.5) and 3-methylbutanoate (FC of 0.6) were present in reduced quantities at the same time. In the stationary phase (T2) 4-methyl-pent-2-enoate (FC of 2.7), 4-methylpentanoate (FC of 2.4) and propanoate (FC of 1.6) were accumulated in the mutant strain. In contrast, 1-butanol (FC of 0.03), 2-methyl-1-propanol (FC of 0.1), 1-propanol (FC of 0.1), 1-pentanol (FC of 0.1), ethanol (FC of 0.2) and 5-methyl-1-hexanol (FC of 0.2) were detected in reduced quantities in the *rnfC* mutant at the same time. However, 1-butanol only occurred at T1 in the wildtype.

The exometabolites and amino acids of the *rnfC* mutant strain compared to the wildtype

Overall, 30 exometabolites were found in the growth medium of the *rnfC* mutant strain and the wildtype strain at T1 and T2. After applying the above-mentioned settings and thresholds (FC 0.67 to 1.5) 20 exometabolites were found significantly changed in the concentrations. Additionally, 12 amino acids and 5-aminovalerate were found in different concentrations in the growth medium (FC values see appendix). Figure 32 shows the compounds and the amino acids that were found in the exometabolome.

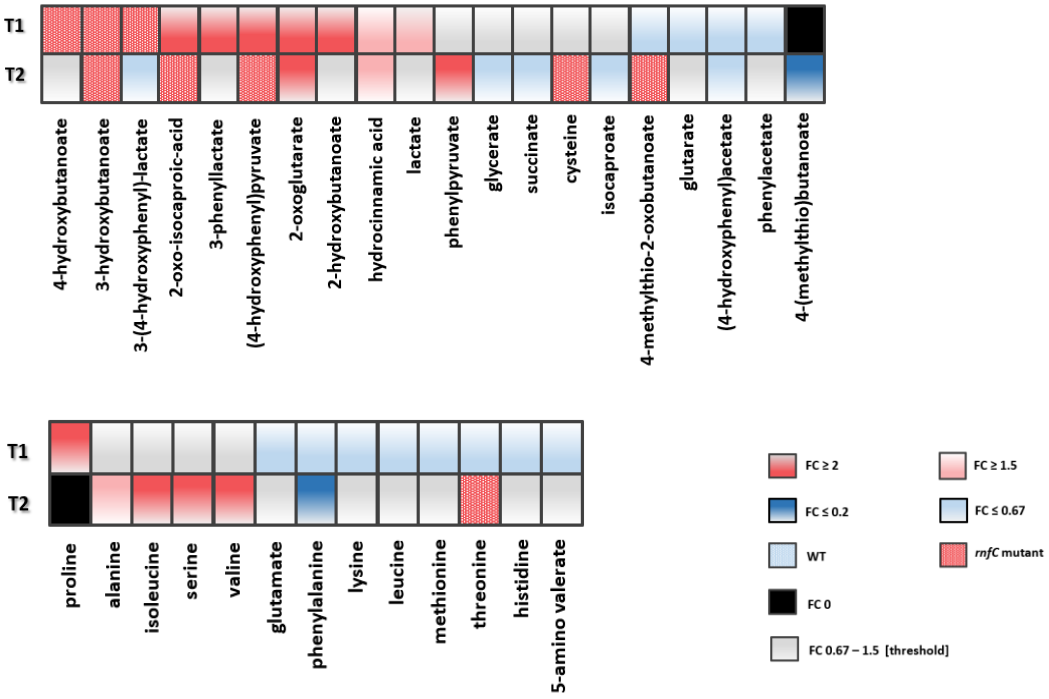

Figure 32: The heatmap of the determined fold changes (FC) of the exomatabolites and amino acids extracted from the growth medium of the *rnfC* mutant strain CD630Δ*erm*_*rnfC*636/637s::*ermB* in comparison to the wildtype CD630Δ*erm* at T1 and T2. The figure shows the FC values of the 20 measured exometabolites, 12 amino acids and 5- amino valerate analyzed from the growth medium of the *rnfC* mutant in comparison to the wildtype at T1 (upper row) and at T2 (lower row). The threshold range were from FC 0.67 to 1.5 (grey) (indicating no significant change between mutant strain and wildtype). Compounds with FC values > 1.5 (red) and < 0.67 (blue) at T1 or T2 were in the focus. Here, 2-oxo-isocaproic-acid (FC of 5.1) and proline (FC of 7.6) at T1 were the highest accumulated compounds. Phenylacetate (FC of 0.4) and threonine (FC of 0.6) were observed in a reduced amount from the *rnfC* mutant strain growth medium at T1. In contrast, phenylpyruvate (FC of 7.9) and isoleucine (FC of 5.2) are highly accumulated at T2 in the mutant strain. 4-hydroxybutanoate and 3-(4-hydroxyphenyl)-lactate at T1 and 2-oxo-isocaproic-acid, (4-hydroxyphenyl) pyruvate, cysteine, 4-methylthio-2-oxobutanoate and threonine at the time point T2 were found in the growth medium of the *rnfC* mutant strain but not in the wildtype (dotted red). Only 3-hydroxybutanoate was observed in the growth medium of the mutant strain.

It is shown that acidic metabolites and amino acids like 2-oxo-isocaproic-acid (FC of 5.1), 3-phenyllactate (FC of 4.7), (4-hydroxyphenyl) pyruvate (FC of 3.3), 2-hydroxybutanoate (FC of 2.3) and proline (FC of 7.6) were highly accumulated at T1 in the growth medium of the *rnfC* mutant strain. Phenylacetate (FC of 0.4), (4-hydroxyphenyl) acetate (FC of 0.5), glutarate (FC of 0.5), histidine (FC of 0.5), threonine (FC of 0.6) and 5-aminovalerate (FC of 0.35) on the other hand were found in reduced quantities at T1. At T2, when the *rnfC* mutant strain entered the stationary growth phase, phenylpyruvate (FC of 7.9),

2-oxoglutarate (FC of 3.0) and hydrocinnamic acid (FC of 1.8) and the amino acids isoleucine (FC of 5.2), valine (FC of 2.5) and serine (FC of 2.4) were found accumulated in the growth medium of the *rnfC* mutant strain. It became also visible that 2-oxoglutarate (FC_{T1} of 2.3; FC_{T2} of 3.0) was highly enriched at T1 and T2.

Interestingly, 4-hydroxybutanoate and 3-(4-hydroxyphenyl)-lactate at T1 and 2-oxo-isocaproic-acid, (4-hydroxyphenyl) pyruvate, cysteine, 4-methylthio-2-oxobutanoate and threonine were only present in the growth medium of the *rnfC* mutant strain at T2. Finally, 3-hydroxybutanoate was only visible at T1 and T2 in the growth medium of the mutant strain.

Transcriptomics and proteomics of the wildtype and the *rnfC* mutant strain

For the comparative analyses of gene expression in the *rnfC* mutant strain CD630Δ*erm_rnfC*636/637s::*ermB* versus the wildtype CD630Δ*erm* transcriptomics and proteomics experiments were performed for both strains at the time points T1 and T2 (see chapter 3.6.2). For transcriptomics, the RNA of the strains (at T1 and T2) were isolated and followed by rRNA depletion and cDNA libraries construction according to the protocol described in chapter 3.6.6. Finally, the cDNA sequencing was performed using the Illumina NextSeq system with the NextSeq 500/550 High Output Kit v2.5 (75 cycles) (Illumina Inc, San Diego, USA). The software Rockhopper version 2.03 (McClure *et al*. 2013; Tjaden 2015) was used to map the cDNA reads to *C. difficile* 630 genome. Afterwards, the mean value of five biological replicates were calculated and the log2 fold change of each transcript of the *rnfC* mutant strain against the wildtype at T1 and T2 were determined (see digital appendix). After RNA isolation the further RNA sample treatment and cDNA libraries preparation/ measurements, RNA mapping, Rockhopper analyses and log2 fold change calculation were performed by Dr. Petra Henke and Dr. Sabine Will (group of Dr. Meina Neumann-Schaal; Bacterial Metabolomics) at the DSMZ in Braunschweig. Afterwards, the data were provided in MS Excel® (Microsoft® Corporation, Washington, USA) for further analyses.

The total amount of transcripts found in the *rnfC* mutant strain and in the wildtype was 1653. Transcripts with a low expression value (<2) for all strains at both time points and transcripts encoding proteins involved in generic cell functions like chaperones, ABC

transporter, cell division/surface proteins, cold shock proteins, DNA ligase/gyrase, polymerases, hypothetical proteins, lipoproteins or multidrug resistance proteins were discared from the study. Ultimately, 1201 transcripts were analyzed closely.

The proteomics was performed using samples from three biological replicates from both strains at T1 and T2 as described in chapter 3.6.6 by Dr. Josef Wissing and Hedwig Schrader at the HZI in Braunschweig (group of Prof. Dr. Lothar Jänsch; Cellular Proteome Research). In total, 1298 proteins were identified in the samples of the strains CD630Δ*erm*_*rnfC*636/637s::*ermB* and CD630Δ*erm* at T1 and 1567 proteins at T2. Afterwards, proteins with a unique peptide value > 1 and occurring in at least two biological replicates for one strain were analyzed more in detail. Therefore, 1004 proteins from T1 and 1323 proteins from T2 were identified. The mean values and the log2 fold change factors of proteins from the *rnfC* mutant strain compared to the wildtype at T1 and T2 were calculated (see digital appendix).

Found proteins and their respective transcripts were further categorized into metabolic pathways or cell functions regarding to their relation to energy production in *C. difficile* and according to previously identified metabolic compounds and the results of the toxin ELISAs. Here, the enzymes responsible for the generation of certain compounds released in a specific metabolic step were determined via KEGG. Obtained log2 fold changes (log2 FC) for the transcripts and abundant proteins for the *rnfC* mutant strain in comparison to the wildtype were included in the table 25 subdivided for the time points T1 and T2. Transcripts and proteins with a log2 FC value of 0 indicate an identical amount of both in the *rnfC* mutant and wildtype. Values > 0 indicate the upregulation of the respective gene or a higher protein abundance in the *rnfC* mutant strain. Consequently, log2 FC values for transcripts and proteins of < 0 indicate a gene down regulation or a low protein abundance in the *rnfC* mutant strain.

Table 25: Determination of the log2 fold changes (log2 FC) of transcripts and proteins for the *rnfC* mutant strain CD630Δ*erm*_*rnfC*636/637s::*ermB* versus the wildtype CD630Δ*erm* at the time points T1 and T2

Metabolic pathway (metabolomic compounds)	Protein description	Transcriptomics (log2 FC)		Proteomics (log2 FC)	
		T1	T2	T1	T2
Reductive Stickland fermentation					
Electron transport complex protein	Electron transport complex protein (***rnfB***)	-3.52	-2.62	-3.94	-2.08
Electron transport complex protein	Electron transport complex protein (***rnfC***)	0.12	0.91	-7.34	-1.31
Electron transport complex protein	Electron transport complex protein (***rnfD***)	-3.09	-2.91	-	-4.41
Electron transport complex protein	Electron transport complex protein (***rnfE***)	-3.34	-3.04	-	-
Electron transport complex protein	Electron transport complex protein (***rnfG***)	-3.05	-2.82	-6.89	-6.60
Proline ↔ D-proline	Proline racemase (***prdF***)	-0.01	3.53	-0.87	0.53
D-proline → 5-amino pentanoate (amino valerate)	D-proline reductase (***prdA***)	0.16	3.15	-1.09	0
D-proline → 5-amino pentanoate (amino valerate)	D-proline reductase (***prdB***)	0.03	2.90	-0.57	0.01
Glycine reduction	glycine/sarcosine/betaine reductase complex protein A (***grdA***)	-0.22	7.20	-	0.54
Glycine reduction	glycine reductase complex component B subunit (***grdB***)	-0.22	7.18	1.30	0.27
Glycine reduction	glycine reductase complex component E subunit (***grdE***)	0.32	7.07	1.45	0.69

Glycine reduction	glycine reductase complex component C subunit (***grdC***)	0.00	6.61	0.93	-0.07
Glycolysis/pyruvate metabolism and pentose phosphate pathway					
Acetyl-CoA → Acetoacetyl-CoA	Acetoacetyl-CoA thiolase 1 (***thlA1***)	-8.97	1.66	1.01	0.05
Acetyl CoA → Malonyl CoA	Acetyl-CoA carboxylase (***accB***)	0.72	-0.36	-0.29	-0.30
Acetyl P ↔ Acetate	Acetate kinase (***ackA***)	1.03	0.92	0.24	0.15
Acetyl CoA → Malonyl CoA	Acetyl-CoA carboxylase (***accC***)	0.86	-0.40	-0.04	-0.49
Acetyl CoA → Malonyl CoA	Acetyl-CoA carboxylase (***accD***)	0.72	-0.36	-0.62	-0.99
Pyruvate ↔ Malate	NAD-dependent malic enzyme	0.89	0.28	-0.18	-0.60
Acetyl-CoA ↔ Pyruvate	Pyruvate-ferredoxin oxidoreductase (***pfo***)	0.34	0.59	0.67	-0.08
Pyruvate ↔ L-Lactate	L-lactate dehydrogenase (***ldh***)	-1.66	-1	-	-1.57
Glycerate-1,3-P2 ↔ 3-phosphoglycerate	Phosphoglycerate kinase (***pgk***)	-0.53	-0.75	0.17	-0.88
Glyceraldehyde-3P → 3-phosphoglycerate	Glyceraldehyde-3-phosphate dehydrogenase ($NADP^+$) (***gapN***)	0.70	0.20	-0.60	-1.18
3-phosphoglycerate ↔ 2- phosphoglycerate	2,3-bisphosphoglycerate-independent phosphoglycerate mutase (***gpmI***)	-0.60	-0.86	0.09	-0.64
D-Fructose-6-P→ D-Fructose-1,6-bisphosphate	6-phosphofructokinase 1 (***pfkA***)	-0.71	0.25	-0.89	-1.92
D-Glucose 6-phosphate ↔ D-Fructose-6-P	Glucose-6-phosphate isomerase (***pgi***)	-1.46	0.08	0.02	-0.50
D-Fructose-1,6-bisphosphate → Glyceraldehyde-3P	Fructose-1,6-bisphosphate aldolase (***fba***)	0,26	-0,20	0,37	-0,15

Glucose-1-P ↔ Glucose-6-P	Phosphoglucomutase (***pgm***)	1.14	0.05	-0.35	-1.04
Acetaldehyde ↔ Ethanol	Bifunctional acetaldehyde-CoA/alcohol dehydrogenase (***adhE1***)	-11.59	-3.89	-1.44	-
Pyruvate ← PEP	Pyruvate kinase (***pyk***)	-0,62	-0,56	0,35	-0,19
Acetyl-CoA → Acetyl-P	Phosphate butyryltransferase (***ptb1***)	-0,15	2,11	-0,05	-0,55
Pyruvate → Oxaloacetate	Pyruvate carboxylase (***pyc***)	0,81	-0,39	0,24	-0,78
TCA Cycle					
Fumarate ↔ Malate	Fumarate hydratase (***fumA***)	1.11	0.30	-0.26	-0.28
Fumarate ↔ Malate	Fumarate hydratase (***fumB***)	1.00	0.18	0.35	-0.06
Citrate ↔ Isocitrate	Aconitate hydratase (***acnB***)	-0.44	-1.27	0.68	-0.72
Isocitrate ↔ 2-Oxoglutarate	Isocitrate dehydrogenase NAD-dependent (***icd***)	-0.51	-1.61	0.89	-1.40
Butanoate metabolism					
Crotonyl-CoA ← Butanoyl-CoA (Butyryl CoA)	Butyryl-CoA dehydrogenase (***bcd2***)	-7.81	1.50	2.31	-0.34
Succinyl-CoA → Succinate semialdehyde	Succinate-semialdehyde dehydrogenase (***sucD***)	-4.00	0.64	-2.49	-0.13
Butanoyl-CoA ↔ Butanoyl-P	Phosphate butyryltransferase (***ptb***)	-0.15	2.11	-0.05	-0.55
Butanoyl-P ↔ Butanoate (Butyryl)	Butyrate kinase (***buk***)	2.41	2.58	0.03	-0.54
3-hydroxybutanoyl CoA ↔ Crotonyl-CoA	3-hydroxybutyryl-CoA dehydratase (***crt2***)	-7.86	1.34	2.08	-0.53
4-hydroxybutanoyl CoA ↔ Crotonyl CoA	Gamma-aminobutyrate metabolism dehydratase/isomerase (***abfD***)	-0.12	0.58	0.67	0.04

Acetoacetyl-CoA ↔ 3-hydroxybutanoyl CoA	3-hydroxybutyryl-CoA dehydrogenase (***hbd***)	-8.31	1.44	0.59	-0.35
4-Hydroxybutanoate ↔ 4-hydroxybutanoyl CoA	4-hydroxybutyrate CoA-transferase (***cat2***)	0.03	1.02	-0.29	-0.94
Butanal → Butanoyl-CoA	Aldehyde-alcohol dehydrogenase (***adhE***)	0.00	0.42	-	-2.78
4-Hydroxybutanoate ↔ Succinate semialdehyde	4-hydroxybutyrate dehydrogenase (***4hbd***)	-0.04	0.74	-0.96	-0.41
Crotonyl-CoA → Butanoyl-CoA (Butyryl CoA)	Electron transfer flavoproteins subunit beta (***etfB3***)	-8.00	1.24	1.87	0.45
Crotonyl-CoA → Butanoyl-CoA (Butyryl CoA)	electron transfer flavoprotein subunit alpha (***etfA3***)	-7.49	1.21	1.75	0.23
Phenylalanine degradation					
3-phenylpropanoyl-CoA → 3-phenylpropionate	Isocaprenoyl-CoA (***hadA***)	-8.35	6.27	0.04	0.18
Phenylpyruvate → Phenyllactate	D-lactate dehydrogenase (***ldhA***)	-8.07	3.00	-0.96	-0.91
3-OH-3-phenylpropionyl-CoA → 2-Enoyl-3-phenylpropionyl-CoA	2-hydroxyisocaproyl-CoA dehydratase (***hadC***)	-8.10	6.12	0.60	-0.05
3-OH-3-phenylpropionyl-CoA → 2-Enoyl-3-phenylpropionyl-CoA	2-hydroxyisocaproyl-CoA dehydratase (***hadB***)	-8.12	6.06	0.41	-0.23
3-OH-3-phenylpropionyl-CoA → 2-Enoyl-3-phenylpropionyl-CoA	Activator 2-hydroxyisocaproyl-CoA dehydratase (***hadI***)	-8.22	5.97	-1.51	-0.02
Phenylalanine ↔ Phenylpyruvateindole-3-acetonitrile	Aspartate aminotransferase (***aspC***)	-0.53	-0.37	0.32	-0.58
3-Enoyl-3-phenyl propionyl-CoA → 3-Phenylpropionyl-CoA	Electron transfer flavoprotein (***etfA1***)	-7.54	6.25	-0.59	-0.12
3-Enoyl-3-phenyl propionyl-CoA → 3-Phenylpropionyl-CoA	Electron transfer flavoprotein (***etfB1***)	-7.55	6.96	-0.36	0.03

3-Enoyl-3-phenyl propionyl-CoA → 3-Phenylpropionyl-CoA	Acyl-CoA dehydrogenase (***acdB***)	-7.40	6.62	0.55	-0.45
Metabolism of amino acids					
4-Hydroxyphenyl) pyruvate ↔ Tyrosine	Histidinol-phosphate aminotransferase (***hisC***)	1.20	1.47	1.50	1.61
Proline ↔ (S)-1-Pyrroline-5-carboxylate	Pyrroline-5-carboxylate reductase (***proC***)	-1.26	-0.61	-0.20	0.39
Ornithine ↔ Proline	Ornithine cyclodeaminase	-0.65	0.99	-0.63	-0.05
2-Oxoglutarate → Glutamate	Aspartate aminotransferase (***aspC***)	-0.53	-0.37	0.32	-0.58
Glutamate ↔ Ammonia	NAD-specific glutamate dehydrogenase (***gluD***)	1.02	1.90	0.52	-0.69
Aspartate → L-Arginosuccinate	Argininosuccinate synthase (***argG***)	-2.24	1.00	-0.50	-0.94
Indole-3-acetaldehyde → Indoleacetate	Aldehyde dehydrogenase (***aldH***)	-0.21	-1.12	-	-
Serine ↔ Gycine	Glycine hydroxymethyltransferase (***glyA***)	-0.84	-0.67	-0.16	-1.45
Threonine ↔ Glycine	Threonine aldolase (***ltaE***)	-0.71	1.20	-0.46	-0.37
Glycerate → 2-Phospho-D-gycerate	Glycerate 2-kinase (***garK***)	-2.00	-0.58	-	-
meso-2,6-Diaminopimelate → Lysine	Diaminopimelate decarboxylase (***lysA***)	-3.52	-0.83	-	-1.55
L,L-2,6-Diaminopimelate ↔ meso-2,6-Diaminopimelate	Diaminopimelate epimerase (***dapF***)	-0.64	0.28	0.29	-1.07
Meso-2,6-Diaminopimelate → UDP-N-acetylmuramoylalanyl-D-glutamyl--2,6-diaminopimelate	UDP-N-acetylmuramoylalanyl-D-glutamate--2,6-diaminopimelate ligase (***murE***)	2.40	-0.51	-0.56	-1.25

L-methionine ← L-Homocysteine	Homocysteine S-methyltransferase	0.26	-0.08	0.09	-1.00
4-Methylthio-2-oxobutanoate → Methionin	Pyridoxal phosphate-dependent transferase	1.78	7.41	1.78	0.32
L-Aspartate → L-Alanine	Aspartate aminotransferase (aspartate 4-decarboxylase)	-0.47	-0.26	-	0.15
Glycerollipid, glyoxylate/ dicarboxylate, propanoate and pyrimidine metabolism					
Glycerol → Glycerol-3-P	Glycerol kinase (***glpK2***)	-0.58	1.35	-	1.04
2-phosphoglycolate → Glycolate	HAD superfamily hydrolase	-0.72	0.82	-0.42	-
2-Oxobutanoate ↔ 2-Hydroxybutanoate	L-lactate dehydrogenase (***ldh***)	-1.66	-1	-	-1.57
Cytosine → Cytidine	Pyrimidine-nucleoside phosphorylase (***pdp***)	0.58	-0.08	0.08	-0.29
Cellular Processes					
Toxin production	Toxin A (***tcdA***)	1.38	2.55	2.33	0.93
Cell motility	Flagellar basal body-associated protein (***fliL***)	0.99	-0.36	-3.56	-2.45

Table 25 shows the log2 FC values for proteins and their respective transcripts in the *rnfC* mutant strain at T1 and T2 in comparison to the wildtype. The analyses showed that during Stickland fermentation the proteins and corresponding transcripts of the Rnf complex (RnfB, RnfC, RnfD, RnfE and RnfG) were present in negligible quantities in the *rnfC* mutant strain at T1 and T2. Interestingly, the log2 FC protein values of the D-proline reductase subunits PrdA and PrdB at T1 indicated a reduced amount in the mutant strain while corresponding transcript values were higher than in the wildtype. At T2 the protein log2 FC values of PrdA and PrdB changed to 0 and indicated the identical protein quantities in both strains. The transcripts for both proteins increased at the same time in the mutant strain.

In addition, the glycine reductase (GrdA, GrdB, GrdE and GrdC) subunits were found enriched in the *rnfC* mutant strain at T1 and mainly at T2. Most of the corresponding transcripts showed only marginally changed log2 FC values in the mutant strain at T1, but very high amounts at T2. Further proteins and corresponding transcripts with significant changed log2 FC values from energy generation pathways (e.g. glycolysis, butanoate metabolism) were also identified in the *rnfC* mutant strain in comparison to the wildtype.

4.5 In vivo *behavior of the* rnfC *mutant strain in a mouse model*

As described above, the *rnfC* mutant strain CD630Δ*erm_rnfC*636/637s::*ermB* was tested in comparison to the wildtype *in vitro* using multi-omic experiments in order to determine the physiological role of RnfC in *C. difficile* 630Δ*erm*. Next, the *rnfC* mutant strain was further tested in a mouse model and compared to the wildtype in terms of infection efficiency. For this purpose, a prepared spore suspension of the strains CD630Δ*erm_rnfC*636/637s::*ermB*_pMTL82151*rnfC*-strep II (complemented strain), CD630Δ*erm_rnfC*636/637s::*ermB*_pMTL82151 (*rnfC* mutant) and CD630Δ*erm*_pMTL82151 (wildtype) was used to infect under sterile conditions (SPF) the mouse wildtype (WTBL/6-SPF1) line of the HZI in Braunschweig as described in chapter 3.7. The experiments were performed by Dr. Nathiana Smit at the HZI in Braunschweig (group of Prof. Dr. Till Strowig; Microbial Immune Regulation).

4.5.1 Single infection experiments of the *rnfC*-mutant strain, the *rnfC*-complemeted mutant strain and the wildtype in a mouse model

Single infection experiments with the wildtype, *rnfC* mutant strain and *rnfC*-complemented mutant strain were performed. For this purpose, the log CFU per gram stool in cecum, colon and feces of day 1 (D1) and day 3 (D3) after infection were determined. The approach differentiated heated (spores) or non-heated (vegetative cells) samples which is illustrated in the next figures.

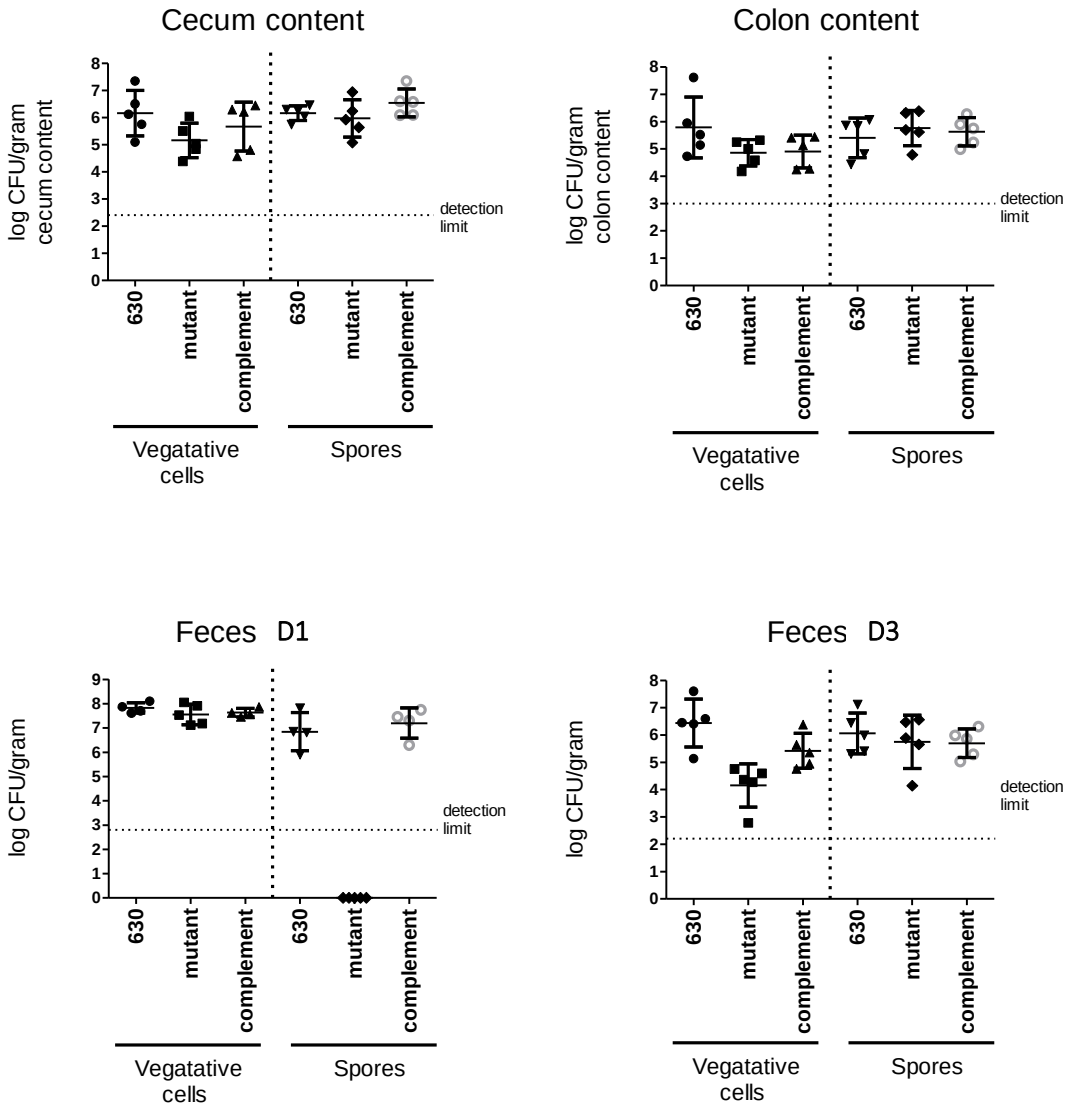

Figure 33: Determined log CFU/gram stool content of cecum (D3), colon (D3) and feces (D1 and D3), separated into heated (spores) and non-heated (vegetative cells) samples after single mice infection experiments with the *rnfC* mutant strain (mutant), wildtype (630) and the *rnfC*-complemented mutant strain (complement). The single mouse infection experiments were performed with the wildtype strain (630), *rnfC* mutant strain (mutant) and the *rnfC*-complemented mutant strain (complement). The feces were collected on day 1 and 3 (D1; D3). The contents of the colon and cecum was isolated on day 3 post infection. The samples were prepared according to outlined protocols (see chapter 3.7). The samples were also divided into unheated and heated samples and were treated accordingly. The log CFU/gram sample was determined and graphically displayed with a detection limit (~3 CFU/gram). The values of all samples were above the detection limit except for the spore sample of the *rnfC* mutant in the feces on day 1 (D1) after the mouse infection. The infection experiments were performed and the illustration was generated by Dr. Nathiana Smit at the HZI in Braunschweig (group of Prof. Dr. Till Strowig; Microbial Immune Regulation) and provided for this work.

The figure 33 shows the log CFU/gram of the heated (spores) and non-heated (vegetative cells) stool content of the cecum, colon and feces of the *rnfC* mutant strain (mutant), wildtype (630) and *rnfC*-complemented mutant strain (complement) obtained after single infection in the mouse model. The graphs are divided into data from cecum (D3), colon (D3) and feces content (D1/D3). The samples of the colon and cecum show that the log CFU/gram stool for the vegetative cells and the spores were above the detection limit (3 log CFU/gram stool). At an average between 5 and 6 log CFU/gram were detected. In the feces of D3 all samples were above the detection limit, whereas the spores of the individual samples were at an average between 5 and 6 log CFU/gram. In contrast, the log CFU/gram of the vegetative cells of the individual strains wildtype (630), *rnfC* mutant strain (mutant) and the complemented strain (complement) showed deviating mean values in the range between 4 and 6.5 log CFU/gram. The *rnfC* mutant (mutant) with a value of ~4 log CFU/gram showed the lowest value, while the wildtype (630) revealed the highest one (~6.5 log CFU/gram). In the feces depicted in D1 of the graph the vegetative cells of the individual strains revealed similarly high mean values in the range between 7 and 8 log CFU/gram. Interestingly, the spore samples of the various strains led to clearly different values. No spores were detected for the *rnfC* mutant strain post infection and the corresponding log CFU/gram value was below the detection limit. On average, the log CFU/gram values of the *rnfC*-complemented mutant strain and the wildtype were between 7 and 8 log CFU/gram.

As clear differences of the various investigated strains were only observed at day 1 for the feces and the experiments were repeated. The identical experiments were performed with only the complemented strain and the *rnfC* mutant strain and data obtained after day 1 post infection (figure 34).

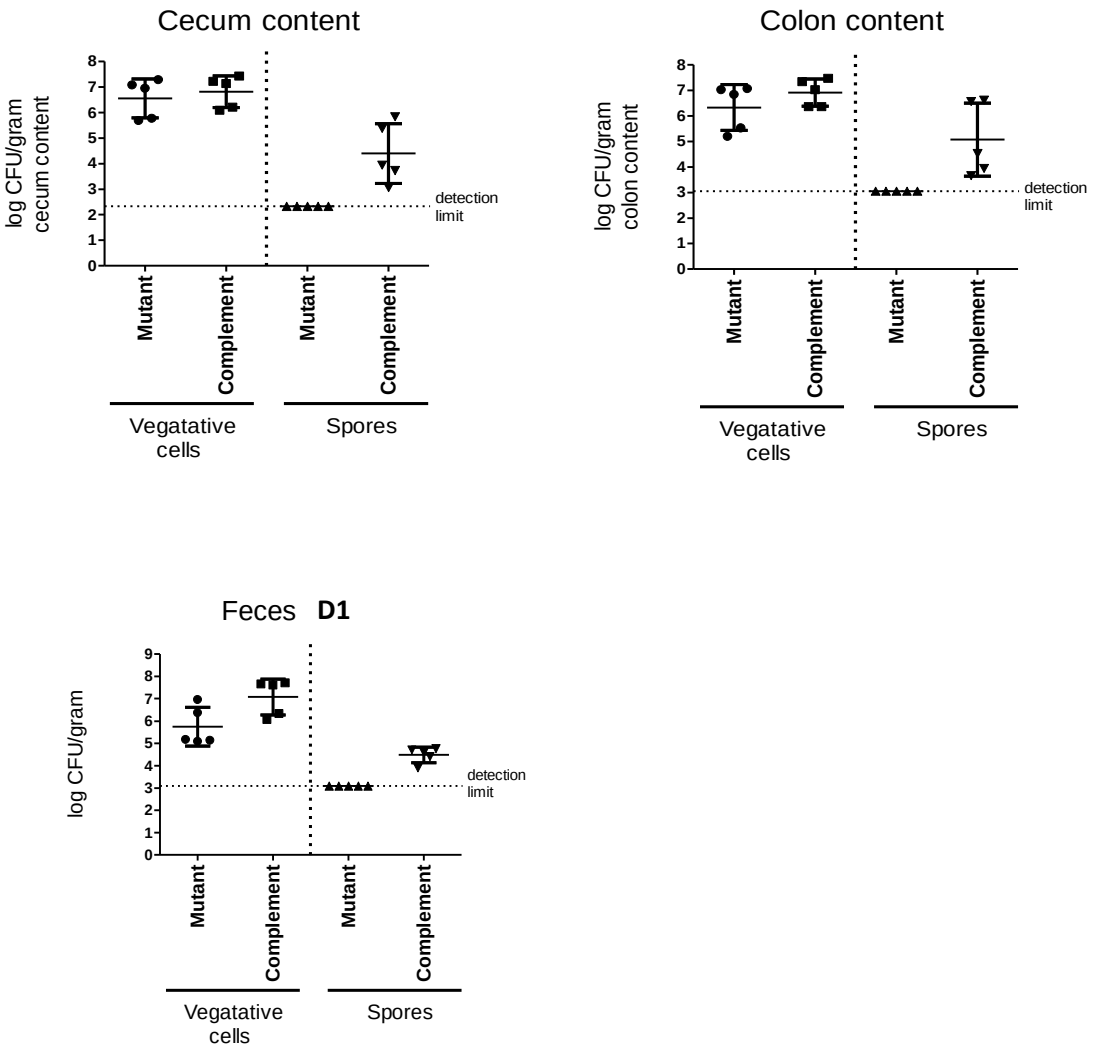

Figure 34: Determined log CFU/gram stool content of cecum (D1), colon (D1) and feces (D1), separated into heated (spores) and non-heated (vegetative cells) samples after single mice infection experiments with the *rnfC* mutant strain (mutant) and the *rnfC*-complemented mutant strain (complement). As described before single mouse infection experiments were performed with the strains *rnfC* mutant strain (mutant) and the *rnfC*-complemented mutant strain (complement). In contrast, the stool contents of the feces, colon and cecum were collected and analyzed at day 1 (D1) after infection. The samples were also seperated into unheated and heated samples and were treated accordingly. The log CFU/gram stool content was determined and illustrated with a detection limit around 3 CFU/gram. Interestingly, only the log CFU/gram values of the *rnfC* mutant spores in cecum, colon and feces were closely at the detection limit. The illustration and the infection experiments were performed by Dr. Nathiana Smit at the HZI in Braunschweig (group of Prof. Dr. Till Strowig; Microbial Immune Regulation) and provided for this work.

For the experiment outlined in figure 34 it is worth to be noted that all spore samples from cecum, colon and feces of the *rnfC* mutant strain (mutant) post infection (D1) showed log CFU/gram values close to the detection limit. In contrast, the *rnfC*-complemented mutant strain (complement) showed log CFU/gram values above the detection limit in a range between 4 and 5 in colon, cecum and feces. The unheated samples, containing the vegetative cells showed values of 6 until 7 log CFU/gram in colon, cecum and feces.

4.5.2 Competition infection experiments of the *rnfC*-mutant strain in comparison to the *rnfC*-complemeted mutant strain in a mouse model

In addition, competition experiments applying both strains, *rnfC* mutant and *rnfC*-complemented mutant strain, were conducted in order to examine the germination and infection behavior when the mouse was infected with both strains simultaneously. For this purpose, five mice were infected. Post infection samples were collected from feces (D1/D3), colon (D3) and cecum (D3) and further processed as described in chapter 3.7. The samples were heated (spore samples) or not (vegetative cells) and spread onto CLO plates (bioMérieux GmbH, Nürtingen, Germany). A total of 100 individual colonies per sample were observed. The identity of the colony as the *rnfC* mutant or complemented strain was tested by PCR (confirmation of plasmid DNA, see chapter 3.3.9). This approach was used to determine the presence of the plasmid pMTL82151 or pMTL82151_*rnfC*-strep II (see appendix) to check for the existence of corresponding specific strain in colon, cecum and feces with or without heating treatment in five replicates. The next graph illustrates the number of identified strains determined via PCR.

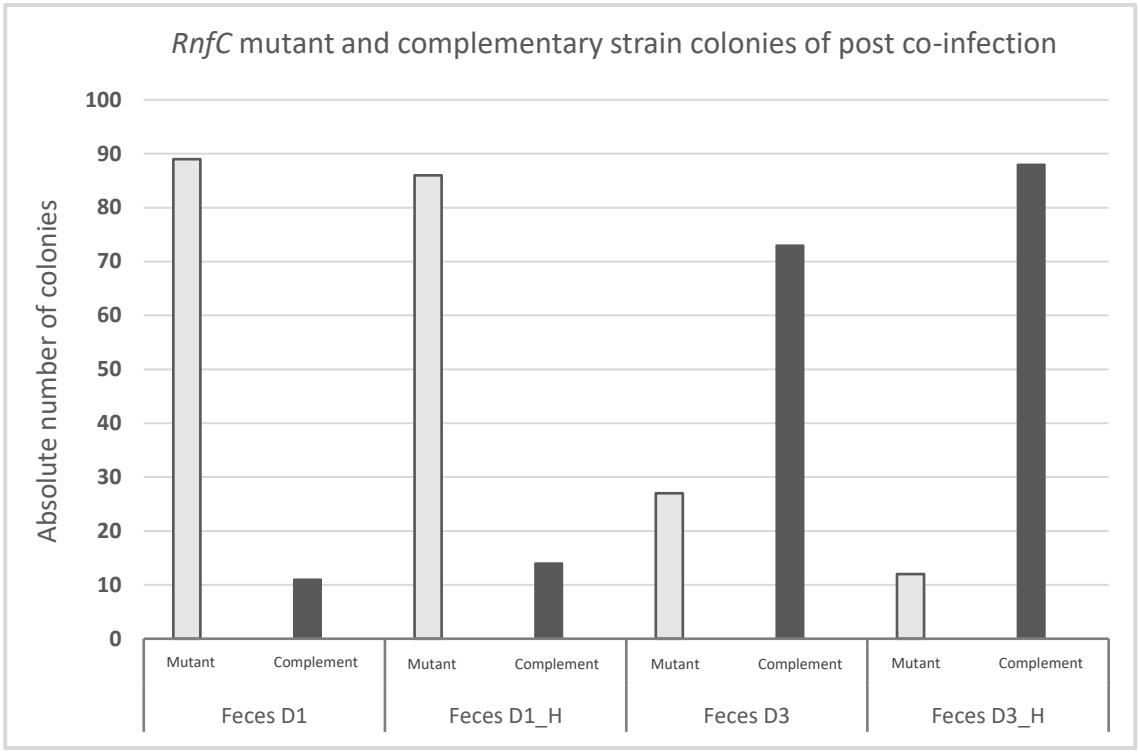

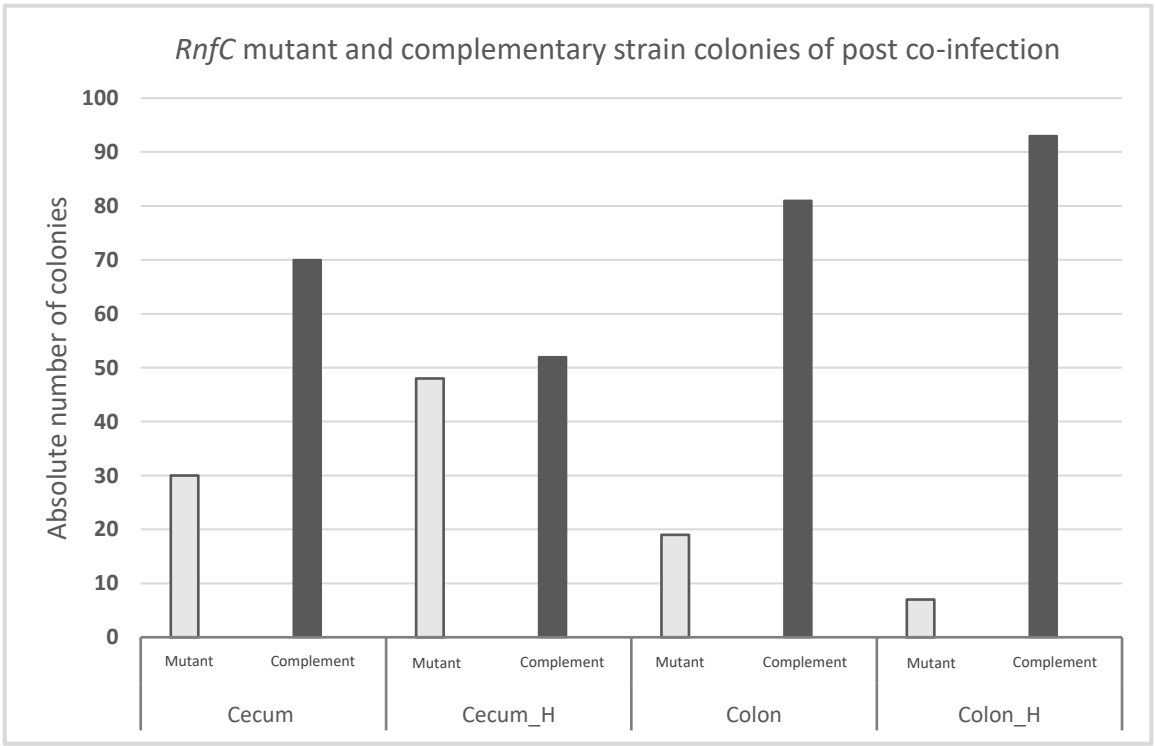

Figure 35: The absolute number of colonies found post infection in mice experiments performed with the *rnfC* mutant strain (mutant) and the *rnfC*-complemented mutant strain (complement). Shown is the distribution and the absolute number of the *rnfC* mutant strain (light grey bar) and its complemented strain (dark grey bar) detected by a PCR analyses of 100 single colonies (from 5 replicates) post co-infection in a mouse. The samples were taken from feces day 1 and day 3 from the mouse after co-infection with both bacteria strains (D1/D3). Colon and cecum samples of the co-infected mouse after day 3 (D3) were collected and separated into heated (H; spores) and non-heated (vegetative cells) samples.

Figure 35 shows the absolute number of identified *rnfC* mutants (light grey bar) and *rnfC*-complemented mutant strains (dark grey bar) in a total 100 tested individual colonies (5 replicates) from post co-infection experiments. Colonies from obtained feces at day 1 and day 3 (D1/D3) from the colon (D3) and cecum (D3) were tested after heating (H; spores) and non-heating conditions (vegetative cells). It became evident that only on day 1 there were more vegetative cells and spores of the *rnfC* mutant (vegetative cells: 89; spores: 86) in the feces compared to the *rnfC*-complemented mutant strain (vegetative cells: 11; spores: 14). On the third day in feces, colon and cecum there were more spores and vegetative cells of the *rnfC*-complemented mutant strain in the tested samples. Here, 88 spores and 73 vegetative cells of the *rnfC*-complemented mutant strain were found in feces D3 and 12 spores, whereas only 27 vegetative cells of the *rnfC* mutant strain were found. In cecum 52 spores and 70 vegetative cells of the *rnfC*-complemented mutant strain were identified, while 48 spore colonies and 30 vegetative cells of the *rnfC* mutant were detected. The content of the colon showed 93 spore colonies and 81 vegetative cells of the rnfC-complemented mutant strain and 7 spore colonies and 19 vegetative cells of the *rnfC* mutant (see digital appendix).

5 Discussion

The hospital-associated human pathogen *C. difficile* is an anaerobic organism that inhabits the intestine and has the ability to cause diseases ranging from diarrhea over pseudomembranous colitis to toxic megacolon. Annually, several thousand people die as a result of *Clostridioides difficile* infections worldwide (Kachrimanidou and Tsintarakis 2020; Czepiel *et al.* 2019; Rao and Safdar 2016). Therefore, research on this pathogen is essential for its containment.

As strict anaerobic organism *C. difficile* is capable of generating energy in the absence of oxygen as electron acceptor. During this process it employs organic compounds which are broken down during a fermentation process producing ATP in turn (Bouillaut *et al.* 2013). This is usually done via substrate-level phosphorylations, as observed for the Wood-Ljungdahl pathway (WLP) or butanoate fermentation pathway. Nevertheless, this organism is able to actively produce a chemiosmotic ion-gradient at the membrane. The ions Na^+/H^+ are generally transported by the Rnf-complex, which enables the ATP synthase to phosphorylate ADP utilizing the produced gradient (Müller and Wiechmann 2017; Aboulnaga *et al.* 2013).

C. difficile conducts specialized amino acid fermentation, called Stickland fermentation which consists of an oxidative and a reductive branch. This study laid its major focus on the energy-relevant reductive branch in which *C. difficile* employs a variety of amino acids to produce ATP and NAD^+. The enzyme D-proline reductase (Prd) uses D-proline as well as NADH to convert the substrate into 5-aminovalerate and NAD^+ (Bouillaut *et al.* 2013). The NAD^+-dependent Rnf complex (*Rhodobacter* nitrogen fixation) generates NADH by the reduction of NAD^+ and the oxidation of ferredoxin during electron transfer (Müller and Wiechmann 2017; Biegel and Müller 2010; Biegel *et al.* 2009). The suggestion that the reductive Stickland pathway, specifically the D-proline reductase (Prd), and the Rnf complex might be associated with each other has already been briefly proposed by Neumann-Schaal *et al.* 2019.

In this thesis the protein-protein interaction between Prd and Rnf was determined for the first time by affinity chromatography coupled with LC-MS/MS and immunogold labeling based of electron microscopy. The production of a mutant strain, which no longer carries RnfC also enabled the elucidation of the adaptational metabolic rewiring when the complex is absent and the assessment of infection impairments in mouse models.

5.1 The high-ordered ion translocating Rnf-proline reductase complex in the Stickland fermentation of C. difficile 630Δerm

A manifold of protein-protein interactions studies have largely relied on the well-described method of affinity chromatography coupled with LC-MS/MS. Interactome mapping is a valuable tool to provide information on the complexity and functionality of the cell (Gingras *et al.* 2007). Protein interactions within the reductive Stickland fermentation specifically between D-proline reductase and the membrane-bound Rnf complex were analyzed in detail using that approach. The bait proteins PrdA (CD630DERM_32440), PrdB (CD630DERM_32410), RnfB (CD630DERM_11420) and RnfC (CD630DERM_11370) were analyzed in a gel-based method with and without formaldehyde cross-linking treatment and in a quantitative gel-free approach. For the verification of a direct interaction, the subunits PrdA, RnfB and RnfC were investigated for co-localization in the immunogold labeling experiment by transmission electron microscopy.

5.1.1 Protein-protein interactions between the Prd and the Rnf complex in the gel-based affinity chromatography coupled with LC-MS/MS

In the first place, the successful purification of the baits PrdA, PrdB, RnfB and RnfC (gel-based affinity chromatographed LC-MS/MS approach without a formaldehyde cross-link treatment) proved the reliability of the chosen experimental design: employment of native promoters and fusion of a C-terminal Strep-tag® II for anaerobic production. For the subunits of D-proline reductase, the relative protein detection via Western blot using C-terminal Strep-tag® II displayed a distinctive band at M_r of ~70.000 for PrdA (68.000) and of ~25.000 for PrdB (26.000) (see chapter 4.1.2, figure 17). The proof of principle to confirm stability of the approach was the appearance of PrdA in the PrdB´s

elution fraction and *vice versa*. The LC-MS/MS was also used to confirm the presence of PrdA and PrdB at their respective elution fraction. It is worth to note that a smaller subunit herein described as PrdA*, which might result from proteolytic processing of the major PrdA subunit was also visualized on the SDS-PAGE and identified by LC-MS/MS as well as by Western blot analysis. It has been reported that the M_r of 68.000 PrdA from clostridial species has a proteolytically susceptible cleavage site, which means that the complete PrdA is divided into two differentially sized proteolytic products (M_r of 23.000 and 45.000) (Kabisch *et al.* 1999; Jackson *et al.* 2006). Conversely, the detection of the membrane-bound Rnf subunits revealed several bands of mostly lower molecular weight. Most likely the sensitive membrane proteins were subjected to degradation by the harsh purification steps and therefore several bands were determined at different relative molecular masses. Nevertheless, the results of the LC-MS/MS analyses also showed that the target proteins RnfB (M_r 35.000) and RnfC (M_r 48.000) were properly produced and purified (see chapter 4.1.3, figure 18). For a better protein purification efficiency, the corresponding protocol and especially the solubilization of the membrane proteins might be adapted e.g using different solubilization detergents instead of Triton X-100.

Remarkably, the cytosolic subunit PrdA was co-purified from the soluble fraction along with the membrane complex subunit RnfC without the need of cross-linker treatment. This indicates strong assotiation of the RnfC and PrdA components. The elutions of the baits RnfB and RnfC also contained the PrdA subunit after protein purification and LC-MS/MS analyses. In contrast, the bait PrdB under same conditions, did show any of the Rnf subunit. The possible direct interplay between the energy generation fermentation procecess and the Rnf complex has already been briefly mentioned by Neumann-Schaal *et al.* 2019. However, these results are determining for the first time a tight interaction of both subunits, which is conceivable if the subunit PrdA is responsible for the transfer of the electron acceptor NAD^+ to the RnfC subunit during the D-proline conversion to generate NADH (NAD^+-channeling). Bouillaut *et al.* 2019 postulates the Prd activity seems the major NAD^+ regeneration pathway in *C. difficile*. In the light of this assumption, the strong interaction of PrdA and RnfC could ensure a rapid NAD^+/NADH regeneration as well as energy production and might prevent the loss of electron transfer during the reductive Stickland fermentation.

In contrast, protein-protein interactions specific to the membrane can be observed more easily after a cross-linker treatment. All four bait proteins were purified from the insoluble fraction of the cell free extract using the Strep-tag® II and analyzed by Western blot analyses and LC-MS/MS measurements. The results of the bait eluates (figure 19 and 20) show that generally more Rnf subunits were found by using the affinity chromatography LC-MS/MS approach and a previously *in vivo* cross-linker treatment with exception of the purified PrdB. Here, only very few identified proteins were detected in LC-MS/MS, but unfortunately no PrdB. However, these results show that the method might not be applicable to PrdB and alternatively indicate that PrdB does not interact with proteins at the membrane level, which was already previously visible without cross-linking due to the missing Rnf association. Alternatively, the interactions may be weak or occurring transiently and were not stable enough, even not with a cross-linker treatment.

Both methods not only analyzed the direct interactions between the Rnf complex and Prd. Furthermore, abundant proteins that play an important role in the different energy generation pathways were identified bound to Prd and Rnf. The tables 18-21 in chapter 4.1.6 show that bait protein containing eluates include a wide spectrum of co-purified proteins that participate in the reductive branch of Stickland fermentation e.g. glycine reductase (Grd), ATP synthase, bifurcating enzymes (e.g. Bcd2/Etf) and proteins from various energy generating pathways and fermentation processes e.g. butanoate metabolism (e.g. Cat2, Crt2). Thus, to achieve a more profound interactomic analysis in order to map to a larger extent protein-protein interaction taking place in a weak or transient manner, quantitative analyses were performed. This is discussed in the next chapter. However, from a global point of view it is visible that a formaldehyde treatment can be benefitial for obtaining increased abundance of potential interaction partners.

5.1.2 Quantitative interactomic analyses of Prd and Rnf using a gel-free affinity chromatography coupled with LC-MS/MS and their validation by electron microscopy co-localization studies

The gel-free quantitative formaldehyde cross-link affinity chromatography coupled with LC-MS/MS approach of the bait-prey interaction of the target proteins PrdA, PrdB, RnfB and RnfC were determined as described in chapter 3.5.6. Prey proteins which were closely identified with a high abundance after the above-mentioned approach from a total of 810 identified proteins are described in chapter 4.2.1. Figure 21 shows that most of these preys were found in all four baits eluates. Due to the different settings applied (unique peptides ≥ 2, protein coverage ≥ 5 %, excluding generic proteins) and the concentration normalization (0.24 mg/mL), the prey proteins were categorized according to Stickland fermentation, butanoate metabolism, fatty acid metabolism, glycolysis, pentose phosphate pathway, pyruvate metabolism and TCA cycle and their functionality (e.g. ATP synthase subunits, electron transfer proteins, PTS system, cellular processes). By highlighting the enrichment factor in table 22-23 in chapter 4.2.1, strong (dark blue), moderate (bright blue) and weak transient interaction (grey) can be quickly spotted.

In conclusion, the table shows strong to moderate transient interactions between the components of D-proline reductase and the Rnf complex. Especially, the chromatographed bait samples RnfB and RnfC showed subunits of the D-proline reductase bound with a high abundance which is evidenced by the very high enrichment factor and indicating a strong interaction. Since the prey proteins were purified natively and the formaldehyde treatment takes place *in vivo*, it might also be the case that preys adopted different oligomeric states (dimer/trimer) when binding to the bait protein to different extents. The analysis of the PrdA, on the other hand, showed a moderate to weak interaction with the Rnf complex depending on the subunits studied, but also with the subunit PrdB.

Obtained results were supported by the immunogold labeling electron microscopy experiments. As seen in chapter 4.3, the TEM images showed a co-localization between Prd and Rnf which based on a semi-quantitative analyses, occured mainly at the membrane. Microscopic analyses clearly demonstrated that there is a strong and direct interaction between Prd and Rnf which leads to the assumption that these proteins were present in a higher ordered ion and electron transfer complex at the membrane of

C. difficile to generate a chemiosmotic ion-gradient. Whether this complex was permanently present in the cell as it is the case for the ATP synthase (De Las Rivas and Fontanillo 2010) should be further studied in future experiments. Potentially, taking samples at different time points of the cell growth could also help to clarify this aspect. The protein composition of an observed multimeric species could also be investigated by using size-exclusion chromatography (SEC) coupled with multi-angle laser light (MALLS) (Mahler *et al.* 2009).

Regarding the other identified prey proteins, the enzyme glycine reductase (Grd), which is also of high importance during reductive Stickland fermentation (Bouillaut *et al*. 2013), revealed a strong to moderate interaction to the Rnf complex components and medium to weak interaction to the Prd subunits. Furthermore, transient interactions were found of the Rnf complex with both types of the ATP synthase (F-type and V-type) and with electron transferring flavoproteins (Etf) of the bifurcating protein complex (Etf/Bcd) and also iron-dependent/transporting proteins. As previously explained, the Rnf complex is able to form a chemiosmotic ion-gradient at the membrane, which in turn can be used by the ATP synthase for ADP phosphorylation (Müller and Wiechmann 2017). Here, the Rnf complex in *C. difficile* interacted particularly strong with most of the subunits of both ATP synthase types. A direct interaction is conceivable, because the Rnf-ATPase supercomplex in *Thermotoga maritima* has already been published very recently (Kuhns *et al.* 2020). Whereby the complex between Rnf and ATP synthase was discovered in liposome experiments (Kuhns *et al.* 2020), which could also be used to verify the interaction between both complexes in *C. difficile*.

Furthermore, it is also known that in a variety of anaerobic bacteria including clostridial species, electron bifurcating protein complexes such as flavoprotein/butyryl-CoA dehydrogenase (EtfAB/Bcd) (Demmer *et al.* 2017) contribute to energy conservation. Electrons are sinked into the butanoate metabolism resulting in reduced ferredoxins which are oxidized at the Rnf complex (specifically RnfB) coupled to electron transfer. The electron acceptor NAD^+ is reduced and NADH regenerated via the subunit RnfC (Aboulnaga *et al.* 2013; Bertsch *et al.* 2013; Neumann-Schaal *et al*. 2019; Köpke *et al.* 2010; Chowdhury *et al.* 2016; Buckel and Thauer 2018). This functional arrangement explains these enzymes are required to interact with the Rnf-Prd complex as subcellular proximity of

this components fosters the electron flow. The potential electron transfer and a rapid NADH/NAD^+ generation would also allow for the production of an ion-gradient at the membrane without time limitations and energy depletion, and thus the ATP synthase could provide ATP to the cell more promptly.

In general, the ion translocating function of the Rnf complex is sustained by electron transport driven by iron sulfur clusters as cofactors (Kuhns *et al*. 2020; Chowdhury *et al.* 2016). An interaction of iron transporting proteins with the Rnf-Prd complex seems to be essential for the further maturation of involved cluster-coordinating enzymes. For instance, this thesis revealed the assoziation of the membrane bound protein subunit FeoB, which transports ferrous iron (Hastie *et al.* 2018; Lau *et al.* 2016) into the cell, and was identified as a potential interactor of the Rnf-Prd complex.

Preys, which are part of alternative fermentation pathways (e.g. butanoate metabolism) and energy supplying processes were already observed in the gel-based experiment. The gel-free quantitative experiment identified enzymes such as Crt2, Cat2, Acc, Adh, LdhA, Fba, GapN, Buk2, PycA, PflE, Pyk, Tkt` or SucD to strongly interact with the core Rnf-Prd complex. Moreover, mostly moderate to weak interactions of these enzymes with the D-proline reductase were encountered. The interaction observed to other sorts of fermentation-related proteins involved in alternative NAD^+ regeneration systems (e.g butanoate metabolism (Bouillaut *et al.* 2019)), might ensure a seamless and rapid electron and NAD^+ cofactor transport from found enzymes to the Rnf-Prd complex. That could be a benefit under conditions of NAD^+ limitation if the Prd activity is reduced (e.g by a nutrient lack), which was postulated as the priority regeneration system of NAD^+ in *C. difficile* (Bouillaut *et al.* 2019).

In conclusion the analyses of the interaction partners of the membrane-bound Rnf-Prd complex, specifically of the Rnf part, provided the strong evidence for the existence of a molecular supercomplex for efficient energy generation in *C. difficile* (figure 36).

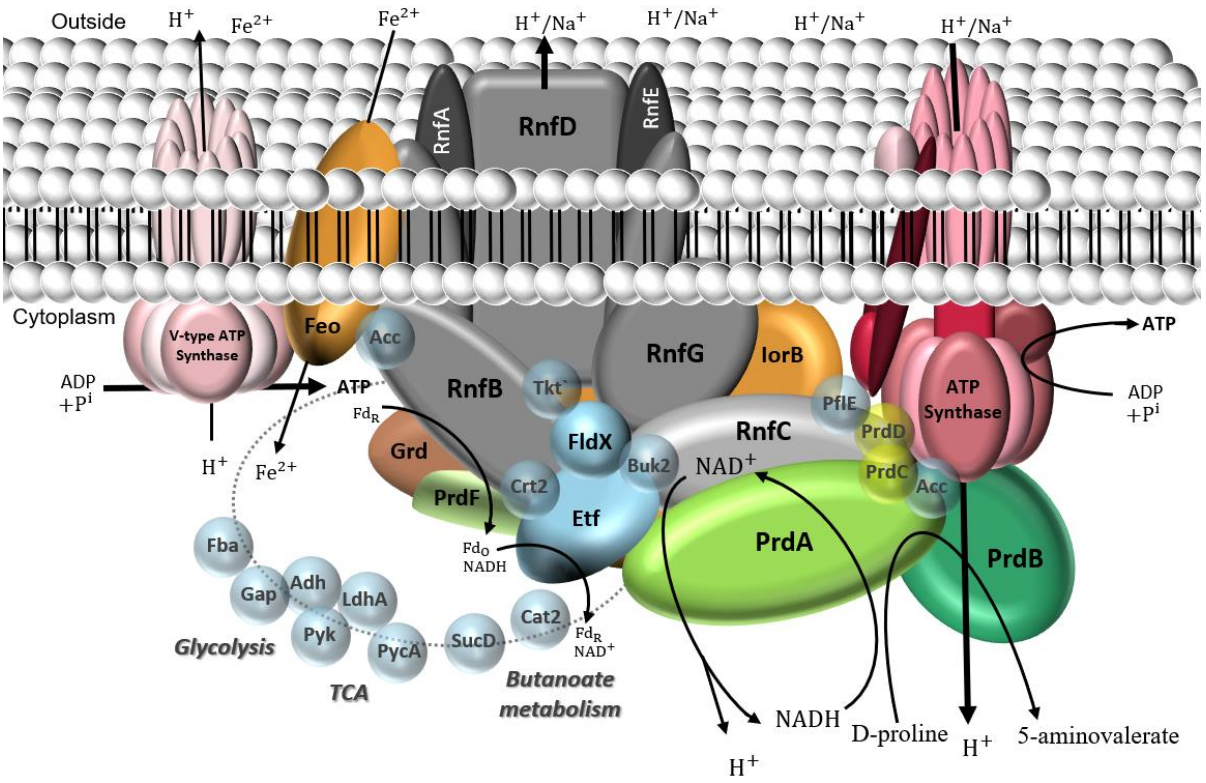

Figure 36: High-ordered ion translocating Rnf-Prd supercomplex in *C. difficile*. Shown are the most likely strong, direct interactions between D-proline reductase (green compounds) and the membrane-bound Rnf complex (grey compounds) identified by affinity chromatography coupled with LC-MS/MS and electron microscopy. Additional, interactions have been identified to proteins which belong to the two ATP synthase types (red compounds) or which are involved in reductive Stickland fermentation, other fermentation pathways (e.g. butanoate metabolism), and in several energy producing processes (brown/blue compounds). Interactions concerning iron transport/containing proteins were also identified (orange compounds). Also, some of these transient interactions are represented by the dotted line with a connection to the complex.

Since this supercomplex, in combination with the ATP synthase and other energy-providing systems, delivers energy to the cell, the significance and importance of the complex was further analyzed by investigating an Rnf lacking strain *in vitro* and *in vivo*.

5.2 *Metabolic rearrangements caused by a non-functional Rnf-Prd complex in* C. difficile

For the better understanding of the impact of the RnfC subunit on the Rnf-Prd complex assembly and functionality, and its influence on the overall metabolism, a *rnfC* mutant strain was generated and regarding to this characterized.

5.2.1 The restricted cell growth of the *rnfC*-lacking *C. difficile* strain

The mutation of the *rnfC* causes the disruption of the Rnf-Prd complex and abolishes its functionality. Firstly, the mutant strain presented an arrested growth behavior compared to the wildtype (figure 25). This is shown by a rather longer restricted exponential growth phase of the mutant strain. Finally, it reaches a lower maximum optical cell density. Depriving *C. difficile* of its RnfC subunit apparently results in an inefficient energy supply which is reflected by its diminished growth. The *rnfC* mutant strain also shows morphological differences (figure 26), like an abnormal formation of the flagellar apparatus or the stacking of secreted proteins on the cell surface. Further experiments such as a swimming motility assay would provide critical information about the functionality of the flagella. However, a deeper look into the cell and into the metabolic behavior via the multi-omic assays (metabolomic, transcriptomic, proteomic) and the determination of the D-proline reductase activity, NAD^+/NADH ratio in the cell and the concentration of secreted toxins, helped to shed light on the *rnfC* mutant physiology at different levels.

5.2.2 Influence of a non-functional ion translocating Rnf-Prd complex on the reductive Stickland fermentation

Proteomic and transcriptomic analyses of the *rnfC* mutant versus the wildtype revealed a drastically decreased amount of all *rnf* operon transcripts and a corresponding lower protein abundance (table 25). Only the partial *rnfC* transcripts were found enriched in the transcriptomic assessment. A higher amount of *rnfC* transcripts compared to a significantly reduced protein amount could be explained by the partial transcription of this gene, which is disrupted in the middle by the introduced intron eluding thereby translation. This is due to the fact that the insertion of the group II intron in the *rnfC* gene

prevented the transcription of the downstream genes which means that the subsequent *rnf* genes were not transcribed and therefore not translated efficiently.

However, the absence of the entire Rnf complex seemed to be detrimental to the D-proline reductase maturation as significantly reduced amounts of the subunits PrdA, PrdB or PrdF (table 25) were found by proteomics especially in the exponential growth phase. This is a hint to the dependence of the components of the Rnf-Prd complex in their formation. Interestingly, the *prd* genes were found upregulated and the amount of transcripts were higher than in the wildtype (at T1/T2) which might an indicative of a transcriptional compensatory effect elicited by the cell, although it was mirrored inefficiently at the protein level. The reduced D-proline reductase protein amount in the exponential growth phase led to an associated reduced 5-aminovalerate formation compared to the wildtype which became obviously visible in the Prd activity test (figure 27) and in the exometabolome/amino acid and 5-aminovalerate measurements (figure 32). In addition, the reduced enzyme amount is responsible for the very high intracellular and extracellular D-proline accumulation compared to the wildtype (figure 29 and 32). In the stationary growth phase, the genes of Prd were upregulated and the amount of Prd proteins increased almost to the wildtype enzyme amount (table 25). This phenomenon was not accompanied by enhanced D-proline reductase activities in the stationary growth phase as shown in figure 27 at T2, presumably due to a malformation of the Prd complex which led to its impared functioning. Bioinformatic analyses using the KEGG database indicated that D-proline can be converted back to proline and then to 4-hydroxyproline or 1-pyrroline-5-carboxylate and may be metabolized in other metabolic processes. Furthermore, via lysine degradation the 5-aminovalerate can be formed and that might explain to a certain extent the extracellular product amount in the *rnfC* mutant strain in the stationary growth phase (figure 32).

It is also evident that glycine reductase (Grd) was influenced by the loss of function of the Rnf-Prd complex as the genes for *grdA, grdB, grdE* and *grdC* were found upregulated (table 25). The corresponding proteins were partly more abundant in both growth phases than in the wildtype. The slightly increase of intracellular glycine in the mutant strain in the exponential growth phase which was then reduced in the stationary growth phase (figure 29) showed that this enzyme is less restricted in its functionality by the

Rnf-Prd complex loss. The ADP phosphorylation during acetate formation in the Grd pathway of the Stickland fermentation (Bouillaut *et al.* 2013), whose amount does not differ intracellularly from the wildtype neither in the exponential nor in the stationary growth phase (see digital appendix), also proved that the Grd pathway is not restricted by the *rnfC* mutation. Since, the acetate in the mutant strain was not significantly higher as in the wildtype, the Grd pathway does not appear to be compensating for the lack of the Rnf-Prd complex.

In summary, these results show that the *rnfC* mutation led to a loss of the membrane-bound Rnf complex. However, it is still unclear how the *rnfC* mutant compensated for this metabolic malfunctioning and preserved, although to lower extend energy conservation. Therefore, the Omic studies were performed in order to identify the alternative ways of supplying energy.

5.2.3 The alternative routes of energy production with an inactive Rnf-Prd complex containing in the *rnfC* mutant strain

Prd in the reductive Stickland fermentation generates NAD^+ as electron acceptor for the Rnf complex through its enzymatic D-proline conversion. This pathway is the main one for NAD^+ production in *C. difficile* (Bouillaut *et al.* 2019). Therefore, by limiting Prd function a reduced amount of the NAD^+ in the cell was presumed. In turn, the lack of RnfC should lead to diminished NADH formation. Therefore, abnormal NAD^+/NADH ratios were expected in the mutant. Surprisingly, the data of the NAD^+/NADH ratio measurement (table 24) show that in the exponential growth phase the mutant strain contained almost identical amounts of NAD^+ as the wildtype which suggests that alternative NAD^+ generating systems (such as the butanoate metabolism (Bouillaut *et al.* 2019)), must be activated in order to compensate for the D-proline reductase. Looking at the NADH value the *rnfC* mutant strain also produced almost twice as much NADH compared to the wildtype at the same growth phase. Here, existing NADH can be generated e.g. via the oxidative Stickland fermentation pathway (Bouillaut *et al.* 2013).

The ratios were reversed in the stationary growth phase. The *rnfC* mutant strain revealed a 164-fold increased NAD^+/NADH ratio in comparison to the wildtype. This underscores the importance of NADH regeneration by the RnfC complex. Furthermore, the NAD^+/NADH ratio indicated that previously formed NAD^+ can be alternatively reduced to NADH, e.g. in the oxidative Stickland metabolism (figure 5), which is obviously not the primary pathway for NADH regeneration. These results may imply that the Rnf-Prd complex is the primary pathway for NAD^+/NADH homeostasis in *C. difficile*.

Regarding the alternative NAD^+ regeneration systems, the butaonate pathway, which is mainly activated in case of redox stress and nutrient starvation is worth to be mentioned (Bouillaut *et al.* 2019). During the employed nutrient-rich conditions the *rnfC* mutant strain presented a significant activation of this pathway and therefore the formation of NAD^+ can be observed already in the exponential growth phase. Thus, most of the butanoate metabolism intermediates were intracellularly accumulated. Moreover, most of the proteins involved in butanoate metabolism were found highly abundant in the cell in the exponential and less of them in the stationary growth phase. The link between that activated pathway, especially the formed product butyrate, and the toxin regulation was mentioned by Karlsson *et al.* 2000 and Bouillaut *et al.* 2019. In this case, the results revealed the activation of the butanoate pathway and therefore the accumulation of compounds, which may influence the toxin formation. This became clear in the toxin ELISA experiment. Directly or indirectly, the upregulation of the butanoate pathway appeared to have a strongly activating influence on TcdA formation, especially in the exponential growth phase, but not on TcdB production (figure 28). It is likely that the enzymes involved in butanoate metabolism or its related by-products had a gene regulatory influence on TcdA synthesis. This might exclude the final product butyrate, whose concentration did not differ highly from that of the wildtype (see digital appendix).

Also noticeable was the high accumulation of various amino acids in the exponential growth phase (figure 29), which was mostly reversed in the stationary growth phase. These include amino acids such as tyrosine, isoleucine, leucine, lysine, serine and valine. Also, many proteins which are involved in amino acid metabolism were found abundant in the *rnfC* mutant strain (table 25). The catabolized amino acids are important energy-

providing sources as their conversion leads to different metabolic intermediates like pyruvate, oxaloacetate or 2-oxoglutarate and the synthesis of ATP via the corresponding pathways (Halsey *et al.* 2017). Especially the relevant electron donors isoleucine, alanine and leucine are used in oxidative Stickland fermentation for ATP generation (Bouillaut *et al.* 2013). In this context, the results show that the *rnfC* mutant strain was able to generate ATP via substrate-level phosphorylation e.g. in an upregulated oxidative Stickland fermentation. Whether the substrate-level phosphorylation derived ATP is adequate for cell physiological maintenance remains still unclear.

In a variety of pathogenic bacteria like *Vibrio cholerae* there are other known closely related ion-transporting complexes such as NADH:quinone oxidoreductase (Na^+-NQR) (Juárez and Barquera 2012; Häse *et al.* 2001). In *C. difficile* the corresponding enzyme is annotated as Hym like protein (CD630DERM_34050; CD630DERM_34060; CD630DERM_34070), which was also identified in the proteome data set (see digital appendix), but not as abundant as in the wildtype. Nevertheless, this complex could be used to transfer ions across the membrane to generate a chemiosmotic ion-gradient by NADH conversion. Obviously, *C. difficile* did not maintain an effective chemiosmotic ion-gradient using this alternative pumping system in the *rnfC* mutant strain (figure 25).

Finally, the Omics experiments using the *rnfC* mutant strain revealed a significant effect of the *rnfC* mutation on energy production and the corresponding electron conversion pathways in the cell. The next figure illustrates metabolic changes in relevant fermentation and energy-producing pathways, which were discussed before, in the *rnfC* mutant strain compared between exponential (T1) and stationary growth phase (T2).

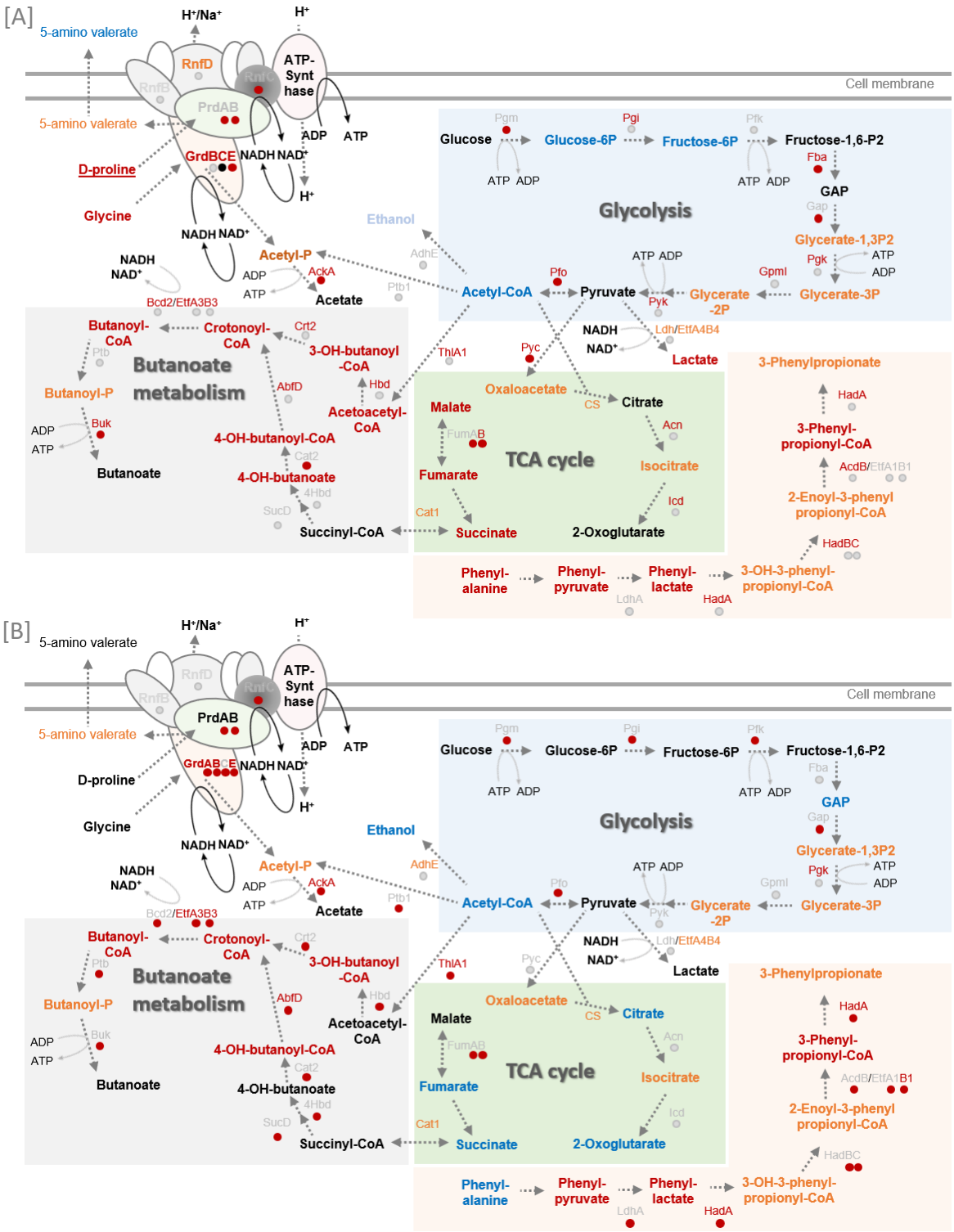

Figure 37: Measured metabolic changes specific to the Stickland fermentation, glycolysis, TCA cycle and butanoate metabolism between the exponential (T1) [A] and stationary (T2) [B] growth phase of the *rnfC* mutant strain in relation to the wildtype. Shown is the most important metabolic changes in the energy production pathways in the *rnfC* mutant strain in relation to the wildtype at T1 [A] and T2 [B]. Accumulated (red) or reduced (blue) intermediates or with no changes (treshhold range [FC: 0.67-1.5]; black) are shown in the respective color code. Enzymes (partly at the arrows) and associated transcripts (dots) which were found highly abundant (log2 FC > 0; red), reduced (log2 FC < 0; grey) or without modification (log2 FC = 0; black) are illustrated. Intermediates which were not formed in the mutant strain in relation to the wildtype are shown in bright blue. Unidentified compounds were shown for completeness (orange). Metabolic changes induced by the lacking Rnf complex are visible e.g. in the reductive Stickland fermentation, an upregulation of the butanoate metabolism, TCA cycle and the phenylalanine degradation. Intermediates and their enzymes of glycolysis tend to indicate a reduced or weakly upregulation.

All results taken together provide strong evidence that the disruption of a functional Rnf-Prd supercomplex has a remarkable metabolic effect on the cell. Finally, it is noteable that an anaerobic lifestyle without a functional Rnf-Prd complex is viable on the expenses of energy losses and extensive phyisiological re-adjustments.

5.3 The negative influence on infection process by a non-functional Rnf-Prd complex tested in a mouse model

Finally, individual infection experiments in the mouse model with the *rnfC* mutant strain and the *rnfC*-complemented mutant strain showed a drastic difference specifically at day 1 after infection. While the complemented strain resembled the expected wildtype behavior (figure 33) produced spores in the cecum, colon and feces at the first day after infection, the mutant was unable to sporulate in the different samples (figure 34). Nevertheless, CFU counting resulted in similar numbers of vegetative cells for both strains in all samples (figure 34). This might imply that the *rnfC* mutant is highly restricted in the sporulation process as a result of a reduced mode of energy generation. Alternatively, important metabolic signal molecules involved in sporulation were missing. It is also likely that germination is diminished for this mutant. Specific experiments on the germination process with the use of bile acids (Sorg and Sonenshein 2008) in comparison with the *rnfC*-complemented mutant strain could provide further insights into this aspect.

In order to determine the competitive fitness of both strains, they were subjected to a co-infection experiment in a mouse model. The experiment demonstrated obviously that at day 1 after co-infection mainly *rnfC* mutant spores but also vegetative cells were excreted. This ratio was reversed at day 3 which was also mirrored by the gut samples (figure 35). Obviously, the co-infection negatively impacted the fitness of the *rnfC* mutant strain. Since many spores were found excreted here, a germination defect was concluded for the *rnfC* mutant strain.

Interestingly, vegetative cells of the *rnfC* mutant were also excreted after co-infection at day 1, which did not have any germination defects (figure 35). In comparison to the *rnfC*-complemented mutant strain, significantly more vegetative *rnfC* mutant cells were

excreted, which indicated that the mutant cells were suppressed by the fitter *rnfC*-complemented mutant strain and did not colonize effectively the gut. Obviously, the vegetative *rnfC* mutant cells were no longer able to adhere sufficiently to the epithelial cells, which may be caused by the abnormal flagellar morphology already visible by SEM (figure 26).

However, only few *rnfC* mutant cells succeed and were identified in the samples at day 3. The weakness of colonization of the *C. difficile rnfC* mutants in the gut has also been observed before with a *prdB* mutant strain (Battaglioli *et al.* 2018), which supports the claim that there is a correlation between effective colonization and an intact Rnf-Prd complex. Hence, in order to investigate observed defects, further adherence surface experiments and moltility assessment studies with the *rnfC* mutant strain might enlighten this phenomenon.

6 Summary

Metabolic processes are central to toxin formation and corresponding infection success of the Gram-positive, anaerobic gut pathogen *C. difficile*. The bacterium utilizes a unique amino acid-based fermentation (Stickland reaction) in conjunction with a membrane-spanning ion-pumping Rnf complex for ATP generation. Here, it was demonstrated by interactomics that one of the major enzymes of the reductive Stickland fermentation D-proline reductase forms a stable supercomplex with the Rnf complex. Other enzymes of Stickland fermentation (subunits of the glycine reductase), of ATP generation (F-type and V-type ATPase), of electron bifurcation (Bcd2/Etf), butanoate metabolism (e.g. Buk2, Cat2, Crt2 and SucD), glycolysis (e.g. Fba, Gap and Pyk) and the TCA cycle (e.g. PycA) are also members of the supercomplex.

Correspondingly, a still viable *rnfC* mutant strain contained an almost inactive D-proline reductase, showed changes in cell morphology, flagella formation and toxin production. Detailed holistic Omics-based analyses of compensatory changes in gene regulation, the protein inventory and metabolite composition revealed a significant reprogramming of the overall cell physiology. The NAD^+/NADH ratio was imbalanced, a compensatory up-regulation of the butanoate metabolism and TCA cycle as well as changes in the amino acid pathways were observed. Finally, the *rnfC* mutant strain showed clear cut defects in the colonization of the host as tested in a mouse model. In summary, obtained results underscores the importance of the Rnf-proline reductase supercomplex for the infection by *C. difficile*.

7 References

Aebersold, R. and Mann, M. (2003): Mass spectrometry-based proteomics. In: *Nature*, 422: 198–207

Aboulnaga, E.; Pinkenburg, O.; Schiffels, J.; El-Refai, A.; Buckel, W. and Selmer, T. (2013): Effect of an oxygen-tolerant bifurcating butyryl coenzyme A dehydrogenase/electron-transferring flavoprotein complex from *Clostridium difficile* on butyrate production in *Escherichia coli*. In: *Journal of Bacteriology,* 195: 3704–3713

Baktash, A.; Terveer, E. M.; Zwittink, R. D.; Hornung, B. V. H.; Corver, J.; Kuijper, E. J. and Smits, W. K. (2018): Mechanistic Insights in the Success of Fecal Microbiota Transplants for the Treatment of *Clostridium difficile* Infections. In: *Frontiers in Microbiology*, 9: 1242

Battaglioli, E.J., Hale, V.L., Chen, J., Jeraldo, P., Ruiz-Mojica, C., Schmidt, B.A., Rekdal, V.M., Till, L.M., Huq, L., Smits, S. A., Moor, W. J., Jones-Hall, Y., Smyrk, T., Khanna, S., Pardi, D.S., Grover, M., Patel, R., Chia, N., Nelson, H., Sonnenburg, J. L., Farrugia, G. and Kashyap, P. C. (2018): *Clostridioides difficile* uses amino acids associated with gut microbial dysbiosis in a subset of patients with diarrhea. In: *Science Translational Medicine*., 10: eaam7019

Bartlett, J. G.; Onderdonk, A. B.; Cisneros, R. L. and Kasper, D. L. (1977): Clindamycin-associated colitis due to a toxin-producing species of *Clostridium* in hamsters. In: *The Journal of Infectious Diseases,* 136: 701–705

Bartlett, J. G.; Chang, T. W.; Gurwith, M.; Gorbach, S. L. and Onderdonk, A. B. (1978): Antibiotic-associated pseudomembranous colitis due to toxin-producing *clostridia*. In: *The New England Journal of Medicine*, 298: 531–534

Bertani, G. (1951): Studies on lysogenesis. I. The mode of phage liberation by lysogenic *Escherichia coli*. In: *Journal of Bacteriology,* 62: 293–300

Bertani, G. (2004): Lysogeny at mid-twentieth century: P1, P2, and other experimental systems. In: *Journal of Bacteriology,* 186: 595–600

Bertsch, J.; Parthasarathy, A.; Buckel, W. and Müller, V. (2013): An electron-bifurcating caffeyl-CoA reductase. In: *The Journal of Biological Chemistry,* 288: 11304–11311

Biegel, E. and Müller, V. (2010): Bacterial Na+-translocating ferredoxin:NAD+ oxidoreductase. In: *Proceedings of the National Academy of Sciences,* 107: 18138–18142

Biegel, E.; Schmidt, S. and Müller, V. (2009): Genetic, immunological and biochemical evidence for a Rnf complex in the acetogen *Acetobacterium woodii*. In: *Environmental Microbiology,* 11: 1438–1443

Bouillaut, L.; McBride, S. M. and Sorg, J. A. (2011): Genetic manipulation of *Clostridium difficile*. In: *Current Protocols in Microbiology*, Unit 9A.2

Bouillaut, L.; Self, W. T.; Sonenshein, A. L. (2013): Proline-dependent regulation of *Clostridium difficile* Stickland metabolism. In: *Journal of Bacteriology,* 195: 844–854

Bouillaut, L.; Dubois, T.; Francis, M.B.; Daou, N.; Monot, M.; Sorg, J. A.; Sonenshein, A. L. and Dupuy, B. (2019): Role of the global regulator Rex in control of NAD^+ -regeneration in *Clostridioides (Clostridium) difficile*. In: *Molecular Microbiology*, 111: 1671-1688

Braun, V.; Hundsberger, T.; Leukel, P.; Sauerborn, M. and von Eichel-Streiber, C. (1996): Definition of the single integration site of the pathogenicity locus in *Clostridium difficile*. In: *Gene,* 181: 29–38

Bruant, G.; Lévesque, M.-J.; Peter, C.; Guiot, S. R. and Masson, L. (2010): Genomic analysis of carbon monoxide utilization and butanol production by *Clostridium carboxidivorans* strain $P7^T$. In: *PLoS ONE,* 5: e13033

Buckel, W. and Thauer R. K. (2013): Energy conservation via electron bifurcating ferredoxin reduction and proton/Na(+) translocating ferredoxin oxidation. In: *Biochim Biophys Acta,* 1827: 94–113

Buckel, W. and Thauer, R.K. (2018): Flavin-Based Electron Bifurcation, A New Mechanism of Biological Energy Coupling. In: *Chemical Reviews*, 118: 3862– 3886

Cartman, S. T. and Minton, N. P. (2010): A mariner-based transposon system for *in vivo* random mutagenesis of *Clostridium difficile*. In: *Applied and Environmental Microbiology,* 76: 1103–1109

Chiang, J. Y. L. (2009): Bile acids: regulation of synthesis. In: *Journal of Lipid Research*, 50: 1955–1966

Chowdhury, N.P.; Klomann, K.; Seubert, A. and Buckel, W. (2016): Reduction of Flavodoxin by Electron Bifurcation and Sodium Ion-dependent Reoxidation by NAD^+ Catalyzed by Ferredoxin-NAD^+ Reductase (Rnf). In: *The Journal of Biological Chemistry*, 291: 11993-12002

Cone, J. E.; del Río, R. M. and Stadtman, T. C. (1977): Clostridial glycine reductase complex. Purification and characterization of the selenoprotein component. In: *The Journal of biological chemistry,* 252: 5337–5344.

Cusick, M.; Klitgord, N.; Vidal, M. and Hill, D. E. (2005): Interactome: gateway into systems biology. In: *Human Molecular Genetics*, 14: R171-R181

Czepiel, J.; Dróżdż, M.; Pituch, H.; Kuijper, E. J.; Perucki, W.; Mielimonka, A.; Goldman, S.; Wultańska, D.; Garlicki, A. and Biesiada, G. (2019): *Clostridium difficile* infection: review. In: *European Journal of Clinical Microbiology & Infectious Diseases: official publication of the European Society of Clinical Microbiology,* 38: 1211–1221

Dannheim, H.; Will, S. E.; Schomburg, D. and Neumann-Schaal, M. (2017): *Clostridioides difficile* 630Δ*erm in silico* and *in vivo* - quantitative growth and extensive polysaccharide secretion. In: *FEBS Open Bio,* 7: 602–615

Demmer, J.K.; Pal Chowdhury, N.; Selmer, T; Ermler, U. and Buckel, W. (2017): The semiquinone swing in the bifurcating electron transferring flavoprotein/butyryl-CoA dehydrogenase complex from *Clostridium difficile*. In: *Nat Commun*, 8: 1577

De Las Rivas, J. and Fontanillo, C. (2010): Protein–Protein Interactions Essentials: Key Concepts to Building and Analyzing Interactome Networks. In: *PLoS Computational Biology*, 6: e1000807

Dineen, S. S.; McBride, S. M. and Sonenshein, A. L. (2010): Integration of metabolism and virulence by *Clostridium difficile* CodY. In: *Journal of Bacteriology,* 192: 5350–5362

Dineen, S. S.; Villapakkam, A. C.; Nordman, J. T. and Sonenshein, A. L. (2007): Repression of *Clostridium difficile* toxin gene expression by CodY. In: *Molecular Microbiology,* 66: 206–219

Dupuy, B. and Sonenshein, A. L. (1998): Regulated transcription of *Clostridium difficile* toxin genes. In: *Molecular Microbiology,* 27: 107–120

Drake, H. L.; Gößner, A. S. and Daniel, S.L. (2008): Old acetogens, new light. In: *New York Academy of Sciences*, 1125: 100–12

Eckburg, P. B.; Bik, E. M.; Bernstein, C. N.; Purdom, E.; Dethlefsen, L.; Sargent, M.; Gill, S.R.; Nelson, K.E. and Relman, D.A. (2005): Diversity of the human intestinal microbial flora. In: *Science (New York, N.Y.),* 308: 1635–1638

Eng, J. K.; Searle, B. C.; Clauser, K. R. and Tabb, D. L. (2011): A Face in the Crowd: Recognizing Peptides Through Database Search. In: *Molecular and Cellular Proteomics*, 10: R111.009522

Fast, A. G. and Papoutsakis, E. T. (2018): Functional Expression of the *Clostridium ljungdahlii* Acetyl-Coenzyme A Synthase in *Clostridium acetobutylicum* as Demonstrated by a Novel *In Vivo* CO Exchange Activity En Route to Heterologous Installation of a Functional Wood-Ljungdahl Pathway. In: *Applied and Environmental Microbiology,* 84: e02307-17

Feng, S.; Zhou, L.; Huang, C.; Xie, K. and Nice, E. C. (2014): Interactomics: toward proteinfunction and regulation. In: *Expert Review of Proteomics,* 12: 37-60

Fonknechten, N.; Chaussonnerie, S.; Tricot, S.; Lajus, A.; Andreesen, J. R.; Perchat, N.; Pelletier, E.; Gouyvenoux, M.; Barbe, V.; Salanoubat, M.; Le Paslier, D.; Weissenbach, J.; Cohen, G.N. and Kreimeyer, A. (2010): *Clostridium sticklandii*, a specialist in amino acid degradation:revisiting its metabolism through its genome sequence. In: *BMC Genomics*, 11: 555

Fortier, L.-C. and Sekulovic, O. (2013): Importance of prophages to evolution and virulence of bacterial pathogens. In: *Virulence,* 4: 354–365

Fraenkel-Conrat, H. and Olcott, H. S. (1948): Reaction of formaldehyde with proteins. VI. cross-linking of amino groups with phenol, imidazole or indole groups. In: *Journal of Biological Chemistry*, 174: 827-843

Fromont-Racine, M.; Rain, J. C. and Legrain, P. (1997): Toward a functional analysis of the yeast genome through exhaustive two-hybrid screens. In: *Nature Genetics*, 16: 277–282

Gingras, A.; Gstaiger, M.; Raught, B. and Aebersold, R. (2007): Analysis of protein complexes using mass spectrometry. In: *Nature Reviews. Molecular Cell Biology,* 8: 645–654.

Guarner, F. and Malagelada, J.-R. (2003): Gut flora in health and disease. In: *The Lancet,* 361: 512–519

Häse, C.C.; Fedorova, N.D.; Galperin, M.Y. and Dibrov P.A. (2001): Sodium ion cycle in bacterial pathogens: evidence from cross-genome comparisons. In: *Microbiology and Molecular Biology Reviews*, 65: 353-370

Hall, I. C. and O'Toole E. (1935): INTESTINAL FLORA IN NEW-BORN INFANTS: WITH A DESCRIPTION OF A NEW PATHOGENIC ANAEROBE, *BACILLUS DIFFICILIS*. In: *Am J Dis Child,* 49: 390–402.

Halsey, C. R., Lei, S., Wax, J. K., Lehman, M. K., Nuxoll, A. S., Steinke, L., Sadykov, M., Powers, R., and Fey, P. D. (2017): Amino Acid Catabolism in *Staphylococcus aureus* and the Function of Carbon Catabolite Repression. In: *mBio*, 8: e01434-16

Hastie, J.L.; Hanna, P.C. and Carlson, P.E. (2018): Transcriptional response of *Clostridium difficile* to low iron conditions. In: *Pathogens and Disease*, 76: fty009

Hattori, M. and Taylor, T. D. (2009): The human intestinal microbiome: a new frontier of human biology. In: *DNA research: an international journal for rapid publication of reports on genes and genomes,* 16: 1–12

Heap, J. T.; Cartman, S. T.; Kuehne, S. A.; Cooksley, C. and Minton, N. P. (2010a): ClosTron-targeted mutagenesis. In: *Methods in Molecular Biology (Clifton, N.J.)*, 646: 165–182

Heap, J. T.; Kuehne, S. A.; Ehsaan, M.; Cartman, S. T.; Cooksley, C. M.; Scott, J. C. and Minton, N. P. (2010b): The ClosTron: Mutagenesis in *Clostridium* refined and streamlined. In: *Journal of Microbiological Methods,* 80: 49–55

Heap, J. T.; Pennington, O. J.; Cartman, S. T.; Carter, G. P. and Minton, N. P. (2007): The ClosTron: a universal gene knock-out system for the genus *Clostridium*. In: *Journal of Microbiological Methods,* 70: 452–464

Heap, J. T.; Pennington, O. J.; Cartman, S. T. and Minton, N. P. (2009): A modular system for *Clostridium* shuttle plasmids. In: *Journal of Microbiological Methods,* 78: 79–85

Hofmann, J. D.; Otto, A.; Berges, M.; Biedendieck, R.; Michel, A.-M.; Becher, D.; Jahn, D. and Neumann-Schaal, M. (2018): Metabolic Reprogramming of *Clostridioides difficile* During the Stationary Phase With the Induction of Toxin Production. In: *Frontiers in Microbiology*, 9: 1970

Hooper, L. V.; Midtvedt, T. and Gordon, J. I. (2002): How host-microbial interactions shape the nutrient environment of the mammalian intestine. In: *Annual Review of Nutrition*, 22: 283–307

Hughes, C. S.; Foehr, S.; Garfield, D. A.; Furlong, E. E.; Steinmetz, L. M. and Krijgsveld, J. (2014): Ultrasensitive proteome analysis using paramagnetic bead technology. In: *Molecular Systems Biology*, 10: 757

Hussain, H. A.; Roberts, A. P. and Mullany, P. (2005): Generation of an erythromycin-sensitive derivative of *Clostridium difficile* strain 630 (630Deltaerm) and demonstration that the conjugative transposon Tn916DeltaE enters the genome of this strain at multiple sites. In: *Journal of Medical Microbiology,* 54: 137–141

Jackson, S.; Calos, M.; Myers, A. and Self, W.T. (2006): Analysis of proline reduction in the nosocomial pathogen *Clostridium difficile*. In: *Journal of Bacteriology*, 188: 8487-8495

Jahn, M.; Jahn, D.; Moran, L. A.; Horton, H.R.; Scrimgeour, K.G. and Perry, M.D. (2020): Horton. Biochemie kompakt. München: Pearson Deutschland GmbH

Juárez, O. and Barquera, B. (2012): Insights into the mechanism of electron transfer and sodium translocation of the Na^+-pumping NADH:quinone oxidoreductase. In: *Biochimica et Biophysica Acta,* 1817: 1823-1832

Jungermann, K.; Thrauer, R. K. and Decker, K. (1967): The Synthesis of One-Carbon Units from CO_2 in *Clostridium kluyveri*. In: *European J. Biochem*., 3: 351-359

Kabisch, U.C., Gräntzdörffer, A.; Schierhorn, A.; Rücknagel, K.P.; Andreesen, J.R. and Pich, A. (1999): Identification of D-proline reductase from *Clostridium sticklandii* as a selenoenzyme and indications for a catalytically active pyruvoyl group derived from a cysteine residue by cleavage of a proprotein. In: *Journal of Biological Chemistry*, 274: 8445-8454

Kabisch, U. C.: Proteinchemische und molekularbiologische Charakterisierung der D-Prolin-Reduktase aus *Clostridium sticklandii*. @Halle, Univ., Diss., 2001. [Elektronische Ressource]. Halle, Saale: Universitäts- und Landesbibliothek. Online verfügbar unter http://nbn-resolving.de/urn:nbn:de:gbv:3-000003052.

Kachrimanidou, M. and Tsintarakis, E. (2020): Insights into the Role of Human Gut Microbiota in *Clostridioides difficile* Infection. In: *Microorganisms*, 8:200

Karlsson, S.; Burman, L. G. and Åkerlund, T. (1999): Suppression of toxin production in *Clostridium difficile* VPI 10463 by amino acids. In: *Microbiology (Reading, England)*, 145: 1683–1693

Karlsson, S.; Lindberg, A.; Norin, E.; Burman, L.G. and Akerlund, T. (2000): Toxins, butyric acid, and other short-chain fatty acids are coordinately expressed and down-regulated by cysteine in *Clostridium difficile*. In: *Infection and Immun*ity, 68: 5881-5888

Karlsson, S.; Dupuy, B.; Mukherjee, K.; Norin, E.; Burman, L. G. and Akerlund, T. (2003): Expression of *Clostridium difficile* toxins A and B and their sigma factor TcdD is controlled by temperature. In: *Infection and Immunity,* 71: 1784–1793

Kho, Z. Y. and Lal, S. K. (2018): The Human Gut Microbiome - A Potential Controller of Wellness and Disease. In: *Frontiers in Microbiology*, 9:1835

Kochan, T. J.; Somers, M. J.; Kaiser, A. M.; Shoshiev, M. S.; Hagan, A. K.; Hastie, J. L.; Giordano, N. P.; Smith, A. S.; Schubert, A. M.; Carlson Jr., P. E. and Hanna, P. C. (2017): Intestinal calcium and bile salts facilitate germination of *Clostridium difficile* spores. In: *PLoS Pathogens*, 13: e1006443

Köpke, M.; Held, C.; Hujer, S.; Liesegang, H.; Wiezer, A.; Wollherr, A.; Ehrenreich, A.; Liebl, W.; Gottschalk, G. and Dürre, P. (2010): *Clostridium ljungdahlii* represents a microbial production platform based on syngas. In: *Proceedings of the National Academy of Sciences,* 107: 13087–13092

Köpke, M.; Straub, M. and Dürre, P. (2013): *Clostridium difficile* is an autotrophic bacterial pathogen. In: *PloS ONE,* 8: e62157

Kuehne, S. A. and Minton, N. P. (2012): ClosTron-mediated engineering of Clostridium. In: *Bioengineered,* 3: 247–254

Kuhns, M.; Trifunović, D.; Huber, H. and Müller, V. (2020): The Rnf complex is a Na^+ coupled respiratory enzyme in a fermenting bacterium, *Thermotoga maritima*. In: *Communications Biology,* 3: 431

Langmead, B. and Salzberg, S. L. (2012): Fast gapped-read alignment with Bowtie 2. In: *Nature Methods,* 9: 357–359

Larance, M., Kirkwood, K. J.; Tinti, M.; Brenes Murillo, A.; Ferguson, M. A. and Lamond, A. I. (2016): Global Membrane Protein Interactome Analysis using *In vivo* Crosslinking and Mass Spectrometry-based Protein Correlation Profiling. In: *Molecular & Cellular Proteomics*, 15: 2476–2490

Larson, H. E.; Parry, J. V.; Price, A. B.; Davies, D. R.; Dolby, J. and Tyrrell, D. A. (1977): Undescribed toxin in pseudomembranous colitis. In: *British Medical Journal,* 1: 1246–1248

Lau, C. K. Y.; Krewulak, K. D. and Vogel, H. J. (2016): Bacterial ferrous iron transport: the Feo system. In: *FEMS Microbiology Rev*iews, 40: 273-298

Lawson, P. A.; Citron, D. M.; Tyrrell, K. L. and Finegold, S. M. (2016): Reclassification of *Clostridium difficile* as *Clostridioides difficile* (Hall and O'Toole 1935) Prévot 1938. In: *Anaerobe*, 40: 95–99

Li, F.; Hinderberger, J.; Seedorf, H.; Zhang, J.; Buckel, W. and Thauer, R. K. (2008): Coupled ferredoxin and crotonyl coenzyme A (CoA) reduction with NADH catalyzed by the butyryl-CoA dehydrogenase/Etf complex from *Clostridium kluyveri*. In: *Journal of Bacteriology,* 190: 843–850

Luckey, T. D. (1972): Introduction to intestinal microecology. In: *The American Journal of Clinical Nutrition,* 25: 1292–1294

Mahler, H. C.; Friess, W.; Grauschopf, U and Kiese, S. (2009): Protein aggregation: Pathways, induction factors and analysis. In: *Journal of Pharmaceutical Sciences*, 98: 2909-2934

Mani, N. and Dupuy, B. (2001): Regulation of toxin synthesis in *Clostridium difficile* by an alternative RNA polymerase sigma factor. In: *Proceedings of the National Academy of Sciences of the United States of America,* 98: 5844–5849

Martin-Verstraete, I.; Peltier, J. and Dupuy, B. (2016): The Regulatory Networks That Control *Clostridium difficile* Toxin Synthesis. In: *Toxins* 8: 153

McClure, R.; Balasubramanian, D.; Sun, Y.; Bobrovskyy, M.; Sumby, P.; Genco, C. A.; Vanderpool, C. K. and Tjaden, B. (2013): Computational analysis of bacterial RNA-Seq data. In: *Nucleic Acids Research;* 41: e140

Metz, B.; Kersten, G. F. A.; Hoogerhout, P.; Brugghe, H. F.; Timmermans, H. A. M.; de Jong, A.; Meiring, H.; ten Hove, J.; Hennink, W. E.; Crommelin, D. J. A. and Jiskoot, W. (2004): Identification of formaldehyde-induced modifications in proteins: reactions with model peptides. In: *Journal of Biological Chemistry,* 279: 6235–6243

Meyer, K. and Selbach, M. (2015): Quantitative affinity purification mass spectrometry: a versatile technology to study protein-protein interactions. In: *Frontiers in Genetics*, 6: 237

Mohr, G.; Smith, D.; Belfort, M. and Lambowitz, A. M. (2000): Rules for DNA target-site recognition by a lactococcal group II intron enable retargeting of the intron to specific DNA sequences. In: *Genes & Development,* 14: 559–573

Müller, V. and Wiechmann, A. (2017): Synthesis of Acetyl-CoA from Carbon Dioxide in Acetogenic Bacteria. In: Geiger O. (Hg.): Biogenesis of Fatty Acids, Lipids and Membranes. Handbook of Hydrocarbon and Lipid Microbiology: Springer

Müller, V.; Aufurth, S. and Rahlfs, S. (2001): The Na^+ cycle in *Acetobacterium woodii*: Identification and characterization of a Na^+ translocating F1F0-ATPase with a mixed oligomer of 8 and 16 kDa proteolipids. In: *Biochimica et Biophysica Acta (BBA) - Bioenergetics,* 1505: 108–120

Mylonakis, E.; Ryan, E. T. and Calderwood, S. B. (2001): *Clostridium difficile*--Associated diarrhea: A review. In: *Archives of Internal Medicine,* 161: 525–533

Neumann-Schaal, M.; Hofmann, J. D.; Will, S. E. and Schomburg, D. (2015): Time-resolved amino acid uptake of *Clostridium difficile* 630Δ*erm* and concomitant fermentation product and toxin formation. In: *BMC Microbiology*, 15: 281

Neumann-Schaal, M.; Jahn, D. and Schmidt-Hohagen, K. (2019): Metabolism the Difficile Way: The Key to the Success of the Pathogen *Clostridioides difficile*. In: *Frontiers in Microbiology*, 10: 219

Nisman, B. (1954): The Stickland reaction. In: *Bacteriological Reviews,* 18: 16–42

Onderdonk, A. B.; Lowe, B. R. and Barlett, J. G. (1979): Effect of environmental stress on *Clostridium difficile* toxin levels during continuous cultivation. In: *Applied and Environmental Microbiology,* 38: 637–641

Perutka, J.; Wang, W.; Goerlitz, D. and Lambowitz, A.M. (2004): Use of computer-designed group II introns to disrupt *Escherichia coli* DExH/D-box protein and DNA helicase genes. In: *Journal of Molecular Biology,* 336: 421–39

Poehlein, A.; Schmidt, S.; Kaster, A.-K.; Goenrich, M.; Vollmers, J.; Thürmer, A.; Bertsch, J.; Schuchmann, K.; Voigt, B.; Hecker, M.; Daniel, R.; Thauer, R. K.; Gottschalk, G. and Müller, V. (2012): An Ancient Pathway Combining Carbon Dioxide Fixation with the Generation and Utilization of a Sodium Ion Gradient for ATP Synthesis. In: *PloS ONE,* 7: e33439

Popoff, M. R.; Rubin, E. J.; Gill, D. M. and Boquet, P. (1988): Actin-specific ADP-ribosyltransferase produced by a *Clostridium difficile* strain. In: *Infection and Immunity,* 56: 2299–2306

Präve, P.; Faust, U.; Sittig, W. and Sukatsch, D. A. (1994): Handbuch der Biotechnologie. 4. Auflage. R. Oldenbourg Verlag GmbH, Münschen, p. 129

Rao, K. and Safdar, N. (2016): Fecal microbiota transplantation for the treatment of *Clostridium difficile* infection. In: *Journal of Hospital Medicine,*11: 56–61

Schirmer, J. and Aktories, K. (2004): Large clostridial cytotoxins: cellular biology of Rho/Ras-glucosylating toxins. In: *Biochimica et Biophysica Acta,* 1673: 66–74

Schmehl, M.; Jahn, A.; Meyer zu Vilsendorf, A.; Hennecke, S.; Masepohl, B.; Schuppler, M.; Marxer, M.; Oelze, J. and Klipp, W. (1993): Identification of a new class of nitrogen fixation genes in *Rhodobacter capsulatus*: a putative membrane complex involved in electron transport to nitrogenase. In: *Molecular & General Genetics,* 241*:* 602–615

Schottelius, M. (1902): Die Bedeutung der Darmbakterien für die Ehrnahrung. II. In: *Arch. Hyg.* 42: 48–70

Schuchmann, K. and Müller, V. (2014): Autotrophy at the thermodynamic limit of life: a model for energy conservation in acetogenic bacteria. In: *Nature Reviews Microbiology,* 12: 809-821

Seto, B. and Stadtman, T. C. (1976): Purification and properties of proline reductase from *Clostridium sticklandii*. In: *Journal of Biological Chemistry* 251: 2435–2439

Seto, B. (1979): Proline reductase. A sensitive fluorometric assay with o-phthalaldehyde. In: *Analytical Biochemistry,* 95: 44–47

Shen, A. (2012): *Clostridium difficile* toxins: mediators of inflammation. In: *Journal of Innate Immunity,* 4: 149–158

Sielaff, M.; Kuharev, J.; Bohn, T.; Hahlbrock, J.; Bopp, T.; Tenzer, S. and Distler, U. (2017): Evaluation of FASP, SP3, and iST Protocols for Proteomic Sample Preparation in the Low Microgram Range. In: *Journal of Proteome Research,* 16: 4060–4072

Smits, W. K.; Lyras, D.; Lacy, D. B.; Wilcox, M. H. and Kuijper, E. J. (2016): *Clostridium difficile* infection. In: *Nature reviews. Disease primers*, 2: 16020

Sorg, J. A. and Sonenshein, A. L. (2008): Bile salts and glycine as cogerminants for *Clostridium difficile* spores. In: *Journal of Bacteriology,* 190: 2505-2512

Stadtman, T. C. (1956): Studies on the enzymic reduction of amino acids: a proline reductase of an amino acid-fermenting *Clostridium*, strain HF. In: *The Biochemical Journal,* 62: 614–621

Stadtman, T. C. and Elliott, P. (1957): Studies on the enzymic reduction of amino acids. II. Purification and properties of D-proline reductase and a proline racemase from *Clostridium sticklandii*. In: *Journal of Biological Chemistry,* 228: 983–997

Stickland, L. H. (1934): Studies in the metabolism of the strict anaerobes (genus *Clostridium*): The chemical reactions by which *Cl. sporogenes* obtains its energy. In: *Biochemical Journal,* 28*:* 1746–1759

Stickland, L. H. (1935a): Studies in the metabolism of the strict anaerobes (genus *Clostridium*): The oxidation of alanine by *Cl. sporogenes*. IV. The reduction of glycine by *Cl. sporogenes.* In: *Biochemical Journal,* 29: 889–898

Stickland, L. H. (1935b): Studies in the metabolism of the strict anaerobes (Genus *Clostridium*): The reduction of proline by *Cl. sporogenes*. In: *Biochemical Journal,* 29*:* 288–290

Tayri-Wilk, T.; Slavin, M; Zamel, J.; Blass, A.; Cohen, S.; Motzik, A.; Sun, X.; Shalev, D.E.; Ram, O. and Kalisman, N. (2020): Mass spectrometry reveals the chemistry of formaldehyde cross-linking in structured proteins. In: *Nature Communications*, 11: 3128

Thoma, S. and Schobert, M. (2009): An improved *Escherichia coli* donor strain for diparental mating. In: *FEMS Microbiology Letters,* 294: 127–132

Tjaden, B. (2015): *De novo* assembly of bacterial transcriptomes from RNA-seq data. In: *Genome Biology*, 16: 1

Trautwein, K.; Will, S. E.; Hulsch, R.; Maschmann, U.; Wiegmann, K.; Hensler, M.; Michael, V.; Ruppersberg, H.; Wünsch, D.; Feenders, C.; Neumann-Schaal, M.; Kaltenhäuser, S.; Ulbrich, M.; Schmidt-Hohagen, K.; Blasius, B.; Petersen, J.; Schomburg, D. and Rabus, R. (2016): Native plasmids restrict growth of *Phaeobacter inhibens* DSM 17395: Energetic costs of plasmids assessed by quantitative physiological analyses. In: *Environmental Microbiology,* 18: 4817–4829

Walhout, A.J., Sordella, R.; Lu, X., Hartley, J. L.; Temple, G. F.; Brasch, M. A.; Thierry-Mieg, N. and Vidal, M. (2000): Protein interaction mapping in C. elegans using proteins involved in vulval development. In: *Science,* 287: 116–122

Wang, S.; Hong, W.; Dong, S.; Zhang, Z-T; Zhang, J.; Wang, L. and Wang, Y. (2018): Genome engineering of *Clostridium difficile* using the CRISPR-Cas9 system. In: *Clinical Microbiology and Infection: the official publication of the European Society of Clinical Microbiology and Infectious Diseases*, 24: 1095–1099

Will, S. E.; Henke, P.; Boedeker, C.; Huang, S.; Brinkmann, H.; Rohde, M.; Jarek, M.; Friedl, T.; Seufert, S.; Schumacher, M.; Overmann, J.; Neumann-Schaal, M. and Petersen, J. (2019): Day and Night: Metabolic Profiles and Evolutionary Relationships of Six Axenic Non-Marine Cyanobacteria. In: *Genome Biology and Evolution,* 11: 270–294

Wolf, J.; Stark, H.; Fafenrot, K.; Albersmeier, A.; Pham, T. K.; Müller, K. B.; Meyer, B. H.; Hoffmann, L.; Shen, L.; Albaum, S. P.; Kouril, T.; Schmidt-Hohagen, K.; Neumann-Schaal, M.; Bräsen, C.; Kalinowski, J.; Wright, P. C.; Albers, S.-V.; Schomburg, D. and Siebers, B. (2016): A systems biology approach reveals major metabolic changes in the thermoacidophilic archaeon *Sulfolobus solfataricus* in response to the carbon source L-fucose versus D-glucose. In: *Molecular Microbiology,* 102: 882–908

8 Appendix

8.1 Vector map of the plasmid pMTL82151

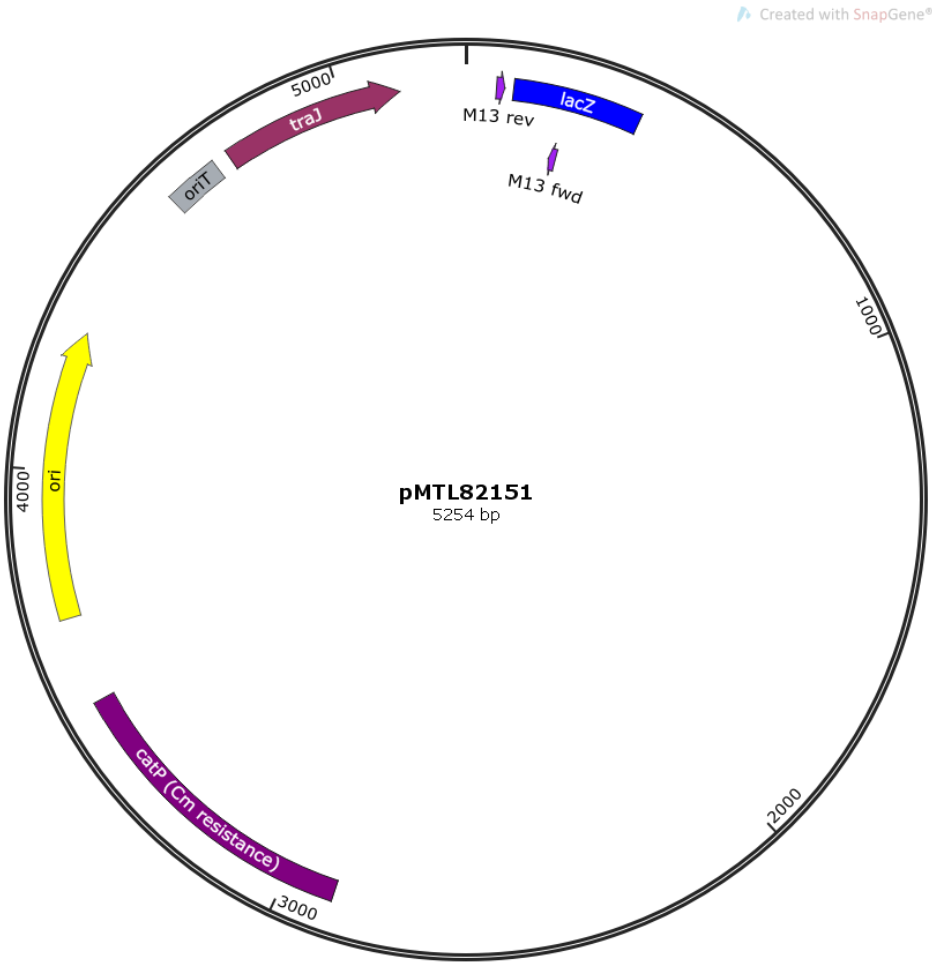

Figure 38: Illustration of the vector pMTL82151. Shown is the commercially available vector pMTL82151 ((Heap *et al.* 2009)/CHAIN Biotechnplogy Ltd; Nottingham, UK) with a size of 5354 bp, which was used as the basis for cloning steps of the constructs: pMTL82151*prdA*-strep II, pMTL82151*prdB*-strep II, pMTL82151*rnfB*-strep II and pMTL82151*rnfC*-strep II (vector card: digital appendix). The vector has the following features: Binding sites for the general primers M13, *traJ* and *oriT* ((ColE1) Gram-negative replicon), *ori* (pBP1, Gram-positiv replicon), *catP* (Cm resistance) and *lacZ*. The vector map was prepared using the program SnapGene® (GSL Biotech LLC; San Diego, CA, USA).

8.2 SDS-PAGEs of the baits PrdA, PrdB, RnfB, RnfC and the wildtype in absence of the cross-linker formaldehyde

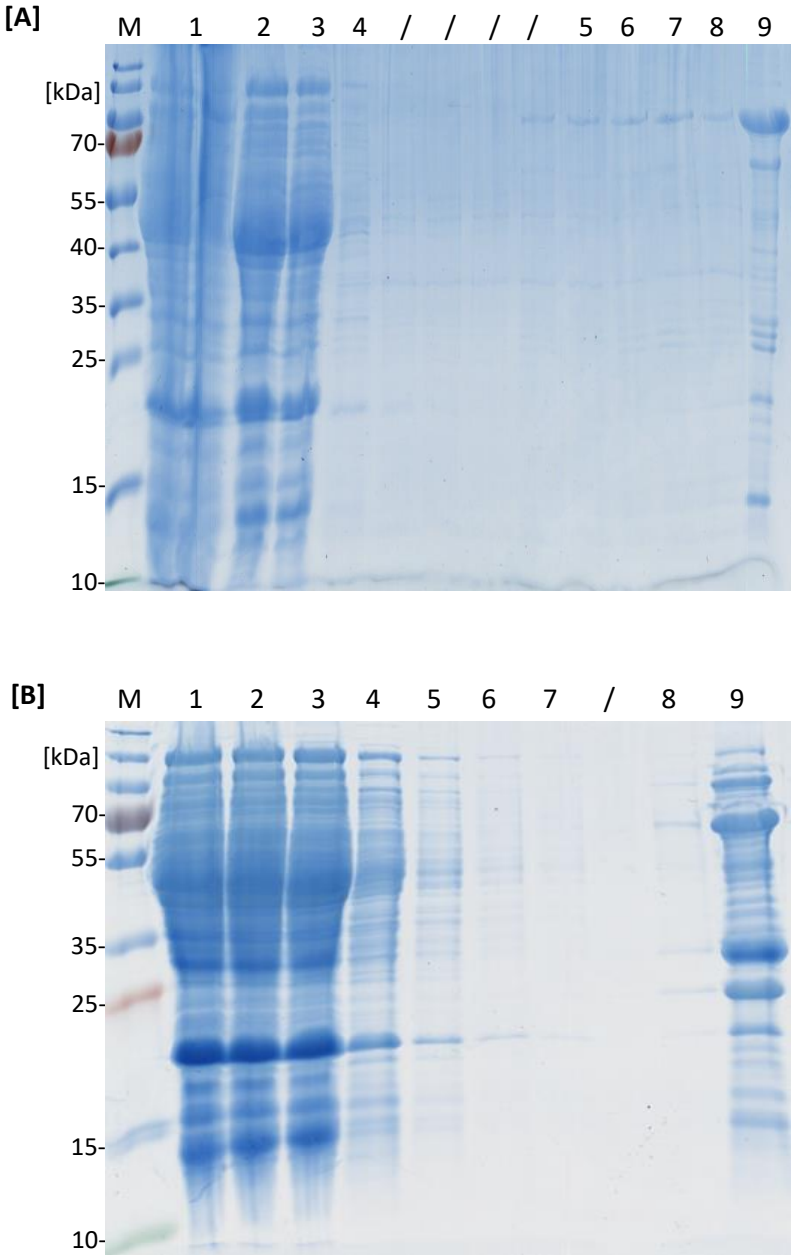

Figure 39: SDS-PAGEs of the baits PrdA [A] and PrdB [B] from *C. difficile* 630Δ*erm*_pMTL82151*prdA*-strep II and *C. difficile* 630Δ*erm*_pMTL82151*prdB*-strep II after affinity chromatography of the corresponding soluble fraction of the cell free extract. The different samples of the Strep-tagged affinity chromatographed bait proteins were loaded on a 15 % SDS-PAGE and separated according to their relative molecular masses at 45 mA for 45 min. The gel was stained with InstantBlue® Protein Stain (Expedeon Ltd, Cambridge, UK) solution. **M**: 5 µL PageRuler™ (Plus) Prestained *Protein Ladder* (Thermo Fisher Scientific, Schwerte, Germany); **lane 1**: 7 µL of the cell-free extract after ultracentrifugation (soluble fraction); **lane 2**: 7 µL flowthrough of the Strep-Tactin® column (Strep-Tactin® Superflow® high capacity, IBA Lifesciences, Göttingen, Germany); **lane 3-7**: 10 µL wash fractions 1 to 5; **lane 8**: 10 µL of the elution fraction of the bait protein PrdA [A] or PrdB [B]; **lane 9**: 10 µL of the 60-fold concentrated elution fraction of the bait protein; **lane /**: empty lanes. The PrdA encoding plasmid was constructed and the subsequent purification steps were performed by Ilka Pusch during her master thesis (2018).

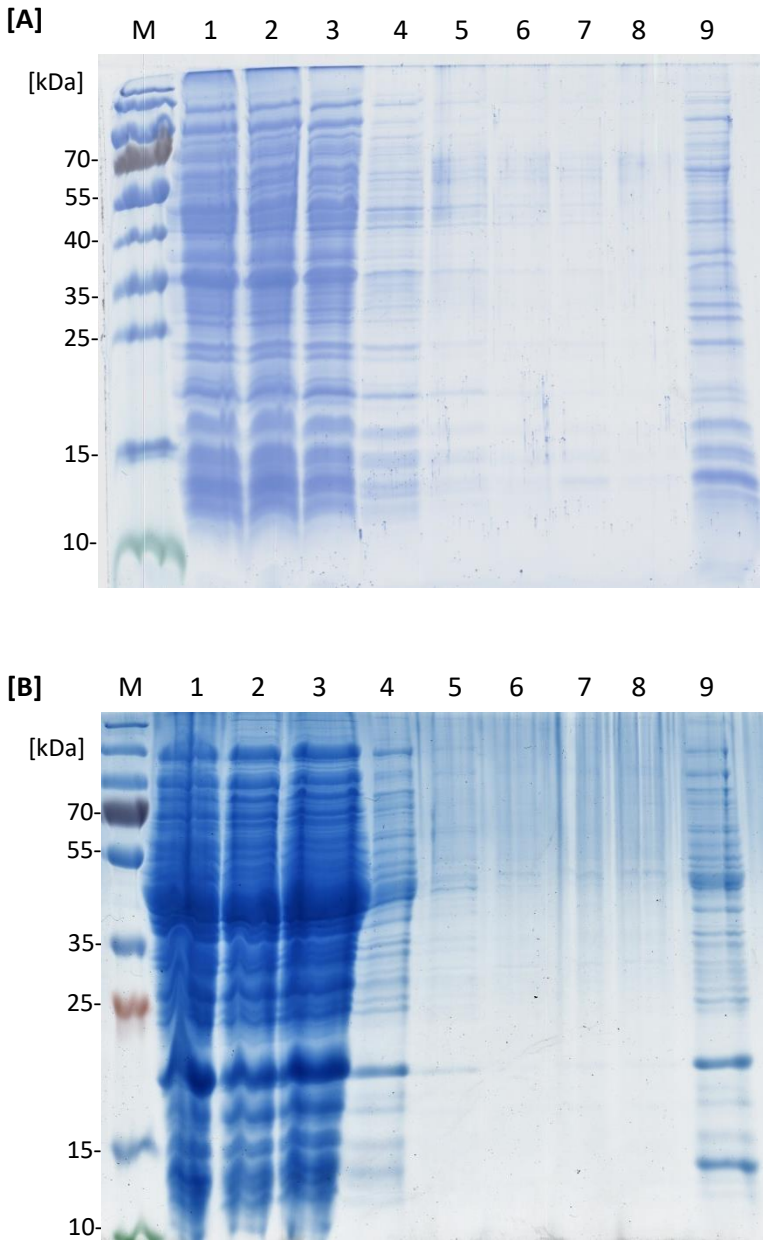

Figure 40: SDS-PAGEs of the baits RnfB [A] and RnfC [B] from *C. difficile* 630Δ*erm*_ pMTL82151*rnfB*-strep II *and C. difficile* 630Δ*erm*_ pMTL82151*rnfC*-strep II after affinity chromatography of the soluble fraction [RnfC] and insoluble fraction [RnfB] of the cell free extract. The samples of the protein purification were loaded on a 15 % SDS-PAGE and separated according to their relative molecular masses for 45 min at 45 mA. The gel was stained with InstantBlue® Protein Stain (Expedeon Ltd, Cambridge, UK) solution. **M**: 5 µL PageRuler™ (Plus) Prestained *Protein Ladder* (Thermo Fisher Scientific, Schwerte, Germany); **lane 1**: 7 µL of the solubilized insoluble fraction in [A] or 7 µL of the cell-free extract after ultracentrifugation (soluble fraction) in [B]; **lane 2**: 7 µL flowthrough of the Strep-Tactin® column (Strep-Tactin® Superflow® high capacity, IBA Lifesciences, Göttingen, Germany); **lane 3-7**: 10 µL wash fractions 1 to 5; **lane 8**: 10 µL of the elution fraction of the bait protein RnfB [A] or RnfC [B]; **lane 9**: 10 µL of the 60-fold (RnfC) and 30-fold (RnfB) concentrated elution fraction of the bait protein

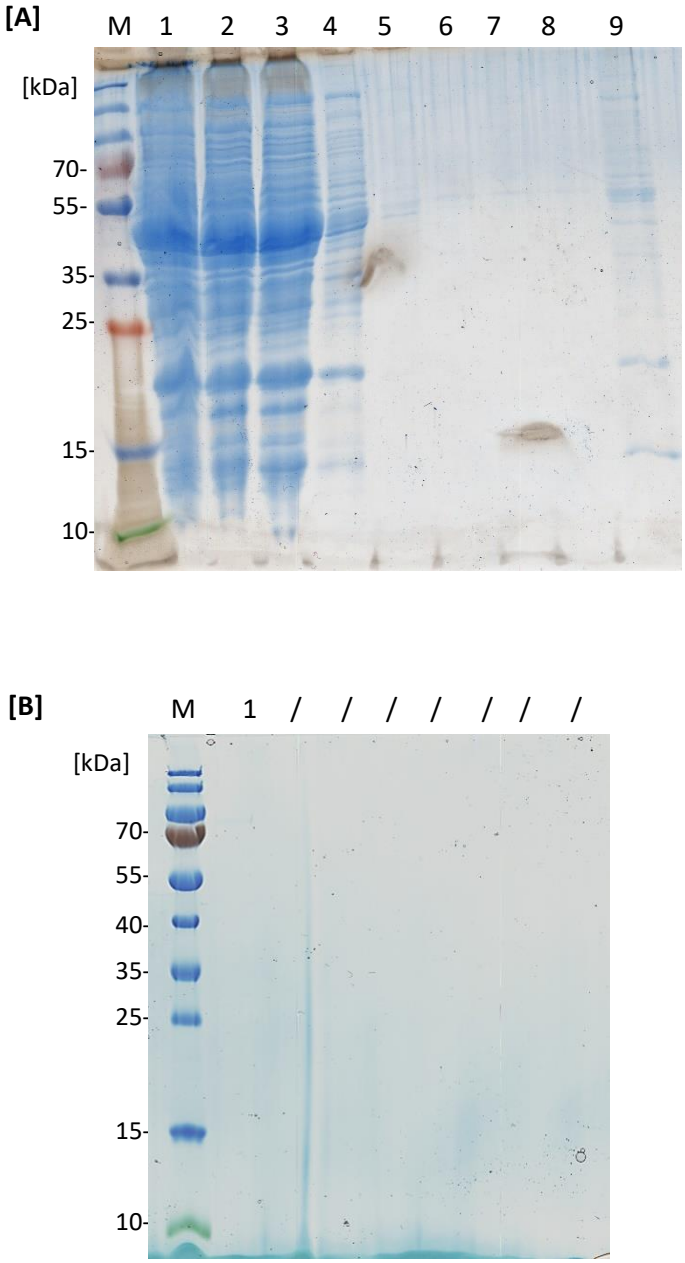

Figure 41: SDS-PAGEs of the affinity chromatographed wildtype proteins from *C. difficile* 630Δ*erm*_pMTL82151 of the soluble fraction [A] and insoluble fraction [B]. The affinity chromatographed protein samples were loaded on a 15 % SDS-PAGE and separated according to their relative molecular masses for 45 min by 45 mA. The gel was stained with InstantBlue® Protein Stain (Expedeon Ltd, Cambridge, UK) solution. **[A]: M**: 5 µL PageRuler™ (Plus) Prestained *Protein Ladder* (Thermo Fisher Scientific, Schwerte, Germany); **lane 1**: 7 µL of the cell-free extract after ultracentrifugation (soluble fraction); **lane 2**: 7 µL flowthrough of the Strep-Tactin® column (Strep-Tactin® Superflow® high capacity, IBA Lifesciences,Göttingen, Germany); **lane 3-7**: 10 µL wash fractions 1 to 5; **lane 8**: 10 µL of the elution fraction; **lane 9**: 10 µL of the 60-fold concentrated elution fraction; **[B]: M**: 5 µL PageRuler™ Prestained *Protein Ladder* (Thermo Fisher Scientific, Schwerte, Germany); **lane 1:** 10 µL of the 30-fold concentrated elution fraction after affinity chromatography of the insoluble fraction of the cell free extract from the wildtype *C. difficile* 630Δ*erm*_pMTL82151; **lane /**: empty lanes. The SDS-PAGE of the insoluble fraction [B] were performed by Ilka Pusch during her master thesis (2018).

8.3 SDS-PAGEs of the baits PrdA, PrdB, RnfB and RnfC in presence of the cross-linker formaldehyde

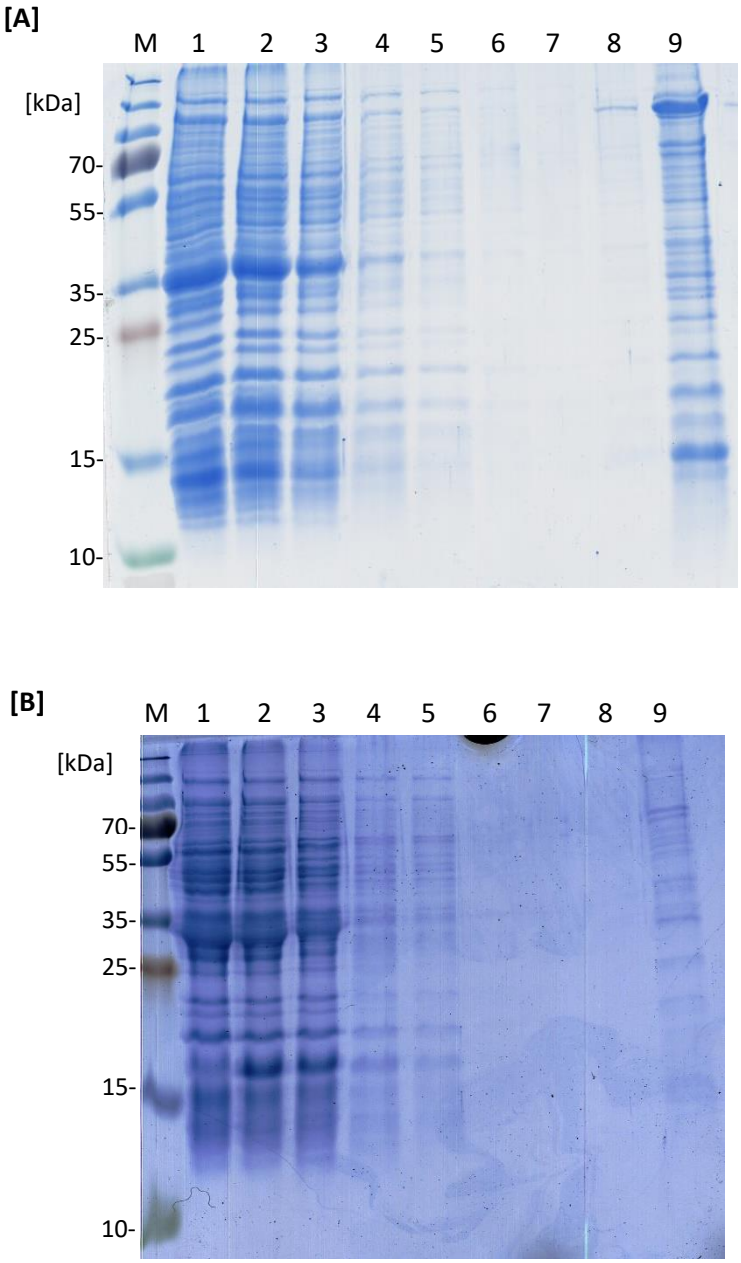

Figure 42: SDS-PAGEs of the affinity chromatographed bait proteins PrdA [A] and PrdB [B] from *C. difficile* 630Δ*erm*_pMTL82151*prdA*-strep II and *C. difficile* 630Δ*erm*_pMTL82151*prdB*-strep II in presence of the cross-linker formaldehyde. The *in-vivo* cross-linked (formaldehyde; $OD_{600\ nm}$ 1 = 0.156 % crosslinker) and Strep-tagged affinity chromatographed bait proteins PrdA and PrdB from the insoluble fractions were loaded on a 15 % SDS-PAGE, respectively. The proteins were separated according to their relative molecular masses at 45 mA for 45 min. Afterwards, the gel was stained with InstantBlue® Protein Stain (Expedeon Ltd, Cambridge, UK) solution. **M**: 5 µL PageRuler™ Plus Prestained *Protein Ladder* (Thermo Fisher Scientific, Schwerte, Germany); **lane 1**: 7 µL of the solubilized insoluble fraction; **lane 2**: 7 µL flowthrough of the Strep-Tactin® column (Strep-Tactin® Superflow® high capacity, IBA Lifesciences, Göttingen, Germany); **lane 3-7**: 10 µL wash fractions; **lane 8**: 10 µL of the elution fraction of the *in-vivo* cross-linked bait PrdA [A] or PrdB [B]; **lane 9**: 10 µL of the 30-fold concentrated elution fraction of the different bait. The PrdA plasmid was constructed and the purification steps were performed by Ilka Pusch during her master thesis (2018).

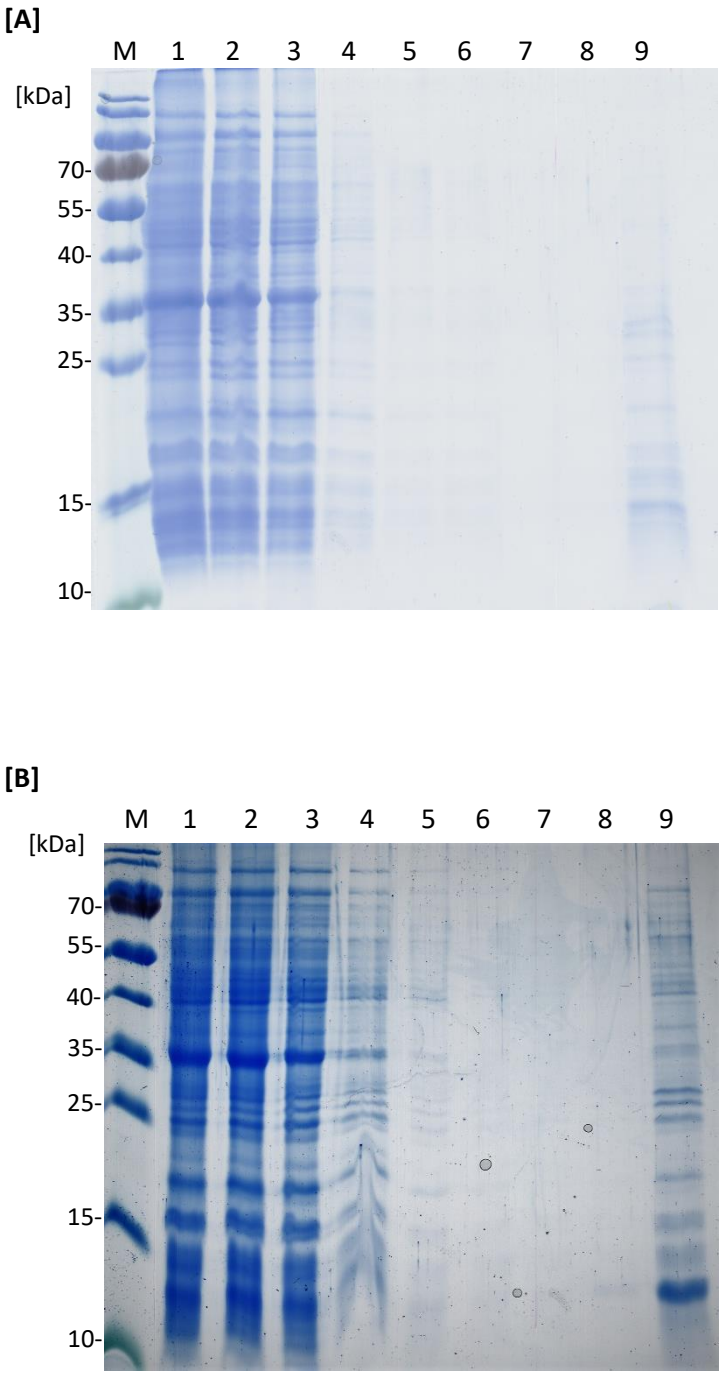

Figure 43: SDS-PAGEs of the fromaldehyde cross-linked bait proteins RnfB [A] and RnfC [B] after affinity chromatography of the insoluble fraction from *C. difficile* 630Δ*erm*_ pMTL82151*rnfB*-strep II *and C. difficile* 630Δ*erm*_ pMTL82151*rnfC*-strep II. The cross-linked (formaldehyde; $OD_{600\,nm}$ 1 = 0.156 % crosslinker) baits RnfB and RnfC after the Strep-tagged affinity chromatography of the insoluble fraction were loaded on a 15 % SDS-PAGE. The seperation of the proteins according to their relative molecular masses were performed at 45 mA for 45 min. The gel was stained with InstantBlue® Protein Stain (Expedeon Ltd, Cambridge, UK) solution. **M**: 5 µL PageRuler™ Prestained *Protein Ladder* (Thermo Fisher Scientific, Schwerte, Germany); **lane 1**: 7 µL of the solubilized insoluble fraction; **lane 2**: 7 µL flowthrough of the Strep-Tactin® column (Strep-Tactin® Superflow® high capacity, IBA Lifesciences, Göttingen, Germany); **lane 3-7**: 10 µL wash fractions; **lane 8**: 10 µL of the elution fraction of the *in-vivo* cross-linked bait protein RnfB [A] or RnfC [B]; **lane 9**: 10 µL of the 30-fold concentrated elution fraction of the respective bait protein.

8.4 *Gel-based LC-MS/MS identified interaction partners of the* C. difficile *baits PrdA, PrdB, RnfB and RnfC in absence/ presence of the cross-linker formaldehyde*

<u>*C. difficile* 630Δ*erm* pMTL82151 wildtype affinity chromatographed as a quality Strep-Tactin® column control</u>

Table 26: List of the LC-MS/MS identified proteins in the cut-out gel-slices C1-C3 after affinity chromatography of the soluble fraction of the cell free extract from* C. difficile *630Δ*erm*_pMTL82151

Definition	Protein	Gene-ID	Protein mass [kDa]	Unique Peptide	Abundances
4-hydroxybutyrate dehydrogenase	**4hbD**	CD630DERM_23380	42	10	6.28E+07
Acetate kinase	**AckA**	CD630DERM_11750	44	21	2.53E+08
Acetoacetyl-CoA thiolase	**ThlA1**	CD630DERM_10590	41	24	1.30E+09
Acryloyl-CoA reductase electron transfer subunit beta	**AcrA**	A0A0N1HW97	37	10	4.39E+07
Acyl-CoA dehydrogenase	**AcdB**	CD630DERM_03990	41	19	2.45E+08
Aldehyde-alcohol dehydrogenase	**AdhE1**	CD630DERM_29660	96	5	3.26E+06
Butyrate kinase	**Buk**	CD630DERM_01130	38	8	2.08E+07
Butyryl-CoA dehydrogenase	**Bcd2**	CD630DERM_10540	41	14	1.95E+08
Carnitine dehydratase	**HadA**	CD630DERM_03950	44	28	7.16E+08
Cysteine desulfurase	**IscS1**	CD630DERM_07530	44	10	3.49E+07
Desulfoferredoxin	**Rbo**	CD630DERM_08270	14	4	2.27E+09
Electron transfer flavoprotein subunit alpha	**EtfA1**	CD630DERM_04010	36	4	3.03E+06
Glutamate dehydrogenase	**GluD**	CD630DERM_01790	46	21	1.19E+09
Glyceraldehyde-3-phosphate dehydrogenase	**GapB**	CD630DERM_17670	36	10	1.49E+07

Phosphoglycerate kinase	**Pgk**	CD630DERM_31730	43	17	1.78E+08
Proline racemase	**PrdF**	CD630DERM_32370	36	9	6.04E+07
Precursor of the S-layer proteins	**SlpA**	CD630DERM_27930	76	27	1.42E+08
Pyruvate carboxylase	**PycA**	CD630DERM_00210	128	6	6.70E+06
Rubrerythrin family protein	**Rbr**	CD630DERM_08250	21	18	5.01E+09
R-phenyllactate dehydratase	**FldB**	D5PZU3	47	9	7.89E+07

Protein-protein interactions of the bait proteins PrdA and PrdB of *C. difficile* 630Δ*erm* pMTL82151*prdA/prdB* strep II in absence of the cross-linker formaldehyde

Table 27: List of gel-based LC-MS/MS identified PrdA and PrdB interactions in the different gel slices (UP: unique peptide; A: abundance)

Definition	Protein (preys)	Gene-ID	Protein mass [kDa]	PrdA		PrdB	
				UP	**A**	**UP**	**A**
ATP synthase							
V-type ATPase subunit D	**AtpD**	CD630DERM_29540	50	**-**	**-**	**14**	**1.26 E+07**
F-type H^+-transporting ATPase subunit gamma	**AtpG**	CD630DERM_34690	32	**-**	**-**	**3**	**1.90 E+06**
F-type H+-transporting ATPase subunit alpha	**AtpA1**	CD630DERM_34700	55	**-**	**-**	**8**	**1.75 E+07**
Electron transfer							
Electron transfer flavoprotein protein subunit alpha	**EtfA1**	CD630DERM_04010	36	**-**	**-**	**15**	**1.19 E+08**
Electron transfer flavoprotein subunit beta	**EtfB1**	CD630DERM_04000	29	**9**	**8.22 E+06**	**15**	**9.77 E+07**
Ferrous iron transport protein B	**FeoB1**	CD630DERM_14790	78	**-**	**-**	**6**	**1.54 E+06**

D-proline reductase							
Putative electron transfer protein	**PrdC**	CD630DERM_32470	47	-	-	**30**	**3.12 E+08**
Proline racemase	**PrdF**	CD630DERM_32370	36	-	-	**26**	**2.81 E+08**
Butanoate-, fatty acid metabolism, glycolysis/glyconeogenesis, pentose phosphate pathway, pyruvate metabolism, TCA cycle							
3-hydroxybutyryl-CoA dehydratase	**Crt2**	CD630DERM_10570	28	-	-	**18**	**8.37 E+07**
3-hydroxybutyryl-CoA dehydrogenase	**Hbd**	CD630DERM_10580	31	**11**	**1.84 E+07**	**14**	**2.42 E+08**
4-hydroxybutyrate CoA-transferase	**Cat2**	CD630DERM_23390	48	-	-	**15**	**3.12 E+07**
4-hydroxybutyryl-CoA dehydratase/vi-nylacetyl-CoA-Delta-isomerase	**AbfD**	CD630DERM_23410	55	**7**	**3.24 E+06**	**21**	**1.28 E+08**
Aldehyde-alcohol de-hydrogenase	**AdhE**	CD630DERM_03340	96	**12**	**2.54 E+05**	**14**	**1.79 E+08**
ATP-dependent 6-phosphofructokinase	**PfkA**	CD630DERM_33950	34	**5**	**3.99 E+06**	**13**	**6.41 E+07**
Butyrate kinase	**Buk**	CD630DERM_01130	38	-	-	**30**	**9.04 E+07**
D-lactate dehydro-genase	**LdhA**	CD630DERM_03940	36	**9**	**6.83 E+06**	**21**	**3.45 E+08**
Fructose-1,6-bisphos-phate aldolase	**Fba**	CD630DERM_04030	33	**10**	**1.58 E+07**	**17**	**1.68 E+08**
Glucose-6-phosphate isomerase	**Pgi**	CD630DERM_32850	50	-	-	**20**	**8.92 E+07**
Glyceraldehyde-3-phosphate dehydro-genase subunit A	**GapA**	CD630DERM_31740	36	-	-	**29**	**9.88 E+08**
Glyceraldehyde-3-phosphate dehydro-genase	**GapB**	CD630DERM_17670	36	**17**	**1.05 E+08**	-	-
Phosphate butyryltransferase	**Ptb**	CD630DERM_01120	33	**6**	**1.30 E+06**	**21**	**3.33 E+07**
Pyruvate carboxylase	**PycA**	CD630DERM_00210	128	**12**	**8.58 E+06**	**43**	**1.21 E+08**
Pyruvate flavodoxin oxidoreductase	**Pfo**	CD630DERM_26820	128	-	-	**82**	**1.16 E+08**
Pyruvate kinase	**Pyk**	CD630DERM_33940	63	-	-	**27**	**1.76 E+08**

Succinate-semialdehyde dehydrogenase	**SucD**	CD630DERM_23420	51	**-**	**-**	**34**	**4.50 E+08**
Oxidoreductase							
Ferritin	**FtnA**	CD630DERM_21950	19	**3**	**4.92 E+05**	**5**	**2.11 E+06**
Glycine reductase subunit B	**GrdB**	CD630DERM_23510	47	**-**	**-**	**7**	**5.84 E+06**
Glycine reductase subunit D	**GrdD**	A0A170WEG3	40	**-**	**-**	**9**	**4.88 E+06**
Indolepyruvate ferredoxin oxidoreductase	**IorA**	CD630DERM_23810	66	**-**	**-**	**3**	**4.28 E+06**

Green highlight: proteins which are included in the list of identified proteins in the strep-tagged chromatographed wildtype (table 26), but in comparison to that the proteins here are highly enriched in the elution fraction of the bait samples.

Protein-protein interactions of the bait proteins RnfB and RnfC of *C. difficile* 630Δ*erm* pMTL82151*rnfB/rnfC* strep II in absence of the cross-linker formaldehyde

Table 28: List of gel-based LC-MS/MS identified RnfB and RnfC interactions in the different gel-slices (UP: unique peptide; A: abundance)

Definition	Protein (preys)	Gene-ID	Protein mass [kDa]	RnfB		RnfC	
				UP	A	UP	A
ATP synthase							
V-type ATPase subunit A	**AtpA**	CD630DERM_29560	65	**9**	**4.68 E+07**	**-**	**-**
V-type ATPase subunit B	**AtpB**	CD630DERM_29550	26	**4**	**1.34 E+07**	**-**	**-**
V-type ATPase subunit D	**AtpD**	CD630DERM_29540	50	**33**	**3.79 E+07**	**10**	**3.69 E+06**
V-type ATPase subunit D	**AtpF**	CD630DERM_29561	20	**14**	**7.54 E+07**	**-**	**-**

F-type H^+-transporting ATPase subunit gamma	**AtpG**	CD630DERM_34690	32	**19**	**7.88 E+07**	**3**	**2.38 E+06**
F-type H^+/Na^+-transporting ATPase subunit alpha	**AtpA1**	CD630DERM_34700	55	**27**	**8.06 E+07**	**12**	**2.03 E+07**
Electron transfer							
Electron transfer flavoprotein protein subunit alpha	**EtfA1**	CD630DERM_04010	36	**-**	**-**	**14**	**6.51 E+07**
Electron transfer flavoprotein protein subunit alpha	**EtfA3**	CD630DERM_10560	36	**22**	**4.94 E+07**	**-**	**-**
Electron transfer flavoprotein subunit beta	**EtfB1**	CD630DERM_04000	29	**22**	**7.17 E+07**	**14**	**6.45 E+07**
Electron transfer flavoprotein subunit beta	**EtfB3**	CD630DERM_10550	29	**26**	**4.76 E+07**	**-**	**-**
Ferrous iron transport protein B	**FeoB1**	CD630DERM_14790	78	**28**	**6.95 E+07**	**4**	**7.18 E+05**
Ferrous iron transport protein B	**FeoB2**	CD630DERM_32740	65	**13**	**6.18 E+07**	**-**	**-**
Flavodoxin	**FldX**	CD630DERM_19990	15	**5**	**3.83 E+07**	**-**	**-**
D-proline reductase							
Putative electron transfer protein	**PrdC**	CD630DERM_32470	47	**23**	**4.32 E+07**	**-**	**-**
Butanoate-, fatty acid metabolism, glycolysis/glyconeogenesis, pentose phosphate pathway, pyruvate metabolism, TCA cycle							
3-hydroxybutyryl-CoA dehydratase	**Crt2**	CD630DERM_10570	28	**9**	**5.61 E+07**	**-**	**-**
3-hydroxybutyryl-CoA dehydrogenase	**Hbd**	CD630DERM_10580	31	**17**	**5.36 E+07**	**-**	**-**
4-hydroxybutyryl-CoA dehydratase/vinylacetyl-CoA-Delta-isomerase	**AbfD**	CD630DERM_23410	55	**-**	**-**	**12**	**1.76 E+07**
4-hydroxybutyrate CoA transferase	**Cat2**	CD630DERM_23390	48	**16**	**5.26 E+07**	**13**	**2.74 E+06**
Aldehyde-alcohol dehydrogenase	**AdhE1**	CD630DERM_29660	96	**62**	**8.71 E+07**	**-**	**-**
ATP-dependent 6-phosphofructokinase	**PfkA**	CD630DERM_33950	34	**12**	**6.91 E+07**	**9**	**1.37 E+07**

Butyrate kinase	**Buk**	CD630DERM_01130	38	**15**	**5.56 E+07**	**13**	**1.98 E+07**
Butyrate kinase	**Buk2**	CD630DERM_23790	38	**10**	**7.99 E+06**	**-**	**-**
D-lactate dehydrogenase	**LdhA**	CD630DERM_03940	36	**18**	**1.02 E+08**	**5**	**2.82 E+06**
Fructose-1,6-bisphosphate aldolase	**Fba**	CD630DERM_04030	33	**16**	**5.16 E+07**	**16**	**1.84 E+07**
Glucose-6-phosphate isomerase	**Pgi**	CD630DERM_32850	50	**13**	**7.72 E+07**	**11**	**9.90 E+06**
Glyceraldehyde-3-phosphate dehydrogenase subunit A	**GapA**	CD630DERM_31740	36	**21**	**6.49 E+07**	**23**	**2.30 E+08**
Iron-containing alcohol dehydrogenase	**-**	CD630DERM_31050	68	**-**	**-**	**22**	**3.02 E+07**
Phosphate butyryltransferase	**Ptb**	CD630DERM_01120	33	**-**	**-**	**9**	**6.98 E+06**
Pyruvate carboxylase	**PycA**	CD630DERM_00210	128	**-**	**-**	**22**	**1.15 E+07**
Pyruvate flavodoxin oxidoreductase	**Pfo**	CD630DERM_26820	128	**71**	**5.38 E+07**	**39**	**1.22 E+08**
Pyruvate kinase	**Pyk**	CD630DERM_33940	63	**22**	**6.23 E+07**	**16**	**3.73 E+07**
Succinate-semialdehyde dehydrogenase	**SucD**	CD630DERM_23420	51	**-**	**-**	**16**	**3.04 E+07**
Oxidoreductase							
Glycine reductase subunit C	**GrdC**	CD630DERM_23490	55	**16**	**6.36 E+07**	**8**	**5.58 E+06**
Indolepyruvate ferredoxin oxidoreductase	**IorA**	CD630DERM_23810	66	**-**	**-**	**14**	**7.42 E+06**
Indolepyruvate ferredoxin oxidoreductase	**IorB**	CD630DERM_23800	21	**11**	**1.02 E+07**	**-**	**-**
Toxins							
Toxin A	**TcdA**	CD630DERM_06630	308	**31**	**6.42 E+07**	**-**	**-**

Green highlight: proteins which are included in the list of identified proteins in the strep-tagged chromatographed wildtype (table 26), but in comparison to that the proteins here are highly enriched in the elution fraction of the bait samples.

Protein-protein interactions of the bait proteins PrdA and PrdB of *C. difficile* 630Δ*erm* pMTL82151prdA/*prdB* strep II in presence of the cross-linker formaldehyde

Table 29: List of gel-based LC-MS/MS identified formaldehyde cross-linked PrdA and PrdB interactions in the gel-slices (UP: unique peptide; A: abundance)

Definition	Protein (preys)	Gene-ID	Protein mass [kDa]	PrdA		PrdB	
				UP	A	UP	A
ATP synthase							
V-type ATP synthase beta chain	**AtpB**	CD630DERM_29550	50	**3**	**4.53 E+06**	-	-
V-type ATPase subunit D	**AtpD**	CD630DERM_29540	50	**9**	**1.05 E+07**	-	-
F-type H^+-transporting ATPase subunit gamma	**AtpG**	CD630DERM_34690	32	**16**	**5.32 E+07**	-	-
F-type H^+-transporting ATPase subunit alpha	**AtpA1**	CD630DERM_34700	55	**22**	**3.49 E+08**	**3**	**1.02 E+07**
Electron transfer							
Electron transfer flavoprotein protein subunit alpha	**EtfA1**	CD630DERM_04010	36	**12**	**3.28 E+08**	-	-
Electron transfer flavoprotein subunit beta	**EtfB1**	CD630DERM_04000	29	**18**	**9.21 E+08**	-	-
Ferrous iron transport protein	**FeoB1**	CD630DERM_14790	79	**12**	**1.67 E+07**	-	-
D-proline reductase							
Proline reductase	**PrdD**	CD630DERM_32400	29	**4**	**1.11 E+07**	-	-
Proline racemase	**PrdF**	CD630DERM_32370	36	**16**	**5.01 E+08**	-	-
Butanoate-, fatty acid metabolism, glycolysis/glyconeogenesis, pentose phosphate pathway, pyruvate metabolism, TCA cycle							
3-hydroxybutyryl-CoA dehydratase	**Crt2**	CD630DERM_10570	28	**13**	**1.30 E+08**	-	-
3-hydroxybutyryl-CoA dehydrogenase	**Hbd**	CD630DERM_10580	31	**8**	**1.15 E+09**	-	-
4-hydroxybutyrate CoA-transferase	**Cat2**	CD630DERM_23390	48	**25**	**3.14 E+08**	-	-

4-hydroxybutyryl-CoA dehydratase/vinylacetyl-CoA-Delta-isomerase	**AbfD**	CD630DERM_23410	55	**16**	**1.77 E+08**	-	-
Acyl-CoA dehydrogenase	**AcdB**	CD630DERM_03990	41	**29**	**7.77 E+09**	-	-
Acryloyl-CoA reductase electron transfer subunit beta	**AcrA**	A0A0N1HW97	37	**14**	**2.38 E+08**	-	-
Aldehyde-alcohol dehydrogenase	**AdhE**	CD630DERM_03340	96	**26**	**5.13 E+07**	-	-
ATP-dependent 6-phosphofructokinase	**PfkA**	CD630DERM_33950	34	**18**	**4.00 E+08**	-	-
Butyrate kinase	**Buk**	CD630DERM_01130	38	**26**	**2.48 E+08**	-	-
Butyryl-CoA dehydrogenase	**Bcd2**	CD630DERM_10540	41	**22**	**2.96 E+09**	-	-
D-lactate dehydrogenase	**LdhA**	CD630DERM_03940	36	**15**	**4.85 E+08**	-	-
Formate acetyltransferase	**PlfB**	CD630DERM_07590	83	**51**	**8.65 E+08**	-	-
Fructose-1,6-bisphosphate aldolase	**Fba**	CD630DERM_04030	33	**14**	**9.22 E+07**	-	-
Fumarate hydratase	**FumA**	CD630DERM_10030	30	**4**	**1.74 E+06**	-	-
Glucose-6-phosphate isomerase	**Pgi**	CD630DERM_32850	50	**20**	**2.22 E+08**	-	-
Glucokinase	**GlcK**	CD630DERM_24590	34	**4**	**4.45 E+07**	-	-
Glyceraldehyde-3-phosphate dehydrogenase subunit A	**GapA**	CD630DERM_31740	36	**18**	**7.01 E+08**	-	-
Phosphate butyryltransferase	**Ptb**	CD630DERM_01120	33	**9**	**9.14 E+06**	-	-
Pyruvate carboxylase	**PycA**	CD630DERM_00210	128	**43**	**5.18 E+07**	-	-
Pyruvate flavodoxin oxidoreductase	**Pfo**	CD630DERM_26820	128	**56**	**4.01 E+08**	-	-
Pyruvate kinase	**Pyk**	CD630DERM_33940	63	**25**	**1.09 E+08**	-	-
Succinate-semialdehyde dehydrogenase	**SucD**	CD630DERM_23420	51	**42**	**1.99 E+09**	-	-

Oxidoreductase							
Dihydroorotate dehydrogenase electron transfer subunit	**PyrK**	CD630DERM_01850	33	**11**	**1.91 E+07**	**-**	**-**
Glycine reductase subunit B	**GrdB**	CD630DERM_23510	47	**12**	**8.18 E+07**	**-**	**-**
Indolepyruvate ferredoxin oxidoreductase	**IorA**	CD630DERM_23810	66	**15**	**2.25 E+07**	**-**	**-**

Green highlight: proteins which are included in the list of identified proteins in the strep-tagged chromatographed wildtype (table 26), but in comparison to that the proteins here are highly enriched in the elution fraction of the bait samples.

Protein-protein interactions of the bait proteins RnfB and RnfC of *C. difficile* 630Δ*erm* pMTL82151*rnfB/rnfC* strep II in presence of the cross-linker formaldehyde

Table 30: List of gel-based LC-MS/MS identified formaldehyde cross-linked RnfB and RnfC interactions in the different gel-slices (UP: unique peptide; A: abundance)

Definition	Protein (preys)	Gene-ID	Protein mass [kDa]	RnfB		RnfC	
				UP	A	UP	A
ATP synthase							
V-type ATPase subunit A	**AtpA**	CD630DERM_29560	65	**-**	**-**	**3**	**3.28 E+05**
V-type ATPase subunit D	**AtpD**	CD630DERM_29540	50	**16**	**4.64 E+07**	**28**	**6.03 E+07**
V-type ATPase subunit F	**AtpF**	CD630DERM_29561	20	**10**	**5.22 E+07**	**18**	**1.08 E+08**
F-type H^+-transporting ATPase subunit gamma	**AtpG**	CD630DERM_34690	32	**6**	**8.74 E+07**	**9**	**3.02 E+06**
F-type H^+/Na^+-transporting ATPase subunit alpha	**AtpA1**	CD630DERM_34700	55	**15**	**5.84 E+07**	**24**	**1.04 E+08**
F-type H^+-transporting ATPase subunit delta	**AtpF1**	CD630DERM_34710	21	**-**	**-**	**7**	**1.13 E+07**

Electron transfer							
Electron transfer flavoprotein protein subunit alpha	**EtfA1**	CD630DERM_04010	36	**14**	**8.37 E+07**	**21**	**1.86 E+09**
Electron transfer flavoprotein protein subunit alpha	**EtfA3**	CD630DERM_10560	36	**9**	**3.32 E+07**	**-**	**-**
Electron transfer flavoprotein subunit beta	**EtfB1**	CD630DERM_04000	29	**13**	**9.57 E+07**	**19**	**2.92 E+08**
Electron transfer flavoprotein subunit beta	**EtfB3**	CD630DERM_10550	29	**13**	**6.17 E+06**	**-**	**-**
Ferrous iron transport protein B	**FeoB1**	CD630DERM_14790	78	**6**	**6.03 E+07**	**14**	**4.48 E+07**
D-proline reductase							
Putative electron transfer protein	**PrdC**	CD630DERM_32470	47	**-**	**-**	**13**	**3.43 E+07**
Proline racemase	**PrdF**	CD630DERM_32370	36	**-**	**-**	**16**	**2.82 E+08**
Butanoate-, fatty acid metabolism, glycolysis/glyconeogenesis, pentose phosphate pathway, pyruvate metabolism, TCA cycle							
3-hydroxybutyryl-CoA dehydratase	**Crt2**	CD630DERM_10570	28	**10**	**9.89 E+07**	**9**	**6.94 E+06**
3-hydroxybutyryl-CoA dehydrogenase	**Hbd**	CD630DERM_10580	31	**-**	**-**	**14**	**4.86 E+08**
4-hydroxybutyryl-CoA dehydratase/vinylacetyl-CoA-Delta-isomerase	**AbfD**	CD630DERM_23410	55	**6**	**7.87 E+07**	**10**	**1.17 E+07**
4-hydroxybutyrate CoA transferase	**Cat2**	CD630DERM_23390	48	**7**	**1.88 E+07**	**20**	**4.20 E+07**
Aldehyde-alcohol dehydrogenase	**AdhE1**	CD630DERM_29660	96	**46**	**6.73 E+07**	**43**	**1.95 E+09**
ATP-dependent 6-phosphofructokinase	**PfkA**	CD630DERM_33950	34	**7**	**3.67 E+07**	**11**	**1.45 E+07**
1-phosphofructokinase	**FruK**	CD630DERM_22700	34	**-**	**-**	**15**	**4.35 E+07**
Butyrate kinase	**Buk**	CD630DERM_01130	38	**-**	**-**	**26**	**6.35 E+07**
D-lactate dehydrogenase	**LdhA**	CD630DERM_03940	36	**12**	**2.58 E+07**	**15**	**8.58 E+07**
Formate acetyltransferase	**PlfB**	CD630DERM_07590	84	**24**	**9.33 E+07**	**15**	**7.90 E+06**

Fructose-1,6-bisphos-phate aldolase	**Fba**	CD630DERM_ 04030	33	**3**	**4.76 E+07**	**10**	**8.87 E+07**
Glucose-6-phosphate isomerase	**Pgi**	CD630DERM_ 32850	50	**-**	**-**	**10**	**2.08 E+07**
Glyceraldehyde-3-phosphate dehydro-genase subunit A	**GapA**	CD630DERM_ 31740	36	**8**	**7.67 E+07**	**20**	**4.24 E+08**
Phosphate butyryltransferase	**Ptb**	CD630DERM_ 01120	33	**5**	**8.89 E+07**	**-**	**-**
Pyruvate carboxylase	**PycA**	CD630DERM_ 00210	128	**44**	**5.54 E+07**	**47**	**1.55 E+08**
Pyruvate flavodoxin oxidoreductase	**Pfo**	CD630DERM_ 26820	128	**33**	**5.69 E+07**	**37**	**1.85 E+08**
Pyruvate kinase	**Pyk**	CD630DERM_ 33940	63	**6**	**9.00 E+07**	**21**	**9.54 E+07**
Succinate-semialde-hyde dehydrogenase	**SucD**	CD630DERM_ 23420	51	**18**	**4.81 E+07**	**19**	**2.94 E+08**
Oxidoreductase							
Ferritin	**FtnA**	CD630DERM_ 21950	19	**-**	**-**	**6**	**2.23 E+07**
Glycine reductase sub-unit B	**GrdB**	CD630DERM_ 23510	47	**-**	**-**	**7**	**8.22 E+06**
Glycine reductase sub-unit D	**GrdD**	A0A170WEG3	41	**-**	**-**	**15**	**1.85 E+07**
Indolepyruvate ferre-doxin oxidoreductase	**IorA**	CD630DERM_ 23810	66	**-**	**-**	**6**	**1.15 E+06**
Toxin							
Toxin A	**TcdA**	CD630DERM_ 06630	307	**-**	**-**	**18**	**4.20 E+06**
Chaperones and folding catalysts							
ATP-dependent Clp protease	**ClpC**	CD630DERM_ 00260	91	**-**	**-**	**49**	**2.34 E+08**

Green highlight: proteins which are included in the list of identified proteins in the strep-tagged chro-matographed wildtype (table 26), but in comparison to that the proteins here are highly enriched in the elution fraction of the bait samples.

8.5 In vitro biochemically characterization of the rnfC mutant strain

8.5.1 Data of growth curves of the *rnfC* mutant strain CD630Δ*erm_rnfC*636/637s::*ermB* compared to the wildtype CD630Δ*erm* in BHI(S)

Table 31: Data of the wildtype CD630Δ*erm *cell density measurement at $OD_{600\,nm}$ in BHI(S)

Time [h]	Replicate 1	Replicate 2	Replicate 3	Replicate 4	Replicate 5	Mean value	Standard deviation
0	0.05	0.06	0.06	0.05	0.05	0.05	0.00
1	0.13	0.14	0.15	0.11	0.13	0.13	0.01
2	0.28	0.27	0.29	0.27	0.27	0.28	0.01
3	0.63	0.59	0.57	0.61	0.62	0.60	0.02
4	1.18	1.05	1.06	1.1	1.07	1.09	0.05
5	1.29	1.23	1.27	1.29	1.24	1.26	0.02
6	1.46	1.4	1.45	1.44	1.43	1.44	0.02
7	1.51	1.51	1.48	1.5	1.52	1.50	0.01
8	1.57	1.56	1.57	1.59	1.57	1.57	0.01
9	1.6	1.6	1.6	1.59	1.57	1.59	0.01
10	1.53	1.53	1.52	1.56	1.55	1.54	0.01
11	1.53	1.5	1.49	1.47	1.55	1.51	0.03
12	1.45	1.48	1.48	1.49	1.47	1.47	0.01
13	1.47	1.48	1.46	1.48	1.47	1.47	0.01
14	1.43	1.44	1.43	1.41	1.41	1.42	0.01
15	1.34	1.36	1.42	1.38	1.32	1.36	0.03
16	1.2	1.24	1.29	1.22	1.25	1.24	0.03

Table 32: Data of the CD630Δerm_rnfC636/637s::ermB cell density measurement at $OD_{600\,nm}$ in BHI(S)

Time [h]	Replicate 1	Replicate 2	Replicate 3	Replicate 4	Replicate 5	Mean value	Standard deviation
0	0.05	0.06	0.05	0.06	0.05	0.05	0.00
1	0.08	0.07	0.07	0.06	0.08	0.07	0.01
2	0.08	0.08	0.1	0.1	0.08	0.09	0.01
3	0.12	0.09	0.12	0.08	0.13	0.11	0.02
4	0.18	0.12	0.17	0.14	0.16	0.15	0.02
5	0.22	0.16	0.2	0.21	0.2	0.20	0.02
6	0.36	0.29	0.37	0.37	0.34	0.35	0.03
7	0.52	0.43	0.51	0.49	0.5	0.49	0.03
8	0.71	0.64	0.71	0.7	0.69	0.69	0.03
9	0.73	0.73	0.75	0.71	0.71	0.73	0.01
10	0.76	0.75	0.75	0.74	0.74	0.75	0.01
11	0.75	0.75	0.79	0.75	0.75	0.76	0.02
12	0.74	0.74	0.76	0.72	0.72	0.74	0.01
13	0.74	0.77	0.77	0.73	0.76	0.75	0.02
14	0.72	0.71	0.72	0.69	0.71	0.71	0.01
15	0.73	0.73	0.75	0.72	0.71	0.73	0.01
16	0.72	0.72	0.75	0.7	0.74	0.73	0.02

8.5.2 Data of the fluorometric assay of the D-proline reductase activity

Table 33: Data of the fluorometric activity assay of the wildtype CD630Δerm for T1 and T2 at 450nm (5-aminovalerate standard of T1 data set: y = 108.28x and T2: y = 94.354x)

	Reaction time [min]	Replicate 1	Replicate 2	Replicate 3	Replicate 1	Replicate 2	Replicate 3
5-aminovalerate determination		**Relative fluorescence intensity (R1) + D-proline**			**Relative fluorescence intensity (R2) neg. control**		
T1	0	586.92	347.14	505.74	484.43	87.44	310.93
	30	485.55	220.11	721.31	399.75	146.84	621.04
	60	**1126.69**	**646.20**	**964.51**	**947.36**	**348.01**	**737.10**
T2	0	586.93	1343.13	1528.35	585.22	1023.18	745.63
	30	580.27	1032.23	833.27	584.07	831.89	629.71
	60	**761.36**	**1373.02**	**1079.30**	**757.32**	**1197.91**	**847.63**
5-aminovalerate determination		**Normalized fluorescence Intensity (R1-R2)**			**Concentration of 5-aminovalerate [nmol] (via standard)**		
T1	0	102.49	259.70	194.82	0.95	2.40	1.80
	30	85.80	73.27	100.27	0.79	0.68	0.93
	60	**179.33**	**298.19**	**227.41**	**1.66**	**2.75**	**2.10**
T2	0	1.71	319.95	782.72	0.02	3.39	8.30
	30	-3.80	200.34	203.57	-0.04	2.12	2.16

	60	**4.05**	**175.11**	**231.67**	**0.04**	**1.86**	**2.46**

5-aminovalerate determination		**Mean value of 5-aminovalerate [nmol]**	**Standard deviation**
T1	0	1.70	0.59
	30	0.80	0.10
	60	**2.17**	**0.45**
T2	0	3.90	3.40
	30	2.14	0.02
	60	**1.45**	**1.03**

Table 34: Data of the fluorometric activity assay of the strain CD630Δ*erm_rnfC*636/637s::*ermB *for T1 and T2 at 450nm (5-aminovalerate standard of T1 data set: y = 105,62x and T2: y = 154,81x)

	Reaction time [min]	**Replicate 1**	**Replicate 2**	**Replicate 3**	**Replicate 1**	**Replicate 2**	**Replicate 3**
5-aminovalerate determination		**Relative fluorescence intensity (R1) + D-proline**			**Relative fluorescence intensity (R2) neg. control**		
T1	0	470.06	476.15	380.49	383.16	425.87	330.73
	30	412.81	509.67	377.08	345.39	417.73	363.29
	60	**365.03**	**635.46**	**415.15**	**325.75**	**604.47**	**363.08**
T2	0	647.27	544.46	546.76	384.64	483.96	446.24
	30	495.64	450.76	385.84	313.46	348.25	340.00
	60	**558.66**	**522.53**	**604.42**	**480.27**	**455.96**	**448.29**
5-aminovalerate determination		**Normalized fluorescence Intensity (R1-R2)**			**Concentration of 5-aminovalerate [nmol] (via standard)**		
T1	0	86.90	50.28	49.76	0.82	0.48	0.47
	30	67.42	91.94	13.79	0.64	0.87	0.13
	60	**39.28**	**30.99**	**52.07**	**0.37**	**0.29**	**0.50**
T2	0	262.63	60.50	100.53	1.70	0.40	0.65
	30	182.19	102.51	45.84	1.18	0.66	0.30
	60	**78.40**	**66.57**	**156.13**	**0.51**	**0.43**	**1.01**

5-aminovalerate determination		**Mean value of 5-aminovalerate [nmol]**	**Standard deviation**
T1	0	0.59	0.16
	30	0.55	0.31
	60	**0.39**	**0.09**
T2	0	0.92	0.56
	30	0.71	0.36
	60	**0.65**	**0.26**

The original fluorescence data and the analysis of the corresponding standards are shown in the digital appendix. The mean value and the sandard deviation of the concentration of 5-aminovalerate after a reaction time of 60 min of the wildtype and *rnfC* mutant strain at the time points T1 and T2 were included for the analysis in this thesis and highlighted in a grey box.

8.5.3 Data of the NAD^+/NADH ratio in the *rnfC* mutant and wildtype strain

Table 35: Data of the NAD^+/NADH ratio measurement of the wildtype CD630Δerm for T1 and T2 (values provided by Dr. Petra Henke, DSMZ in Braunschweig)

	NAD^+ and NADH	Replicate 1	Replicate 2	Replicate 3	Replicate 4	Replicate 5	Mean value	Standard deviation	Standard error
T1	**mg dry weight**	1.66	1.85	1.85	1.72	1.79			
	NAD^+ [nM]	1302.37	2978.39	1318.95	1068.64	1595.78			
	NAD^+ [nM/mg dw]	784,56	1609.94	712.94	621.30	891.50	**924.05**	395.97	197.99
	NADH [nM]	24.45	18.60	25.93	17.04	21.21			
	NADH [nM/mg dw]	14.73	10.06	14.01	9.90	11.85	**12.11**	2.22	1.11
T2	**mg dry weight**	4.81	4.86	4.85	4.88	4.82			
	NAD^+ [nM]	11438.31	11349.22	10721.12	12380.58	12421.66			
	NAD^+ [nM/mg dw]	2378.03	2335.23	2210.54	2537.01	2577.11	**2407.58**	150.35	75.18
	NADH [nM]	1575.56	1229.53	1158.25	308.93	459.41			
	NADH [nM/mg dw]	327.56	252.99	238.82	63.31	95.31	**195.60**	111.95	55.98

Table 36: Data of the NAD⁺/NADH ratio measurement of the strain CD630Δerm_rnfC636/637s::ermB for T1 and T2 (values provided by Dr. Petra Henke, DSMZ in Braunschweig)

	NAD⁺ and NADH	Replicate 1	Replicate 2	Replicate 3	Replicate 4	Replicate 5	Mean value	Standard deviation	Standard error
T1	mg dry weight	1.23	1.16	1.21	1.24	1.32			
	NAD⁺ [nM]	1024.53	997.10	995.49	1457.07	1578.86			
	NAD⁺ [nM/mg dw]	832.95	859.57	822.72	1175.06	1196.11	**977.28**	190.77	95.39
	NADH [nM]	29.47	33.48	30.58	38.16	31.07			
	NADH [nM/mg dw]	23.96	28.87	25.27	30.77	23.53	**26.48**	3.19	1.59
T2	mg dry weight	5.09	4.74	4.47	4.14	4.38			
	NAD⁺ [nM]	7629.41	7472.90	8182.21	9308.59	5603.25			
	NAD⁺ [nM/mg dw]	1498.90	1576.56	1830.47	2248.45	1279.28	**1686.73**	370.68	185.34
	NADH [nM]	58.46	55.97	61.75	20.49	41.59			
	NADH [nM/mg dw]	11.49	11.81	13.81	4.95	9.49	**10.31**	3.37	1.68

8.5.4 Data of the TcdA and TcdB concentration in the *rnfC* mutant and willdtype strain supernatant performed via the toxin ELISA test

Table 37: Data of the TcdA and TcdB concentration measurement of the strains CD630Δerm (WT) and CD630Δerm_rnfC636/637s::ermB (rnfC mutant) for T1 and T2 (TcdA standard: y = 0.1389x + 0.019; TcdB standard: y = 0.1275x + 0,01)

OD 450 nm - 620 nm			Replicate 1	Replicate 2	Replicate 3	Replicate 4	Replicate 5
TcdA	WT	T1	0.019	0.021	0.022	0.022	0.022
		T2	0.046	0.042	0.046	0.043	0.029
	rnfC mutant	T1	0.085	0.082	0.066	0.137	0.054
		T2	0.044	0.043	0.038	0.042	0.042
TcdB	WT	T1	0.024	0.022	0.036	0.028	0.015
		T2	0.021	0.024	0.024	0.026	0.025

TcdB	*rnfC* mutant	T1	0.028	0.033	0.020	0.024	0.018
		T2	0.020	0.019	0.022	0.027	0.025
Concentration [ng/mL] (via standard)							
TcdA	WT	T1	0.000	0.014	0.022	0.022	0.022
		T2	0.194	0.166	0.194	0.173	0.072
	rnfC mutant	T1	0.475	0.454	0.338	0.850	0.252
		T2	0.180	0.173	0.137	0.166	0.166
TcdB	WT	T1	0.094	0.078	0.188	0.125	0.024
		T2	0.071	0.094	0.094	0.110	0.102
	rnfC mutant	T1	0.125	0.165	0.063	0.094	0.047
		T2	0.063	0.055	0.078	0.118	0.102

Concentration [ng/mL]			**Mean value**	**Standard deviation**
TcdA	WT	T1	**0.016**	**0.009**
		T2	**0.160**	**0.045**
	rnfC mutant	T1	**0.474**	**0.205**
		T2	**0.164**	**0.015**
TcdB	WT	T1	**0.102**	**0.054**
		T2	**0.094**	**0.013**
	rnfC mutant	T1	**0.099**	**0.043**
		T2	**0.083**	**0.024**

The original fluorescence data of 450 nm and 620 nm as well as the analyses of the standard curve TcdA and TcdB are shown in the digital appendix. The mean value and the sandard deviation of the concentration of TcdA and TcdB of the wildtype and *rnfC* mutant strain at the time points T1 and T2 were included for the analyses in this thesis (highlighted in a grey box).

8.5.5 Fold change data of the metabolomics experiments

Table 38: Fold change (FC) data of the metabolite and CoA derivates MS measurement of the CD630Δerm_rnfC636/637s::ermB (rnfC mutant) versus CD630Δerm (WT) at T1 and T2 (FC: mean normalized peak area$_{rnfC\ mutant}$ / mean normalized peak area$_{WT}$)

Metabolites	Fold change T1	Fold change T2	CoA derivates	Fold change T1	Fold change T2
Proline	60.02	0.86	Crotonoyl-CoA	9.35	4.12
Ribose	7.81	1.54	3-Hydroxyhexanoyl-CoA	7.46	2.94
Phenyl-pyruvate	7.36	7.85	Butanoyl-CoA	7.15	2.52
Adenine	6.07	0.41	2-Methyl-3-oxo butanoyl-CoA	6.02	1.25
3-phenyl-lactate	5.32	6.07	3-Hydroxybutanoyl-CoA	5.75	4.86
Fructose	4.10	2.85	2-Isocaprenoyl-CoA	5.36	1.38
Succinate	2.82	0.23	Acetoacetyl-CoA	3.29	0.99
Tyrosine	2.77	0.19	3-phenylpropanoyl-CoA	2.27	2.69
Isoleucine	2.32	2.15	4-Hydroxyphe-nylacetyl-CoA	2.26	2.28
Indole-3-acetalde-hyde	2.21	WT	Phenyllactyl-CoA	2.00	3.20
lysine	2.21	0.94	3-Hydroxyisovaleryl-CoA	1.59	1.94
Serine	2.20	0.61	4-Hydroxybutanoyl-CoA	1.51	1.57
2-hydroxy-butanoate	2.15	1.21	D-2-hydroxyisoca-proyl-CoA	1.48	1.91
Xylose	2.13	1.01	Lactoyl-CoA	1.44	4.11
Valine	2.11	1.18	NADPH	1.15	0.47
Ribose-5-phosphate	2.09	0.69	2-Heptenoyl-CoA	1.10	0.53
N-acetyl-glucosamine	1.97	1.34	Hexenoyl-CoA	0.91	2.68
Threonine	1.96	1.44	Propanoyl-CoA	0.91	2..11
Cysteine	1.94	0.00	Phenylacetyl-CoA	0.68	2.32
N-acetyl-putrescine	1.93	0.00	CoA	0.65	1.35

4-hydroxy butanoate	1.85	1.23	Heptanoyl-CoA	0.63	0.75
Ornithine	1.84	0.53	ADP	0.62	0.54
2-phospho glycolate	1.80	0.00	5-Methyl-2-hexenoyl-CoA	0.61	1.05
Phenylala-nine	1.79	0.39	CoA-disulfide	0.60	1.36
Glutamate	1.74	0.85	NAD	0.59	0.52
Aspartate	1.74	0.66	ATP	0.55	0.44
Leucine	1.74	1.10	Isocaproyl-CoA	0.49	0.97
Cytosine	1.70	0.51	Malonyl-CoA	0.46	0.55
Gluconic-acid	1.64	1.18	(S)-2-Methyl-butanoyl-CoA	0.46	0.56
Glycine	1.63	1.23	AMP	0.45	0.89
Hydrocinna-mic acid	1.59	1.27	(4-Hydroxyphenyl) lactoyl-CoA	0.44	0.88
Malate	1.58	0.75	3-Oxopentanoyl-CoA	0.43	1.19
Fumarate	1.57	0.54	Acetyl-CoA	0.43	0.57
Lactate	1.57	0.71	Isovaleryl-CoA	0.38	0.70
(4-hydroxy-phenyl) acetate	1.55	0.58	NADH	0.32	0.32
Acetoacetate	1.33	Mut	3-Hydroxypentanoyl-CoA	0.30	3.96
Citrate	1.19	0.61	5-Methyl-hexanoyl-CoA	0.30	1.67
Nicotin-amide	1.18	0.31	2-Pentenoyl-CoA	0.28	1.65
Thymine	1.18	0.51	4-Methylthio-butyryl-CoA	0.27	0.74
AMP	1.15	0.27	Pentanoyl-CoA	0.21	1.60
Tryptophan	1.10	0.37	Hexanoyl-CoA	Mut	0.42
Methionine	1.05	0.65			
2-oxogluta-rate	0.93	0.46			
3-phospho glycerate	0.89	0.58			
(4-hydroxy-phenyl) pyruvate	0.87	0.33			
Sorbitol-6-phosphate	0.77	0.48			
Glycerate	0.66	0.99			

Glycerol-3-phosphate	0.64	0.45			
Nicotinic acid	0.60	0.39			
Iminodi acetate	0.34	2.21			
Fructose-6-phosphate	0.33	1.35			
Glucose-6-phosphate	0.29	0.83			
3-(4-hydro-xyphenyl) - lactate	0.12	WT			
Alanine	0.05	2.46			
4-(methyl-thio) butanoate	0.00	2.33			
Hexanoate	WT	0.84			

Table 39: Fold change (FC) data of the volatile acids (cell content), exometabolites (culture supernatant), amino acids (culture supernatant) and 5-aminovalerate (culture supernatant) measurement of the CD630Δerm_rnfC636/637s::ermB (rnfC mutant) against CD630Δerm (WT) at T1 and T2 (FC: mean normalized peak area$_{rnfC\ mutant}$ / mean normalized peak area$_{WT}$)

Exometabolites	Fold change T1	Fold change T2	Volatile acids	Fold change T1	Fold change T2
2-oxo-isocaproic-acid	5.05	Mut	3-Methyl-1-butanol	1.55	1.35
3-phenyllactate	4.66	0.84	4-Methyl-pent-2-enoate	1.44	2.65
(4-hydroxyphenyl) pyruvate	3.31	Mut	Pentanoate	0.83	0.43
2-oxoglutarate	2.27	3.03	5-Methyl hexanoate	0.81	0.58
2-hydroxybutanoate	2.27	0.93	3-Methyl butanoate	0.58	0.77
Hydrocinnamic acid	1.65	1.80	4-Methyl pentanoate	0.48	2.37
Lactate	1.55	0.68	2-Methyl butanoate	0.46	0.76

Phenylpyruvate	1.39	7.94	Propanoate	0.45	1.56
Glycerate	1.18	0.52	2-Methyl propanoate	0.37	0.70
Succinate	1.05	0.58	2-Methyl-1-propanol	0.00	0.09
Cysteine	0.91	Mut	1-Propanol	0.00	0.10
Isocaproate	0.71	0.53	1-Pentanol	0.00	0.12
4-methylthio-2-oxo butanoate	0.65	Mut	Ethanol	0.00	0.15
Glutarate	0.50	0.74	5-Methyl-1-hexanol	0.00	0.17
(4-hydroxyphenyl) acetate	0.49	0.34	1-Butanol	WT	0.03
Phenylacetate	0.43	1.06	**Amino acids**	**Fold change T1**	**Fold change T2**
4-(methylthio) butanoate	0.00	0.20	Proline	7.63	0.00
3-(4-hydroxyphenyl) -lactate	Mut	0.59	Alanine	0.87	1.74
4-hydroxybutanoate	Mut	1.15	Isoleucine	0.74	5.20
3-hydroxybutanoate	Mut	Mut	Serine	0.74	2.37
			Valine	0.68	2.52
			Glutamate	0.67	0.84
			Phenylalanine	0.67	0.06
			Lysine	0.67	0.78
			Leucine	0.66	0.97
			Methionine	0.65	1.13
			Threonine	0.61	Mut
			Histidine	0.54	0.77
			5-amino vale-rate	*0.35*	*0.99*

8.6 In vivo *characterization of the* rnfC *mutant strain*

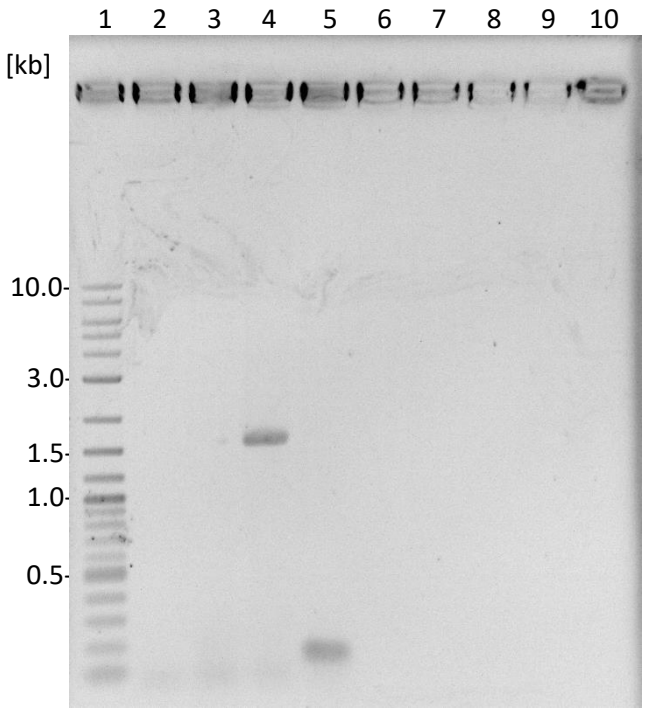

Figure 44: DNA agarose gel of the amplified DNA fragments of PCR samples from the wildtype *C. difficile* 630Δ*erm* strain (without pMTL82151), *rnfC* mutant strain (CD630Δ*erm*_*rnfC*636/637s::*ermB*_pMTL82151) and *rnfC*-complemented mutant strain (CD630Δerm_*rnfC*636/637s::*ermB*_pMTL82151*rnfC*-strep II) using the primer M13_fw/M13_rev. Shown is an agarose gel containing amplified DNA fragments by using the primers M13_fw/M13_rev binding to the vector pMTL82151 or pMTL82151*rnfC*-strep. After DNA extraction from the respective *C. difficile* strain, PCR "Confirmation of the constructed *C. difficile* pMTL82151 strains by PCR" (see chapter 3.3.10) was performed. Based on the different amplified DNA fragment sizes, conclusions can be reached about the previous strain for mouse infection experiments (see chapter 3.7). The expected amplified DNA target fragment of pMTL82151 has a size of ~150 bp and pMTL82151*rnfC*-strep II of ~1690 bp. The PCR samples were load onto a 1 % agarose gel and the fragments were separated for ~ 50 min and 100 V. **1**: 7µL DNA ladder Quick-Load® Purple 1 kb Plus DNA Ladder (New England Biolabs GmbH; Frankfurt am Main, Germany); **2**: 10 µL PCR sample of dH_2O as PCR template, negative control; **3**: 10 µL PCR sample from the wildtype; **4**: 10 µL PCR sample of amplified pMTL82151*rnfC*-strep II from *rnfC*-complemented mutant strain; **5**: 10 µL PCR sample of amplified pMTL82151 from *rnfC* mutant strain; **6 – 10**: empty

Acknowledgement

Zuerst möchte ich mich ganz herzlich bei meinem Doktorvater Prof. Dr. Dieter Jahn bedanken. Ich danke Dir, dass Du mir die Möglichkeit gegeben hast, an so einem interessanten und spannenden Thema mitwirken zu können. Mir Vertrauen und Mut geschenkt hast, um mich Verwirklichen zu können. Ich danke Dir, dass Du Dir immer Zeit für tolle und hilfreiche Diskussionen und Gespräche genommen hast. Deine Unterstützung, Ratschläge, Vorschläge und Energie während der gesamten Studien-und Promotionszeit haben mir gezeigt, dass „alles gut wird“. Vielen Dank! *Come on Eileen*.

Anschließend möchte ich mich von ganzem Herzen bei Dr. José Borrero-de Acuña bedanken. Du hast mich immer bestens unterstützt und gefördert, mich geformt und mir Grenzen gezeigt an denen ich wachsen konnte. Ich bin sehr dankbar, dass ich die Dissertation als Deine erste Doktorandin durchführen konnte. Ich bin stolz darauf, dass ich die Anfänge Deiner Arbeitsgruppe miterleben und mit formen durfte und auf das, was wir erreicht haben. Wir haben soviele schöne wissenschaftliche und private Momente miteinander erlebt, die ich nie vergessen werde. Du warst immer für mich da, in schwierigen und in schönen (Labor-) Zeiten. „Das Telefonat dauert nur fünf Minuten, José!“ – *60 Minuten später*. Diese Zeit werde ich nie vergessen. Danke für ein zweites Zuhause!

Bei Prof. Dr. Lothar Jänsch möchte ich mich herzlich bedanken, dass Sie diese Arbeit mit der großartigen Unterstützung Ihrer Arbeitsgruppe soweit gefördert haben, dass sie das werden konnte, was sie nun ist. Daher war es für mich eine Selbstverständlichkeit und wirklich schön zu hören, dass sie eingewilligt haben als 2. Referent meine Dissertation zu übernehmen.

Bei Prof. Dr. Ralf Mendel möchte ich mich zuerst ganz herzlich bedanken, dass ich die Möglichkeit bekommen habe bei der GradSchool PROCOMPAS Mitglied zu werden. Ich denke, so eine Chance hat nicht jeder und daher weiß ich es umso mehr zu schätzen. Ebenfalls danke ich Ihnen, dass Sie den Vorsitz für diese Arbeit bilden und somit PROCOMPAS Teil meiner Arbeit sein kann.

Zunächst möchte ich mich ganz herzlich bei der AG Borrero für eine tolle Arbeitsatmosphäre und der wirklich wunderbaren Zusammenarbeit bedanken. Danke Dr. Hao Zhang, Ilka Pusch, Annika Michel, Viktoria Otto, Ayten Mustafayeva und Finja Rieper. Danke für die wirklich wunderbare Zeit! Ebenfalls möchte ich all meinen betreuten Studenten, besonders Ilka und Finja, danken, dass sie sich dafür entschieden haben, in der AG Borrero die Abschlussarbeit/Praktika zu absolvieren und somit mit mir an Clostridien zu forschen und wunderbare Ergebnisse zu generieren!

An dieser Stelle möchte ich mich ganz herzlich bei meinen Kooperationspartnern für die tolle und erfolgreiche Zusammenarbeit bedanken:

Ich danke Dr. Josef Wissing und Hedwig Schrader (Gruppe von Prof. Dr. Lothar Jänsch; Cellular Proteome Research, HZI in Braunschweig) für die Übernahme der Durchführung der LC-MS/MS bei den Interactomics/Proteomics Studien und die immer freundliche, hilfsbereite Unterstützung bei technischen oder analytischen Fragen.

Bei Dr. Meina Neumann-Schaal, Dr. Sabine Will und Dr. Petra Henke (Bacterial Metabolomics, DSMZ in Braunschweig) möchte ich mich für die sehr gute Zusammenarbeit an den Metabolom/Transkriptom Experimenten bedanken. Ich danke euch für die prima Unterstüzung bei der Probenaufbereitung der Bakterienstämme, das Messen und Bereitstellen der Daten des Metabolom, der CoA-Ester, volatile acids, Exometabolom, Aminosäuren (5-Aminovalerat) sowie der NAD^+/NADH Gehalts Messung.

Ebenfalls möchte ich mich ganz herzlich bei Dr. Mathias Müsken und Ina Schleicher (Gruppe von Prof. Dr. Manfred Rohde; Central Facility for Microscopy, HZI in Braunschweig) für die immer hilfsbereite und freundliche Zusammenarbeit bedanken. Ich danke euch für die Übernahme der Durchführung der Immunogoldlabeling Experimente im TEM sowie den SEM Aufnahmen der *C. difficile* Proben.

Des Weiteren möchte ich mich für die sehr gute Zusammenarbeit und die experimentelle Übernahme der Mausinfektionsexperimente bei Dr. Nathiana Smit (Gruppe von Prof. Dr. Till Strowig; Microbial Immune Regulation, HZI in Braunschweig) herzlich bedanken.

Vielen Dank Dr. Julia Hofmann (Gruppe von Prof. Dr. Karsten Hiller, Bioinformatics and Biochemistry, TU Braunschweig, BRICS) für die Bereitstellung der Geräte und sehr freundliche Hilfestellung bei Fragen während des Toxin ELISA Experimentes.

An dieser Stelle möchte ich mich ebenfalls bei den Mitgliedern des CDiff Konsortiums /CDInfect (Sprecher: Prof. Dr. Dieter Jahn; Förderung im Rahmen des NZMG durch den Niedersächischen Vorabs der VolkswagenStiftung) für die tollen wissenschaftlichen Diskussionen innerhalb der Treffen und Veranstaltungen bedanken. Auch den Mitgliedern meiner Graduiertenschule PROCOMPAS (Sprecher: Prof. Dr. R.-R. Mendel; DFG gefördert) möchte ich für die hilfreichen Seminartreffen und Vorträge herzlich Danke sagen. Ebenfalls möchte ich mich an dieser Stelle für die ausgezeichnete, berufliche Unterstützung im Rahmen von Fortbildungen/Konferenzen bedanken. An dieser Stelle möchte ich der Koordinatorin Dr. Dagmar Zwerschke für die tolle Organisation und die immer freundliche Hilfestellung danken.

Über PROCOMPAS durfte ich tolle neue Menschen in der Wissenschaft kennenlernen, wodurch einige wertvolle Kontakte geknüpft wurden. Wenn aus Kollegen Freunde werden – an dieser Stelle möchte ich mich bei zwei ganz besonderen Menschen herzlich

bedanken: Nicole Beier und Maurice Diwo. Ich danke euch für die tolle berufliche und private Untersützung während den letzten drei Jahren – und hoffentlich darüber hinaus!

Anschließend möchte ich mich bei meinen Kollegen bedanken, die mich durch diese spannende Zeit begleitet haben. Zuerst wären da drei ganz besondere Menschen zu nennen, die nicht nur Arbeitskollegen, sondern auch wirklich tolle Freunde sind: Ilka Pusch, Katrin Müller und Hilger Jagau (Hilger, du fehlst hier!). Ilka, Du bist die beste Laborpartnerin, die man sich vorstellen kann. Danke, dass Du Deine Masterarbeit damals mit mir gemacht hast. Katrin, was kann ich sagen, außer „eine Eule brauch einen Delfin". Danke, dass wir so schöne Momente auf unseren (Dienst-)reisen (Neuseeland, USA,…) gemeinsam verbringen konnten. Hilger, Deine Ruhe und lieben Worte haben mich immer bestärkt in all dem was ich tun wollte. Vor Deiner Gelassenheit habe ich immer großen Respekt gehabt. Ich danke Dir für all deine Hilfe und Unterstützung.

Wenn ich über die Anfänge meiner Doktorarbeitszeit, aber auch darüber hinaus nachdenke, möchte ich mich ganz herzlich bei der Arbeitsgruppe von Dr. Martina Jahn und Prof. Dr. Michael Steinert bedanken. Danke Dir Martina, dass Du mich ebenfalls „aufgenommen" hast (Heide Park) und dass somit die AG Jahn mit Katrin Müller, Stefan Barthels, Davina Hiller, Toni Mingers und Juan José Vargas Guerrero einen besonderen Stellenwert, neben der AG Borrero, für mich besitzt! Can, bei Dir möchte ich mich ganz besonders bedanken, dass Du Dich meiner *C. difficile*-Einarbeitung so geduldig und immer hilfsbereit angenommen hast! Ohne Dich würde wahrscheinlich immer noch nichts wachsen!

Ebenfalls danke ich dem ganzen Institut für Mikrobiologie für die wundervolle und tolle Zeit. Für eure hilfsbereitschaft und die schöne Arbeitsatmosphäre. Besonders aber möchte ich mich bei Dr. Jürgen Moser für die wunderbare Bachelorarbeitszeit bedanken, wodurch der Grundstein der Arbeit in der Mibi gelegt wurde. Danke Dir Dr. Elisabeth Härtig, dass der Weg hier weitergehen sollte und ich meine Masterarbeit in Deiner Arbeitsgruppe anfertigen durfte. Ebenfalls danke ich ganz herzlich Alina Rommerskirch und Anja Hartmann für Tipps und Tricks sowie schöne Momente. Danke Dr. Rebekka Biedendieck für deine bedingungslose Hilfsbereitschaft und dein „offenes Ohr" in jeglichen Situationen. Ein großer Dank geht an das wunderbare Team Barbara und Dagmar. Danke für eure tolle Arbeit, die die Experimente unterstützen. Ich möchte mich auch bei unserem immer hilfsbereiten und freundlichen Sekretariat bedanken, Gunhild Voss und Christina Nitzsche, ohne euch würde soviel bürokratischer „Kram" nicht so leicht gehen. Du warst immer für die finanziellen und privaten Probleme offen: Danke Dir Daniela Schnobel! Danke Dir, dass Du mich in ganz schwierigen Zeiten so stark aufgefangen hast. Das werde ich Dir niemals vergessen!

Ein besonderer Dank geht an meine besten Freunde, die immer an meiner Seite waren, in schönen sowie in traurigen Momenten. Ihr habt mich immer aufgefangen, gestärkt und begleitet. Ich danke Dir Stephen Heß, Gina Hoga, Miriam Mege und Anna Hirsch. Ebenfalls möchte ich mich bei Ümran Karsli und Jasper Liedtke für die tolle Freundschaft und der mentalen Unterstützung, vorallem in der Schreibphase der Doktorarbeit, herzlich bedanken!

Zum Abschluss möchte ich noch den Menschen danken, die mich lieben, unterstützen, formen und prägen: Mama, Papa, Tom und Oma.
Danke, dass ihr immer für mich da seid, mir ein Zuhause gebt und immer an mich geglaubt habt. Ohne euch wäre ich nicht da, wo ich jetzt bin. Ich bin stolz, dass wir uns immer gegenseitig Halt geben. Ich liebe euch!